THE EFFECT OF BARIUM HYDROXIDE ON THE PHYSICOCHEMICAL PROPERTIES OF LIME-BASED CONSERVATION MORTARS

IOANNIS KARATASIOS

A thesis submitted to the Faculty of Art and Design in partial fulfilment of the requirements of the degree of Doctor of Philosophy

De Montfort University
Leicester

SEPTEMBER 2005

ABSTRACT

The research undertaken concerns the study of new mortars, for conservation purposes, which present enhanced resistance to sulphates. The thesis focuses on the effect of barium hydroxide, as an additive, to both the physico-chemical properties and the durability of conservation mortars. The analysis of original Byzantine mosaic mortars served as the basis to evaluate the potential benefits and limitations of analytical methods and techniques, which found application in the analysis of mortars.

Both binary pastes and mortar mixtures, containing varying amounts of barium hydroxide, were prepared and their physico-chemical properties and durability determined. Comparisons were made with a reference mixture containing no barium hydroxide.

The durability of the mortar mixtures against sulphate action was studied through the use of accelerated aging tests; crystallisation of soluble salts; electrochemical degradation; sulphate fixation; and resistance to leaching of cementing material. The results of these tests were considered together with the physical properties of the mortars, since these also influence their durability.

From the interpretation of the results it was shown that the setting of lime-based barium mixtures can be described by two mechanisms; the carbonation process of calcium hydroxide and barium hydroxide; and the precipitation of a barium calcium carbonate [$BaCa(CO_3)_2$] solid solution.

It has also been shown that barium hydroxide can be used as an additive material in lime-based conservation mixtures, and therefore enhance their durability against sulphate attack.

CONTENTS

LIST OF FIGURES

LIST OF TABLES

ABBREVIATIONS

AAS	Atomic Absorption Spectroscopy
AD	Anno Domini
BC	Before Christ
C_3A	Tricalcium Aluminate
CAH	Calcium Aluminate Hydrate
C_3S	Tricalcium Silicate
CSH	Calcium Silicate Hydrate
DTA	Differential Thermal Analysis
EC	European Commission
EDX	Energy Dispersive X-ray Analysis
EMRS	European Materials Research Society Meeting
EMY	Hellenic National Meteorological Service
E-SEM	Environmental Scanning Electron Microscope
FTIR	Fourier Transformed Infrared Spectroscopy
ICCM	International Committee for the Conservation of Mosaics
ICCROM	International Centre for the Study of the Preservation and Restoration of Cultural Property
ICP	Inductively Coupled Plasma Spectroscopy
MIP	Mercury Intrusion Porosimetry
NCSR	National Centre for Scientific Research
nd	Not Detected
PM	Petrographic Microscope
PPL	Plain Polarised Light
RH	Relative Humidity
RILEM	International Union of Testing and Research Laboratories for Materials and Structures
SEM	Scanning Electron Microscope
TAN	Technical Advisory Note
TC	Technical Committee
TEI	Technological Educational Institution
TG	Thermogravimetric Analysis
XPOLS	Crossed Polars
XRD	X-ray Diffraction

ACKNOWLEDGEMENTS

I would like to specially acknowledge my supervisors Dr David Watt and Dr Belinda Colston for their constant support and patience during the past years, as well as for their valuable comments on the final text. Also, many thanks to Dr Vassilis Lampropoulos, who helped me in the initial stage of my thesis.

This work was carried out in the Institute of Materials Science - Laboratory of Archeometry at the National Centre for Scientific Research (NCSR) 'Demokritos', Greece, under the supervision of Dr Vassilis Kilikoglou. Additionally, he provided financial support for the project, whenever this was necessary, and was happy to discuss the progress and any problems faced. I would like to express my sincere gratitude to him for his unconfined support.

Special thanks are given to Dr Panagiotis Theoulakis from the Department for Conservation of Antiquities and Works of Art, TEI of Athens, for introducing me to mortars and for a fruitful cooperation. Also, to Dr Georgios Panagiaris, Head of the Department, for providing access to SEM equipment.

I would like also to thank Demitris Fragoulis, Dr Aris Papageorgiou and Dr Demitris Papageorgiou from TITAN Cement Industry, Greece, for providing access and training in E-SEM, Thermal and X-ray Diffraction analysis.

Special thanks go to Dr Christos Trapalis and Dr Giorgos Kordas, at the Institute of Materials Science, for providing access and running ICP analysis, as well as to Dr Vassilis Verganelakis for providing training in FTIR spectroscopy.

Special thanks are due to the following people, with whom I collaborated during my research:

Dr Nikolaos Kanellopoulos, at the Institute of Physical Chemistry, NCSR Demokritos, for providing access to Mercury Porosimetry equipment, as well as Yiorgos Pilatos and Andreas Sapalides for running the measurements.

Dr Niki Miltiadou, director of the Directorate for Technical Research on Restoration, Hellenic Ministry of Culture for providing access to compressive test equipment, as well as Sofia Anagnostopoulou and Anna Kalagri for their help.

Dr Giorgos Vekinis, at the Institute of Materials Science, for his contribution to the study of mechanical properties, and Dr Ioannis Bassiakos for discussing the petrography.

Dr Nikos Zacharias, Paulina Gavala, Despina Kavousanaki, the personnel and PhD students of the Institute of Materials Science for their collaboration.

Many thanks go to Dr Anno Hein for discussing my 'out of the blue' questions and for taking-care of the soundtrack for my writing up period, as well as to Noemi Muller, for her support on chemistry issues and, Thanasis Karampotsos for providing technical support in SEM examination.

Haris Koilakou and Aspasia Ntina, directors of the 1st and 7th Eforates of Byzantine Monuments, are also acknowledged for providing licences for sampling mosaic mortars from Thebes and Nea Anghialos. Many thanks also to Demitrios Maltezos, archaeological conservator, for his help on the sampling procedure and for providing background information on mosaics conservation.

Last, but not least, I wish to thank my parents and Maria for their unfailing support and patience throughout this work.

DECLARATION

The work discussed in this thesis was carried out whilst the author was registered with the Faculty of Art and Design, De Montfort University, Leicester, between September 1998 and September 2005. It is the original work of the author.

This thesis has not been submitted for any other degree at this or any other university.

Ioannis Karatasios

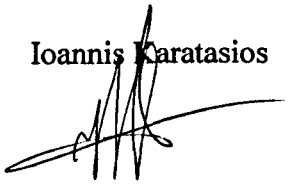

September 2005

1 INTRODUCTION

Today, with the majority of cement-based mortars have been proved to be incompatible with ancient and historic building materials, and the know-how on the manufacture and application of traditional lime mortars has mostly been lost (Lanas and Alvarez, 2003), the development and study of compatible conservation lime-based mortars with enhanced durability are issues with a wide range of applications in the field of cultural heritage conservation.

This research programme deals with the analysis of original Byzantine mortars and the study of new lime-based mixtures for conservation purposes, which present enhanced resistance against sulphate compounds. The thesis focuses on the potential impact of barium hydroxide [$Ba(OH)_2$] as an additive material, both to the physicochemical properties and the durability of conservation mortars.

1.1 CONSERVATION OF CULTURAL HERITAGE

During the past decade, a series of incremental changes concerning the conservation of cultural heritage has been undertaken, wherein the term conservation is used as an umbrella to describe all the actions planned for the protection of cultural heritage and the strengthening of its role within the complex of today's societies (Cassar et al., 2004).

Cultural heritage includes all traces of human activity in the physical environment. These are irreplaceable sources of information on people's lives and activities, and on the historical development of artistic and technical skills. Today, cultural heritage is no longer simply valued for its age or beauty, but has long been recognised as a source of national unity, especially arising from the acknowledgement of great architecture and monuments (English Heritage, 2003). Ancient monuments and historic buildings are

only part of a nation's cultural heritage, and along with archaeological sites, landscapes, townscapes, parks and designed landscapes form the main constituents of built heritage (Historic Scotland, 2000:3).

The potential for the conservation and maintenance of cultural heritage is now recognised to play a proactive role in enriching and enhancing the quality of life, in delivering answers to basic questions about our historic origins, in providing solutions to environmental and construction-related problems, and in interacting with other social, economic and political drivers (Cassar et al., 2004). Therefore, the preservation of cultural heritage is the key objective of any cultural policy (UNESCO, 1985), wherein 'conservation' is taken as an umbrella term to describe a wide range of measures aimed at preventing damage and protecting cultural assets (European Parliament, 2001:8-19).

1.2 WEATHERING OF BUILDING MATERIALS

As part of the total environment, the elements of architectural heritage are subjected to the natural and relatively slow weathering processes. However, these processes have been accelerated during past decades, due to changes of air quality and air pollution phenomena, to such an extent that costly maintenance is necessary (Building Effects Review Group, 1989; Yates, 2003). Today, historic buildings and monuments, which form a vital part of Europe's cultural heritage, are particularly vulnerable to the effect of air pollutants such as carbon dioxide, nitrogen oxides, ozone, sulphur oxides and particulate matter (Amoroso and Fassina, 1983a).

The importance of preserving architectural heritage and its contents has been acknowledged by the European Community in the adopted Directive on Ambient Air Quality Assessment and Management' (EC 96/62). The Directive is concerned with the effects of air pollution on human health, environment, damage to materials and cultural heritage (EUROPA, 2004).

Consequently, several research projects have been supported in planned actions for cultural heritage, mainly under the Science and Technology for Environmental

Protection (STEP) Programmes (CORDIS, 2000). The effects of air pollution and acid rain on building monuments and their constituents have been widely studied over the past few years by the research community and heightened interest catalysed by this important environmental issue has fostered an increase in research on material damage by air pollutants (Skoulikides and Papakonstantinou, 1981; Baer, 1982; Amoroso and Fassina, 1983a; Baer and Sabbioni, 1988; BERG Report, 1989; Camuffo, 1992; Schuster et al., 1994; Okochi, 1995; Kucera and Fitz, 1995; Torfs and Van Grieken, 1997; Striegel et al., 2003).

Among other pollutants, sulphur dioxide (SO_2) is the most important in determining the rate of deterioration of a number of building materials, including stonework and mortars. Although SO_2 concentrations have decreased in recent decades, sulphur dioxide still remains an important air pollutant that causes great damage to building materials (Brimblecombe and Sabbioni, 2002). Sulphur compounds are present in the atmosphere as gases, mainly sulphur dioxide (SO_2), sulphur trioxide (SO_3) and hydrogen sulphide (H_2S). Sulphur oxides are produced by the burning of materials and fuels containing sulphur. The formation of SO_x can be described by the following simplified reactions (Amoroso and Fassina, 1983b; Zappia et al. 1994):

$$S + O_2 \leftrightarrow SO_2 \tag{1.1}$$

$$2SO_2 + O_2 \leftrightarrow 2SO_3 \tag{1.2}$$

Gaseous SO_3 in the atmosphere exists only if the water vapour concentration is very low. Normally water vapour is present in amounts sufficient to combine with SO_3 to form droplets of sulphuric acid, according to the reaction:

$$SO_3 + H_2O \rightarrow H_2SO_4 \tag{1.3}$$

Lime mortars are one of the most widely used materials in ancient and historic monuments. They have been used for different purposes, including plastering and rendering of walls, bedding and pointing of masonry units, adhesion or supporting of

decorative constructions (mosaics, tiles, wall-paintings), waterproof linings, and grouting (Ashurst, 1983; Moropoulou et al., 2000; Hughes and Valek, 2003:15). Therefore, the preservation condition of mortars strongly affects the preservation condition of the whole architectural construction and any degradation usually has both structural and economic consequences to the monument.

Previous research has investigated the effects of multi-pollutants on the durability of lime-based mortars in terms of composition, chemical stability and typologies of damage. Laboratory simulation and field exposure tests have been carried out on samples taken from historic buildings and on different mixtures designed for conservation purposes. The aim of such projects has been to provide a better understanding of the deterioration mechanisms of mortars, as well as the interactions between the composition of mortars and durability against environmental pollution (Van Balen et al., 1999; Zappia et al. 1994, Sabbioni et al. 2001, Martinez-Ramirez et al. 1996, Hoffmann and Niesel 1995, Moriconi et al. 1994; Teutonico et al, 1994).

Sulphate attack of mortars and their subsequent degradation is a highly complex process and the mode of failure depends upon a wide range of factors, which include the type of sulphates, microclimatic conditions, mortars composition and microstructure. Mortars, because of their high porosity, present greater reactivity with SO_2 than stone.

Although no universal mechanism is involved, the main deterioration process that takes place when lime mortars are exposed to sulphur dioxide and/or other sulphate pollutants is the transformation of calcium carbonate ($CaCO_3$) into calcium sulphate ($CaSO_4$) following two main mechanisms (Brimblecombe and Sabbioni, 2002):

1) Dry deposition of SO_2 and its transformation into sulphate at the surface of the material, giving rise to the formation of gypsum ($CaSO_4 \cdot 2H_2O$).
2) Wet deposition of SO_4^{2-}, which directly attacks the calcitic binder, leading to the formation of a gypsum layer.

In both cases, calcium carbonate, that is produced during the setting of lime putty, is converted, in the external layers of mortar, to gypsum. Gypsum is more soluble than calcium carbonate ($K_{sp}=3.14\cdot10^{-5}$ at 25°C), and is easily dissolved and removed by rainwater (Livingston, 1992). The last mechanisms describe the chemical dissolution and the washing out of the binding medium from mortar matrix. Moreover, SO_2 deposition and recrystallisation of gypsum may induce mechanical stresses and flaking in the external layers of mortars (Yates, 2003).

From the very first studies it was obvious that pure lime mortars were vulnerable to sulphate attack, while hydraulic and cement-based mixtures proved to be more durable (Torrii et al., 1995; Hoffmann and Niesel, 1995; Wild et al., 1997). This partially explains the reasons for the extensive use of cement-based mortars on monuments during the 20th century.

1.3 DEVELOPMENT OF CONSERVATION MORTARS

Understanding the durability of ancient and historic mortars and how this is affected by their binder type, composition and microstructure is essential for planning future conservation treatments and developing adequate conservation strategies for monuments and historic buildings (Frohnsdorff and Masters, 1980). During planned conservation actions, such as pointing, grouting and/or filling of lacunae, it is important that the physical properties of the replacement mortars closely match those of the substrate in order to minimize potential incompatibility between the materials. Scientific investigations on test mixtures, manufactured and cured under standardized conditions, can lower the risk of failure and increase the durability of the restorative intervention (Getty, 2001).

Today, where extensive damage of masonry and decorative elements of historic buildings due to incompatibility of cement mortars with original materials has been clearly established, much attention is given to the use of traditional materials and their

compatibility with original materials (Rodriguez-Navarro et al., 1998; Moropoulou et al., 2002; Degryse et al., 2002; Lanas and Alvarez, 2003).

Cement-based mortars contain high amounts of soluble salts, potentially damaging for the original elements of the structures (Rodriguez-Navarro et al., 1998), and are less permeable than lime mortars, retaining excess water that initiates alteration phenomena. Moreover, their high values of compressive strength have been proved to be a source of further problems as they are not able to accommodate slight movement of the structures, resulting from creep or thermal effects. Repair mortars with low elasticity restrain movement, leading to stress that can cause failure of the original building elements (Hendry, 2001; Mosquera et al., 2002).

Scientific interest in the analysis and characterization of ancient and historic mortars and plasters, their deterioration mechanisms and the performance and compatibility of new repair mortars goes back to the 1980s and continues today. Apart from publication of research in scientific journals, reviews of the knowledge and experience gained to date have also been produced during relevant scientific meetings. ICCROM recognised the vital role that the properties of mortar play in the function and protection of a structure and its decorative parts, and organised the first conference devoted to mortars and grouts in old buildings in Rome during1981. This conference included both the study of original materials and the use of new ones.

The Technical Committee on 'Characterisation of old mortars with respect to their repair' (TC 167-COM) of the International Union of Testing and Research Laboratories for Materials and Structures (RILEM) considering the demand for improved guidance on conservation practice and reviewing current knowledge, and organised an international workshop on 'Historic Mortars: Characteristics and Tests' in Paisley during 1999. The workshop covered issues of sampling, analysis and testing of historic mortars, as well as specifications, composition and properties of new conservation mortars.

Finally, extensive literature reviews on lime mortars have been published by Historic Scotland (Hughes and Valek, 2003) and the Getty Conservation Institute (2003). These documents cover specific research areas in the field of lime mortars, such as the analysis and characterization of mortars and plasters, the study of the compatibility parameters of historic lime mortars and new repair materials, and the elucidation of the effects of traditional practices (processing procedures and additives) in order to estimate the influence of the composition and formulation procedures for repair and replacement materials.

1.4 RESEARCH AIMS AND OBJECTIVES

In addressing the problem of dissolution of binding material caused by sulphate attack, many research projects have focused on the development and study of mixtures with high strength values and enhanced resistance against sulphates. One effective method to achieve this is to partially replace the binder with different amounts and qualities of pozzolanic materials, such as natural pozzolana, ground brick clay, fly ash, and condensed silica fume (Wild et al., 1997). The main disadvantage of this approach is that it is not always possible to achieve both increased durability and compatibility with original mortars and other architectural elements, especially with regard to the physical and chemical properties of new mortars, and with the interaction between mortar and masonry or other architectural elements.

The present study considers the problem of sulphate resistance of conservation mortars by adopting a different approach that combines issues of compatibility and durability. Experience from architectural conservation has shown that these principles are considered more sustainable, because they are more realistic and enable future treatments to take advantage of the progress in scientific knowledge.

In the above context, different mixtures of conservation mortars were designed according to the raw materials, mix proportions and physical properties identified in the original mortars wherein sulphate resistance requirements were achieved by the addition of a material that could potentially fix and stabilize sulphate ions. Based on

conservation-related literature, the material that was selected for this purpose was barium hydroxide [$Ba(OH)_2$].

The use of barium hydroxide in conservation has a long history. Barium carbonate, precipitated from barium hydroxide, has been initially considered as an alternative consolidant for carbonate stones. Consolidation of stone is achieved through the formation of a barium-calcium carbonate ($BaCO_3$-$CaCO_3$) solid solution, which bridges the original calcite crystals (Lewin and Baer, 1974).

Moreover, barium hydroxide solutions have been used for the consolidation of sulphated stones, sculptures and wall-paintings. This procedure is known as the 'Florentine method' (Matteini, 1991). According to this method, sulphated surfaces are treated with ammonium carbonate [$(NH_4)_2CO_3$] and barium hydroxide. Sulphate ions are fixed in the form of barium sulphate ($BaSO_4$) wherein calcium hydroxide obtained from the above reactions (with excess of barium hydroxide) is converted to calcium carbonate and barium carbonate, which results in a further consolidating action (Ambrosi et al., 2000).

Barium hydroxide was first introduced by the cement industry as an additive material, in order to fix sulphates produced by gypsum and form barium sulphate ($BaSO_4$). The idea was abandoned, because the fixation of sulphates was causing quick setting of the cement mortars (Skoulikidis, 1996). Some years later, in an initial study, Lambropoulos et al., (2000) studied the effect of barium hydroxide on the microstructure and sulphate resistance of lime-cement mortars. Their results were encouraging and proposed further study on the potential of using barium hydroxide to increase the sulphate resistance of conservation mortars.

Chemically, barium hydroxide [$Ba(OH)_2$] is significantly more soluble in water (K_{sp}= $5 \cdot 10^{-3}$ at 25°C) than calcium hydroxide [$Ca(OH)_2$] (K_{sp}= $5.5 \cdot 10^{-6}$ at 25°C). However, barium carbonate ($BaCO_3$), formed after carbonation is chemically very similar to calcium carbonate –they are both alkaline-earth carbonates, with relatively low solubilities (Hansen et al., 2003).

The contribution of barium hydroxide to the durability of conservation mortars could be summarised in the fixation of sulphate ions by barium compounds. This reaction leads to the formation of a barrier external layer, consisting of the insoluble barium sulphate. Compared to calcium carbonate ($CaCO_3$) (K_{sp}= $2.8 \cdot 10^{-9}$ at 25°C) and calcium sulphate ($CaSO_4$) (K_{sp}= $9.1 \cdot 10^{-6}$ at 25°C), barium sulphate ($BaSO_4$) is a compound of very low solubility (K_{sp}= $1.1 \cdot 10^{-10}$ at 25°C), even in acidic environments (Hansen et al., 2003). Through this mechanism, the amount of binding material that is dissolved and washed out of the mortar matrix may be reduced, resulting in less damage on conservation mortars. Bearing in mind all the above, the main aims and objectives of this research are as follows:

a) to consider the synthesis and technology of original, historic mortars;
b) to asses the physico-chemical properties and microstructure of the above mortars;
c) to establish the criteria and methodology for the production of new conservation mortars, based on the results of the original historic mortar analysis;
d) to produce new conservation mixtures containing different amounts of barium hydroxide; and
d) to asses whether the addition of barium hydroxide in conservation mortars results in enhanced resistance to sulphate attack.

Original mortar samples were collected from six different Byzantine floor mosaics in Greece, and served as a case study for the development and assessment of appropriate analytical methodology. The characterisation of original mortars (see a-c above) served as the basis to evaluate the potential benefits and limitations of analytical methods and techniques, which are applied to the analysis of mortars. The analysis of mosaic mortars and the elaboration of the derived results was an individual part of the research, which offered the opportunity for better understanding of the basic principles of the analytical techniques used and, consequently helped on the interpretation of different analytical methodologies proposed in research papers.

Barium hydroxide was proposed so that it could play an active role within the mortar mass during setting, and to produce a mixed binding material with lime, eventually

behaving in a similar way to the one described by Lewin and Baer (1974) for the consolidating action of the barium-calcium carbonate ($BaCO_3$-$CaCO_3$) solid solution. If barium carbonate had been used, it would only have behaved as filler, and not as an admixture.

New conservation mixtures containing different proportions of barium hydroxide were prepared, by slightly modifying directives described in British standards for testing cements (BS EN 196, 1995). Mortars with similar composition and mix proportions to those studied in this programme very often appear in Roman, Byzantine, and later buildings and constructions. Their physicochemical properties and durability have been compared to those of a reference mixture containing no barium hydroxide.

Further issues investigated in this research, in relation to the addition of barium in conservation mortars, were:

a) the monitoring of the setting process of mixtures containing barium hydroxide;
b) the effect of barium hydroxide on the microstructure, physical and mechanical properties of mortars under consideration;
c) the impact of barium hydroxide on the durability of mortars against acid attack and crystallization tests;
d) the potential effect of the amount of barium hydroxide initially added in mixtures to the washing-out of the binding medium;
e) the microstructure of mortars during accelerating aging tests; and
f) the practical application of such mortars along with standardisation, ease of application, and appearance.

In this work, the term 'durability' is considered as the relative resistance of mortars to degradation caused by the effect of sulphate compounds in aquatic solutions. The development and study of such mortars are issues with a wide range of applications in architectural and archaeological conservation, when monuments are exposed in a sulphates-rich environment.

Apart from the laboratory work, a considerable number of references in the field of mortars analysis, deterioration and other relevant topics have been reviewed, providing documentation and a theoretical background on the above mentioned tasks, as well as on all the topics discussed in this thesis.

As a result, this thesis contributes to the on-going need for research on the development of modern materials for the conservation and protection of architectural heritage, durability, and compatibility with original materials.

2 HISTORIC MORTARS

2.1 TECHNOLOGICAL DEVELOPMENT

Mortars are one of the most commonly used materials for structural (i.e. bedding, jointing, grouting), protective (i.e. covering, rendering, sacrificial) and decorative (i.e. plasterwork, stucco, fresco, mosaic) purposes (Zacharopoulou, 1998). Generally, mortars are constituted with a binding agent, mixed with different types of aggregates and water. After mixing, they harden and gradually develop their adhesive and mechanical properties.

The technological development of mortars has a more local character for each community, and depended on the social and economic development of each civilization as well as on access to and availability of raw materials. Some key events concerning the evolution of mortars are given in Table 2.1.

Mud and clays seem to be the first materials that were utilized as binders in the construction of prehistoric shelter structures in hills or by lakes (lake-settlements). The materials employed in prehistoric constructions were those available in the area of the settlements. Sun-dried mud bricks and stones used to build the walls were joined with a thin layer of mud, while additionally tree branches and reeds used either for roofing or walls were covered with a thick layer of mud to provide extra protection (Hourmouziadis, 1982:19).

Table 2.1: Summary of key events in the history of mortars and concretes (University of Illinois, Urbana/Champaign, 2000).

Date	Event
12,000 BC	Reactions between limestone and soil shale during spontaneous combustion occurred in Israel to form a natural deposit of cement compounds. The deposits were characterised by Israeli geologists in the 1960s and '70s.
3,000 BC Egyptians	Mud mixed with straw used to bind dried bricks. They also used gypsum mortars and mortars of lime in the construction of the pyramids.
Chinese	Cementitious materials used to hold bamboo together in boats and in the Great Wall.
800 BC Greeks, Crete and Cyprus	Lime mortars used, which were much harder than later Roman mortars.
300 BC Babylonians and Assyrians	Bitumen used to bind stones and bricks.
300 BC – AD 476 Romans	Pozzolanic cement used from Pozzuoli (near Mt. Vesuvius) in Italy to build the Appian Way, Roman baths, the Coliseum and Pantheon in Rome, and the Pont du Gard aqueduct in south France. Lime used as a cementitious material. Pliny reported a mortar mixture of 1 part lime to 4 parts sand. Vitruvius reported a mixture of 2 parts pozzolana to 1 part lime. Animal fat, milk and blood were used as admixtures (substances added to cement to increase specific properties).
1200 – 1500 Middle Ages	The quality of cementing materials deteriorated. The use of burning lime and pozzolana (i.e. admixture) was lost, but reintroduced in the 1300s.
1678	Joseph Moxon wrote about a hidden fire in heated lime that appears upon the addition of water.
1779	Bry Higgins was issued a patent for hydraulic cement (stucco) for exterior plastering use.

1793	John Smeaton found that the calcination of limestone containing clay gave a lime that hardened under water (hydraulic lime). He used hydraulic lime to rebuild Eddystone Lighthouse in Cornwall (England), which he had been commissioned to build in 1756, but had to first invent a material that would not be affected by water. He wrote a book about his work.
1796	James Parker of England patented a natural hydraulic cement by calcining nodules of impure limestone containing clay, called Parker's Cement or Roman Cement.
1802	In France, a similar Roman Cement process was used.
1810	Edgar Dobbs received a patent for hydraulic mortars, stucco and plaster, although they were of poor quality due to a lack of kiln precautions.
1812–13	Louis Vicat of France prepared artificial hydraulic lime by calcining synthetic mixtures of limestone and clay.
1818	Maurice St Leger was issued patents for hydraulic cement. Natural cement was produced in the USA. Natural cement is based on limestone that has the appropriate amounts of natural clay to make the same type of concrete as John Smeaton discovered.
1820–21	John Tickell and Abraham Chambers were issued hydraulic cement patents.
1822	James Frost of England prepared artificial hydraulic lime like that of Vicat and called it British Cement.
1824	Joseph Aspdin of England invented Portland cement by burning finely-ground chalk with finely-divided clay in a lime kiln until carbon dioxide was driven off. The sintered product was then ground and called Portland cement after the high-quality building stone quarried at Portland (England).

The beginning of lime calcinations around 12,000BC introduced the production of slaked lime. The first dated sample of lime was found in a wooden shaft and was used as an adhesive material to fix a stone blade (Kingery et al., 1988). Other early applications of slaked lime, such as wall and floor plasters, pottery coatings and plastered sculptures, which have been found in Anatolia, Syria, Palestine, Turkestan, Sinai and Jericho dated from 7,000–3,500BC, suggest the development of the first

rudimentary kilns (Gourdin and Kingery, 1975; Elert et al, 2002). The first documented appearance of a lime kiln, and hence evidence for larger scale production of lime is at the Natufian site, Hayonim Cave, dated between 14,000–10,000 BC (Siddall, 2000).

The production technology and use of lime mortars for laying floors and covering walls was well known since the Early Bronze Age, while during the Mycenaean period mortars were used for more exacting applications such as waterproofing agent for cisterns, reservoirs, water channels and baths (Siddall, 2000).

Gypsum mortars and plasters were also used in antiquity along with lime mortars. Typical examples of gypsum mortars were analysed in samples from the Pyramid of Cheops (Wallace, 1865) and earlier monuments of Ancient Egypt (Gourdin and Kingery, 1975; Klemm and Klemm, 1990).

During the Classical period in Greece, which is acknowledged for its monumental architecture, lime was mainly used for rendering and decorative purposes. Lime mortars for jointing, bedding and plastering purposes were mostly used in common house building. Marble blocks used in most monumental buildings were precisely cut and the surfaces in contact were carefully polished. Such construction did not require any bedding or jointing mortar. When sandstone is used instead of marble, the surface of the architectural parts is covered with lime mixed with finely crushed marble fragments in order to imitate the texture of marble. The thickness of these rendering layers has been found to be 2–3mm (Doganis et al., 2003), while in the external layer, lime is probably mixed with a proteinous medium. The thickness of those layers, the orientation of the aggregates, and the smooth surface of the renders leads to the assumption that mortar layers should be polished. Vitruvius (Morgan, 1960), in *Ten Books on Architecture*, mentions that careful polishing of lime plasters with stones and leather helps mortars to restrain shrinkage and cracking, while it also attributes waterproofing properties.

The procedure of polishing fresh mortar in order to produce a compact, durable and impermeable surface seems to have first appeared in the Mask of Jericho (7,000BC) in Palestine. Later examples of the same technology were confirmed in Mycenaean and

Minoan settlements (1,500BC) and in many buildings of Phestos and Malia, in Crete (Malinowski, 1981).

The presence of volcanogenic material, either as a coarse aggregate or fine powder, in the matrix of mortars from water channels found in Olympia, Peloponnesus (800-700BC); the metallurgical, waterproofed cisterns (500BC) in Laurion (Conophagos, 1982), and the water cistern of Kameiros (500BC) in Rhodes (Malinowski, 1981) provide evidence that Greeks knew the production technology of hydraulic mortars (Dix, 1982) through the use of mortar admixtures. Further research is necessary to evaluate the intentional inclusion of pozzolanic material in Hellenistic and earlier mortars, mainly because of a lack of information about the methodology used for the analysis of the above samples (Siddall, 2000).

However, Greeks and Romans knew the effect of pozzolanic additives on the properties of lime mortars (Baronio et al., 1997). The first pozzolanic additives utilized in mortars were different types of volcanic ash or finely crushed volcanic, lightweight rocks that could be found on the earth's surface. Pozzuoli in Italy, Santorini (Thira) and Milos islands in Greece were known locations for providing natural pozzolans in antiquity. Pozzolans in the above areas are formed through the fast cooling of a molten material, the magma. Therefore, the associated silica and alumina compounds of the resulted material have a glassy, amorphous structure, which enables their faster reactivity with lime. The main constituents of the different types of pozzolans are SiO_2 and Al_2O_3, Fe_2O_3, CaO, MgO, Na_2O, K_2O as well as traces of TiO_2 and SO_3. Chemical composition varies widely, depending on the origin of the material.

The development of the Roman Empire and the new demands of construction works lead to the development of the Roman concrete or *opus caementicium*. The Roman concrete was a special mixture of mortar with coarse aggregates of 50-150mm thickness (Harries, 1995), which was used in masonry and wall construction. Because of the large size of aggregates it was placed by layering. Aggregates varied from large stone fragments to crushed bricks (Hughes and Valek, 2003:6).

During the late Roman period, ceramic powder and thin fragments of crushed bricks were introduced into lime mortars to act as artificial pozzolana. These mortars were mainly used for rendering and for the upper layers of floors, while large fragments were present in masonry mortars (Moropoulou et al., 2005a). Romans spread their use throughout their empire into Europe, northern Africa and west Asia. During the early Byzantine period, the use of crushed bricks in the joints of load-bearing walls became more frequent, while the thickness of the horizontal joints gradually increased from 10–15 mm to 60–70 mm (Papagianni and Karaveziroglou, 1993; Baronio et al., 1997; Binda et al., 1999).

In the late 1700s, Smeaton discovered that burning limestone with clay impurities above 1,000°C resulted in limes which could also gain their strength by reacting directly with water. Later, during the 19th century, the further increase of clay content and gradual increase of firing temperature to around 1,450°C resulted first in the production of natural cements and, finally, in Portland cement (Charola and Henrigues, 1999; Maurenbrecher et al., 2001).

2.2 SETTING AND HARDENING OF LIME-BASED MORTARS

Depending on the type of the binding material, mortars can be classified as follows (Rossi-Doria, 1986; Moropoulou et al, 1995):

- lime mortars;
- hydraulic-lime mortars;
- crushed-brick lime mortars;
- lime mortars with natural pozzolans;
- gypsum mortars; and
- clays.

Consequently, mortars may be classified according to their setting process in three categories, namely air-hardening, hydraulic, and mixed-type or pozzolanic (Zacharopoulou, 1998; Van Balen et al., 1999a:1). Air-hardening mortars are produced by mixing slaked (non-hydraulic) lime and inert aggregates. Hydraulic mortars are produced by using hydraulic lime and inert aggregates, while mixed-type mortars are produced by mixing slaked lime with pozzolanic (natural or artificial) materials (Charola and Henriques, 1999).

2.2.1 Setting of Air Hardening Mortars

Lime is produced by burning limestone, chalk or other calcareous materials of high content in calcium carbonate ($CaCO_3$). High calcium limestones containing at least 95% pure calcium carbonate are recommended for the production of pure high-quality fat limes (Swallow and Carrington, 1995; TAN 1, 2003:9). The production of lime involves the processes of calcinations and slaking.

During calcinations, limestone is burnt at a temperature in excess of 900°C and releases carbon dioxide and moisture (Equation 2.1). The product of this process is quicklime (CaO), which is collected from the kilns and graded. The process of slaking involves the mixing of quicklime with water (Equation 2.2). Depending on the quantity of water added, slaked lime may be available as dry powder or lime putty (Boyton, 1966:290; Swallow and Carrington, 1995; TAN 1, 2003:13). Lime putty occurs when an excess of water is added to quicklime, while dry powder is formed when just sufficient water is present to complete slaking. Finally, curing or maturing of lime putty is required in order to improve the quality of the material before use. Alternatively, quicklime can be mixed directly with water and other mortar constituents and produce a 'hot mix'.

$$CaCO_{3(s)} + \text{heating}\,(900^{\circ}C) \rightarrow \underset{\textit{quicklime}}{CaO_{(s)}} + CO_{2(g)} + H_2O_{(g)} \quad \text{(calcination)} \qquad (2.1)$$

$$\underset{\textit{quicklime}}{CaO_{(s)}} + H_2O_{(l)} \rightarrow \underset{\textit{hydrated lime}}{Ca(OH)_{2(s)}} + \text{heating} \quad \text{(slaking)} \qquad (2.2)$$

The setting and hardening of lime mortars take place through carbonation. Carbonation is a very slow process that requires years and sometimes centuries to be completed. Its evolution determines the performance of mortars as a building material (Rodrigues-Navarro et al., 2002). Carbonation proceeds in two stages. Initially, carbon dioxide (CO_2) dissolves in water (Dheilly et al., 2002) and forms carbonic acid (Equation 2.3).

$$CO_{2(g)} + H_2O_{(l)} \leftrightarrow H_2CO_{3(l)} \quad (2.3)$$

In the second stage (Equation 2.4), carbonic acid reacts with the dissolved calcium hydroxide, the mortar binder, and results in the precipitation of calcium carbonate. Depending on the storage conditions, calcium carbonate crystallizes as calcite, aragonite or vaterite. Calcite is the most thermodynamically stable of the three, followed by aragonite and vaterite in that order (Cole and Kroone, 1960; Martnez-Ramirez et al., 2003).

$$Ca(OH)_{2(l)} + H_2CO_{3(l)} \rightarrow CaCO_{3(s)} + 2H_2O_{(l)} \quad (2.4)$$

This process depends on relative humidity, temperature and CO_2 concentration (Moorehead 1986; Dheilly et al., 2002; Martinez-Ramirez et al., 2003). The relative humidity of the atmosphere and the water content of mortars play an important role in the diffusion of carbon dioxide in the lime, as the diffusion coefficient in water is much lower than in the air. Thus, carbonation speed is reduced when the mixture is saturated with water. The optimum water content is that which corresponds to maximum absorption on the pores surface before capillary condensation (Moorehead 1986; Van Balen and Van Gemert, 1994). The solubility of carbon dioxide and calcium hydroxide in water decreases with increasing temperature, whereas chemical reactions in general are faster as temperature increases (Dheilly et al., 2002). Thus, the optimum carbonation temperature is around 20°C (Van Balen and Van Gemert, 1994). Finally, the solubility of lime in water depends on the particle size and therefore on the curing time of slaked lime (Cazalla et al., 2000)

Carbonation of lime results in the precipitation of the colloid-size calcium carbonate once a certain supersaturation threshold is reached in pores with pore radius below 0.1μm (Rodrigues-Navarro et al., 2002). This process also results in an increase in mass, caused by the transformation of portlandite into calcite (Cultrone et al., 2005). Therefore pores larger around 1μm in diameter are significantly reduced upon carbonation, while the total porosity reduction reaches 10% (Moorehead 1986).

Both, diffusion of carbon dioxide and carbonation of lime are time-dependent processes, which are controlled by the porosity and pore-structure of the binder. Pore space characteristics of lime mortars affect their hydroscopic behaviour and therefore water content and carbon dioxide diffusion. Hence the carbonation of lime mortars is a self-limiting process in which CO_2 uptake and diffusion decreases as the process progresses toward the core of the mortar (Cultrone et al., 2005).

2.2.2 Setting of Hydraulic Mortars

Hydraulic limes can be produced by burning limestones with a high clay content (6.5–20%) at 1,000–1,250°C or, alternatively, by mixing clay minerals with finely ground limestones (Allen et al., 2003:3; TAN 1, 2003:15). The reactions between calcium, aluminum and silica during the calcination process leads to the formation of calcium silicates and aluminates. Calcium silicates (C_2S, C_3S), calcium hydroxide (CH), gehlenite (C_2AS) and calcium aluminate (C_3A) are the main phases formed during calcination (Lanas et al., 2004). The fundamental properties of hydraulic binders are their ability to set and harden when water is added to the dry binder and their ability to harden under water (Sabbioni et al., 2001; Sabbioni et al., 2002). According to the nomenclature used in cement chemistry (C) corresponds to CaO, (A) to Al_2O_3, (S) to SiO_2 and (H) to H_2O respectively (Lea, 1971).

Setting and hardening of hydraulic mortars is partially attributed to the carbonation of calcium hydroxide and partially to the hydration of the aluminium-silicates, which provide higher strength and the ability to harden under water (Torraca, 1988; Collepardi, 1990). The amounts of calcium hydroxide produced during the hydration reactions are

converted to calcium carbonate according to Equations 2.3 and 2.4. The hydration process of aluminium-silicates is described by the following simplified reactions (Zacharopoulou, 1998). The reactions are not balanced and indicate only the products formed.

$$C_2S + C_3S + C_2A + H_2O \rightarrow CSH + CAH + Ca(OH)_2 \quad (2.5)$$

(calcium and aluminium silicates)

$$CSH + CAH + CO_2 \rightarrow \text{intermediate products} \rightarrow CaCO_3 + SiO_2 + Al_2O_3 + H_2O \quad (2.6)$$

hydrous silica gel

Hydraulic lime mortars form the same compounds as Portland cement during setting. However, their identification is not easy because of the varying degrees of crystallinity of the products formed and their small particle size. In many cases, the most clearly seen evidence of the hydraulic components is the fibrous-acicular crystal growth, typical of Portland cement (Charola and Henriques, 1999). X-ray diffraction analysis (XRD) of laboratory-produced hydraulic-lime mortars could not identify any hydraulic components. However, scanning electron microscope (SEM) examination showed that the surfaces of the sand (quartz) granules were covered with needle-like, fibrous material, typical of the crystallization forms of CSH gel (Lewin, 1981).

2.2.3 Setting of Pozzolanic Mortars

The term 'pozzolan' refers to an additive material able to transform an air-hardening mortar into a hydraulic mortar, even though the binder used (lime) is air-hardening itself. The effect is principally due to the presence in pozzolans of silica (SiO_2) and alumina (Al_2O_3), that, due to their amorphous, vitreous state and high specific surface area, react with lime and water to form calcium silicates and aluminate hydrates (Van Balen et al., 1999a:2). The same effect is obtained by substituting ordinary sand with ground fired clay (chamotte) or 'cocciopesto' (finely ground bricks or tiles).

The pozzolanic reactivity is influenced by the amount, the mineralogical composition, the grain-size distribution, and the specific surface area of the pozzolan added to the mixture. Concerning ceramic material, their reactivity is also affected by the calcination temperature (Moropoulou et al., 2004a)

The main mechanism of hardening of mixed-type mortars is due partly to the carbonation of calcium hydroxide and partly to the reaction between lime and the aluminium-silicates. The pozzolanic reactions in traditional pozzolanic mortars (Equations 2.7 and 2.8) are controlled by the dissolution of the siliceous phases in the aqueous solution that lead to the formation of the hydrated phases of aluminium-silicates (Gregerova and Pospisil, 2001; Moropoulou et al., 2004b).

$$Ca(OH)_2 + A.S + H_2O \rightarrow CAH + CSH \qquad (2.7)$$

(aluminium-silicates)

$$CSH + CAH + CO_2 \rightarrow \text{intermediate products} \rightarrow CaCO_3 + SiO_2 + Al_2O_3 + H_2O \qquad (2.8)$$

hydrous silica gel

The C-S-H phase formed during the pozzolanic reactions has a similar micro-morphology to that developed by the hydration of the C_2S and C_3S found in Portland cement and it contributes significantly to the mechanical strength of mortars. The exact structural and chemical composition of the above phases depends on the reactants (Moropoulou et al., 2004a).

The identification of the hydraulic phases formed in lime-pozzolana or lime-crushed brick mortars is very difficult due to the variability of composition of pozzolanic materials, the conditions of the pozzolan-lime-water reaction, and the rapid loss of water during the setting of the mortar, resulting in very small sized reaction products (Furlan, 1991; Charola and Henriques, 1999). In a work made by Lewin (1981), mineralogical analysis by XRD of the phases resulting from the setting of a 1:1 by volume lime putty-natural pozzolan mixture identified the presence of calcium aluminate hydrate ($Ca_4Al_2O_7 \cdot H_2O$), calcium silicate hydrate ($5Ca_2SiO_4 \cdot 6H_2O$) and portlandite [$Ca(OH)_2$] .

In the above mixtures, portlandite crystals were again confirmed after further curing of two months, along with monohydrocalcite ($CaCO_3 \cdot H_2O$), prehnite ($Ca_2Al_2Si_8O_{10}$), already present in the pozzolan by itself, and leucite ($KAlSi_2O_6$) (Lewin, 1981).

The increase of the mechanical strength caused to lime mortars by the addition of brick/ceramic fragments has been attributed to the hydraulic reaction occurring at the edge of the brick particles (Papayianni and Karaveziroglou, 1993). This reaction is favoured when clays are burned at temperatures between 600°C and 900°C. At these temperatures, the crystal structure of their minerals is destroyed, resulting in an amorphous mixture of silica and alumina capable of reacting with calcium hydrate (Baronio et al., 1997). The reactions that take place between calcinated ceramics and lime in the presence of water lead to the formation of tetracalcium aluminate hydrate (C_4AH_{13}), tricalcium aluminate hydrate (C_3AH_6), hydrated gehlenite (C_2ASH_8), and tobermorite (CSH) (Charola and Henriques, 1999).

2.2.4 Development of Bond Strength

The setting and hardening processes are responsible for the mechanical properties of the mortars. These properties originate with the development of bonds between the binding material and aggregates, as well as between the binder and the surface of the construction material (Lanas and Alvarez, 2003). The development of bond strength in masonry mortars incorporates two main mechanisms (Reda Taha and Shrive, 2001). These are the chemical bonds, where covalent or Van der Waal bonds form between aggregates/construction materials and the setting phases of binders, and the mechanical bond due to the interlocking of the setting products with the surface pores of the aggregates/construction materials. The mechanical interlocking of the binder to the surface of the aggregates has been proved to have greater influence on the mechanical properties than the chemical bond (Kampf, 1963; Dubovoy and Ribar, 1990).

Bond strength is controlled by two physical processes: densification and de-watering (Groot, 1997; Lange et al., 1999). Densification refers to the qualitative characteristics of the setting products and represents the consolidation of the hydration products at the

binder/aggregate interface. Dewatering represents the reduction in the amount of water available to complete the hydration process at the interfacial zone as a result of binder/aggregate suction. The limited degree of hydration observed for most hydration products at the binder/aggregate interface compared with the mortar core favours this explanation (Goodwin and West, 1982; McGinley, 1990; Reda Taha and Shrive, 2001).

Bond strength is dependent upon many interrelated factors affecting bond development, such as surface texture and water absorption of aggregates and construction materials, composition, pore structure, water retention and curing conditions of mortars and, workmanship (Reda Taha and Shrive, 2001). In this context, it is suggested that the increase in compressive strength observed in mortars that contain crushed brick fragments is due to the better bond between the binder and the rough porous surface of the brick aggregates (Charola and Henriques, 1999). The quality of the mortar and the surface absorption of the construction materials are the most significant parameters in developing good bond and bond strength (Goodwin and West, 1982; McGinley, 1990).

In air-hardening mortars, the bond between the binding material and aggregates is achieved through the precipitation of the colloid-size calcium carbonate in the pores of the lime binder (Rodrigues-Navarro et al., 2002). When calcareous aggregates participate in the mortar matrix, calcite crystals present in aggregates provide nucleating areas for the crystal growth of the precipitated calcium carbonate crystals and therefore enhance the binder-aggregate interface (Heikal et al., 2000).

In pozzolanic mortars, strength development is attributed to the type of the phases formed during setting and the microstructure of the interfacial zone. SEM examination showed that the hydrated phases of calcium aluminate and calcium silicate form needle-like, polygonal crystallites that grow around the pozzolan particles. The surface of the particles is extensively etched, while the portlandite crystals tend to adhere to and thoroughly coat the glassy pozzolana shards (Lewin, 1981).

The increase in mechanical strength of crushed-brick lime mortars is also attributed to the reactions occurring at the edge of the brick particles. Examination of historic renders

containing powdered brick using petrographic microscopy and SEM showed a reaction rim between the brick fragments and the calcareous matrix. This rim was more evident on the finer ground particles (Binda and Baronio, 1988). Elemental microprobe analysis indicated the presence of silicon (Si), calcium (Ca) and aluminum (Al). The presence of this thin irregular layer on the mortar side of this binder-brick interface was attributed to (a) the formation of the hydraulic phases during the reaction of lime with the clay minerals of brick fragments, and (b) the reaction of lime with the dissolved silicates and aluminates in the alkaline medium (hydrated lime) and therefore the formation of new hydrates. On the brick side of this interface, a calcite enriched layer, nearly 1mm thick, was observed and has been related to the carbonation of the migrated lime. Calcite crystals fill the empty space between the two materials and hydraulic phases and therefore increase their adhesion (Charola and Henriques, 1999).

The differences in the performance of different types of pozzolans are attributed not only to their pozzolanic activity (i.e. converting the weak CH crystals to strong CSH gel). The bond strength of the interface is governed by a number of interrelated factors including the ability of the pozzolan to enhance the workability and water retentivity of the mortar mix, and the size of the pozzolan particles (Reda Taha and Shrive, 2001).

2.3 MOSAICS AND MOSAIC MORTARS

2.3.1 Technology of Mosaics

The term 'mosaic' is primarily used to describe the technique of insetting pieces of suitable material, cut more or less to the shape of a cube and with sizes not more than 4 or 5cm across, in mortar (Dunbabin, 1999). Mosaics can be divided broadly into two main categories: those that decorated floors and those that decorated walls or vaults. The two categories eventually acquired different names, *opus tessellatum* and *opus museum* or *misivum* respectively. Such mosaics were initially decorated with patterns including geometric and vegetal motifs. Figure compositions were used from the fourth century BC to the early Byzantine (Christian) period (Ling, 1998). The first materials

used for the construction of floor mosaics were natural pebbles (black and white) in lime mortar. During the middle Hellenistic period the pebbles were replaced by small cut pieces of stones, glass and terracotta called 'tesserae' (Neal, 1976; Istoria tou Ellinikou Ethnous, 1985).

The technique of preparing floor mosaics through ages is quite similar to that described by Vitruvius (Dunbabin, 1999). Surviving pavements generally are composed of two or three preparatory layers, including an initial layer of rubble and one or two layers of coarse lime mortar (Mosaics in Situ Project, 2003). Above this, a finer surface layer is used to join the tesserae (Figure 2.1). Each layer is described by a specific name, which is typical for the level of the layer in mosaic's stratigraphy and the maximum size of aggregates participating in the mortar:

- **Statumen:** is the first preparatory layer which is made of large stones laid on the ground, previously leveled and rammed.
- **Rudus:** is the second preparatory layer, which is spread over the statumen. This layer is typical made of lime mixed with coarse aggregates.
- **Nucleus:** is the third preparatory layer which is spread over the rudus in a thinner layer. The nucleus is made of a mortar with fine aggregates.
- **Bedding layer:** is the final preparatory layer of mortars. The tesserae are inserted in this layer before the mortar sets.
- **Tessellatum:** this layer constitutes the mosaic surface and is composed of tesserae and mortar filling the interstices between them.

Despite the changes that followed the development of mosaic patterns through ages, the basic structural character of mosaics and the technical method of laying them remained almost the same, with only minor changes through the centuries. The main changes concerned the type of materials used and the technology applied for the constructions of mosaics through ages (Neal, 1976). The stratigraphy described above (graphically represented in Figure 2.1) has been derived from surviving pavements and ancient literary sources and therefore should be regarded only as a general reference. In practice, all mosaics do not necessarily display this stratigraphy.

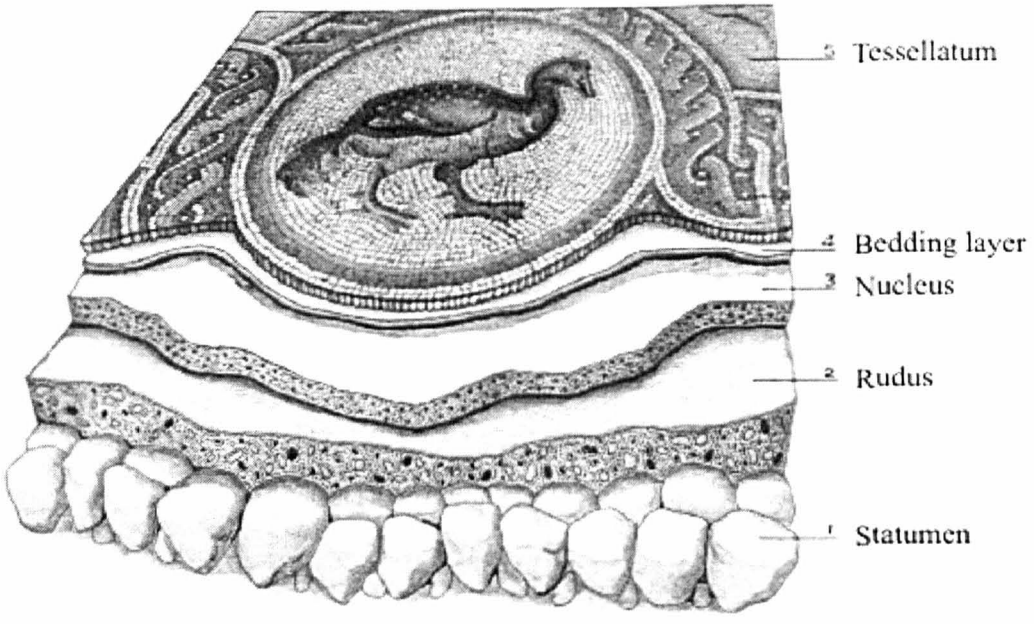

Figure 2.1: Diagram of the layers of a mosaic pavement (Mosaics in situ project, 2003).

2.3.2 Types and Functions of Mosaic Mortars

Considering the technique of preparing mosaics it is obvious that mortars play a multifunctional role. In floor mosaics, the mortar mixtures used for the preparatory layers have to provide a flat, durable substratum, able to support the weight of the bedding layer and tesserae, as well as the vertical loading caused by external forces (e.g. people's walking, superficial constructions, heavy objects). The preparatory mortar layers also provide the floor with the necessary slope of the surface, in order to avoid water stagnant. Basic requirements for those layers are the high level of mechanical strength values and the coarse pore structure, in order to minimise water absorption by capillarity. In general, preparatory mortar layers consist of coarse aggregate fragments mixed with hydrated lime putty. Lime may contain additionally some amounts of natural or artificial pozzolan. Aggregates may consist of both, stone and ceramic fragments. Their size depends on the thickness of the preparatory layer (2-35cm). Aggregates size usually varies between 5mm and 10cm diameter (Dunbabin, 1999).

Wall mosaics usually consist of one or two preparatory mortar layers and the surface bedding layer. Preparatory layers are primary applied on the wall in order to provide a smooth surface for insetting tesserae. They contain a rich amount of hydrated lime binder, mixed with fine aggregates (<3mm) (Istoria tou Ellinikou Ethnous, 1985). The thickness of those layers does not exceed 2-3cm. In many cases, lime binder is mixed with both aggregates and hays, in order to increase adhesion between continuous layers, while iron nails were also used for the same reason (Sear, 1976).

The surface mortar forms the bedding layer, which is used to join the tesserae. Both in floor and wall mosaics, this layer has to be able to penetrate between the tesserae and provide good adhesion ability. Depending on the size of tesserae, the gap between them usually ranges from 0.3mm to 5mm or more (Istoria tou Ellinikou Ethnous, 1985; Ling, 1998). In floor mosaics, bedding mortar is thinly applied in small sections over the nucleus and the craft persons insert the tesserae in this layer. This is a time consuming process and therefore the mixture must provide sufficient working time before the setting process starts. In order to achieve good penetration and adhesion ability, and provide sufficient working time, bedding mortars are very rich in lime. They usually contain high amounts of pozzolanic material and low content of thin aggregates. The maximum size of aggregates, when present, is set close to the one third of the gap between tesserae. In wall mosaics the bedding layer does not contain any aggregates (Dunbabin, 1999; Sear, 1976).

In the above context, the degradation of mosaic mortars during their service life, while buried or after excavation, is of particular interest as it usually causes loss of cohesion between mortar layers, loss of adherence between wall and preparatory mortar layers, and/or bedding mortar and mosaic tesserae (Puertas et al., 1994). This process gradually leads to the collapse of the mosaic. Therefore, the preservation condition of mosaics is strongly related to the preservation condition of the preparatory and bedding mortar layers.

Finally, the deterioration and damaging of mosaics during their service life may be direct, caused by the mechanical effect of walking on the mosaic pavements, ground

instability, earth-quakes or other natural destructions, and vandalisms during war attacks.

2.4 DETERIORATION OF MORTARS

The deterioration of lime-based mortars, plasters, and stuccos, found on archaeological sites and historic buildings is complex and controlled by both the intrinsic properties of mortars and the qualitative characteristics of the deterioration environment.

The main intrinsic parameters that control the durability of mortars are the mineralogical composition of the binder and aggregates, as well as the pore space properties of their mass. The type of binder (i.e. hydrated lime, hydraulic lime, lime and pozzolan, cement), the type of aggregates (calcareous, siliceous, ceramics) and the mix proportions of the mixture determine their strength and the type of chemical reactions that will take place. Consequently, the pore space properties of hardened mortars, such as porosity, water absorption and permeability control the diffusion of the deterioration solutions into the mortar mass and therefore the extent of damage. The deterioration mechanisms of mortars may be categorised in the following processes (Moriconi et al., 1994; Bland and Rolls, 1998:58):

- **physical**: freeze-thaw, crystallisation of salts, insolation weathering, ground instability and stress corrosion;
- **chemical**: leaching of Ca ions, salt formation, alteration of the binding material, precipitation phenomena; and
- **biological**: plants, algae, lichens and fungi.

2.4.1 Deterioration of Mortars in a Burial Environment

The main factors that influence the deterioration of buried mortars on archaeological sites are the type of soil, its hydraulic conductivity, the underlying geology, the natural salts contained in the soil, the effect of any additional salts, the water-retentive capacity

of the soil, and the local hydrological regime (Corfield, 1996). The latter is determined by the sources of water supply, the level of water table, the quality of water, the annual fluctuations of water retained by soil, and finally the presence of micro-organisms.

Water may function as a simple solvent, in which soil substances are dissolved, controlling its pH and therefore any precipitation phenomena. Water may also participate in deterioration mechanisms as an active component in a chemical process, like the decalcification of the binding material and the hydrolysis of silicates present in soil (Theoulakis et al., 2004). The mechanisms of decalcification involve the dissolution of calcium hydroxide [$Ca(OH)_2$] crystals as well as the partial dissolution of C-S-H (hydraulic) phases and calcite ($CaCO_3$) in the pores solution (Adenot and Buil, 1992; Delagrave et al., 1997; Catinaud et al., 2000). Decalcification is linked with an increase in porosity and therefore a decrease of strength values (Carde et al., 1996; Catinaud et al., 2000).

The presence of water solutions is also connected to the crystallisation of soluble salts and the damage caused by crystal growth. It is well known that the precipitation of salts on and beneath the surface of a porous material depends on the solution supply and the evaporation rate according to the surrounding conditions and the effective pore structure (Theoulakis and Moropoulou, 1999). In the first phase, salt crystals grow favorably in the larger pores, connecting with the empty evaporation channels, and being supplied by solution from the next smaller pores. In a second phase, the crystals already exceed the pore size and overlap other smaller pores. As the rate of evaporation exceeds the solution supply, the substrate dries out, the area where the crystal contacts the solution is reduced, and consequently columnar crystals grow. The pressure exerted by crystallization against the pore walls, when the crystals filling entirely the coarse pores continue growing, leads to disruption of the material (Theoulakis and Moropoulou, 1999; Flatt, 2002).

The physical weathering process mainly therefore depends on water supply and percolation in the burial environment, while acidity and basicity of the aqueous

solutions are considered the most important features controlling the chemical weathering of the binding medium.

In contrast, stationary water conditions in soil, slight alkaline pH values, and high values of soil water content favour the precipitation of less soluble soil compounds and the formation of compact crust layers on the surface of buried mortars (Corfield, 1996, Theoulakis et al., 2004). The problem is magnified when the surface of those mortars is decorated with mosaics or wall paintings. Finally, ground instability results in a variety of problems due to extensive crack formation and fragmentation of mortar.

2.4.2 Deterioration of Mortars in an Open Environment

Atmospheric pollution is the main agent responsible for the deterioration of lime-based mortars and calcareous stones in urban areas (Shelley et al., 2001). Air pollutants exist in three states: gaseous (oxides), solid (air borne particles), and liquid (pollutants dissolved in water). During the last decade the problem of acid rain has received great attention in a large part of Europe. This acidification of rain is due to the effect of sulphuric (H_2SO_4) and nitric (HNO_3) acids, which are respectively formed from the reaction of SO_2 and NO_2 with the water. The dilute acids formed (with pH values between 4 and 4.5) react with the calcareous phases of mortars and give place to the formation of calcium sulphates, nitrates and bicarbonates. (Skoulikides and Papakonstantinou, 1981; Amoroso and Fassina, 1983a; Baer and Sabbioni, 1988; Camuffo, 1992; Striegel et al. 2003). Among the gaseous pollutants SO_2 is the most important, while NOx and ozone contributes to the transformation of sulphur dioxide to sulphuric acid (Brimblecombe and Sabbioni, 2002). Laboratory studies on sulphate attack have also revealed the importance of physical factors such as porosity and microcracking on the above process (Rendell and Jauberthie, 1999).

It is generally accepted that the interaction between atmospheric SO_2 and building materials takes place through two mechanisms, namely dry deposition and wet deposition (acid rain) process. In both cases, calcium carbonate that is produced during the setting of lime putty is converted, in the external layers of mortars, to gypsum

($CaSO_4 \cdot 2H_2O$) (Martinez-Ramirez et al., 1997; Martinez-Ramirez et al., 1998). In dry deposition, the rate of reaction between the lime or hydraulic mortar components and the atmospheric SO_2 increases according to the following order (Martinez-Ramirez et al., 1996):

$$SO_2 \quad < \quad SO_2 + O_3 \quad < \quad SO_2 + H_2O \quad < \quad SO_2 + O_3 + H_2O$$

The chemical reaction of SO_2 with the setting products of lime mortar is twice as quick if the reaction takes place in the presence of any other oxide. For mortars exposed to a polluted environment, the rate of conversion of SO_2 to sulphate increases when the binder/water ratio of mortars decreases. In the case of acid rain, an increased water/cement ratio results in an increase in gypsum formation at the surface of the affected specimens (Martinez-Ramirez et al., 1997; Martinez-Ramirez et al., 1998).

The interaction of SO_2 with lime and lime-pozzolan mortars (sulphation process) may take place following two mechanisms (Zappia et al., 1994; Zappia et al., 1998). In wet deposition, the sulphuric acid formed in the atmosphere directly attacks the calcitic binder, leading to the formation of a gypsum layer (Equation 2.9):

$$CaCO_{3(s)} + H_2SO_{4(aq)} + H_2O \rightarrow CaSO_4 \cdot 2H_2O_{(s)} + CO_{2(g)} \qquad (2.9)$$

During the dry deposition process, SO_2 reacts with calcite and is initially deposited as sulphite ($CaSO_3 \cdot 0.5H_2O$), which is consequently oxidised to sulphate (Equations 2.10 and 2.11), giving rise to the formation of gypsum ($CaSO_4 \cdot 2H_2O$).

$$CaCO_{3(s)} + SO_2 \cdot H_2O_{(aq)} \rightarrow CaSO_3 \cdot 0.5H_2O_{(s)} + CO_{2(g)} + 0.5H_2O_{(l)} \qquad (2.10)$$

$$CaSO_4 \cdot 0.5H_2O_{(s)} + 1.5H_2O \rightarrow CaSO_4 \cdot 2H_2O_{(s)} \qquad (2.11)$$

The amount of sulphate and sulphite formed depends on the physical and chemical characteristics of each type of mortar and is independent of the $CaCO_3$ content (Zappia et al., 1998).

The effect of sulphate attack on the degradation of mortars may be summarized as follows: the expansive action of gypsum results in a dislocation of aggregates, and therefore an increase in micro-cracking at the surface of mortars (Rendell and Jauberthie, 1999). Additionally, the surface formations of gypsum are easily washed away when they are exposed to rain, eroding the surfaces and increasing porosity due to its greater solubility compared with the original carbonate compounds (Martinez-Ramirez et al., 1998; Martinez-Ramirez and Thompson, 1999). Finally, the formation of gypsum through dry deposition favours the development of black surface crusts (Sabbionni et al., 1997; Brimblecombe and Sabbioni, 2002).

In hydraulic mortars, a secondary damaging product, ettringite, is additionally identified (Sabbioni et al., 2001). Ettringite is a water-insoluble sulphate, which precipitates from the reaction between the gypsum, being dissolved by rain and migrating towards the internal mass of the mortar, and the calcium aluminate hydrates (C-A-H) of the hydraulic binders (Equation 2.12):

$$3(CaSO_4)\cdot 2H_2O + 3CaO\cdot Al_2O_3\cdot 6H_2O + 20H_2O \rightarrow 3CaO\cdot Al_2O_3\cdot 3CaSO_4\cdot 32H_2O \quad (2.12)$$

The precipitation of ettringite is controlled by the presence of water and the amount of the water-soluble CO_2. Ettringite is a highly expansive product, which results in severe stress within the pores of the mortar structure and extensive micro-cracking that can lead to a total failure of the material (Sabbioni et al., 2002).

2.5 ANALYSIS OF HISTORIC MORTARS

2.5.1 The Importance of Studying Historic Mortars

Since ancient times, the development of mortar technology has been closely related to improvements in the quality of raw materials, the use of new materials, the importation

of new raw materials, and the transfer of knowledge from other regions or countries. As a result, there is a wide range of different mortar types used through the ages, depending on the region, historic period, and type of monument or construction.

Although mortars appear to be a common and simple material, they are very complicated multi-phase systems. Their matrices consist of crystalline and amorphous phases containing both inert and reactive aggregates. Chemical reactions that take place during setting and weathering cause the formation of new compounds that are difficult to differentiate from the older ones (Chiari et al, 1992). Thus, ancient or historic mortars of the same mineral and chemical composition do not necessarily have the same microstructure, physical properties or durability. Moreover, the characterisation of original mortars and other construction materials, as well as the study of their physicochemical properties and deterioration mechanisms, are essential for planning conservation actions (Goins, 1999). The study of mortars is therefore of great significance, as it provides a wide range of information about:

- production technologies;
- raw materials used and proportions of the constituents;
- physicochemical and mechanical properties;
- preservation conditions and extent of deterioration; and
- understanding of decay agents and deterioration mechanisms.

Elaboration of the above information contributes to the selection of repair mortars and, in addition, helps to extract archaeological, historical and architectural data (Puertas et al. 1992; Schafer and Hilsdorf, 1993).

2.5.2 Microstructure and Physical Properties

The main physical properties concerning the characterisation of mortars are:

- colour;

- surface hardness;
- size, shape and granular distribution of inert aggregates; and
- porosity, pore-size distribution, density and total surface area.

The study of the microstructure may be undertaken using both polished and fractured samples, with the following microscopic examination techniques:

- stereomicroscopy;
- petrographic microscopy (PM), in thin- and polished-sections; and
- scanning electron microscopy (SEM).

Microscopic examination helps to define the different types of mortar according to their colour and raw materials (sand, aggregates, or other inorganic materials like pebbles and pieces of brick), as well as organic materials (plant fibres, coal). By obtaining a fractured or polished section of mortar, it is possible to extract information on the texture and lime particle distribution through the mortar mass. In addition, the distinction of mortars from different periods is also possible (Lewin, 1981; Alessandrini et al., 1992; Riccardi et al., 1998; Middendorf et al., 1999)

Petrographic examination of thin and polished sections of mortars provides information on the type and distribution of binder, the type and shape of aggregate, their structure, and finally the shape, distribution and quantity of the pores (Elsen et al., 2001).

Porosimetric measurements, by means of mercury porosimetry, are used to determine the porosity and pore-size distribution of historic mortars (Moropoulou et al., 1998). Porosity and pore-size distribution may be expressed as a function of pore radius (μm) for each sample versus the cumulative volume (mm^3/g). These two features are mainly correlated with the preparation technology and composition of the mortars.

Grain-size distribution analysis of aggregates is usually carried out using standard sieves, after physical separation of their constituents (Middendorf et al., 1999). The results are expressed in terms of the percentage of the mass passing through the sieves

versus the mesh size of the sieve. Alternatively, this can be expressed by the percentage values of mass between two continuous sizes of sieves.

2.5.3 Mineralogical Analysis

Mineralogical analysis of mortars is usually carried out by means of XRD, in order to identify (Lewin, 1981; Newton and Sharp, 1987; Alessandrini et al., 1992; Van Balen et al., 1999b):

- binder type (hydraulic or non hydraulic) and setting products;
- type of aggregates; and
- alteration products.

Additionally, petrographic examination of thin-sections yields information concerning:

- binder matrix;
- type of setting products; and
- type, size and granular distribution of inert aggregates; and
- alteration products.

2.5.4 Chemical Analysis

Qualitative and quantitative chemical analyses are additionally used to determine the chemical composition of the binder and aggregates, characterization of the pozzolanic materials, and identification of some typical products of deterioration. Fourier transformed infrared spectroscopy (FTIR) and differencial thermal-gravimetric (DTA/TG) analyses of powder samples, as well as energy dispersive X-ray (EDX) analysis of both polished and fractured samples, may serve successfully in this direction (Adams et al., 1998; Bakolas et al., 1998; Paama et al., 1998; Alvarez et al., 2000a; . Finally, total conductivity and pH measurements, along with elements concentration analysis through spectroscopic techniques (AAS, ICP) and wet chemical analysis, may

provide further data on the study of deterioration mechanisms (Alvarez et al., 1999; Franzini et al., 2000; Alvarez et al., 2000b).

2.5.5 Mechanical Properties

Determination of the compressive strength and modulus of elasticity of mortars provides data on their mechanical behaviour, such as strength and deformation, which may be correlated to their microstructural characteristics (i.e. porosity, binder type and ratio, granulometric distribution) and deterioration mechanisms (Papayianni and Karaveziroglou, 1993; Christaras, 1998; Anzani et al., 1998).

3 DESIGN OF CONSERVATION MORTARS

3.1 CRITERIA FOR CONSERVATION MORTARS

Current research in the field of architectural conservation is moving towards the application of traditional materials and techniques along with the development of new standards and requirements for repair materials. Recent research funded by the European Commission (e.g. Raphael-COMARECH, 1998; COMPASS, 2001; ROCEM, 2002) and parallel organized conferences focusing on conservation materials (e.g. EMRS Spring Meeting Symposium, 1994; Raphael-COMARECH Conference, 1998; RILEM International Workshop, 1999) successfully contributed to the establishment of a new status concerning the properties of materials used for the protection and conservation of the European cultural heritage.

The design of new mortars should be based on the performance and durability criteria decided for the specific project, encompassing the compatibility parameters, which are based on the scientific examination of the original mortars and other construction materials (Goncalves, 1998; Hughes and Valec, 2003:43). Additional requirements address practical application (e.g. workmanship, quality control) and side effects on the existing materials and structures (Zacharopoulou, 1998; Fischer, 1999).

The terms 'durability' and 'compatibility' are widely used in conservation documents and research reports, but from several points of view. The durability of mortars and building materials is closely related to performance, and provides a qualitative description of the material linked to the deterioration environment (Fronsdorff and

Masters, 1980). Performance of building materials is generally understood to be behaviour in relation to the use for which they are selected, and can be related to bearing capacity, stability, strength, visual appearance, and reversibility. Performance, as a function of time, is affected by various external factors (degradation factors). In this way, performance is linked to the concept of durability, which is the property expressing the ability of a material to maintain its required performance (Theoulakis et al., 2004, RILEM TC 130-CSL Report, 1996).

The performance of building materials depends both, on the deterioration environment and their intrinsic durability (Lewin, 1989). The durability of mortars against a specific deterioration environment depend not only on the chemical, mineralogical and physical parameters of the mixture (Figure 3.1), but also on how they are applied and cured in field, as well as on maintenance after application (Maurenbrecher et al., 2001).

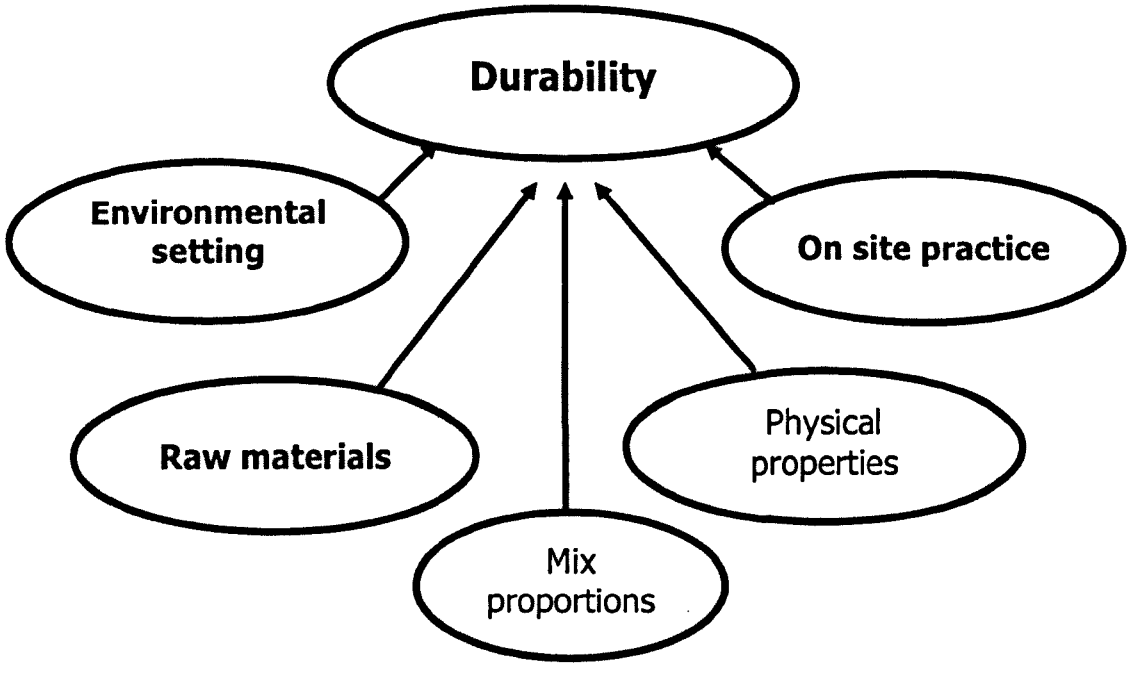

Figure 3.1: Parameters that affect the durability of conservation mortars.

Compatibility parameters (Figure 3.2) involve a variety of criteria, such as philosophical and ethical issues, physicochemical and mechanical properties, interaction of mortars

with other building materials, protection of original materials, and prevention of deterioration mechanisms (Rodrigues, 1998; Papayianni, 1998).

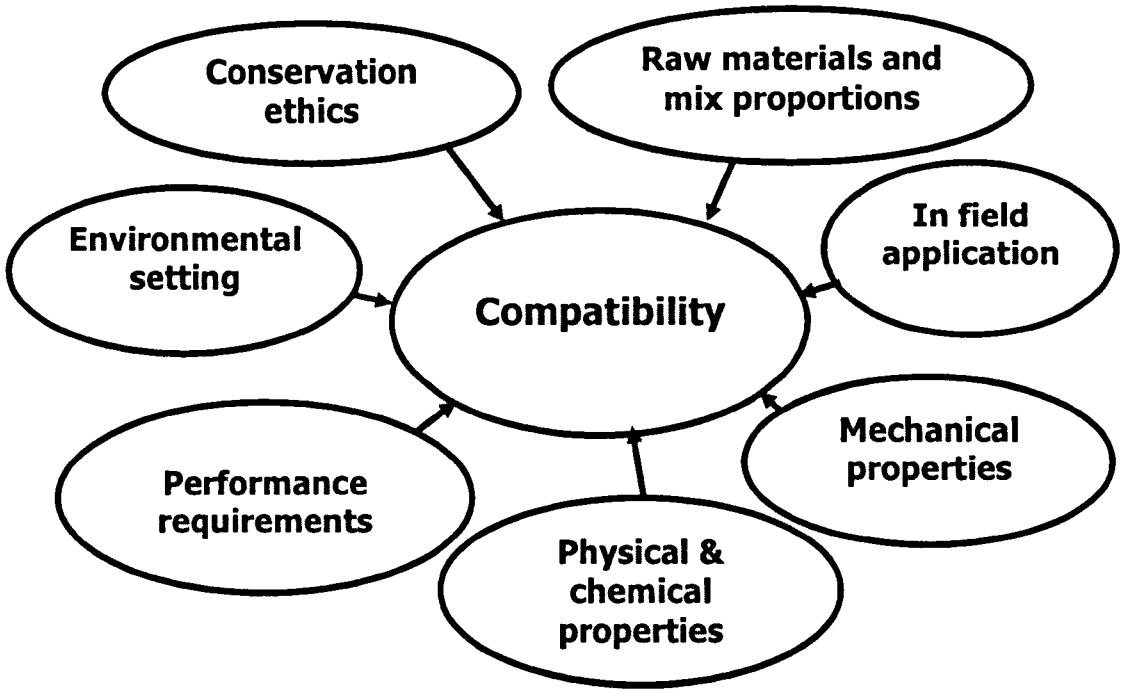

Figure 3.2: Parameters that affect the compatibility of conservation mortars.

Conservation ethics, as laid out in international conservation charters, dictate that new materials used for restoration should be distinguishable and, at the same time, not alter the artistic, aesthetic and historic values of the monument (Venice Charter, 1964; ICOMOS Charter, 2003). In this context, basic specifications for repair mortars advise the use of the same or similar raw materials and the application of traditional techniques (Ashurst, 1983:8). Moreover, regarding compatibility in terms of microstructure and of mechanical properties, repair mortars have to fit the microstructural and mechanical properties of the original mortars and should collaborate with all the construction materials without disturbing the functional behaviour of the original fabric (Papayianni, 1998).

According to the above approach, it became obvious that the design and development of suitable repair mortars requires particular knowledge of the mechanical and physical

properties of historic mortars in addition to information concerning their chemical and mineralogical composition (Schafer and Hildsdorf, 1993; Franzini at al., 2000, Moropoulou et al., 2000). Obtaining the above-mentioned information through material analyses may also assist in determining the best characteristics that a hypothetical repair mortar might possess.

Finally, the durability of restoration mortars should be tested both in the laboratory and on-site in order to make sure that the mixture satisfies the performance criteria gained from the study of the environmental setting and deterioration mechanisms that apply to the monument (Fassina et al., 2002; Lanas and Alvarez, 2003).

Performance requirements and parameters that control durability may serve as the basis for the design and assessment of new compatible repair mortars (Maurenbrecher et al., 2001).

British Standards (BS) describe in detail the procedure that should be followed for the quality control of raw materials, the mixing process, and the preparation of test specimens (BS EN 196-1, 1995; BS 4551, 1998; BS EN 459-1, 2001; BS EN 459-2, 2001). Standard tests for mortars to be used in restoration work should not necessarily follow standard tests for modern mortars (Rossi-Doria, 1986; Charola and Henriques, 1998). International standards may be taken into consideration, but it is essential that test procedures must be carefully designed and adapted to the specific performance requirements of each site.

Basic requirements for restoration mortars are listed below:

Practical application

The mixture should be practical in application to encourage good workmanship by providing satisfactory workability and be able to set in a reasonable time in both dry and wet environments (Peroni et al., 1981; Maurenbrecher et al., 2001). Moreover, the mixture must be accompanied by instructions for on-site preparation and application.

Appearence

Colour, texture and surface roughness should match those of the original mortar and do not cause confusion about the authenticity of the original construction materials (Papayianni, 1998, Karaveziroglou et al., 1990). Time usually affects the initial appearance of the fresh mortars.

Dimensional stability

Dimensional stability of conservation mortars, as it is described by thermal and hygral expansion, should lie within the range of other existing materials. Dimensional variations due to thermal or hygral expansion introduce damaging stresses (Peroni et al., 1981; Charola and Henriques, 1998; Papayianni, 1998). Additionally, low shrinkage is required from conservation mortars in order to avoid extensive micro-crack formation during setting and hardening. The granular distribution of sand, water/binder ratio and curing conditions usually influence shrinkage during setting (Maurenbrecher et al., 2001).

Adhesion

Repair mortars are expected to provide good adhesion between the original mortar and other existing construction materials. Good adhesion and low shrinkage reduce the risk of fine cracks forming at the interface between the masonry unit and mortar (Goncalves, 1998; Papayianni, 1998).

Strength (compressive and flexural strength)

Mortars of lower strength have less stiffness and greater creep, and therefore may absorb slight deformation without cracking and do not apply stress on the construction materials. In future repairs it is also easier to remove them without damaging the other construction materials. It must be also noted that lime-based mortars increase their strength gradually. Moreover, the modulus of elasticity and deformability should fit those of the existing construction materials (Zacharopoulou, 1998; Papayianni, 1998; Maurenbrecher et al., 2001).

Microstructure

The porosity, pore-size distribution, water vapour permeability, and density of repair mortars should match those of the original mortars and building materials. The new mortar should allow the evaporation of water from the original material through renders and mortar joints without creating impermeable areas. A more porous/permeable mixture will also encourage salt solutions present in the monument to migrate out through the new mortar instead of the original contruction materials (Goncalves, 1998; Papayianni, 1998; Charola and Henriques, 1998; Maurenbrecher et al., 2001; Fassina et al., 2002).

Soluble salt content and release

A fundamental requirement of all conservation mortars is that they do not contain or introduce soluble salts (Peroni et al., 1981; Rossi-Doria, 1986; Goncalves, 1998).

Accelerated weathering tests

The durability of the new mortars should be additionally studied under conditions that simulate the deterioration environment. Accelerated weathering tests must be very carefully designed in order to approach accurately the degradation mechanism of the mortars and the original materials in natural conditions. Determination of the resistance of mortars cannot be used in isolation. The results of accelerated aging tests have to be considered in comparison with other physical tests, which affect the durability of new mixtures (Rossi-Doria, 1986; Goncalves, 1998; Papayianni, 1998; Charola and Henriques, 1998; Maurenbrecher et al., 2001). Finally, when possible, on-site tests should also be carried out.

Acceptability limits

The range, within which the values of the above parameters must fall for optimum performance, should be established after the interpretation of the accelerated aging results and comparison of the characteristics of new mortars with those of the original materials (Rossi-Doria, 1986; Charola and Henriques, 1998; Zacharopoulou, 1998).

3.2 FACTORS AFFECTING THE PERFORMANCE OF LIME-BASED CONSERVATION MORTARS

3.2.1 Type and Quality of Binder

The most common binders used in conservation mortars are hydrated lime putty, hydrated lime powder, natural hydraulic lime (NHL) of different classes, and mixed binders. Mixed binders usually consist of lime putty mixed with a natural (e.g. volcanic ash deposits) or an artificial (e.g. brick or clay powder) pozzolanic additive (Ashurst and Ashurst, 1988:11; Baronio et al., 1997; Elert et al., 2002 TAN 1, 2003:15).

The type of binder controls the setting mechanism of the mortars, while additionally it determines the minimum time required for hardening and levels of maximum strength. Hardening of mortars is associated with the development of bond strength and mechanical properties. The range of compressive strength values for typical air-hardening and hydraulic mortars is presented in Figure 3.3. The diagram clearly indicates that there is a distinct increase in the compressive strength of the mixtures when the amount of the hydraulic phases in the binder increases (Schafer and Hilsdorf, 1993).

Setting and hardening of lime relies on the carbonation of the portlandite to calcite. This process requires access to atmospheric carbon dioxide and a balance of moisture and temperature (Van Balen and Van Gemert, 1994). This is a slow process that sometimes takes year to be completed. Therefore lime mortars reach their mechanical properties gradually after a long setting period (Lanas and Alvares, 2003).

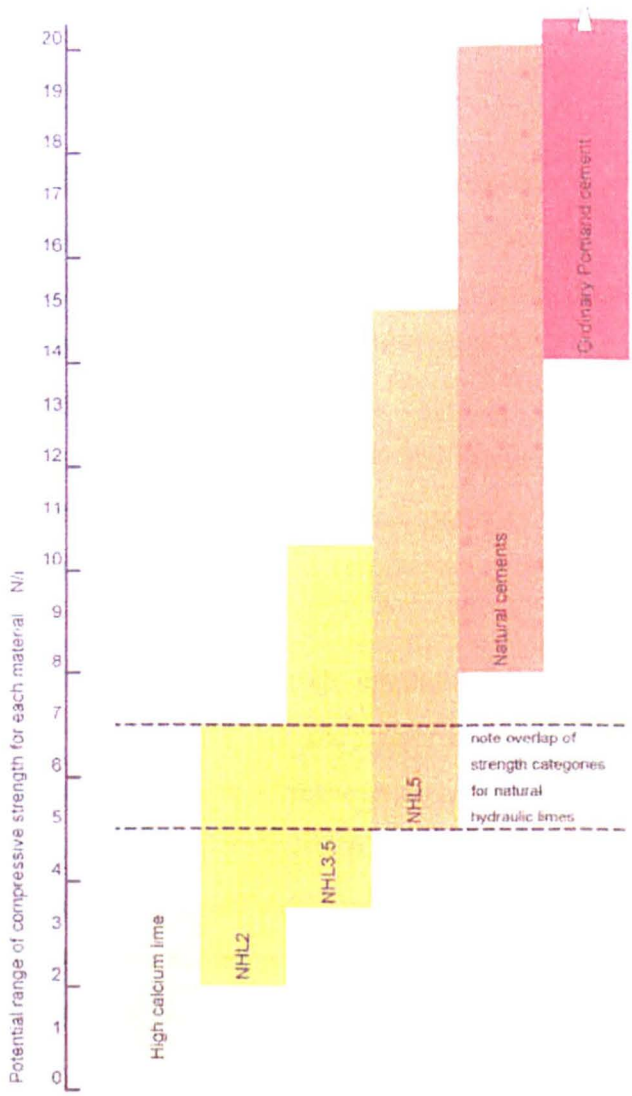

Figure 3.3: Approximate compressive strengths of typical air-hardening and hydraulic mortars (after TAN 1, 2003:18).

Hydraulic limes set and harden through a reaction with water in a process called hydration. Depending on the phases formed, this is a very fast reaction that can take place under water and results in mortars with enhanced strength (Mishara, 1982). Hydraulic limes are classified into strength classes of 2.0, 3.5 and 5.0 according to the minimum compressive strength in MPa achieved at 28 days in laboratory specimens (BS EN 459, 2001). Lime-pozzolan mixtures set and harden in wet conditions through the reaction of lime with the finely powdered reactive aluminium-silicates of the pozzolanic additives (Zacharopoulou, 1998). The last reaction requires more time than

the hydration of pure hydraulic limes, but it is much faster than the carbonation of pure lime mortars.

Another parameter that influences the resulting properties of the hydrated lime is the slaking and aging period. The aging of lime putty, by storing the slaked lime under an excess of water for long time periods, is described in many documents (Boynton, 1966; Ashurst, 1990; Bokan Bosiljkov, 2001; TAN 1, 2003) as an essential procedure for improving the quality of hydrated lime. The extensive storage of slaked lime under water contributes to the fully hydration of the lump quicklime and prevents the exfoliation or 'popping' of calcium oxide (CaO) particles that hydrates after application (Cowper, 1927: after Cazalla et al., 2000).

During the aging of lime putty, portlandite crystals undergo a considerable crystal size reduction, which is accompanied by the generation of plate-like, nanometer-scale portlandite crystals that result in an increase in their surface area (Rodriguez-Navarro et al., 1998; Cazzalla et al., 2000). The small, plate-like crystals may adsorb large amounts of water, which results in the reported increase in plasticity, water retentivity, and workability of lime mortars. Moreover, the small grain size and the large surface area contribute to the faster carbonation of matured limes (Cazzalla et al., 2000).

3.2.2 Binder to Aggregate Ratio

Mortars are composite materials that consist of aggregates and a binding material. The role of the binder is to fill the voids between the particles of the aggregates and produce a homogeneous, compact material (TAN 1, 2003). The void ratio is the percentage of voids within a given volume of dry sand. This percentage corresponds to the lime volume that is required in order to fill all the voids of the sand fraction. Depending on both the granular distribution and the shape of the aggregate particles, the void ratio between different sands varies. It is therefore essential to determine the required volume of lime for different aggregate fractions prior to use.

The required volume of binding material is expressed as the ratio between the volume of the binder and the volume of the aggregates (b/a ratio). When a mixture contains less than the required amount of the binder, the mortar is characterized as 'meager', while when the amount of the binder is greater the mixture is 'fat' (Maurenbrecher et al., 2001). In well graded sands, the void space left over is assumed to be about one-third of the sand volume. This explains the binder to aggregate ratio of 1:3 seen in most specifications (Hayen et al., 2001; Maurenbrecher et al., 2001). This ratio varies, depending on grading and particle shape, and on the binder.

The evaluation of data obtained by mercury intrusion porosimetry has shown that the binder/aggregate ratio has a clear influence on the porosity and pore-size distribution of lime mortars (Hayen et al., 2001). Mortars with binder content below the required amount (meager mortars) have a higher total pore volume, consisting of mainly larger pores with pore diameters in the order of 6 μm to 15 μm (Schafer and Hilsdorf, 1993). In contrast, mortars with a high binder content seems to have a larger capillary water suction capacity, since these mortars mainly have capillary pores ranging from 0.1μm to 1μm in diameter.

The coarser pore structure of meager mortars enables a faster carbonation of the mixtures. This pore structure increases the diffusion coefficient of the carbon dioxide into the mortar, while the lower lime content requires lower amounts of carbon dioxide for a similar carbonation depth than fat mortars (Cazzala et al., 2000; Hayen et al., 2001). Mixtures with very low binder content present poor workability, require additional water, and present very low strength values.

In contrast, when the amount of binder increases up to an optimum ratio, the mixture presents better workability and higher strength values (Mosquera et al., 2002). When this limit is exceeded, the strength is reduced and the risk of shrinkage cracks is increased (Maurenbrecher et al., 2001). The influence of binder/aggregate ratio to both porosity and compressive strength values is presented in Figure 3.4.

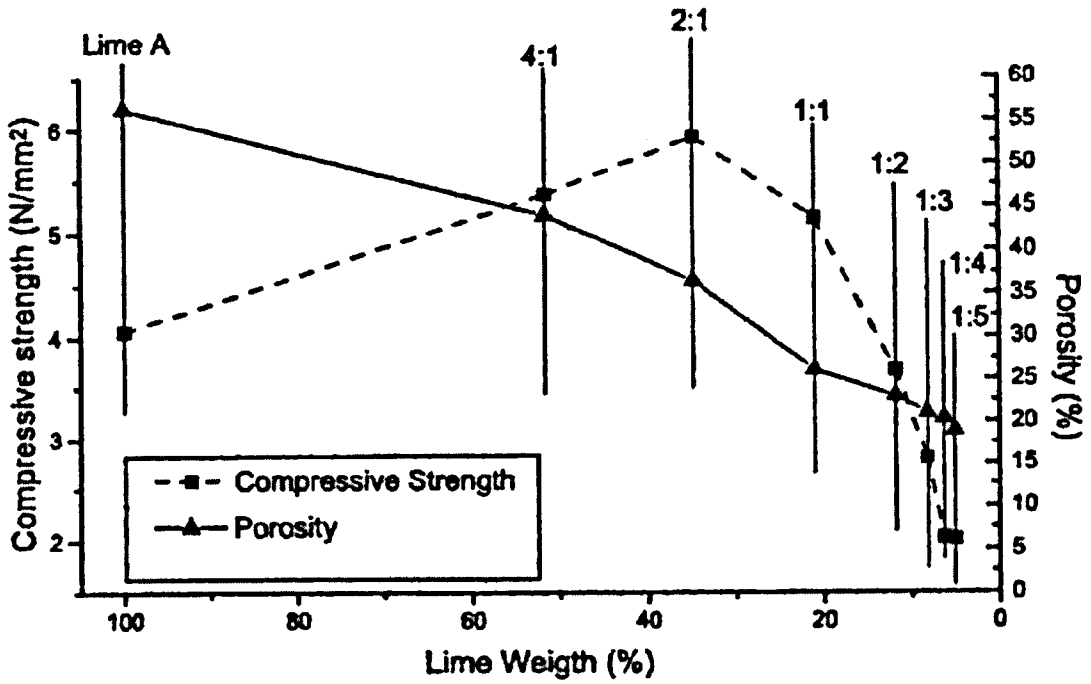

Figure 3.4: The effect of lime content on the total porosity and compressive strength of mortars cured for 365 days (after Lanas and Alvarez, 2003).

Finally, optimization of the properties of fresh and hardened mixtures regarding the effect of binder/aggregate ratio should have reference to the optimum amount of binder required to fill the voids of the aggregate fraction, and not simply to the usual 1:3 ratio. Deviations between the results of different researchers may otherwise be noted (Lanas and Alvarez, 2003).

3.2.3 Water/Binder Ratio

The water demand of fresh mixtures is directly related to their workability. Workability is a property of fresh mixtures that determines their ability to be placed, compacted and finished (Taylor, 2000:61). The amount of water required to produce a workable mixture depends on the type and amount of binder as well as on the type and particle size of aggregates. The required water volume is expressed as a ratio to the binder volume used (w/b).

For a given type of mortar, when the binder content in the mixture is decreased, additional water is required to produce a workable mix (Figure 3.5). The amount of water and the manner in which it evaporates during setting affects the open porosity and pore structure of the mixture. Therefore, when more water is added to the binder, the pore volume of the mixture increases, which consequently results in a reduction of density and mechanical strength values (Schafer and Hilsdorf, 1993).

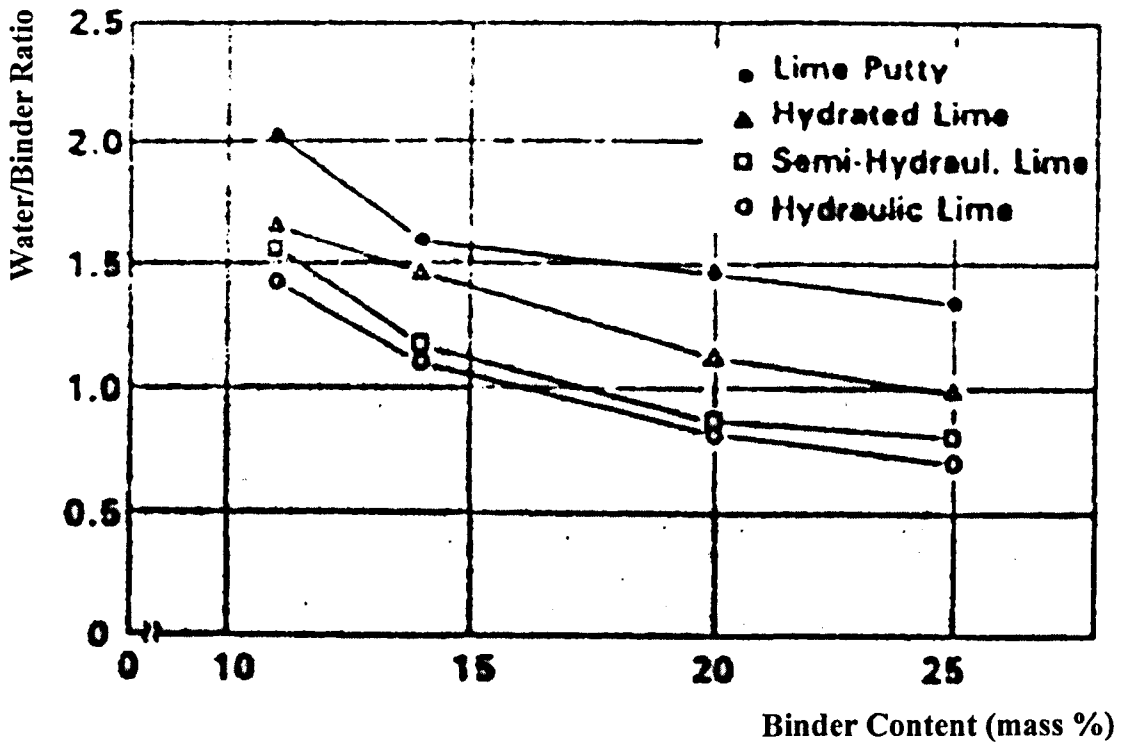

Figure 3.5: Water/binder ratio as a function of the binder content of the mortar, for four different types of lime (after Schafer and Hilsdorf, 1993).

Water is also essential for the hydration reactions and hardening of hydraulic binders. Therefore, if the water/binder ratio is very low, a significant part of the hydraulic binder will never hydrate due to inadequate water. Since the development of strength bonds depends on the hydration process, at water binder ratios below 0.4 the resulting mixture will present decreased strength values. At water/binder ratios 0.3-1 the strength of hydraulic mortars increases progressively as the amount of water is decreased (Taylor, 2000:66).

The addition of fine aggregates or finely grounded pozzolanic materials (grain size below 50μm) to the mixtures increases the surface area of the binder fraction. More water is therefore absorbed within small particles, which results in an increase of capillary pores (Hoffmann and Nielsen, 1993).

Finally, water/binder ratio along with the granular distribution of aggregates has a strong influence on the setting shrinkage of mortar mixtures. An increase in water content results in increased shrinkage due to evaporation (Sanchez et al., 1997).

3.2.4 Granular Distribution and Type of Aggregates

The most commonly used aggregates are sand particles from natural deposits, crushed limestones, and crushed bricks/low-fired ceramics. Aggregates usually consist of particles that range between an upper and a lower limit. Normally, the smaller particles between this range fill the space between particles of larger sizes (Figure 3.6). The cleanliness, grading and particle shape of aggregates have an important influence on the workability, retraction, adhesion, mechanical properties and durability of mortar mixtures (Henriques et al., 2004).

Grain-size distribution has an important influence on the mechanical properties and the pore space characteristics of the mortars (Figures 3.7 and 3.8). An increase in water required for the production of a workable mixture with mortars containing fine aggregates, leads to hardened mortars with increased porosity and lower strength and elasticity values (Papayianni and Karaveziroglou, 1993; Henriques et al., 2004).

Fine aggregates also result in a larger volume of capillary pores and increased water absorption (Henriques et al., 2004), expressed both in terms of the capillary rise coefficient ($kg/m^2 \cdot s^{1/2}$) and the asymptotic values (kg/m^2). Differences in pore volumes measured in mixtures prepared with a fine and a coarse fraction of aggregates range from 5% to 10% (Hayen et al., 2001). Eventually, the density values of mortars decrease with the decrease of the aggregates particles size.

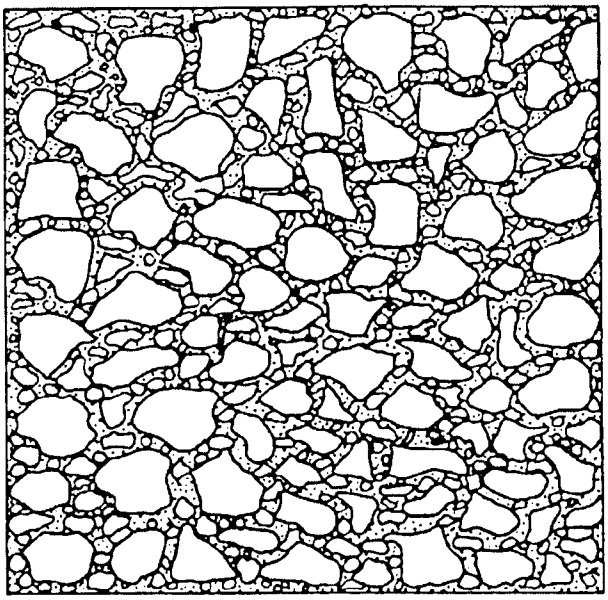

Figure 3.6: The distribution of aggregate particles within the mortar matrix. Spaces between larger particles are filled with progressively smaller particles (after Taylor, 2000).

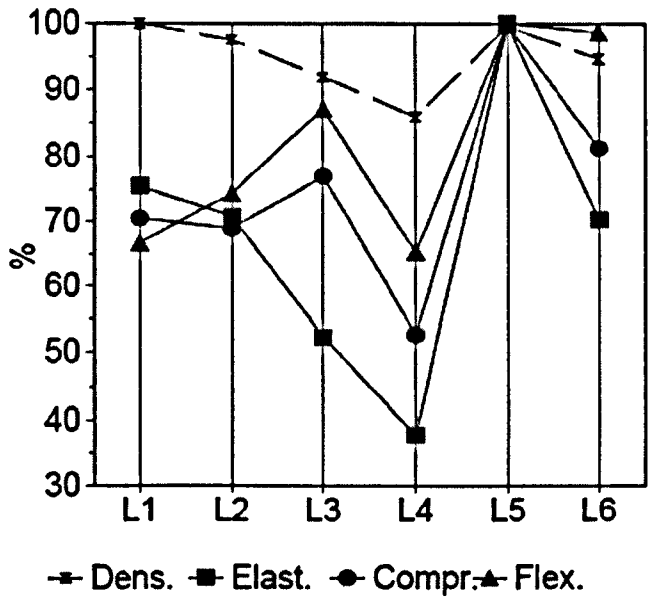

Figure 3.7: Differences in density (Dens.), modulus of elasticity (Elast.), compressive (Compr.) and flexural (Flex.) strength between mortars containing coarse (L1), fine (L3), extra fine (L4), mixture of coarse (L5) and mixture of fine (L6) aggregates. Mortars contain the same binder/aggregate ratio (after Henriques et al., 2004).

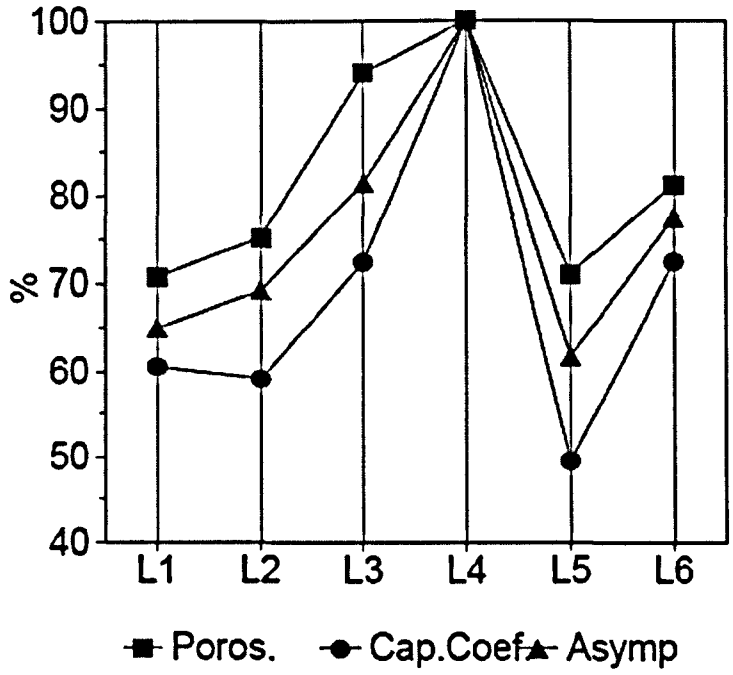

Figure 3.8: Differences in porosity (Poros.), water absorption coefficient (Cap. Coef) and asymptotic values of water absorption (Asymp) between mortars containing coarse (L1), fine (L3), extra fine (L4), mixture of coarse (L5) and mixture of fine (L6) aggregates. Mortars contain the same binder/aggregate ratio (after Henriques et al., 2004).

Coarser aggregates tend to attribute higher mechanical strength to the hardened mixtures, while the formation of larger pores in such mixtures improves their resistance to frost action and salt crystallisation. Moreover, larger grains prevent the formation of micro-cracks due to extensive shrinkage of mortars during setting (Maurenbrecher et al., 2001).

Considering the type of the aggregates, low-fired (<900°C) ceramic fragments usually exhibit a pozzolanic character, which is expressed by the reactions between the lime and the ceramic material. These reactions are accelerated when the size of the particles is decreased, and hence the specific surface area is increased. Pozzolanic reactions can also take place on the external surface of larger ceramic fragments, resulting in increased strength properties (Baronio et al., 1997).

Ceramic aggregates have an effect on the water amount required for optimum workability. Being highly porous, they absorb and retain part of the water added to the mixture. Thus mixtures that contain ceramic aggregates require additional water in order to avoid the formation of micro-cracks during setting. This is also the reason why recommendations for traditional mortar mixes suggest the application of pressure during the curing of crushed brick-lime mortars (Cazalla et al., 2000; Biscontin et al., 1981).

Finally, the granulometry of aggregates has no direct influence on the carbonation depth of mortars, although this is influenced by the effect of aggregates on the pore structure of mortars. Thus mortars containing finer aggregates have a much larger carbonation speed than those containing coarser aggregates (Hayen et al, 2001).

3.2.5 Shape of Aggregates

Aggregates used in mortar mixtures originate from natural deposits, including natural sands, gravels and shells, or they are produced by crushing quarry stone blocks, such as limestone, or low-fired bricks and ceramics. In general, crushed aggregates are considered more angular (sharp), while natural aggregates vary from semi-angular to rounded (TAN 1, 2003:19). Rounded aggregates are very often present in historic mortars.

The shape of the aggregates influences plastic properties and strength development of fresh mortar mixtures. The good packing of the aggregate with angular edges and the lack of discontinuities between the binder matrix and the angular aggregates has been shown to improve the strength of hardened mortars (Lanas and Alvarez, 2003).

Mixtures containing natural aggregates present better plasticity and workability, while they are easier to compact (Taylor, 2000:65). Crushed aggregates result in a larger specific surface area than rounded aggregates and therefore an increase in water demand for producing workable mixtures. They also provide better interlocking between particles, so reducing shrinkage phenomena.

3.2.6 The Effect of Pozzolanic Additives

The ability of pozzolanic materials to enhance the long-term strength and durability of lime mortars has been known since antiquity. Pozzolans are natural or artificial alumino-silicate materials that are not hydraulic by themselves, but form hydraulic compounds when they are mixed with hydrated lime (Charola end Henriques, 1999). The most common pozzolanic materials used historically in mortars include volcanic ash deposits, fine bricks/ceramic powder, and aggregate fragments with mild pozzolanic properties (Baronio et al., 1997). Wood ash, coal ash and plant ashes may also possess pozzolanic properties (TAN 1, 2003).

The addition of pozzolans into the lime mixtures promotes a chemical character in the setting of such mortars, which enables to them to harden and develop strength under water or in humid conditions (Charola end Henriques, 1999). The setting is controlled by the dissolution of the siliceous phases in the aqueous solution (Moropoulou et al., 2004b). During this process, the weak calcium hydroxide crystals are converted to the strong calcium silicate hydrate and calcium aluminate hydrate fibrous gel (Reda Taha and Shrive, 2001; Moropoulou et al., 2004a). These phases have a similar microstructure to the products developed by the hydration of modern cements and they attribute to pozzolanic mortars their hydraulic properties. Hydrated phases in pozzolanic mortars are formed at room temperature, although the reactivity of pozzolanic materials is enhanced when they are mixed with hot slaked lime (TAN 1, 2003).

The setting of pozzolanic mortars requires weeks or even months to be completed; therefore the effect of pozzolans on strength development has a long-term character (Reda Taha and Shrive, 2001). The effect of different types of pozzolans on the properties of hardened mortars depends on the amount of material added, along with the chemical and mineralogical composition, microstructure, and fineness of the material (He et al., 1995; Shannag and Yeginobali, 1995).

While the reactivity of the pozzolans is needed to improve bond strength, the effect of the other factors should not be neglected when selecting a suitable pozzolan for a specific mortar mixture (Reda Taha and Shrive, 2001). The incorporation of pozzolans

affects the water requirement of fresh mortar, water retention, and shrinkage of the hardened mixture.

An increase in pozzolanic material results in an increased water demand in order to achieve sufficient workability (Shannag and Yeginobali, 1995). The increased water content usually results in greater shrinkage and micro-crack formation, along with an increase in the amount of capillary pores (Bokan-Bosiljokov, 2001). The water requirements of differed types of pozzolans varies, depending on the crystal chemistry and the specific surface area of natural (raw) and artificial (calcinated) pozzolans (He et al., 1995; Charola et al., 2004). Concerning ceramic materials, finely powdered (<50μm) ceramics, fired below 900°C exhibit better reactivity than high-temperature ceramic materials (He et al., 1995; TAN 1, 2003).

Finally, curing conditions influence the reactivity of pozzolanic materials and the properties of the hardened mortars. Setting in humid or wet conditions favours the hydration reactions and attributes higher strength values to mixtures (Moropoulou et al., 2004b).

3.2.7 The Role of Admixtures

Ingredients may also be added to the mortar to change its colour or improve workability, water retentivity, water repellancy, bond with masonry units, and/or frost resistance. Additives are usually discouraged in restoration mortars except for pigments for colour and air-entraining agents in frost susceptible areas.

Air-entraining agents can enhance frost durability (hydrated lime can be obtained with an integral air-entraining agent; masonry and mortar cement and most pre-mix mortars also have it added). These agents do not work well in very dry pointing mortar mixes. Excessive air-entrainment reduces the bond to the masonry unit (normal recommended range is 10–15% air) (TAN 1, 2003).

3.2.8 On-Site Practice

The performance of conservation mortars depends much more on preparation and site application than on the materials themselves. Detailed technical instructions have been published in different countries in order to ensure good practice in conservation works (Ftikos and Kalos, 1985; Ashurst and Ashurst, 1988; TAN 1, 2003). The British Standard Institution also provides a number of references concerning quality specifications and performance requirements of building materials (BS 1199 and 1200, 1976; BS 890, 1995; BS 459, 2001). The batching of raw materials, mixing process, preparation of the mortars substrate, and maintenance after application all have an important influence on the long-term performance of mortars.

Measuring

The accurate measuring and batching of mortar ingredients is essential for optimum performance and consistency in the final mortar (Hayen et al., 2001). The measuring of mortar ingredients by weight gives better consistency than batching by volume, but batching by volume is still the most common procedure. Volume batching may introduce larger variations in the quantities measured.

Hydrated lime powder from different manufacturers usually have different bulk densities, due to different particles size. Thus, in volume batching of dry hydrated lime, different weights may result. The finer the lime, the less weight for a given volume (Maurenbrecher et al., 2001). In the case of lime putty, it usually contains more lime than an equivalent volume of dry hydrated lime. Lime putties made with hydrated limes from different manufacturers were found to have 16 to 56% more lime than the equivalent volume of dry hydrated lime (Phillips, 1994). If no attention is paid to these aspects, the quantity of lime in a mortar can vary, leading to mortars with differing properties (i.e. porosity, strength, adhesion).

Moreover, differentiation from the initial mix proportions may occur due to differences between dry and wet bulk volumes of sand. Sand that contains 2-6% moisture occupies more volume than dry sand and, therefore, if sand is measured dry, more sand is added into the mixture than if the same volume of damp sand was used (Philips, 1994,

Maurenbrecher et al., 2001). The problem is more intense in the case of pozzolanic additives, which naturally absorb water from air humidity when they are stored in a loose condition. Volume changes of aggregates and/or pozzolanic additives cause additional changes to the flow values of the mixture and to the volume of required water.

Finally, depending also on the free-water content of ceramic aggregates, variations may occur in the water required and hence to the water to binder ratio. Dry ceramic fragments have a high water capacity and have a tendency to absorb water from the mixture. If no additional water is provided, shrinkage micro-cracks may be caused during setting and hardening of the mixture.

Mixing

Proper mixing and beating of lime mixtures is essential to provide better performance to lime mortars. Mortars should always be mixed in a standard paddle mixer, while the mixing time must be controlled in order to avoid excessive air content. Poor mixing may result in the production of a heterogeneous, crumbly mixture or in insufficient hydration of hydraulic compounds. Mortars with hydraulic binders have to be used within a certain period. The mortar may be allowed to stand for a period after mixing to allow pre-hydration, and thereby reduce shrinkage and improve workability (TAN 1, 2003:25). Finally, before establishing instructions for transfer of laboratory results to site, researchers and practitioners must be involved together in testing the performance of the proposed mixtures on the monument.

Substrate preparation.

Raking out and cleaning of the substrate are essential in order to ensure good contact between the mortar and the masonry, as poor contact usually inhibits moisture transfer. Before application, the substrate is usually pre-wetted to limit its water absorption rate. This can affect the bond of the mortar to the masonry units. A study on modern bricks and pointing mortars found that the amount of the remaining water in the mortar affects durability, hydration and strength (Elsen et al., 1993).

3.2.9 Curing Conditions – Time

Lime mortars may require many years to complete their carbonation process and possess optimum mechanical properties. The required time is usually reduced when hydraulic or pozzolanic components appear in the mixture. However, the age at which lime mortars reach their maximum strength is unknown. Also unknown is the exact correlation between composition, strength values, curing time, and the degree of carbonation or hydration (Lanas and Alvarez, 2003).

Curing conditions have a stronger influence on the development of properties in hardened mortars than time. Curing conditions for conservation mortars have therefore been much debated, especially when there is the risk of frost (TAN 1, 2003:39, Maurenbrecher et al., 2001). Rapid drying of the mortar should be avoided as it can cause detachment from the substrate, formation of a crumbly mortar, bring the lime to the surface and block surface pores, and increase the risk of shrinkage cracks. Furthermore, it may not leave enough moisture for curing and hydration of hydraulic components in pozzolanic or hydraulic mortars (TAN 1, 2003:39).

Standard recommendations suggest curing in moist, but not wet, conditions for a period of two to seven days, depending on ambient environmental conditions (Maurenbrecher et al., 2001). Required humidity may be achieved by wet burlap covered in plastic and/or regular misting of the mortars. Any protection (i.e. plastic sheets) should not prevent the access of air to the surface of mortar. Moreover, water should not run off, otherwise staining may result from lime leaching out of the mortar. Freshly applied mortars should therefore be protected from rain.

Finally, it is essential for good performance that mortars should not be prepared and applied in extremely hot or cold conditions. Conservation works should therefore be carefully planned prior to works being undertaken on site.

3.2.10 Maintenance

Good durability is not only a design and construction consideration. On-going maintenance has a large influence on performance as well. Regular visual inspections coupled with a maintenance guide will ensure good performance of conservation works. If initial micro-cracking occurs in non-hydraulic lime mortars it can be reworked and pressed back, providing the material has not been allowed to dry out (TAN 1, 2003:39). In pozzolanic mortars applied for waterproofing or rendering purposes, fine mist spraying with clear water accompanied by pressing and/or tapping of the surface is suggested to avoid shrinkage cracking (Biscontin et al., 1981).

3.3 THE USE OF BARIUM COMPOUNDS IN BUILDING CONSERVATION

Barium carbonate, precipitated from barium hydroxide, has been initially considered as an alternative consolidant for carbonate stones because barium hydroxide is more soluble in water than calcium hydroxide. Barium carbonate is considered a somewhat similar material to calcium carbonate, both being alkaline-earth carbonates with relatively low solubilities (Hansen et al., 2003). Barium hydroxide solutions have also been given preference in certain situations because gypsum can be converted into barium sulphate when treated with ammonium carbonate followed by barium hydroxide. The procedure is known as the 'Florentine method' (Matteini, 1991).

3.3.1 Chemical Properties

Barium hydroxide is the strongest base and has the greatest water solubility of all the alkaline-earth elements. It may be formed as the octahydrate [$Ba(OH)_2 \cdot 8H_2O$], the monohydrate [$Ba(OH)_2 \cdot H_2O$], and the anhydrous material [$Ba(OH)_2$]. The octahydrate form, followed by the monohydrate, is the most common, with the apparent pentahydrate being a result of a mixture of the two (Kirkpatrick, 1978; DiBello et al., 1992).

Barium hydroxide octahydrate occurs as white monoclinic crystals and melts in its water of crystallisation at 77.9°C. Its solubility depends strongly on water temperature. Solubility and vapour pressure, at different temperatures, are given in Figure 3.9. The octahydrate form is also soluble in methanol and slightly soluble in ethanol. Barium hydroxide solutions are highly alkaline and readily absorb carbon dioxide.

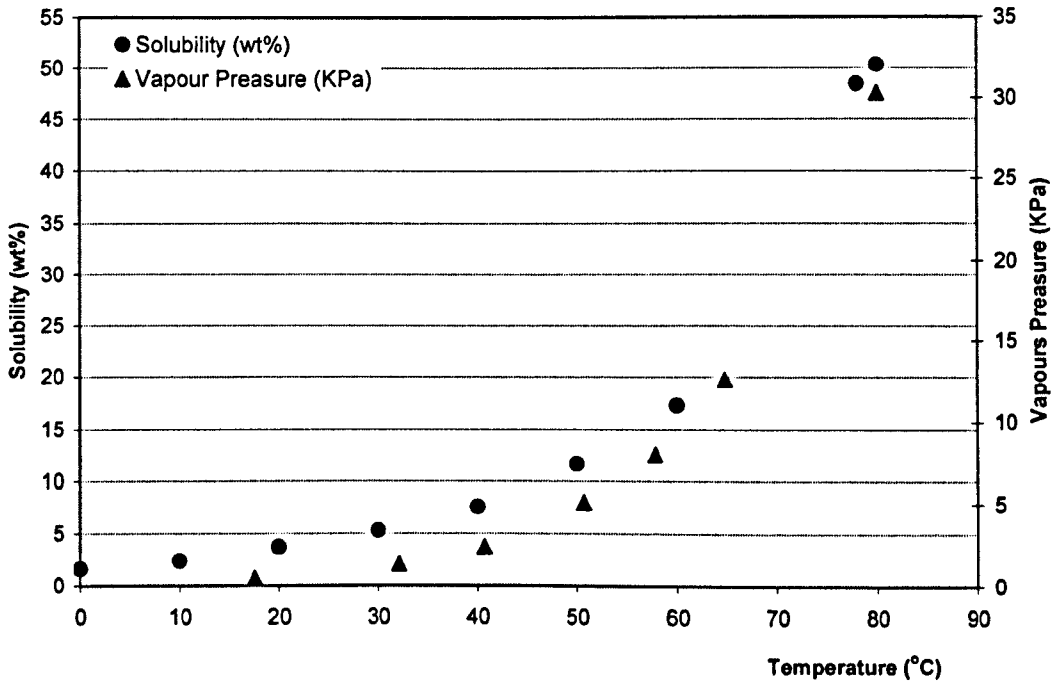

Figure 3.9: Graphical representation of the variation in solubility and vapour pressure of barium hydroxide octahydrate with temperature (values provided by Kirkpatrick, 1978 and DiBello, 1992).

Barium hydroxide may be produced by dissolving barium oxide in hot water, obtaining crystals of the octahydrate form upon cooling, while a different commercial process involves the use of barium silicate. Crystal properties of barium and calcium compounds are presented in Table 3.1, along with their solubility product (K_{sp}).

Today, barium hydroxide finds application in the protection of stone objects made from limestone and in the conservation of sulphated wall paintings. Barium hydroxide may serve in stone conservation to convert calcium sulphate to barium sulphate, and thereby

reduce damage due to the dissolution and re-crystallization of calcium sulphate, to deposit a coating of barium carbonate, which will be more resistant than calcium carbonate to acid rain and, finally, to consolidate the stone through the formation of solid solutions of barium calcium carbonate (Price, 1996:18).

3.3.2 Consolidation Based on Barium Hydroxide

Barium hydroxide was initially introduced into conservation at the end of the 19th century when Rust (1861), Church (1862, 1904), Ransome (1868), and Dennstedt (1884) proposed the use of barium hydroxide solution for the consolidation of limestone. Even from those first attempts barium hydroxide had been correlated with the presence of sulphate compounds and its potential effect on the protection of calcareous stones from sulphate salts decayed action was highlighted.

In the approach described by Rust, the role of barium hydroxide was to reduce the porosity of the stone by filling the pores with an inert insoluble compound. According to this approach, the stone is first treated with a solution of barium hydroxide and afterwards with a second solution containing a substance that forms an insoluble precipitate with barium ions, such as silicic acid, fluorosilicic acid, or sulphuric acid. This method was not generally favoured (Lewin, 1966).

Table 3.1: Crystal properties and solubility product (K_{sp}) of barium and calcium minerals formed during conservation treatments with calcium and barium hydroxides (Lewin, 1974; Deer et al., 1996).

Compound	Mineral	Formula	Symmetry	Lattice Dimensions Å	K_{sp} at 25°C
Calcium hydroxide	Portlandite	$Ca(OH)_2$	Hexagonal	$a_o = 3.593$ $c_o = 4.909$	$5.02 \cdot 10^{-6}$
Barium hydroxide octa-hydrate		$Ba(OH)_2 \cdot 8H_2O$	moniclinic	$a_o = 11.84$ $b_o = 9.277$ $c_o = 9.292$ $\beta = 98°96'$	$2.55 \cdot 10^{-4}$
Calcium carbonate	Calcite	$CaCO_3$	Trigonal	$a_o = 6.412$ $\alpha = 101°55'$	$3.36 \cdot 10^{-9}$
	Aragonite		Orthorombic	$a_o = 7.968$ $b_o = 5.741$ $c_o = 4.959$	$6.0 \cdot 10^{-9}$
	Vaterite		Pseudohexagonal Orthorombic	$a_o = 4.13$ $c_o = 8.55$ $a_o = 4.13$ $b_o = 7.15$ $c_o = 8.48$	
Barium carbonate	Witherite	$BaCO_3$	Orthorombic	$a_o = 6.5490$ $b_o = 5.2556$ $c_o = 8.8345$	$2.58 \cdot 10^{-9}$
Calcium sulphate di-hydrate	Gypsum	$CaSO_4 \cdot 2H_2O$	Monoclinic	$a_o = 5.68$ $b_o = 15.18$ $c_o = 6.29$ $\beta = 113°50'$	$3.14 \cdot 10^{-5}$
Calcium sulphate	Anhydrite	$CaSO_4$	Orthorombic	$a_o = 6.99$ $b_o = 7.00$ $c_o = 6.24$	$4.93 \cdot 10^{-5}$
Barium sulphate	Baryte	$BaSO_4$	Orthorombic	$a_o = 8.88$ $b_o = 5.45$ $c_o = 7.15$	$1.08 \cdot 10^{-10}$

Later, Church used barium hydroxide to fix and stabilize sulphate salts present in stone, such as calcium sulphate, formed by the action of sulphur oxides present in the polluted atmosphere on calcium carbonate, and convert them to the less soluble barium sulphate, according to the following, simplified, reaction:

$$CaSO_4 + Ba(OH)_2 \rightarrow BaSO_4 + Ca(OH)_2 \quad (3.1)$$

Through the above process, the defects caused by the migration of sulphates could be avoided by producing immobile (insoluble) sulphate salts. The calcium hydroxide also produced could further act as consolidant.

Despite the theoretical effectiveness of the model, neither method found acceptance. The main problem was probably the low penetration of the solution as well as the relatively quick precipitation and deposition of barium carbonate on the surface. Thus, the initial consolidation achieved only a surface effect, leading to exfoliation of the surface-hardened layer of barium carbonate and/or barium sulphate (Heaton, 1921; Lewin, 1966; Clifton, 1982; Honeyborne et al., 1998:165). The above defects have been also attributed to the anisotropic crystal growth of barium carbonate and barium sulphate (Warnes, 1926; Marsh, 1926).

During the following years, different methods involving barium hydroxide have been proposed for the consolidation of limestone (Twilley, 1984; Hansen et al., 2003). That proposed by Lewin (1966, 1971) and Sayre (1971) provided alternatives to the early precipitation of barium carbonate at the surface. These methods have been applied on a large number of monuments, with results and comment gained over several years reported on by Rossi-Manaresi and Torraca (1972).

The differences of this method from previous ones include the precipitation of barium carbonate from an aqueous solution of barium hydroxide and urea, and the exchange of barium and calcium ions in the calcite crystal surfaces (Lewin and Baer, 1974). The object to be treated is either immersed in a hot, concentrated solution (if its size permits) or otherwise covered with a mixture of the above solution with glycerin for a period of

about three weeks. The role of glycerin is to prevent the solution from drying out during this period.

During hydrolysis of urea in water, ammonia and carbon dioxide are produced and the required amount of carbon dioxide to react with barium ions is provided to the solution (Equation 3.2). By controlling the rate of this reaction, precipitation of barium carbonate from a 'homogenous solution' (Equation 3.3) can take place for longer period, thus possibly increasing the depth of penetration (Clifton, 1982; Hansen et al., 2003). The effectiveness of this method is dependent on the type of stone and its intrinsic properties (such as composition, colour, pore structure and water permeability) (Lewin, 1974).

$$NH_2\text{–}CO\text{–}NH_2 + H_2O \rightarrow CO_2\uparrow + 2NH_3\uparrow \quad (3.2)$$

$$Ba(OH)_2 + CO_2 \rightarrow BaCO_3\downarrow + H_2O \text{ (consolidating action)} \quad (3.3)$$

This method is based upon the principle that a high concentration of barium ions in a film of liquid is maintained in contact with the pore surface of stone for a prolonged period of time. During this period a significant degree of exchange between barium and calcium ions is achieved in the surfaces of calcite crystals (Equation 3.4). Through this process a 'solid solution' of barium-calcium carbonate is formed on the surface of calcite crystals. The concentration of barium gradually decreases from almost 100% at the solid-liquid interface to 0% in the internal layers of the crystal (Lewin and Baer, 1974). Further amounts of barium carbonate (precipitated from the barium hydroxide solution) upon this newly formed solid-solution layer can be directly bound to the substrate, resulting in the deposition of a mineral phase within the pores of the stone that is permanently bound to the original stone.

$$Ba(OH)_2 + CaCO_3 \rightarrow BaCO_3 + Ca(OH)_2 \text{ (consolidating action)} \quad (3.4)$$

Moreover, the calcium hydroxide that is formed during the ion exchange between barium hydroxide and calcite crystals (Equation 3.4) provides further consolidation of the carbonate stone (Equation 3.5).

$$Ca(OH)_2 + CO_2 \rightarrow CaCO_3 + H_2O \quad \text{(consolidating action)} \quad (3.5)$$

Following treatment, further action by sulphur compounds is expected to be brought to a standstill by the insoluble layer of barium sulphate that would develop in depth.

3.3.3 Desulphation and Indirect Protection

The use of barium hydroxide was also suggested for the fixation of sulphate salts already present in the substrate of wall paintings and the external layers of stone in the late 1960s (Ambrosi et al., 2000; Baglioni et al., 2004). Ferroni and Dini (1981) verified that the consolidation of deteriorated marble using barium hydroxide may be achieved in depth, providing successful results, while at the same time gypsum present on the surface of the marble could be transformed into calcium carbonate (Matteini, 1999). The above method was initially introduced for the desulphation and consolidation of wall paintings, the so-called 'Florentine method', and consisted of two stages.

Initially, the sulphated surface is treated with an ammonium carbonate [$(NH_4)_2CO_3$] solution (Equation 3.6), followed by the addition of a concentrated barium hydroxide solution. The fixation of sulphate ions and the consolidation action of barium compounds are described by the following reactions:

$$(NH_4)_2CO_3 + CaSO_4 \rightarrow (NH_4)_2SO_4 + CaCO_3 \quad \text{(desulphation)} \quad (3.6)$$

$$(NH_4)_2SO_4 + Ba(OH)_2 \rightarrow BaSO_4\downarrow + 2NH_3\uparrow + 2H_2O \quad \text{(fixation)} \quad (3.7)$$

$$Ba(OH)_2 + CO_2 \rightarrow BaCO_3\downarrow + H_2O \quad \text{(consolidation)} \quad (3.8)$$

When ammonium carbonate is not used, calcium hydroxide obtained from the reaction of gypsum with an excess of barium hydroxide converts upon carbonation to calcium carbonate and barium carbonate, providing further consolidating action (Hansen et al., 2003). In this case, the above reactions are modified as following:

$$CaSO_4 \cdot 2H_2O + Ba(OH)_2 \rightarrow BaSO_4\downarrow + Ca(OH)_2 + 2H_2O \quad \text{(desulphation)} \quad (3.9)$$

$$Ca(OH)_2 + CO_2 \rightarrow CaCO_3\downarrow + H_2O \quad \text{(consolidation)} \quad (3.10)$$

$$Ba(OH)_2 + CO_2 \rightarrow BaCO_3\downarrow + H_2O \quad \text{(consolidation)} \quad (3.11)$$

Today, after more than 30 years of application and experience, this method is widely used for the fixation of sulphate ions in both stone monuments and wall paintings. According to the published literature the method is efficient, compatible, and durable. Physicochemical characterization of the original materials must, however, precede treatment in order to avoid chemical alterations and undesirable deterioration effects due to inappropriate conservation procedure (Dei et al., 1997).

Further work has been undertaken either to improve the technique (Ambrosi et al., 2000; Baglioni et al., 2004), or to develop alternatives also involving barium hydroxide (Matteini, 1991, 1999; Matteini et al., 1994; 1996). Nanoparticle treatment offers the logical evolution of the Ferroni-Dini method, and can replace it in most cases with advantages (Baglioni et al., 2004).

3.3.4 Barium Compounds in Mortars

Barium compounds, such as barium carbonate ($BaCO_3$), have been previously used as admixtures in mortars. A thin powder of barium carbonate is added to lime mortars and lime-cement mortars in order to fix the sulphate ions after setting and form the nearly insoluble barium sulphate. Through this method, the amount of efflorescence which appears on the surface of mortars in the form of soluble sulphate salts is reduced (The Northwest Masonry Guide, 2000).

Further to the above application, barium compounds find also use in the cement industry. The effect of barium carbonate on the kinetics of tricalcium silicate formation has been studied by Katyal et al. (1999). Burnability studies in mixes of calcium

carbonate, quartz and barium carbonate showed accelerated rates of clinkerisation through mineralising action. The addition of $BaCO_3$ significantly reduced the time and temperature of the tricalcium silicate (C_3S) formation.

Finally, studies of salt damage in cement mortars, have shown that a higher amount of chloride ions are fixed during the hydration of tricalcium aluminate (C_3A) synthesized in the presence of barium sulphate (Umenura et al., 1998; Tsuyuki et al., 2000).

4 CHARACTERISATION OF MOSAIC MORTARS

The analytical procedure followed for the analysis of the original mosaic mortars is described in this chapter. The characterisation of mosaic mortars was served as the basis to evaluate the potential benefits and limitations of analytical methods and techniques, which are applied in the analysis of mortars. The analysis of the sampled Byzantine mosaic mortars and the elaboration of the derived results was an individual part of the research, which offered the opportunity for better understanding of the basic principles of the analytical techniques used and, consequently helped on the interpretation of different analytical methodologies proposed in research papers.

The study of historic mortars is of great significance as it provides a wide range of information about production technologies, raw materials, mix proportions, physico-chemical and mechanical properties, preservation condition and extent of deterioration, as well as understanding of the decay agents and deterioration mechanisms. Therefore, the analysis of original mortars is regarded as a source of technical, archaeological, historical and architectural data for the monuments (Puertas et al 1992; Schafer and Hilsdorf, 1993). Moreover, the correlation between the physico-chemical and mechanical properties of the mortars under consideration, their function, and the deterioration environment of the monument provides the required data for the development of new mortars for conservation purposes (RIBA CPD Course, 2003; Frohnsdorff and Masters, 1980; Hoffmann, 1979; Rossi-Doria, 1986; Moriconi et al., 1994; Martin-Gil et al., 1999; Fassina et al., 2002).

However, in this thesis, the mosaic mortars analysed are regarded as a case study for the analysis of historic mortars. Consequently, the mixtures prepared for studying the effect of barium hydroxide on lime-based mortars were not based on the results derived from the analysis of mosaic mortars.

Laboratory mixtures were prepared according to the directives described in British standards for testing cement (BS EN 196, 1995).

4.1 DEVELOPMENT OF METHODOLOGY

Mortars generally consist of a binding agent mixed with different types of aggregates and water. Although mortars appear to be a common and simple material, they are very complicated multi-phase systems. Their matrices consist of crystalline and amorphous phases containing both inert and reactive aggregates. Chemical reactions that take place during setting and weathering cause the formation of new compounds that are difficult to differentiate from the older ones (Chiari et *al.*, 1996, Bakolas et *al.*, 1998). Thus, mortars of the same mineral and chemical composition do not necessarily have the same microstructure, physical properties, or durability.

Interest in the systematic study of mortars is relatively new. In 1981, ICCROM organised the first conference focusing on the study of both historic and repair mortars. Although many researchers have been involved in the study of ancient or historic mortars by employing different techniques, the development of a standard methodology for their characterisation is still under consideration – the reported results and guidelines are not always in agreement with each other (Vecchio et *al.*, 1993; Phillips, 1994).

Stewart and Moore (1981), in a desire to find the advantages and limitations of some commonly-used and well-known procedures, compared three techniques proposed for the analysis of historic mortars. These techniques were those of Jedrzejewska (1960), and Cliver (1974).

Of the three techniques studied, that of Jedrzejewska seemed to have the greatest applicability to the analysis of historic mortars. The technique determines three properties of mortars: (a) the carbon dioxide content, which is mathematically converted to calcium carbonate content by volumetric analysis; (b) the sand content, which is determined gravimetrically; and (c) the complex silicates content, which is determined by the difference between the total mass and the soluble fraction.

Charola (Charola et *al.*, 1986) suggested that mortars should be characterised by their mineralogical composition and microstructural appearance, wherein Alessandrini (Alessandrini et *al.*, 1992) suggested a comparison between the results of chemical and petrographical methods. Additionally, microstructural parameters such as granular distribution, porosity, pore size distribution and mechanical characteristics were found to affect the preservation condition of mortars, resulting changes on their chemical and mineralogical composition as well as, on their physical properties (Moropoulou et *al.*, 1993).

In recent projects, the importance of the sampling procedure has been acknowledged (Chiari et al., 1996; Hughes and Callebaut, 2000) and much attention has been given to the separation of binding material from the aggregates fraction and their further study by means of wet chemical analysis and instrumental techniques. The elaboration of the above results along with mineralogical – petrographic analysis and microscopic examination of both polished and freshly fractured sections contributes to the classification of mortars to hydraulic or non-hydraulic and the complete characterization of their constituents (Moropoulou et al., 2000; Van Balen et al., 1999; Alvarez et al., 2000b; Franzini et al., 2000; Hughes and Valek, 2003:31).

Further to the above, petrographic analysis of thin-sections may contribute to the determination of the sources and the provenance of raw materials. Different varieties of stone aggregates may be identified and distinguished, based on their optical and mineralogical properties. In addition, composition and microstructure of lime inclusions may provide clues for their origin, and for the assessment of the composition and

provenance of raw materials (limestone) initially burned for their production (Hughes et al., 2001).

Taking into account the results and suggestions of the above researchers, the following methodology was adopted for studying the Byzantine mortars and providing information on their characteristics and production technologies (Goins, 2000; Veiga et al., 2001; Karatasios et al., 2002) (see Figure 4.1):

- **Sampling**
- **Environmental setting**
- **Microstructure examination**
  - Microscopic examination
  - Grain size distribution of aggregates
- **Physical properties**
  - Porosity
  - Pore-size distribution
- **Mineralogical analysis**
- **Chemical analysis**
- **Mechanical properties**
  - Compressive strength
  - Modulus of elasticity
  - Flexural strength.

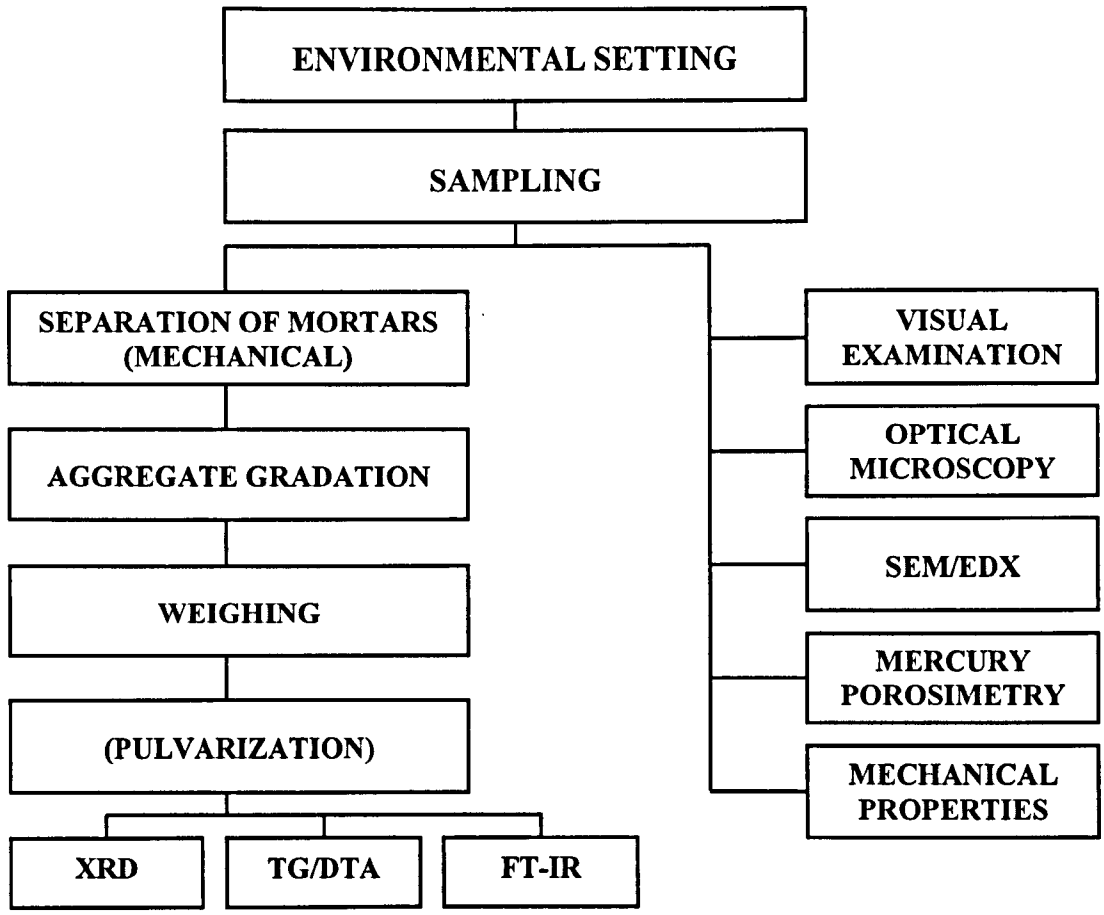

Figure 4.1: Procedure followed for the analysis and classification of historic mortars.

It is obvious that the study of original mortars is of great importance before any conservation action takes place, as it provides a wide range of information concerning their production technologies, raw materials used and proportions of their constituents, physico-chemical and mechanical properties, preservation condition and extent of deterioration and, finally, determination of the decay agents and understanding of their deterioration mechanisms.

Evaluation of the above information contributes to the selection of proper repair mortars and, in addition, helps to extract archaeological, historical, and architectural data (Puertas et al. 1992; Schafer and Hilsdorf, 1993).

4.1.1 Sampling

The mortars analysed were sampled from mosaic pavements found in two different archaeological sites, Thebes and Nea Anghialos, both located in central Greece (Figure 4.2). Samples were collected from three different mosaics at each site, representing fourth, fifth and sixth centuries AD.

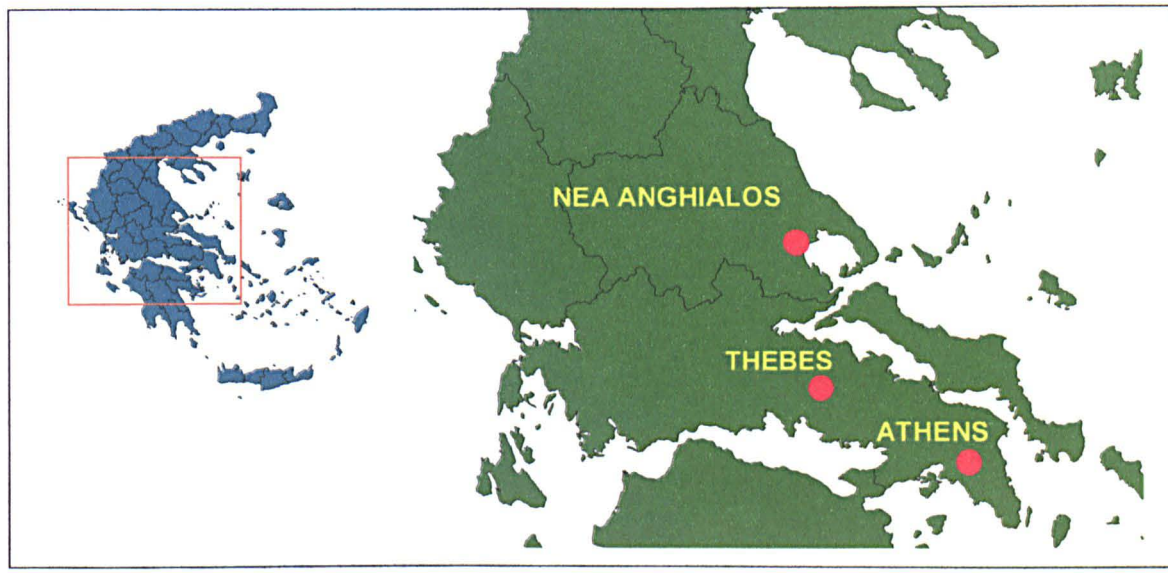

Figure 4.2: Map of Greece, indicating the archaeological sites selected for sampling.

Mosaic pavements from Thebes were buried under the foundations of the modern city. They were excavated in early '80s, during the construction works for the installation of the new water supply system. The names attributed to the mosaic samples have their origin to the names of the streets, where the pavements have been excavated. The pavements have been fragmented and removed from the original archaeological sites to the storehouse of the 1st Eforate of Byzantine Monuments. Mosaic fragments have been placed face down and sampling was therefore carried out without affecting their surface. The only surveying mortar layer after the detachment of mosaics from their background was the bedding layer. Since the archaeological study of the above mosaics have not yet been completed, further archaeological data and surface pictures of the fragments were not available. The archaeological number (excavation code) of the mosaic fragments selected for sampling is given in Table 4.1. Material was taken from different areas of each fragment in order to provide representative samples of each mosaic pavement.

Sampling was carried out only on the bedding layer. Figure 4.3 is a line draw of the mosaic pavement in Pindarou street. The marks indicate the fragments (areas), from which samples have been collected. Graphic or photographic records for mosaics from Kadmeio and Kevitos were not available.

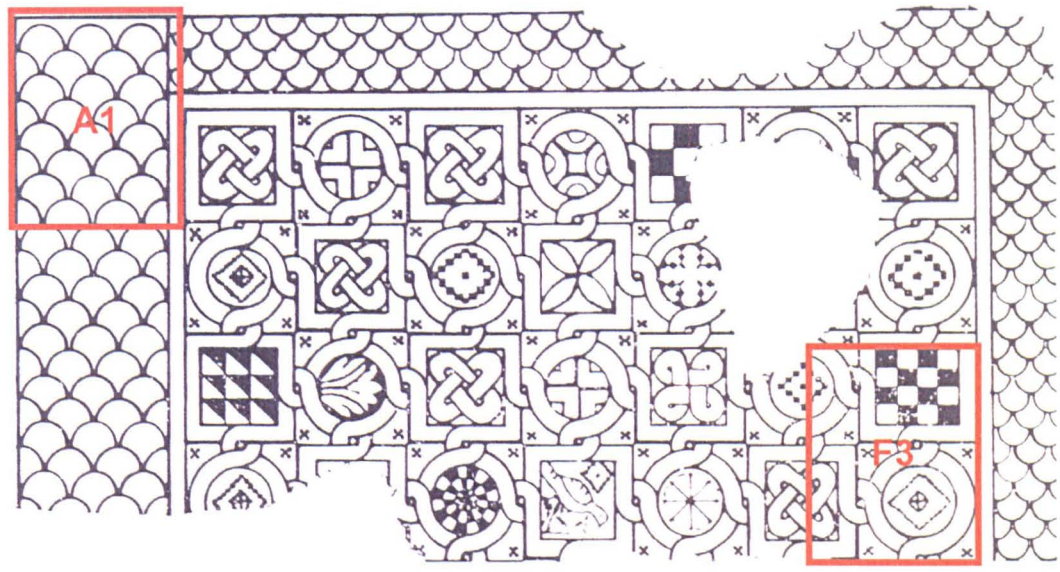

Figure 4.3: Line draw of the mosaic pavement in Pindarou street (after Assimakopoulou-Atzaka, 1987:248).

In the case of Nea Anghialos, samples were collected from the Prelate Peter Basilicas complex. This is considered as the most important basilica excavated in the archaeological area of Nea Anghialos and it is dated on the 6th century BC. Both, the northern and southern aisles of the basilica are decorated with polychrome floor mosaics (Figure 4.4). The excavations, which are today still in progress, revealed that the basilica is built on the ruins of two previous basilicas dated on the 4th and 5th century BC respectively. Their pavements were also decorated with floor mosaics (Ntina, 1990a). The mosaics were excavated and left in the archaeological site, thus sampling was carried out from lacunae, areas where tesserae have been lost.

Samples were collected from mosaics pavements of all the three archaeological periods, on the areas marked on Figure 4.5. The archaeological study of the excavated mosaics in Nea Anghialos sets the doctoral thesis of the supervising archaeologist. Thus, no

permission for other than already published pictures and detailed documentation of sampling procedure was given. Same as in mosaics from Thebes, sampling was carried out only on the upper layer of the mosaics, the bedding layer.

Figure 4.4: Decorative motives of Byzantine floors mosaics from Nea Anghialos archaeological site (after Ntina, 1990b:88).

Mortars were sampled using a small hammer and a chisel. Before sampling, a layer of 1-2mm was removed from the exposed surface of the mortars, in order to avoid any contamination of the samples. Details of all the samples taken are given in Table 4.1.

The bedding layer is the most important for the preservation of the mosaic, as it is the one that connects the tesserae and, usually, the only one remaining after the excavation and removal of the mosaic, as the rest of the layers are destroyed. This is also the layer that concentrates the main interest during any repair interventions, as this is the only visible layer within the tesserae and therefore, there is great interest on functional and aesthetic compatibility with original mortar.

As in archaeological mortars, a standard preparation procedure was not followed, and craftsmen prepared the setting-bed for tesserae in portions, usually presenting some variability in their proportions and properties. This must always be taken into account, both during sampling and interpretation of the analytical results.

Figure 4.5: The basilicas complex of Prelate Peter at the main archaeological site of Nea Anghialos (after Ntina, 1990b:89). The marks indicate the sampling areas.

Table 4.1: Archaeological data of mosaic mortars sampled.

Sample	Site	Location	Area/ Archaeological Code	Date
TH-KAD	Thebes	Kadmeio	Kad/North/ M-F2,4	3rd - 4th Century AD
TH-KEB	Thebes	Kevitos Street	Kev/ W-F5,8	5th Century AD
TH-PIN	Thebes	Pindarou Street	Pind/S-A1, F3	6th Century AD
NA-IV	Nea Anghialos	Complex of Prelate Peter Basilicas	North aisle. External edge of lacunae (IV-A8)	4th Century AD
NA-V	Nea Anghialos	Complex of Prelate Peter Basilicas	North aisle. External edge of lacunae (V-C2)	5th Century AD
NA-VI	Nea Anghialos	Complex of Prelate Peter Basilicas	North aisle. Lacunae (VI-D3)	6th Century AD

The classification of the collected samples was initially achieved by their appearance (colour and tint) followed by a more detailed examination and description of the samples carried out under stereomicroscope. Stereomicroscopy allowed the extraction of primary information on the mortar constituents (natural stone aggregates, ceramic fragments, plant material), their mix quality (air voids, micro-cracks, binder and aggregates distribution), binder content (rich or meagre mixtures), and their preservation condition.

4.1.2 Environmental Setting

During burial, the main factors that influence archaeological structures and its components are the type of soil, its hydraulic conductivity, the underlying geology, the natural salts contained in the soil, the effect of any additional salts, the water-retentive capacity of the soil and, the local hydrological regime. The latter is determined by the source of water supply, the level of water table the quality of water, the annual fluctuations of water retained by soil and, finally, the presence of micro-organisms (Corfield, 1996).

After excavation, microclimatic conditions affect physical and chemical weathering phenomena associated to the degradation of archaeological finds. Temperature and relative humidity values control the formation, movement and diffusion of aquatic solutions, chemical reactions and crystallization of soluble salts (Watt and Colston, 2000; Delalieux, 2001). Thus, the determination of the deterioration agents and the description of the environmental setting form two key parameters for estimating the deterioration mechanism(s) of both mosaics and mortars.

In this context, it was necessary to consider the potential of microclimatic conditions on the above archaeological areas. Environmental data about air temperature (^{o}C) and relative humidity (RH%) were provided by the National Meteorological Service (EMY) of Greece. These data provided both average maximum and minimum temperatures, as well as mean relative humidity levels for each month, from 1980 to 1997.

4.1.3 Microstructure Examination

The microstructure of the mortars was studied on both freshly fractured surfaces and moulded and polished samples using different microscopic examination techniques, such as optical microscopy (OM) and scanning electron microscopy (SEM). Petrographic examination of thin-sections was carried out in transmitted light, both in crossed and parallel Nichols, while cross sections were studied in reflected light under the optical microscope.

Mortar fragments of approximately 1.5-2.0cm^3 volume were used for the preparation of both thin- and polished-sections. The samples were embedded in epoxy resin (Struers EPOFIX, for petrographic examination) in two stages. Half of the samples volume was initially covered with the resin and it was allowed to absorb the resin and release any air content at room pressure. The rest of the samples volume was covered after 10minutes. The resin gives about 20-30 minutes of working time, before the setting starts. No fluorescence dye or any other additive was added to the resin. Cross sections were grinded and polished by using silicon carbide paper (Struers) from 360 to 2400 abrasive size. Special care was given to the thickness of thin sections, in order to satisfy requirements for SEM examination. Thin sections were grinded up to a thickness of about 20-30μm using silicon carbide paper. They were additionally polished with a silicon carbide fining paste of 5 microns. Grinding and polishing were achieved using a non-aqueous lubricant (Struers), in order to prevent the washing away of water-soluble constituents of the samples.

Examination of polished-sections was used for the determination of the different types of aggregates, their shapes and granular distribution, as well as air voids and micro-cracks. An estimation of the amount of binder within the mortar mass and some preliminary information on porosity and the original mix proportions of raw materials were also achieved (Luxan and Dorrego, 1996; Riccardi et al., 1998). Reflected light was additionally used to determine particular areas of interest for further study by SEM.

Petrographic examination of thin-sections allowed a more detailed examination of the sample's matrix. The information gained concerned the type and quality of binder

matrix, type of setting products, the identification of the type, size, and granular distribution of inert aggregates and pozzolanic additives, as well as the study of binder composition and production technology (Whitbread, 1986; Whitbread 1989; Elsen et al., 2001; Hughes et al., 2001).

Polished- and fractured-sections were examined under a JEOL 5310 SEM coupled to an Oxford energy dispersive X-ray analyser (EDX), using secondary electron emission, in order to collect information on the microstructure and chemical composition of the binder and aggregates, as well as the size, shape and distribution of aggregates. Back-scattered electron image was not available in the above instrument. Lindqvist (Lindqvist et al., 1994) recommended that microscopical examination of cross- and thin-sections should always complement a chemical analysis when evaluating the chemical composition of historic mortars. Such examinations can yield information on the content of any organic materials present, such as coal and plant traces, and give a better estimation of the volume of pores and voids.

4.1.4 Physical Properties

Physical properties of mortars, such as density, total surface area (A), pore volume (p_o) and pore-size distribution were determined by means of mercury intrusion porosimetry (MIP) (Quantachrome PoreMaster Mercury Porosimeter). The pore volume and pore-size distribution are mainly correlated with the preparation technology and composition of the mortars. Porosity influences the physical and mechanical characteristics of the mortars, such as water absorption and compressive strength, and is associated with the majority of deterioration mechanisms (Hoffmann and Nielsen, 1992; Nielsen and Hoffmann, 1992; Puertas et al., 1994; Martys and Ferraris, 1997; Fassina et al., 2002; Lanas, 2003).

The above properties were determined in the samples (0.6-1g) in the range of 2.21 nm to 4310.89 nm, with the porosimeter at a maximum pressure of 18980 MPa. Measurements were carried out in triplicate (n=3). The results were expressed as graphs

of pore-size distribution ($DV(r)$ vs. log r) and of the percentage of the cumulative pore volume (P_{mo}) versus the pore radius (log r).

Finally, representative portions from each of the mortars were mechanically separated into their constituents and granulometric distribution analysis was carried out using a DIN sieve series (0.063μm – 8.00mm). The smallest fraction (<0.063μm) is considered to consist almost exclusively of the binding material (Bakolas et al., 1998) but small amounts of binder may be attached to the surface of larger grains of aggregates. The results were expressed in terms of the percentage of the mass passing through the sieves versus the mesh size of the sieve.

4.1.5 Mineralogical Analysis

Additionally to the petrographic examination, mineralogical analysis of mortars was carried out by means of X-ray diffraction (XRD).

XRD can provide valuable data on the type of binder (hydraulic or non-hydraulic), the presence of pozzolanic materials, the phases that were formed during the setting of the mortars, the type of aggregates and, finally, the presence of any alteration products (Lewin, 1981; Moropoulou et al., 1995; Manzano et al., 1999; Middendorf et al., 2000; Blauer Bohn, 2000).

XRD analysis was performed on the fractions obtained from the separation and sieving of the binding material and aggregates, in order to distinguish between the mineral phases within the mortars. In this way, the data gained from the analysis revealed more precise information about the composition of the single components and their interrelations than would have been achieved by analysing bulk samples.

Powder samples (0.9-1.2g) were analysed in double a Siemens D-500 diffractometer working with the Cu-K_α radiation (λ=1.5406 Å) and a graphite monochromator in the diffraction beam at 1.2 kW (40 kV, 30 mA). Spectra were collected in the range of 2-

60° 2θ, with a step of 0.03°/sec. The evaluation of diffractograms was carried out using the DIFFRACT/AT program provided by Siemens.

4.1.6 Chemical Analysis

Qualitative and quantitative chemical analyses were used for the evaluation of chemical composition of the binder and inert aggregates, the characterization of pozzolanic materials, and for the determination of some typical products of deterioration.

EDX was used to identify elements present in the mineral and amorphous phases of the mortars. Polished samples were analysed using SEM examination. Elemental analysis was performed on the binder matrix and aggregates, whilst special attention was given to the interface areas between pozzolanic materials and binder. Elements mapping was additionally used in those areas in order to achieve more information on the formation of hydraulic phases. Samples were analysed by a JEOL 5310 Scanning Electron Microscope, equipped with an Oxford energy dispersive X-ray analyzer. Analysis was performed using Link ISIS software.

Accelerating voltage was set at 20KV. Calibration for quantitative analysis was carried out by analysing pellets of two Geological Standard Reference Materials with known, certified values: SOIL-7 (International Atomic Energy Agency) and GSP-1 (US Geological Survey). The concentrations calculated were in agreement with the published values, with 5% of maximum error. Quantitative analysis was performed in areas of approximately 5X5μm (except otherwise stated in the text), collecting 700.000 counts per spectrum. Quantitative results were expressed in terms of element oxides (%), normalised by oxygen. The background signal was collected and subtracted. For elements maps, 700-800 frames per area were captured, which corresponds to approximately 45-60 minutes of live-time analysis. During the above time, 900.000-1.200.000 counts per image were collected. Finally, the resolution of pictures was set at 1024X768, while 3 frames per image were collected.

The finest fraction of all samples was analysed by means of Fourier–transform infrared spectroscopy (FT-IR), differential scanning calorimetry and thermo-gravimetric analysis (DSC/TG). Both techniques were used in combination with X-ray diffraction analysis, in order to extract more information about the pozzolanic materials, the type of binder, and the evolution of hydraulic phases (Luxan and Dorrego, 1996). Thermal analysis techniques provided qualitative and quantitative data about the chemical composition of binding material, according to the thermal transitions and weight loss that are taking place during controlled heating of the sample (Vecchio et al., 1993; Moropoulou et al., 1995; Adams et al., 1998). The combination of thermal-gravimetric analysis (DTA/TG) results and the elaboration of the above results along with data derived from sieve gradation may provide a first estimation of the binder/aggregates ratio (Moropoulou et al., 1995).

Both FT-IR and DSC/TG techniques are very helpful in determining the presence of pozzolanic materials and the monitoring of hydrated and hydraulic phases that are formed within mortars matrix by the reactions between lime and pozzolans, carbonation of lime and hydration of pozzolans.

FT-IR analysis was carried out on a BRUKER EQUINOX 55/S spectrometer, using OPUS v3.0 software for evaluating spectra, and a NETZSCH STA 409 simultaneous thermal analyzer was used for the thermal analysis. Analysis was performed in KBr pellets, using 40 scans per sample. DSC/TG measurements were performed in 30-50mg of sample, in static air with a heating rate of 10°C/min in the range of 30–1000 °C.

4.1.7 Mechanical Properties

Mechanical testing reveals information about the strength characteristics of a mortar, the modulus of elasticity and its hardness. Those data may be elaborated further and correlated to the microstructural characteristics of mixtures, such as binder type and ratio, porosity, granulometric distribution, type and shape of aggregates (Schafer and Hilsdorf, 1993; Papayianni and Karaveziroglou, 1993; Zhang, 1998; Lanas, 2003).

However, the study of mechanical properties is not always possible due to the difficulties faced because of the required quantities of sample, specimen size, shape and number (Groot et al., 2000).

In order to overcome these difficulties, an indirect procedure for the estimation of the mechanical behaviour of mortars was followed, based on the monitoring of mortar's deformability during continuous point loading (Vekinis and Kilikoglou, 1998). The test was slightly modified in order to fulfil limitations posed by the nature of the samples.

Cube-like fragments of Byzantine mortars of about 25mm edge were mounted in epoxy resin using moulds of 30mm diameter. Samples were cross-sectioned and grounded on silicon carbide (SiC) paper, producing disc-shaped specimens of 10-12mm height, having polished and parallel sides. A steel ball of 8.5mm diameter was placed at the centre of the specimen and the load applied to the ball with a displacement rate of 109μm/min was monitored as a function of displacement, up to the fracture (Figure 4.4). Tests were carried out on a 5000N INSTRON universal tester with computer data acquisition.

Data provided from this procedure were not used for estimating the absolute values of strength (Hertzian fracture strength), but for monitoring and comparing the behaviour of different mortars under continuous loading. A grouping of samples according to the type of the load-displacement curves has been additionally undertaken.

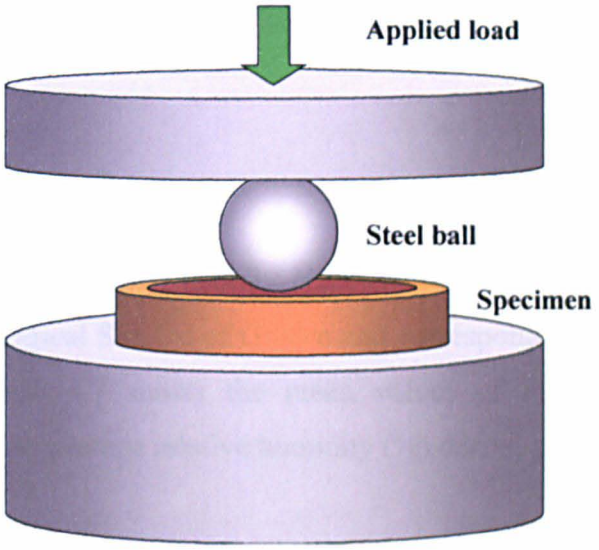

Figure 4.6: Schematic diagram of the test setup for monitoring the behaviour of different mortars under continuous loading.

4.2 ANALYTICAL RESULTS

4.2.1 Environmental Setting

Relative humidity and temperature data for Nea Aghialos and Thebes were provided by the National Meteorological Service of Greece and corresponded to the period between 1972 and 2001. Figure 4.7 shows the mean values of maximum and minimum temperature (°C) and the average relative humidity (%) during this period.

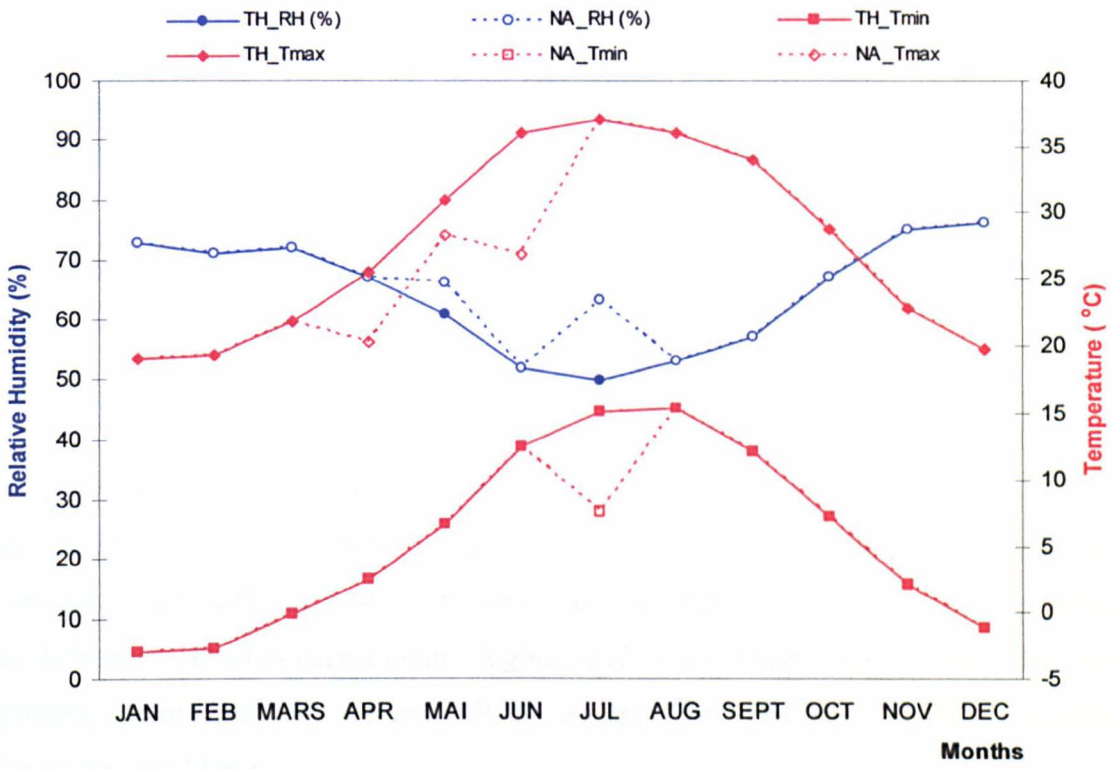

Figure 4.7: Mean values of minimum and maximum temperature, and average values of relative humidity for the areas of Nea Aghialos and Thebes.

The microclimatic environment in Nea Aghialos is considered to be coastal, as the archaeological sites are located very close to the sea (about 200m). Temperature values have minima in January and maxima in July. The lowest temperatures (-3°C) have been recorded in January and February, whereas the highest (38°C) have been recorded in

July. The difference between each month's highest and lowest temperature is in the range of 15-20°C.

Being located in a typical marine environment, the main deterioration agent affecting archaeological materials in Nea Aghialos is the presence of salt solutions. However, for damage to occur, salts must move into and within the pore system of the materials. This requires the presence of water (liquid) and/or moisture (water vapour).

Relative humidity (RH) values present minima (51%) in June and August, and maxima (71-77%) between November and March. Maximum RH values critically exceed 75% (the ERH of NaCl) in November and December. During the other months, the RH values are lower, preventing dissolution and diffusion of sodium chloride salts (Price, 2000:5) in the mass of building materials and archaeological finds.

The archaeological sites of Thebes are located inland, and so are clear of the presence of sea-salt, although microclimatic conditions are not so different from those of Nea Aghialos.

Temperature values in Thebes form smooth sinusoidal curves, with minima in January and maxima in July. The lowest temperatures (-3°C) have been recorded in January and February, whereas the highest (38°C) have been recorded in July. It is noteworthy that the difference between each month's highest and lowest temperature is 20°C. Relative humidity values present minima (50%) in July and maxima (71-78%) between November and March.

4.2.2 Microstructure Examination

In this chapter, the results of petrographic examination and scanning electron microscopy of thin sections are presented, along with the description of freshly fractured surfaces under stereo-microscope. Due to the limited theoretical background on petrography, the examination of thin sections was mainly focused on the

microstructural characteristics of the samples. However, where possible, mineralogical/ petrographic data are also presented.

4.2.2.1 Microscopy

Examination of freshly fractured samples under the stereomicroscope identified the raw materials used, the size of aggregates, the compactness of different mixtures, as well as the presence of micro-cracks and air voids. Polished- and thin-sections were also examined under a petrographic- and scanning electron microscope, providing more accurate data on the mortar microstructure and boundary reactions between binding material and aggregates. The SEM, in combination with EDX analyser, contributed to the determination of the chemical composition of both aggregates and binding medium.

The binding material of all the samples was found to be lime, which, in some cases, was mixed with fine- to medium-grained ceramic fragments. Medium to large-size lime lumps were randomly sorted within the binder mass in all the samples. The presence of lime lumps/conglomerates indicates the use of poorly-slaked lime. Fine- to medium-grained aggregate fragments were well embedded in the cementing material in most samples.

The fraction of aggregates consisted of natural aggregates and crushed ceramic fragments. The examination of ceramic aggregates in SEM revealed an early vitrification stage, which indicates that they were fired below 900°C (Maniatis and Tite, 1981; Kilikoglou, 1994). Additionally, EDX analysis resulted low calcium (Ca) content. Their colour was mainly reddish but, in some of them, turned to brown-yellow. Natural aggregates consist mostly of rounded-shape rock fragments, along with some small angular pieces of quartz and calcareous limestone. Petrographically, apart form quartz and calcite, they consisted of feldspars (orthoclase) and sheet-silicates minerals (biotite, talc, antigorite). In samples from Thebes, aggregate fractions contained some fragments of bioclastic limestone.

Table 4.2: Summary of information derived from microscopic examination of the archaeological mortars concerning production technology and microstructure characteristics.

Sample	Strength	Binding material	Aggregate type	Max. aggregate size	Micro-structure	Other
NA-IV	Medium	Lime and soil material	Natural and ceramic fragments	4mm	Extensive micro-cracks, air voids	Lime lumps, plant material
NA-V	Low	Lime and ceramic powder	Ceramic fragments and natural	5mm	micro-cracks, air voids	Lime lumps plant material
NA-VI	High	Lime and ceramic powder	Ceramic fragments and natural	3-4mm	Air voids	Lime lumps
TH-KAD	Medium	Lime and ceramic powder	Ceramic fragments and natural	3-4mm	Micro-cracks	Lime lumps, coal traces
TH-KEB	High	Lime and ceramic powder	Natural and ceramic fragments	10-15mm	Micro-cracks	Lime lumps, coal traces
TH-PIN	Very high	Lime and ceramic powder	Ceramic fragments and natural	5-7mm	Air voids	Lime lumps, coal traces

A network of micro-cracks, probably formed during setting and hardening of the mortars, was observed in most of the samples within the mortars mass. Moreover, imprints of plant material and wood pieces were randomly observed in some samples. A summary of the results derived from the microscopic examination, concerning the production technology and microstructure characteristics, is presented in Table 4.2.

The classification of the mortars according to their strength was based on the resistance that they exhibited against hand-made fracture. In this context, the strength of the samples was classified as low, medium, high and very high strength, in an attempt to distinguish them.

Samples NA-IV

Samples NA-IV presented poor strength and were very easily crushed by hand. The aggregate fraction in the mortar matrix mainly consisted of natural, rounded and partially elongated aggregates of maximum 8mm diameter.

Medium size lime lumps with an average of 4mm diameter were randomly sorted within the mortar mass, while fine, red ceramic fragments of maximum 1mm diameter were rarely distinguished. The binding material was quite rich and consisted mainly of lime, with a small amount of soil material. The colour was whitish to light brown. Imprints and traces of plant fibres/material were randomly observed (Figure 4.8).

Samples NA-IV presented compact microstructure, although an extensive network of micro-cracks (formed during the setting and hardening of the mortar) spread through the binder mass and around the surface of inert aggregates. This type of micro-crack is due to shrinkage when water evaporates. Examination of the above areas in large magnification showed that the internal of the above cracks does not contain any precipitated material (re-crystallised calcite or soil material). The presence of ceramic fragments might have an additional effect on this process, since they absorb some of the water initially added to the mortar (Figure 4.9).

The examination of thin sections under SEM (Figure 4.10) showed that mortar samples present a compact structure around ceramic materials, while shrinkage micro-cracks have maximum length of 1mm. Overlay of elements X-ray maps in conjunction with elemental analysis (EDX) and petrographic examination helped to extract information on the type of aggregates (ceramic or rock fragments), the identification of some mineral phases and their distribution within the mortar matrix. The spectrum presented at the end of Figure 4.10 corresponds to the line scan of the area presented in the secondary electrons (SE) image. Elemental analysis (EDX) proved that ceramic material consists of potash silicates (K-silicates), while small amount of silicates participates in the binding material (Table 4.5).

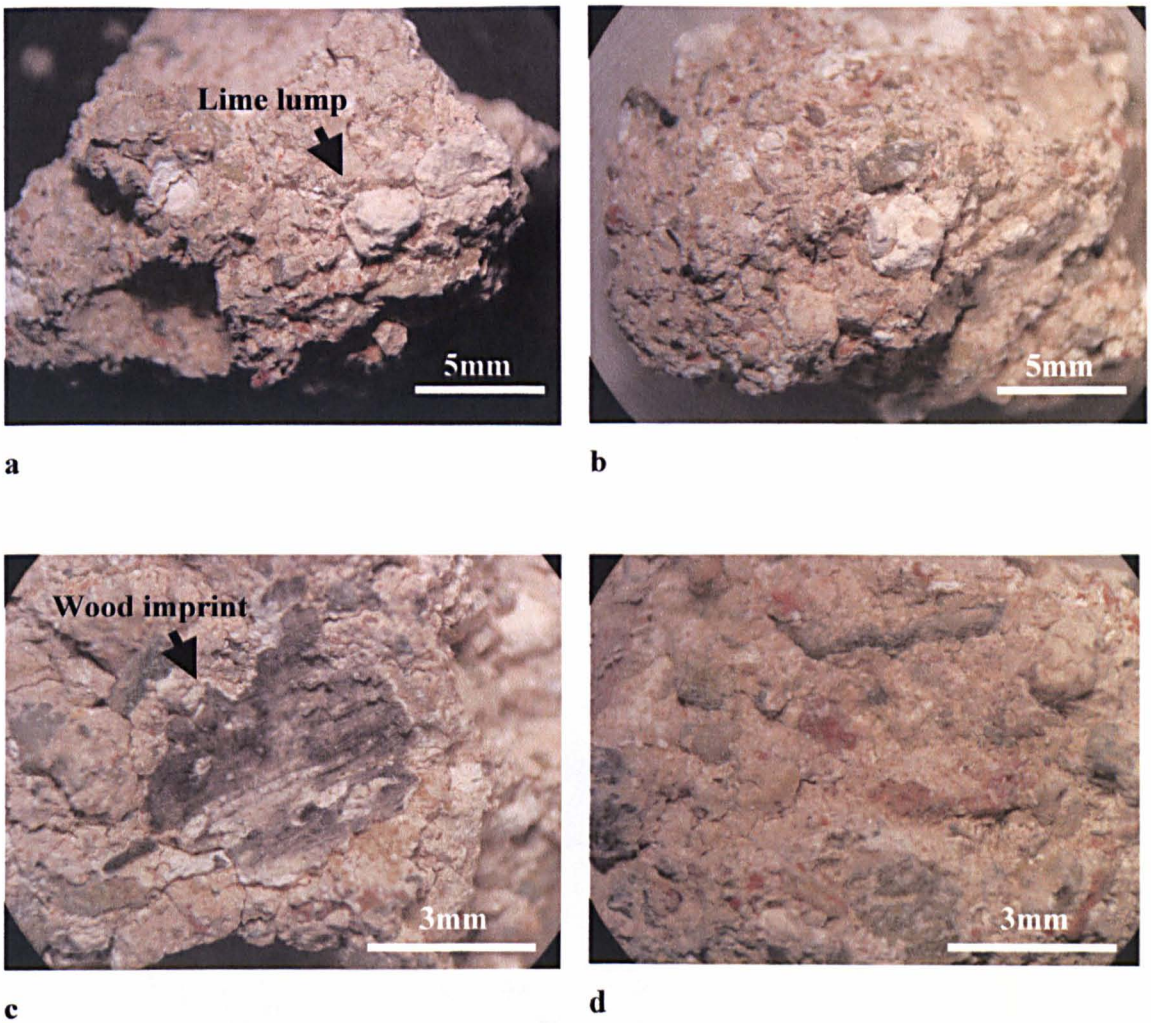

Figure 4.8: Sample NA-IV. Images of freshly fractured surfaces under the stereo-microscope. The mortar mass consists of lime, mixed with both ceramic fragments and natural aggregates (d). Lime lumps have a normal distribution within the mortar mass (a, b), while plant imprints are also present (c).

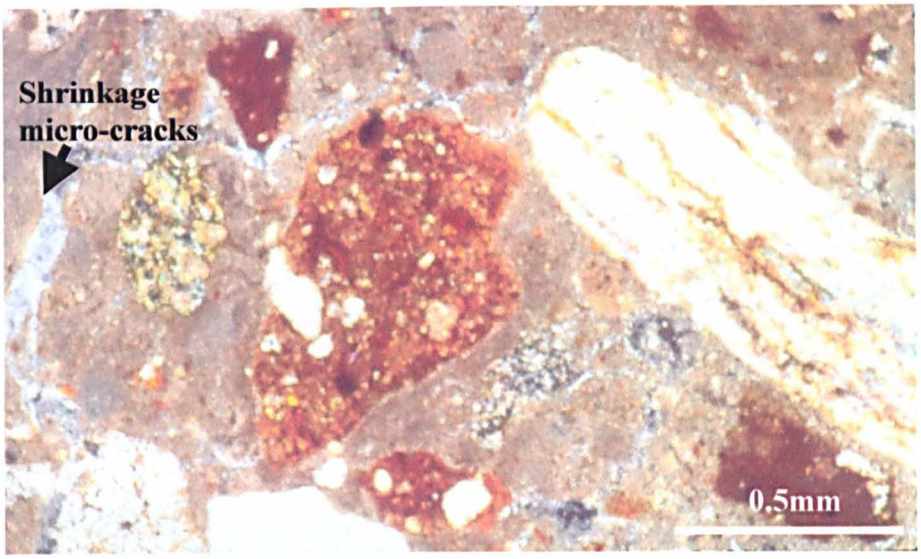

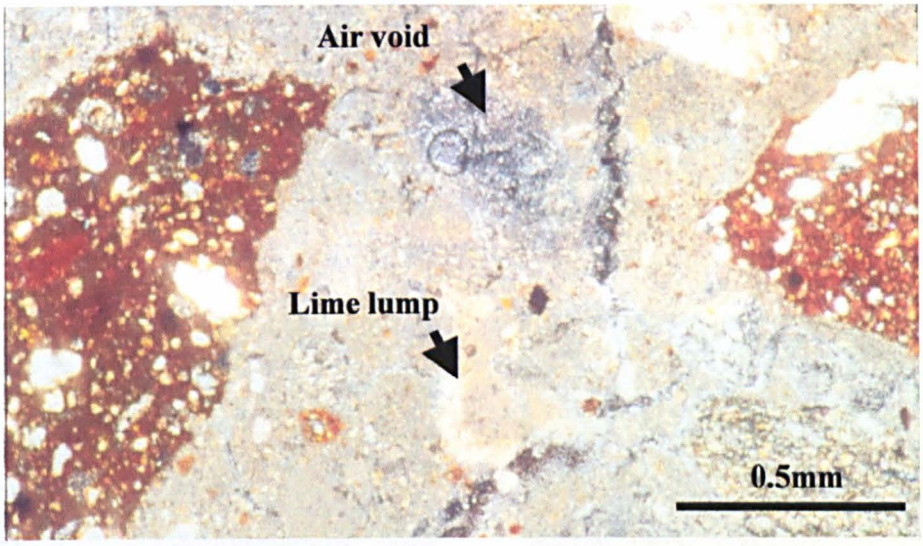

Figure 4.9: Sample NA-IV. Thin-sections in plane polarised light (PPL). Photomicrographs showing different types and grain shapes of aggregates (ceramic and clastic fragments) participating in the mortar matrix. Lime lumps, air-voids and shrinkage micro-cracks are also observed in the binding medium. Very small ceramic fragments are embedded within the binder mass.

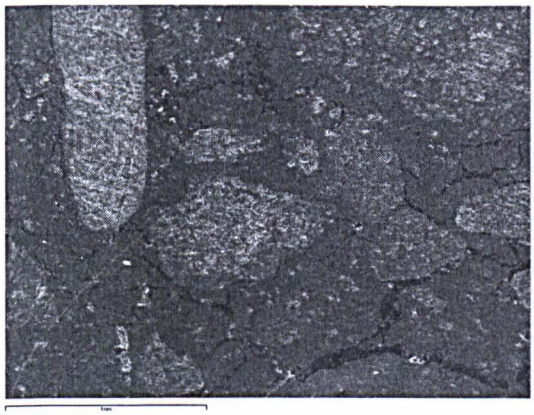

SE image (X50)

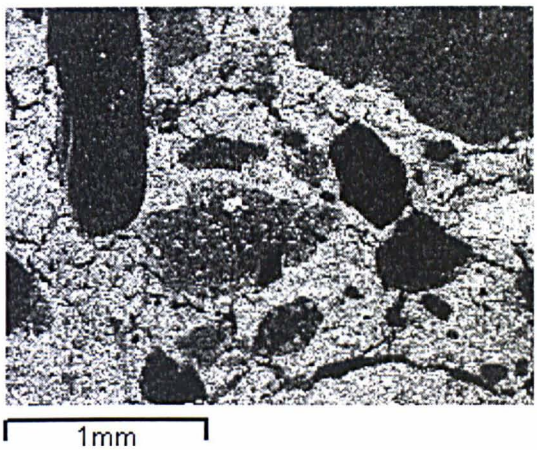

X-ray map: Ca

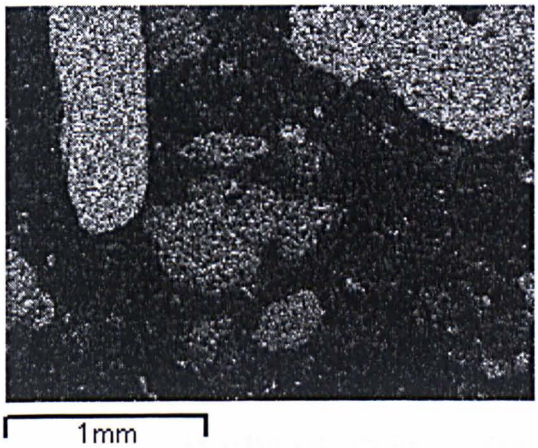

X-ray map: Al

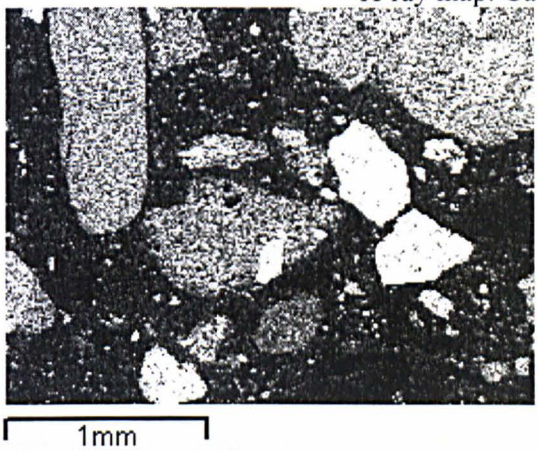

X-ray map: Si

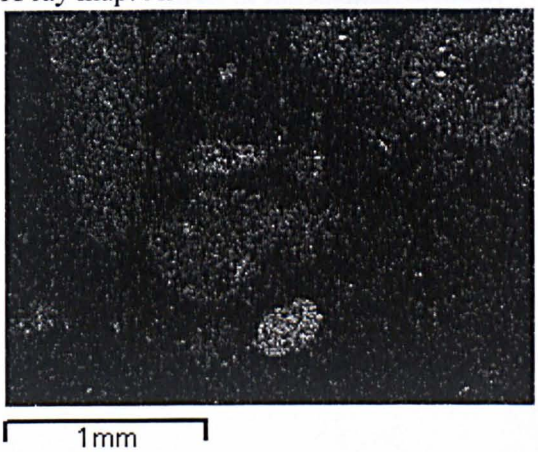

X-ray map: Fe

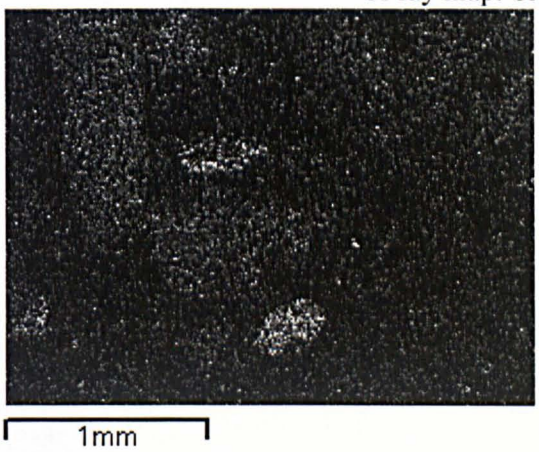

X-ray map: Mg

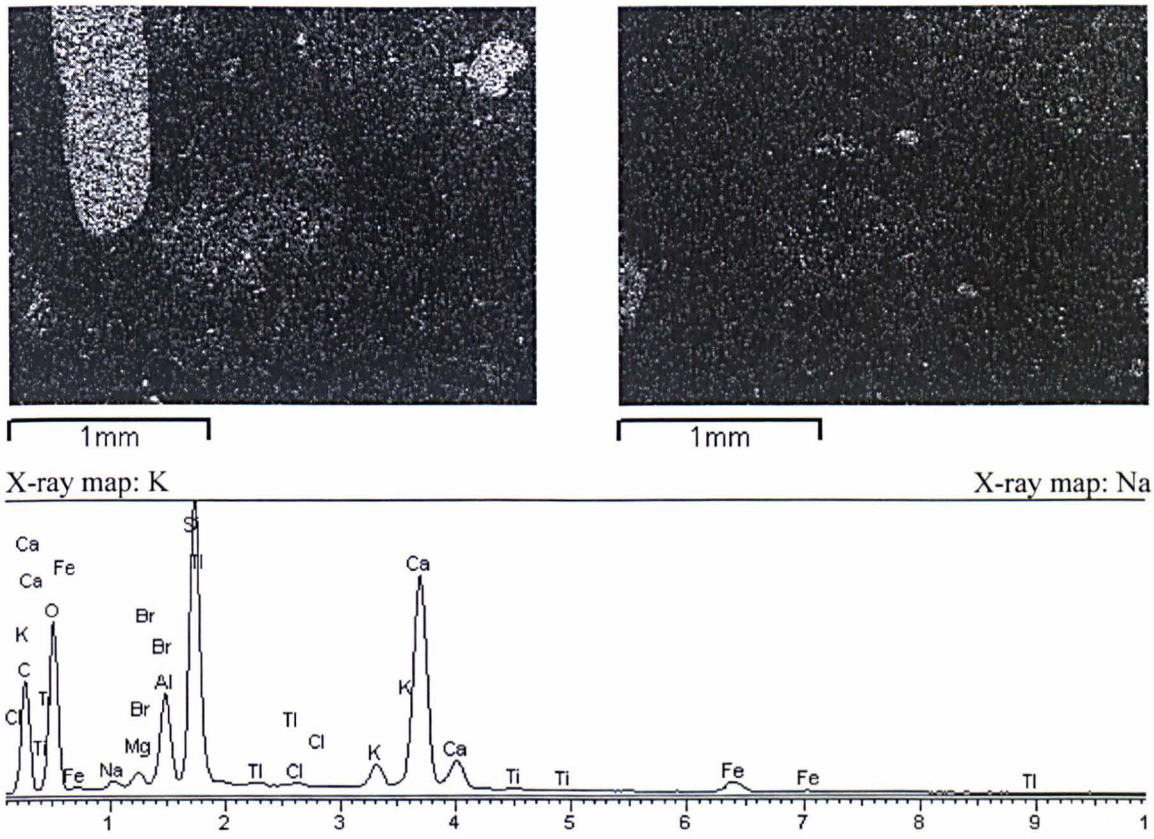

Figure 4.10: Thin-section of NA-IV sample examined under SEM. X-ray maps of elements provided data on the nature of aggregates in the mortar mass, as well as on the type of the binding material.

Samples NA-V

Samples NA-V contained rich amounts of binder and exhibited enhanced strength characteristics, as they were relatively difficult to cut by hand. The binder fraction consisted of slaked lime and ceramic powder in an amount between 10 and 15%. The presence of ceramic powder resulted in a reddish colour to the binding material.

The aggregates contained both natural, rounded-shaped aggregates of maximum 5mm diameter and ceramic fragments of up to 2mm diameter. Ceramic fragments constituted 40–50% per volume of the aggregate fraction. The aggregates were well sorted within the mortar matrix. Thus, a compact microstructure resulted (Figure 4.11).

Small to medium size lime lumps were randomly present in the mortar mass, having maximum diameter of 3mm. Micro-cracks formed during setting were not extensive and only infrequently observed. The small air-bubbles observed are attributed to the air enclosed in the mixture during preparation. This is typical in mixtures with a high lime content and an inadequate mixing procedure (Figure 4.12).

Samples NA-V exhibited a quite compact microstructure under SEM examination (Figure 4.13), presenting small amount of micro-cracks. Elemental analysis (EDX) verified the presence of silicate rock fragments well sorted within the mortars mass.

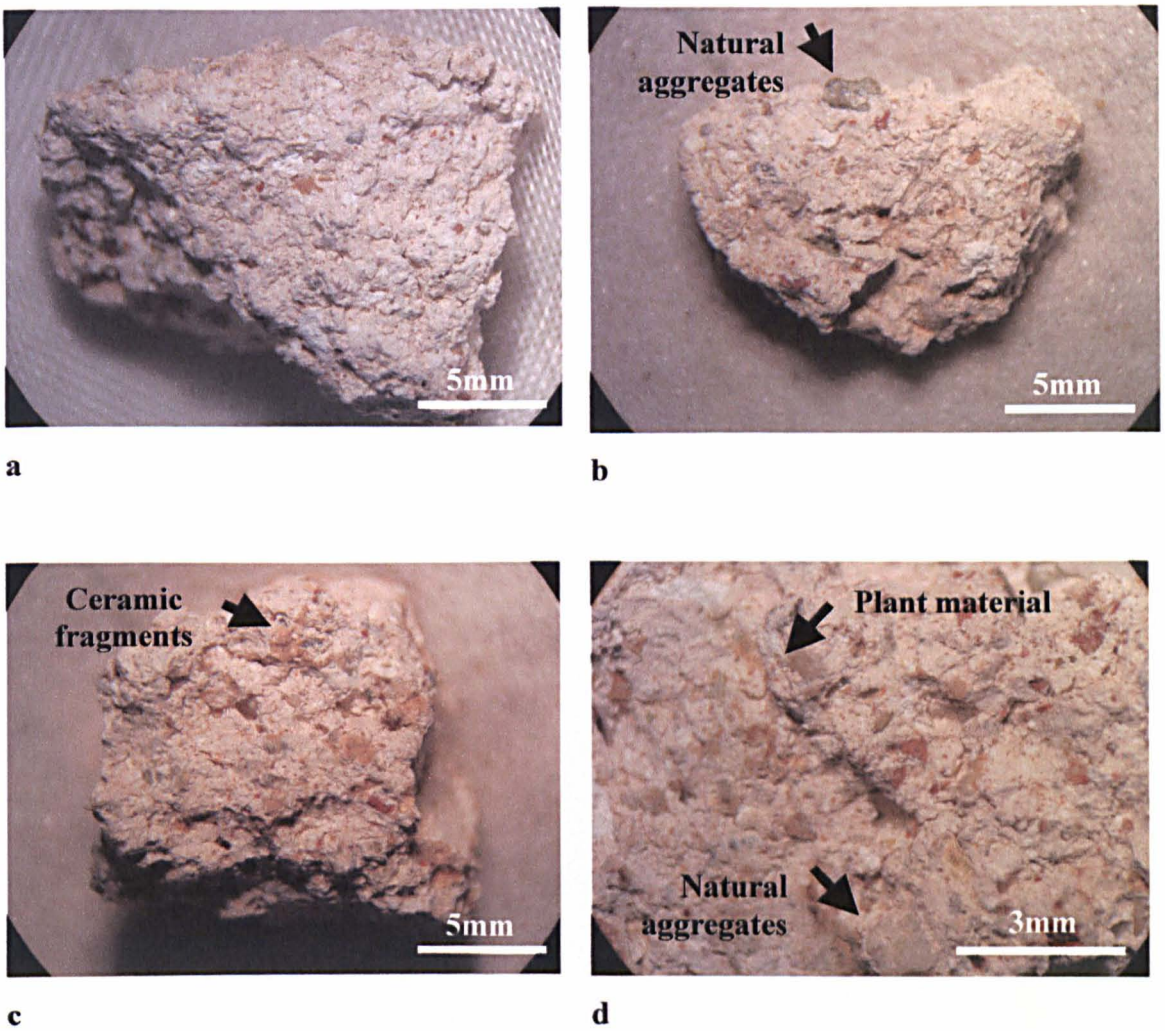

Figure 4.11: Sample NA-V. Examination of freshly fractured surfaces under the stereo-microscope. Mortar mass consists of slaked lime mixed with both ceramic fragments and natural aggregates (c, d). Compact microstructure and small size of aggregates characterise the mixture.

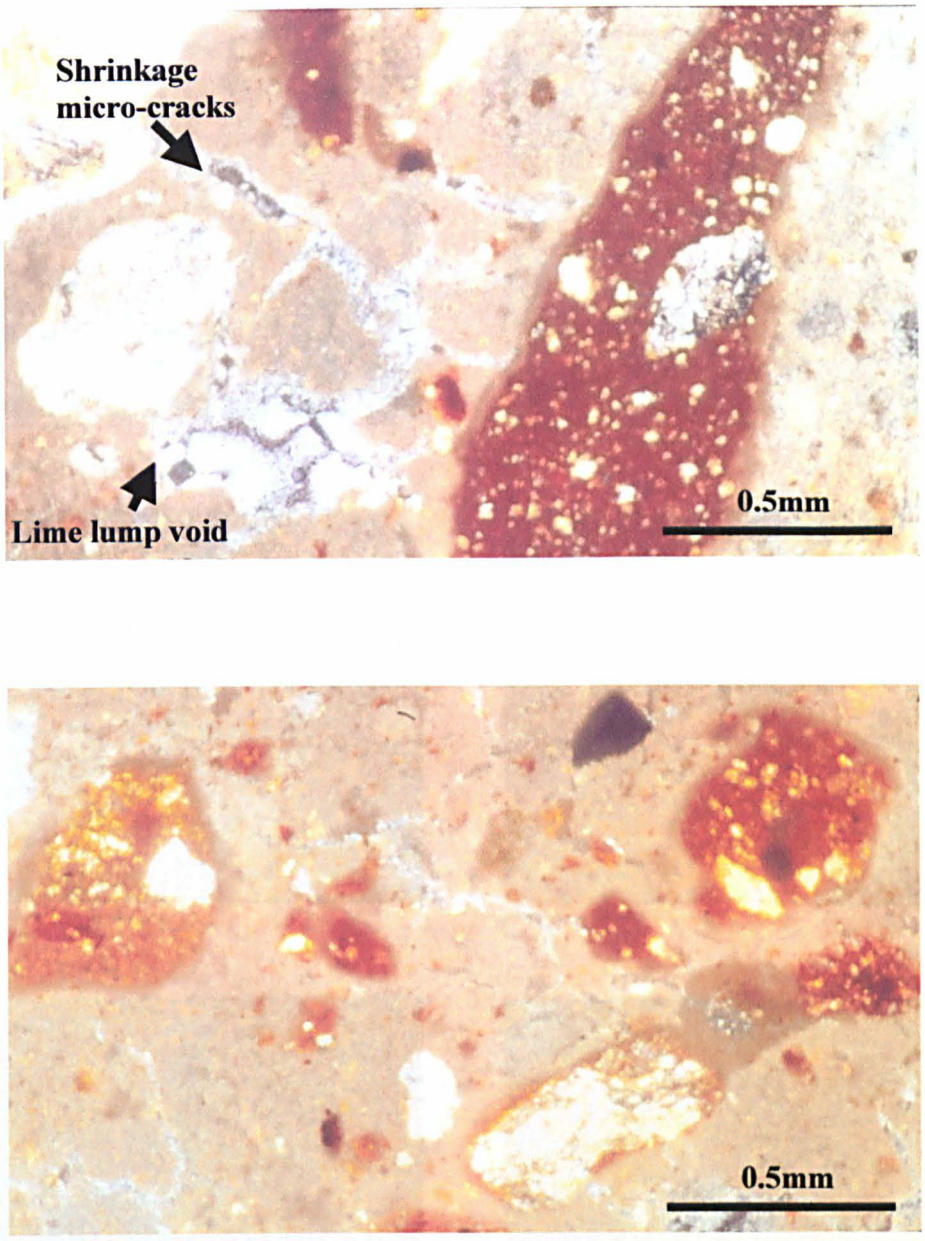

Figure 4.12: Sample NA-V. Examination of thin-sections in plane polarised light. Photomicrographs show different types of ceramic fragments participating in the mortar matrix. Air-voids and shrinkage micro-cracks are also observed in the binding medium. Large amount of ceramic powder and thin ceramic fragments are present in the binder mass.

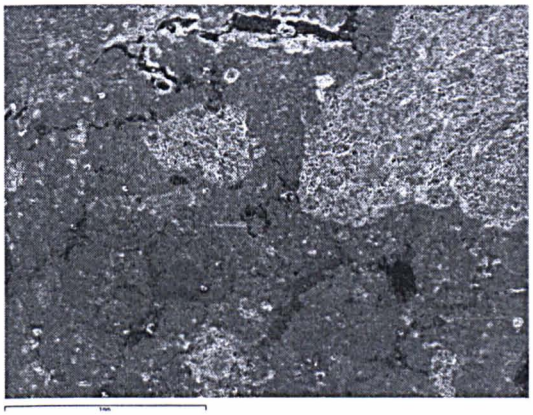

SE image (X50)

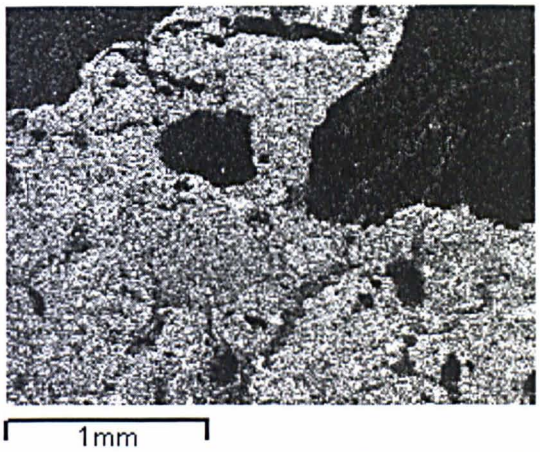

X-ray map: Ca

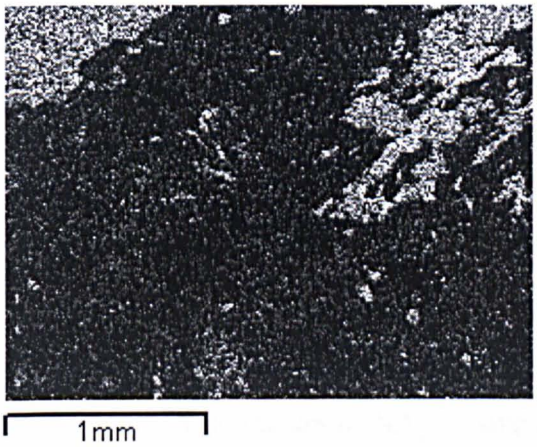

X-ray map: Al

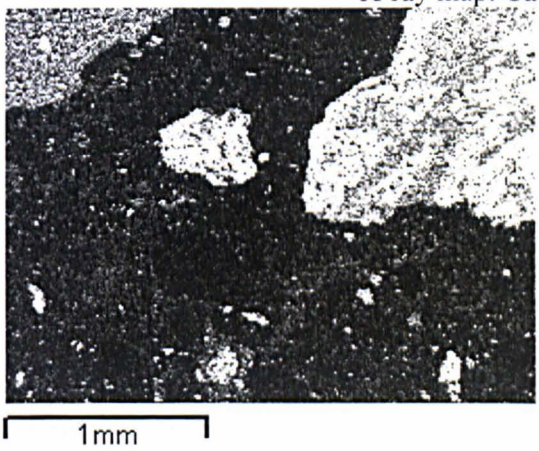

X-ray map: Si

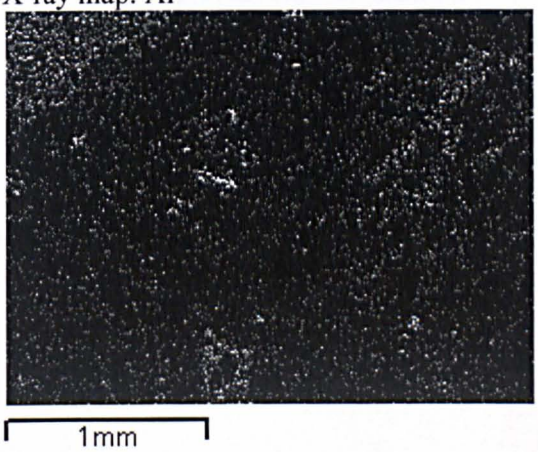

X-ray map: Fe

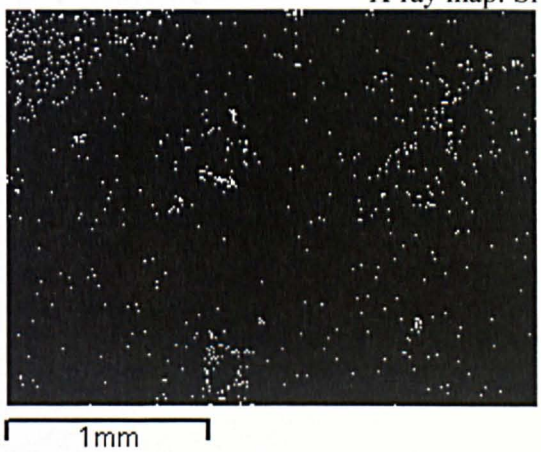

X-ray map: Mg

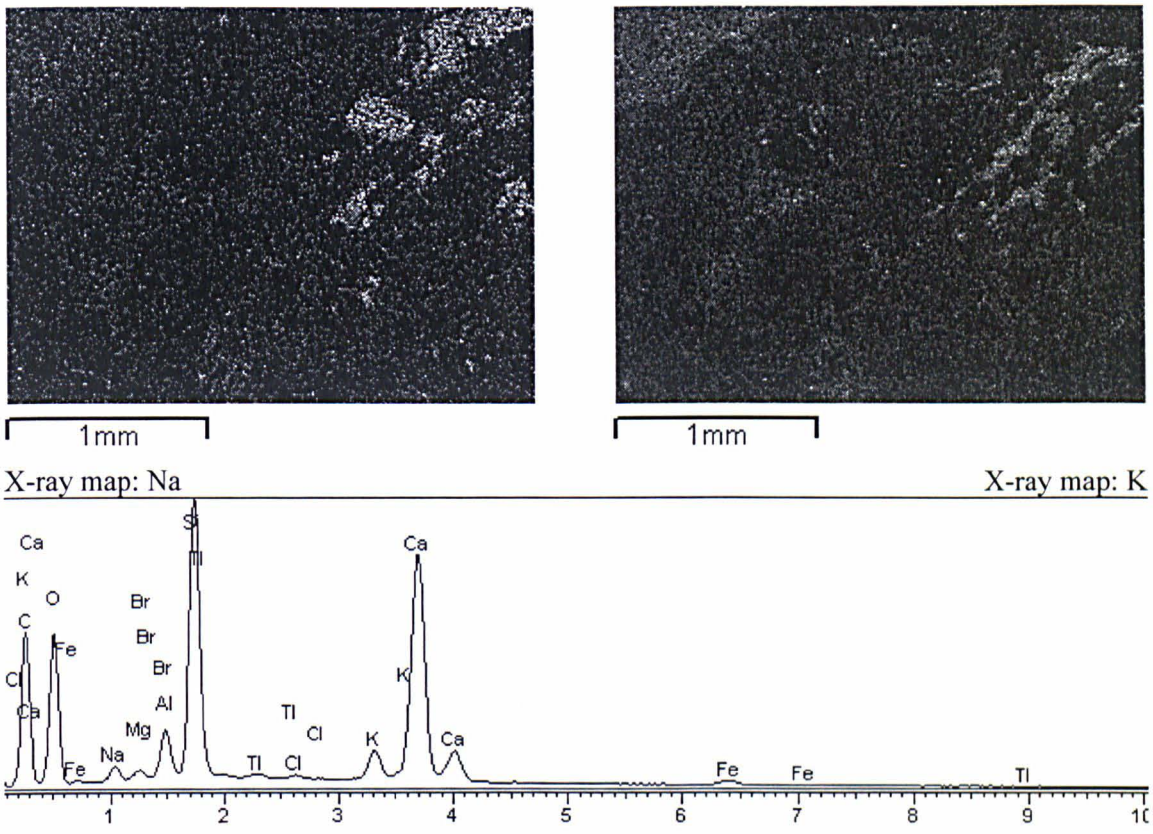

Figure 4.13: Thin-section of NA_V sample examined under SEM. X-ray maps of elements provide data on the nature of aggregates participating in the mortar mass, as well as on the type of binding material.

Samples NA-VI

Samples contained a rich amount of binder and exhibited enhanced strength characteristics. The binder fraction consisted of slaked lime and ceramic powder (15–20%), which resulted in a reddish colour to the mixture.

The aggregate fraction consisted of red and dark-brown ceramic fragments of maximum size 3–4mm, as well as of natural, rounded-shaped rock fragments that had a maximum size of 1mm. The majority of ceramic material in the fraction was 0–0.125mm in diameter. Finally, large amounts of lime lumps (4–10mm) were distributed in the mixture (Figures 4.14 and 4.15).

Examination of thin sections under scanning electron microscope, coupled with EDX analyser (Figure 4.16) revealed a compact microstructure for mortars NA-VI. Small ceramic fragments are very well sorted in the cementing material, along with some angular silicate rock fragments.

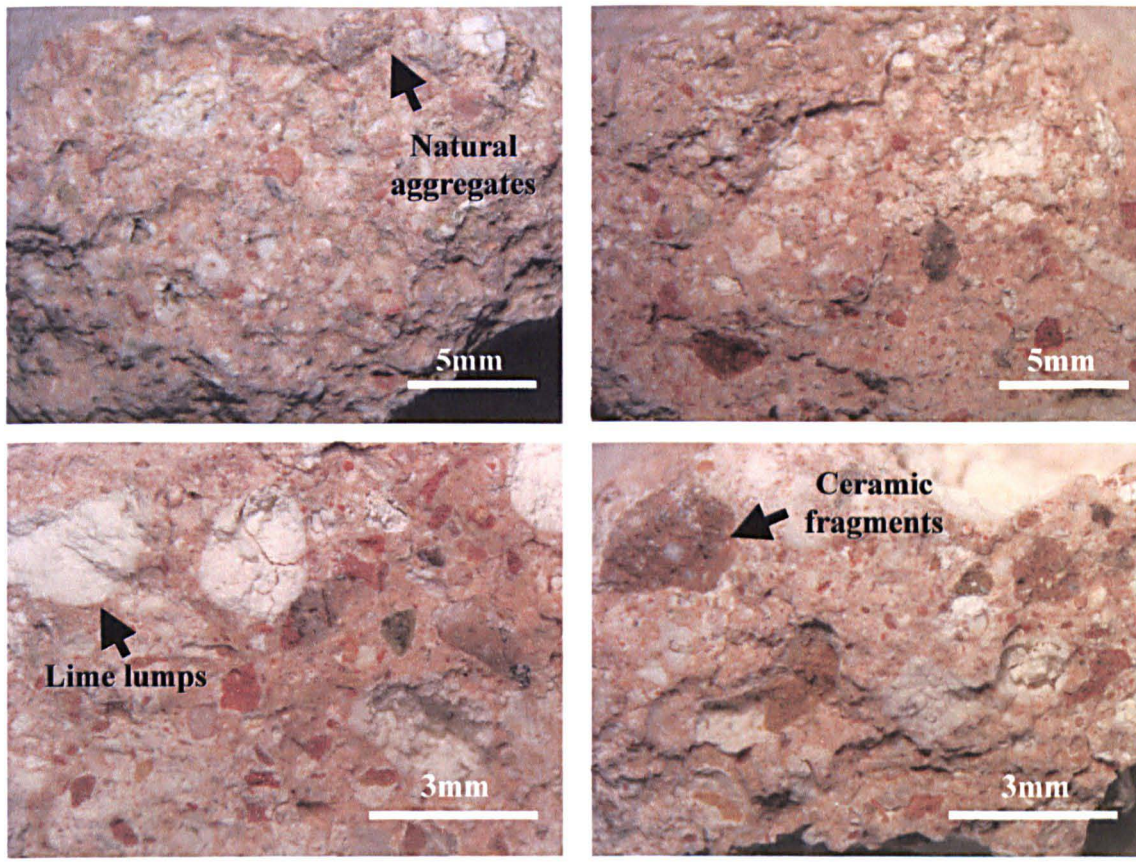

Figure 4.14: Sample NA-VI. Examination of freshly fractured surfaces under a stereo-microscope. Mortar mass consists of slaked lime mixed with both ceramic fragments and natural aggregates. Large lime lumps have a normal distribution within the mortar mass.

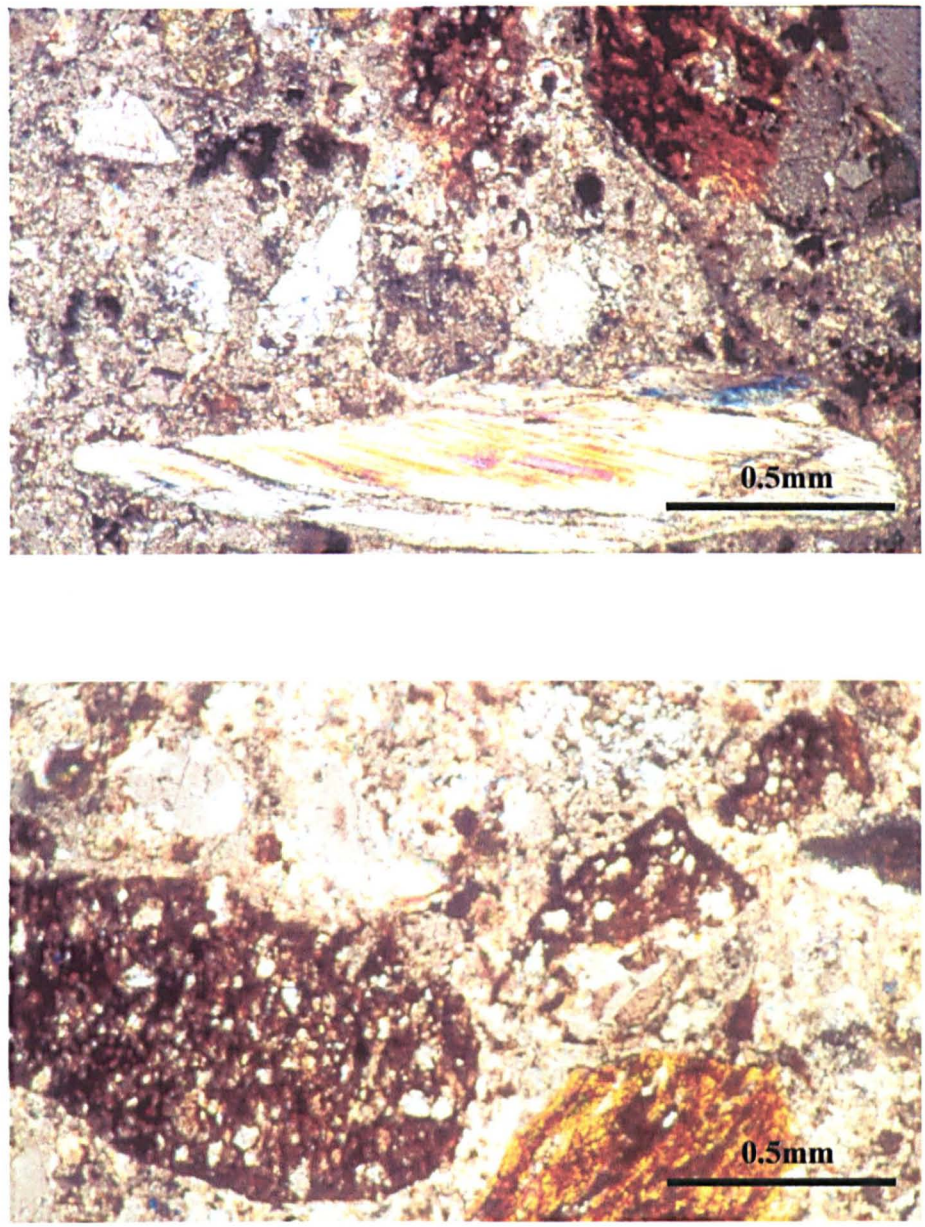

Figure 4.15: Sample NA-VI. Examination of thin-sections in polarising microscope (XPOLS). Photomicrographs show different types of ceramic and rock fragments within the mortar matrix. A large amount of ceramic powder is present and thin ceramic fragments are well sorted in the micro-crystalline matrix of cementing material, along with some angular quartz fragments.

SE image (X50)

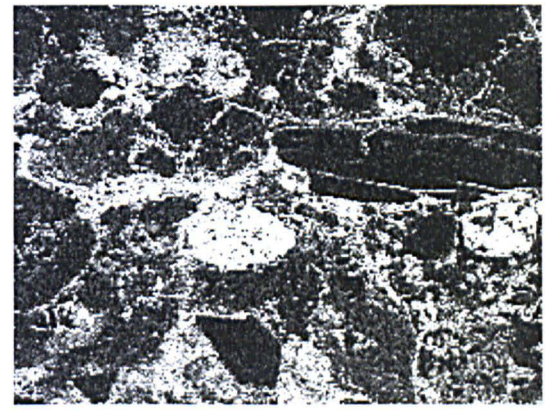

X-ray map: Ca

X-ray map: Al

X-ray map: Si

X-ray map: Fe

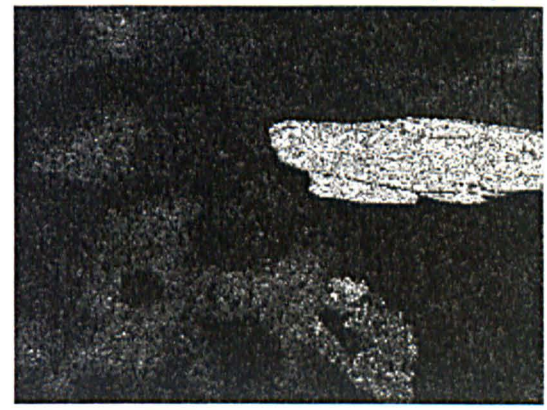

X-ray map: Mg

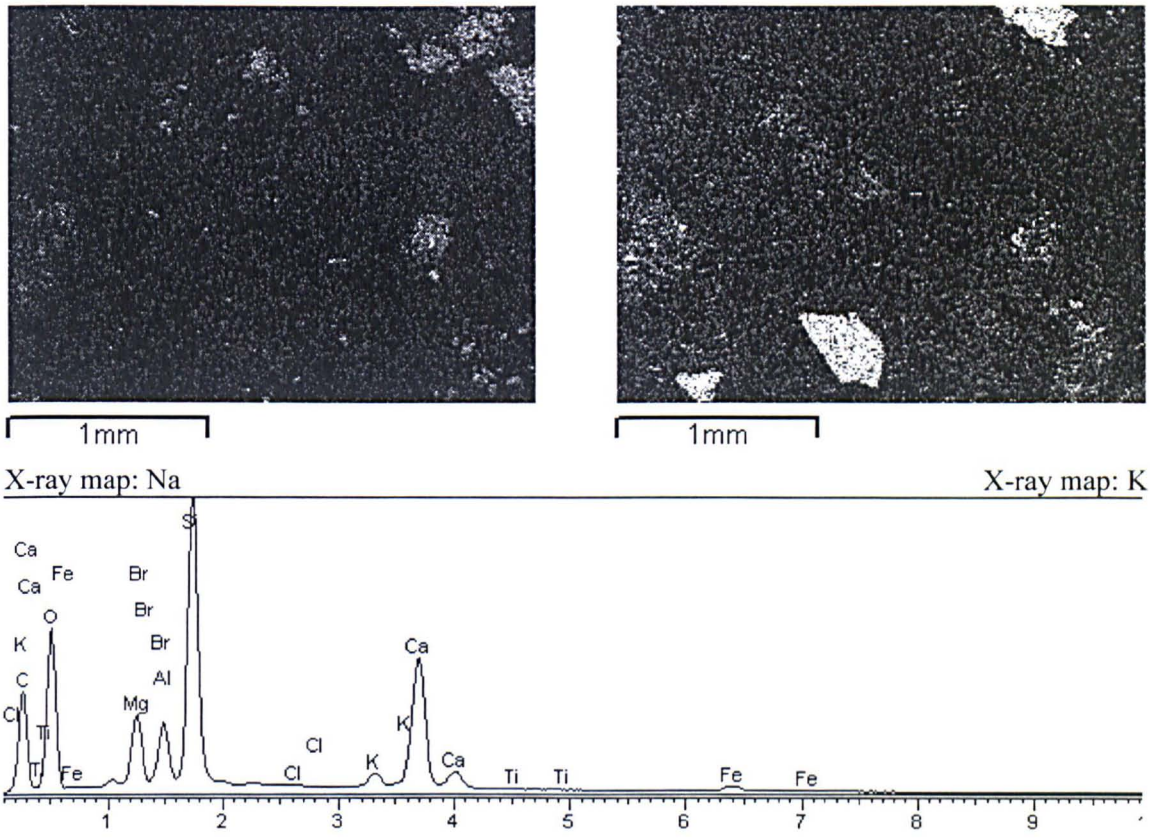

Figure 4.16: Thin-section of NA-VI sample examined under SEM. X-ray maps of elements provide data on the nature of aggregates participating in the mortar mass as well as on the type of binding material.

Samples TH-KAD

The TH-KAD samples were typical lime-based mortars and exhibited medium to low strength characteristics. The binder/aggregate ratio was quite low, and a very small amount of thin ceramic fragments (maximum 5%) was dispersed throughout the binder mass.

The aggregate fraction consisted of large ceramic and local limestone fragments. The maximum size of aggregates was 4mm, with the majority of the material being reddish ceramic fragments. Stone pieces consisted of alumino-silicate and microfossil fragments that were bound together by a large amount of cementing material. Finally, coal traces and lime lumps of about 0.5–0.7mm thickness were often observed within the mixture mass (Figure 4.17).

Large aggregate fragments and low binder content prevented the formation of an extensive micro-crack network due to shrinkage, but locally, the binder was detached from the surface of the ceramic aggregates. This type of shrinkage phenomenon takes place during the setting and hardening of the mixtures when the water content of the binder is absorbed by ceramic and/or other aggregate fragments (Figure 4.18).

SEM examination of thin sections (Figure 4.19) showed that micro-cracks are eliminated, while X-ray element maps proved that aggregate fragments consist of magnesium-rich alumino-silicates.

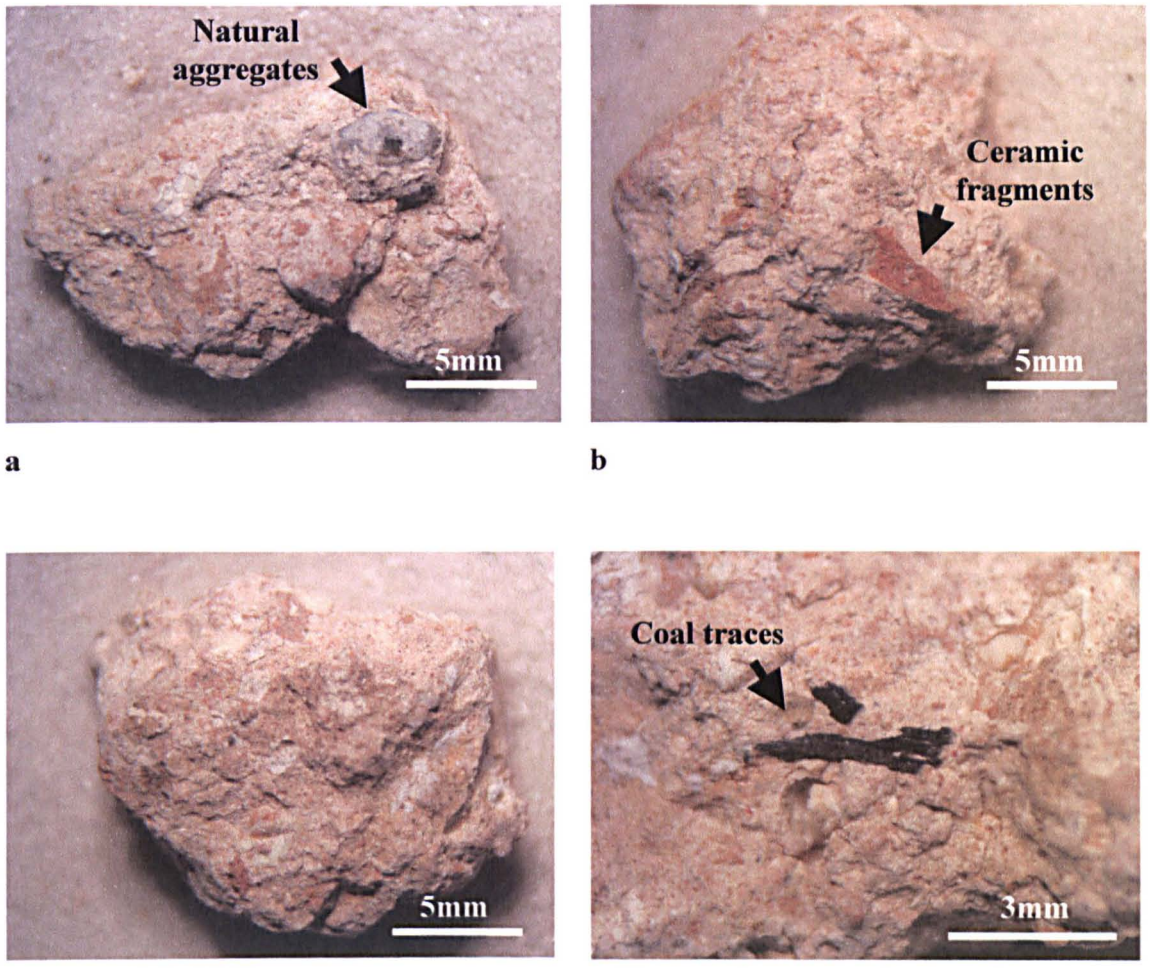

Figure 4.17: Sample TH-KAD. Examination of freshly fractured surfaces under a stereo-microscope. The mixture is compact but heterogeneous and is characterised by the low binder content and the use of large aggregate fragments. Coal traces and lime lumps are often observed within the mixture mass (c, d).

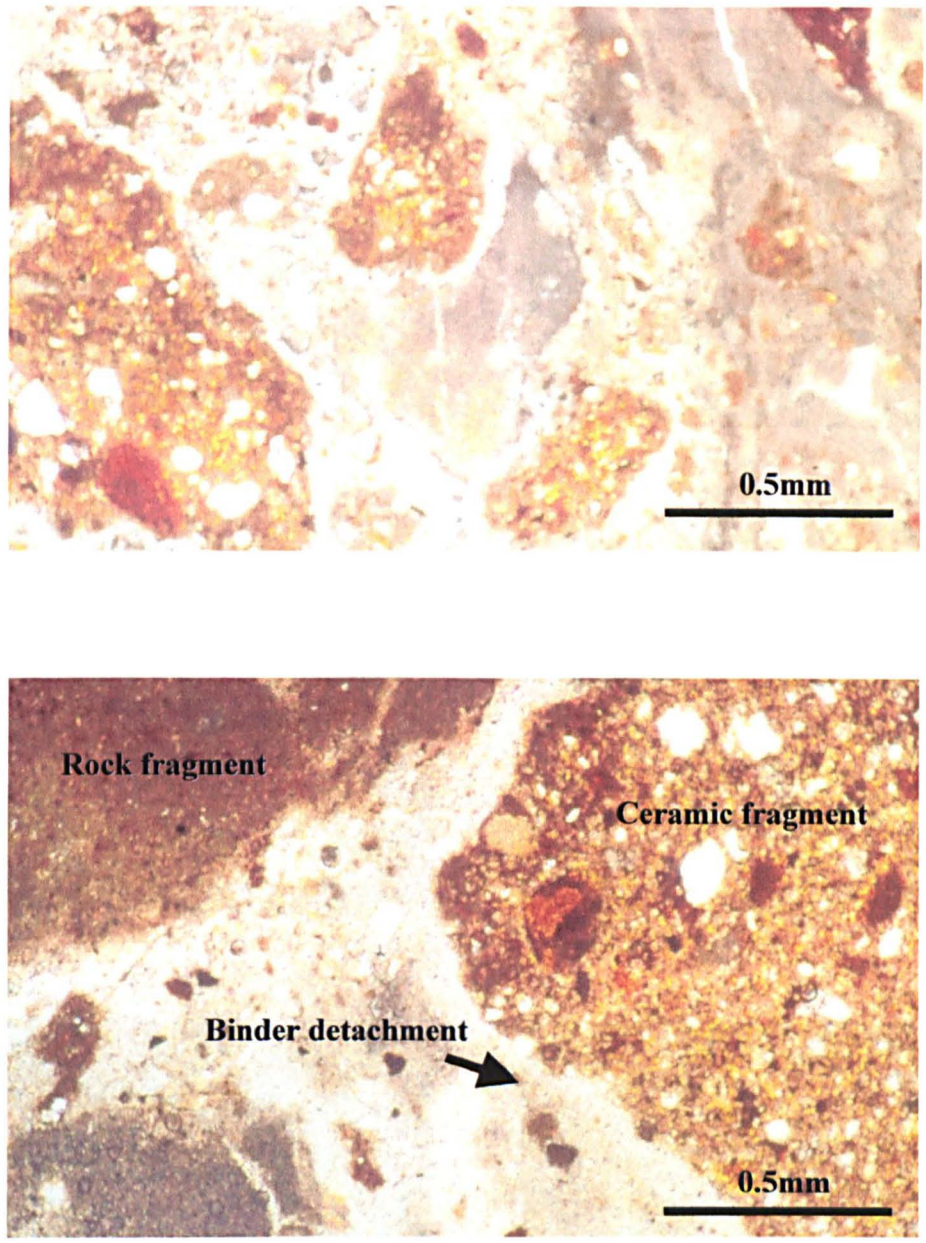

Figure 4.18: Sample TH-KAD. Examination of thin-sections in plane polarised light. Photomicrographs show different types of aggregates within the mortar matrix. Voids, caused by binder shrinkage during setting, are indicated.

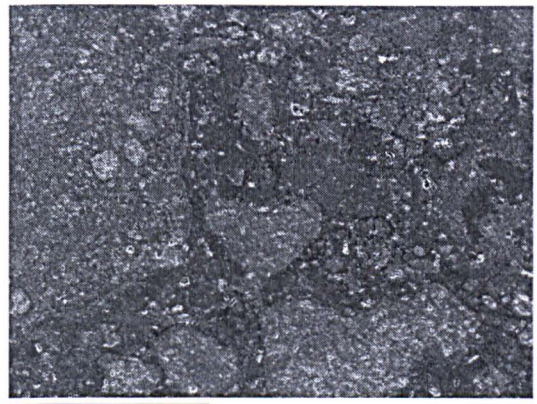

SE image (X50)

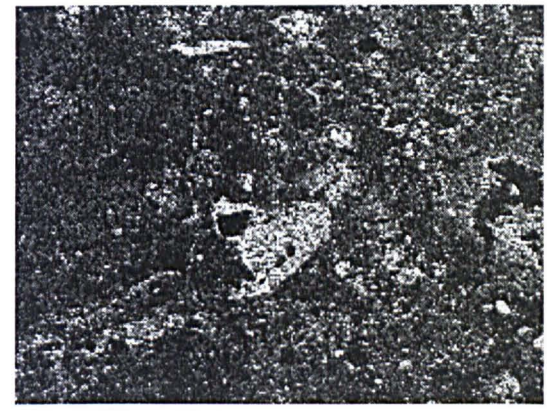

X-ray map: Ca

X-ray map: Al

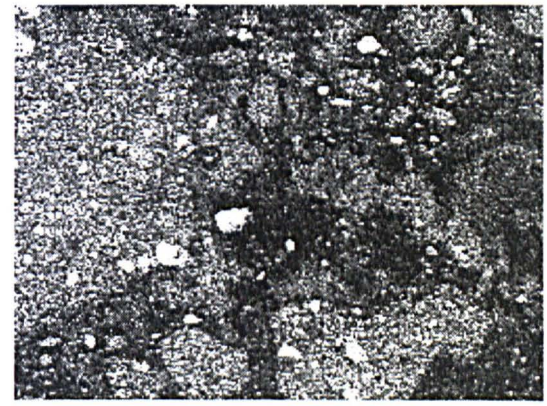

X-ray map: Si

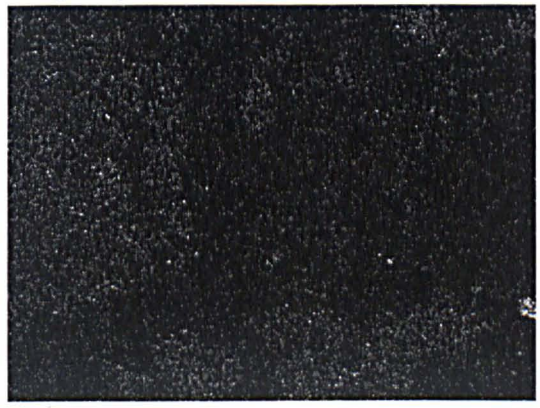

X-ray map: Fe

X-ray map: Mg

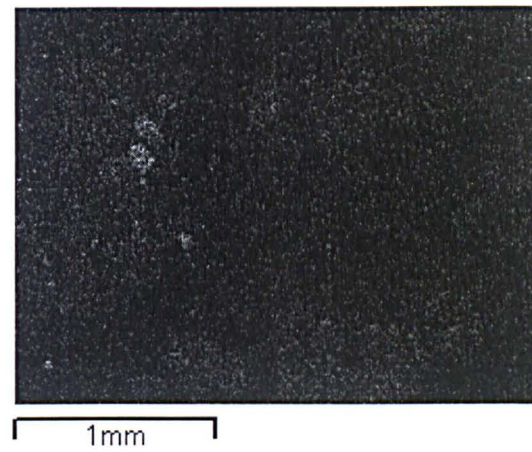

X-ray map: K

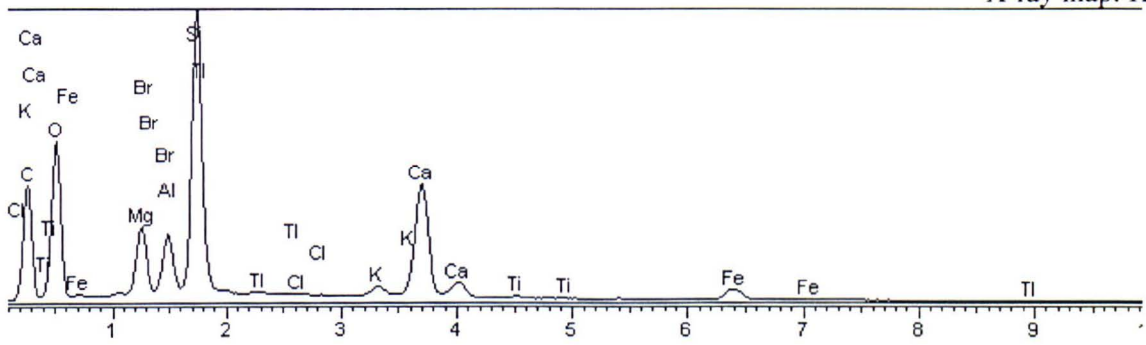

X-ray spectrum

Figure 4.19: Thin-section of TH-KAD sample examined under SEM. X-ray maps of elements provide data on the nature of aggregates within the mortar mass, as well as on the type of binding material.

Samples TH-KEB

The TH-KEB mortar is a lime mixture that contained two different types of aggregates and a small amount (5-10%) of ceramic powder in the binding material. The samples exhibited high strength characteristics, according to their resistance against hand-made fracture.

The mixture contained a large amount of slaked lime, whilst aggregate fragments were well embedded within the binder. Lime lumps were randomly distributed within the mortar mass, the majority being in the range of 3mm diameter, although bigger lumps (1-2cm) were also observed. Imprints of plant material were identified on the lime mass (Figure 4.20).

The aggregates consisted of both spherical, partially elongated rock pieces (local limestone) and ceramic fragments. The ceramic fragments were a reddish colour, and the stone fragments a yellow/brown. Additionally, some angular, dark aggregates were also distinguished. The maximum size of the aggregates was about 4mm diameter. Thus, some individual, larger aggregate fragments (1.5–2.0cm diameter) that were observed, may be attributed to the underneath layer (Figure 4.21).

Finally, discontinuities randomly appeared and a limited network of micro-cracks was apparent. This can be attributed to poor mixing and the small amount of water initially added to the mixture and during the preparation process.

Examination of thin sections under SEM/EDX showed that the binding material is rich in spherical aggregates bellow 0.5mm (Figure 4.22).

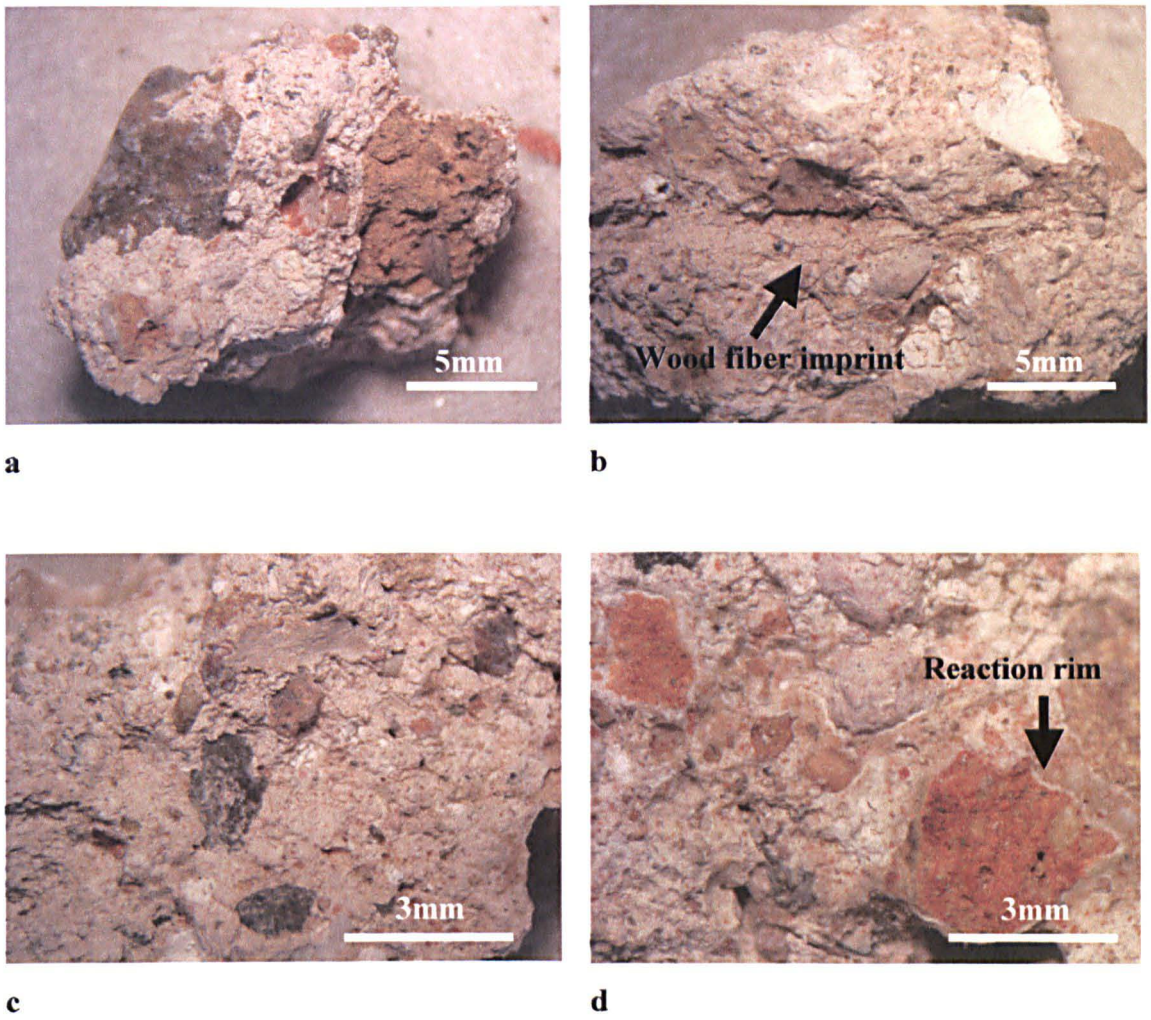

Figure 4.20: Sample TH-KEB. Examination of freshly fractured surfaces under a stereo-microscope. The mixture contains a rich amount of binding material which results in a compact microstructure with enhanced strength characteristics. The mixture shows some local discontinuities that are probably caused by a poor mixing process. Aggregates are very well embedded in the mortar mass, whilst some ceramic fragments exhibit a reaction rim around their granules (d). Finally, wood and plant material imprints are often observed within the mixture mass (b).

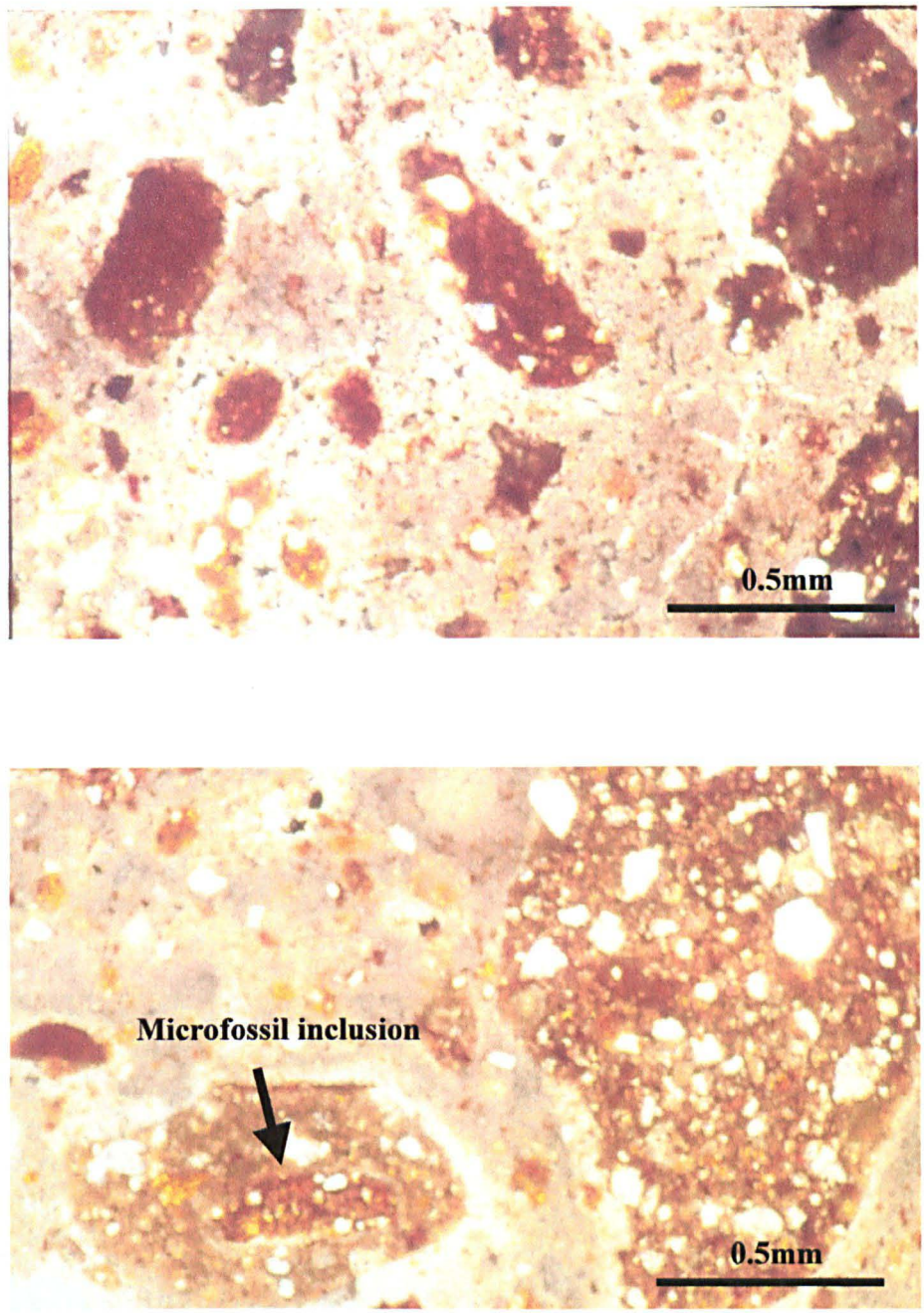

Figure 4.21: Sample TH-KEB. Examination of thin-sections in plane polarised light. The mixture shows a compact microstructure with limited shrinkage micro-cracks. Ceramic fragments (upper picture) and limestone pieces (lower picture), up to 0.5mm, have a normal distribution in the binding material and fill the gaps between the larger fragments.

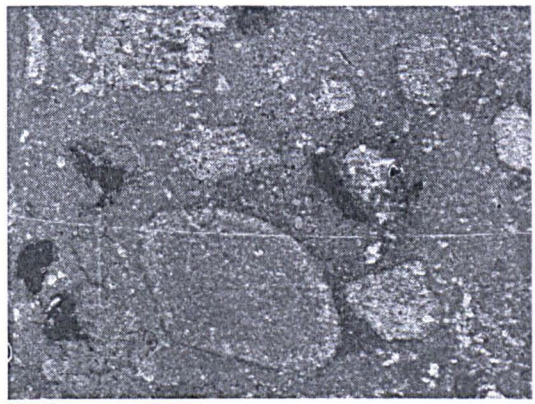

SE image (X50)

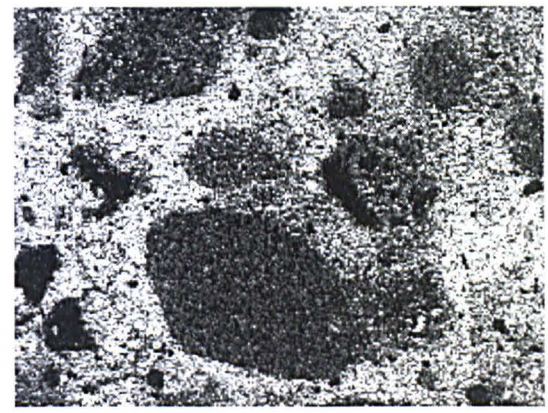

X-ray map: Ca

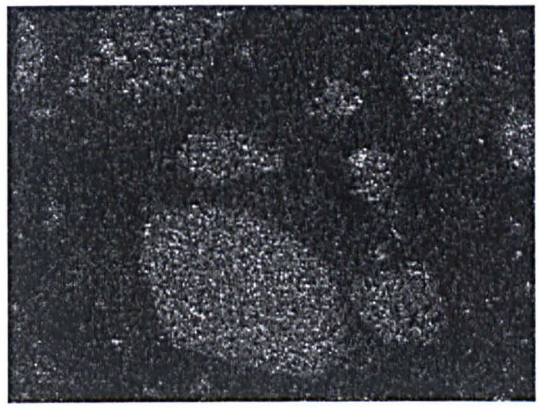

X-ray map: Al

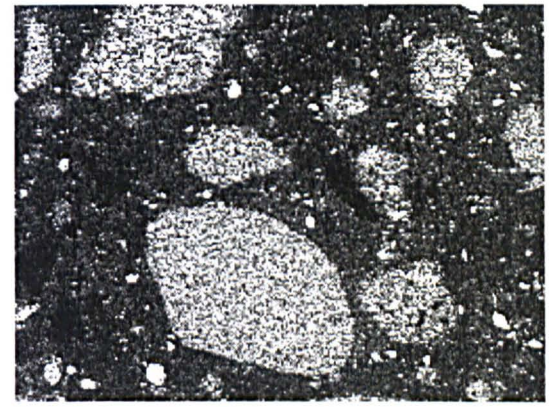

X-ray map: Si

X-ray map: Fe

X-ray map: Mg

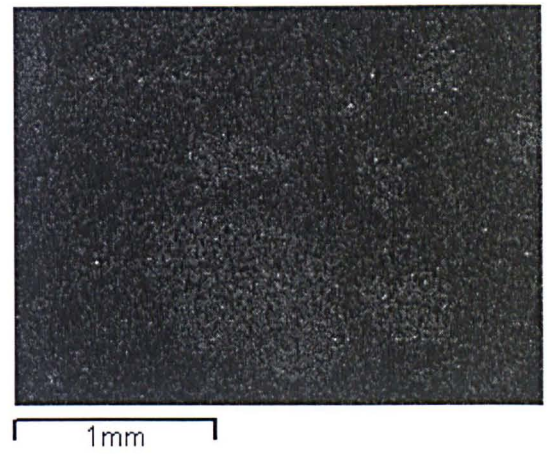

Figure 4.22: Thin-section of TH-KEB sample examined under SEM. X-ray maps of elements provide data on the nature of aggregates within the mortar mass, as well as on the type of binding material.

Samples TH-PIN

The TH-PIN mortars were lime-based mixtures that exhibited high strength characteristics and enhanced hardness. The binder consisted of slaked lime mixed with about 20% by volume of ceramic powder. Lime lumps (2–7mm diameter) were randomly distributed within the mortar mass without affecting their compactness.

The mixture had a reddish colour, caused by the ceramic fragments that constituted the majority of the aggregate fraction. A small amount, up to 30% by volume, of limestone pieces participated, additionally, in the aggregate fraction. The maximum size of aggregates was 4mm in diameter. Small black inclusions, of 1–2mm maximum size, were very often observed in the mortar mass (Figures 4.23 and 4.24).

Samples TH-PIN exhibited a quite compact microstructure under SEM examination (Figure 4.25), presenting small amount of micro-cracks. Elemental analysis (EDX) showed that ceramic material consist of potash silicates (K-silicates) and that silicate rock fragments are well sorted within the mortars mass.

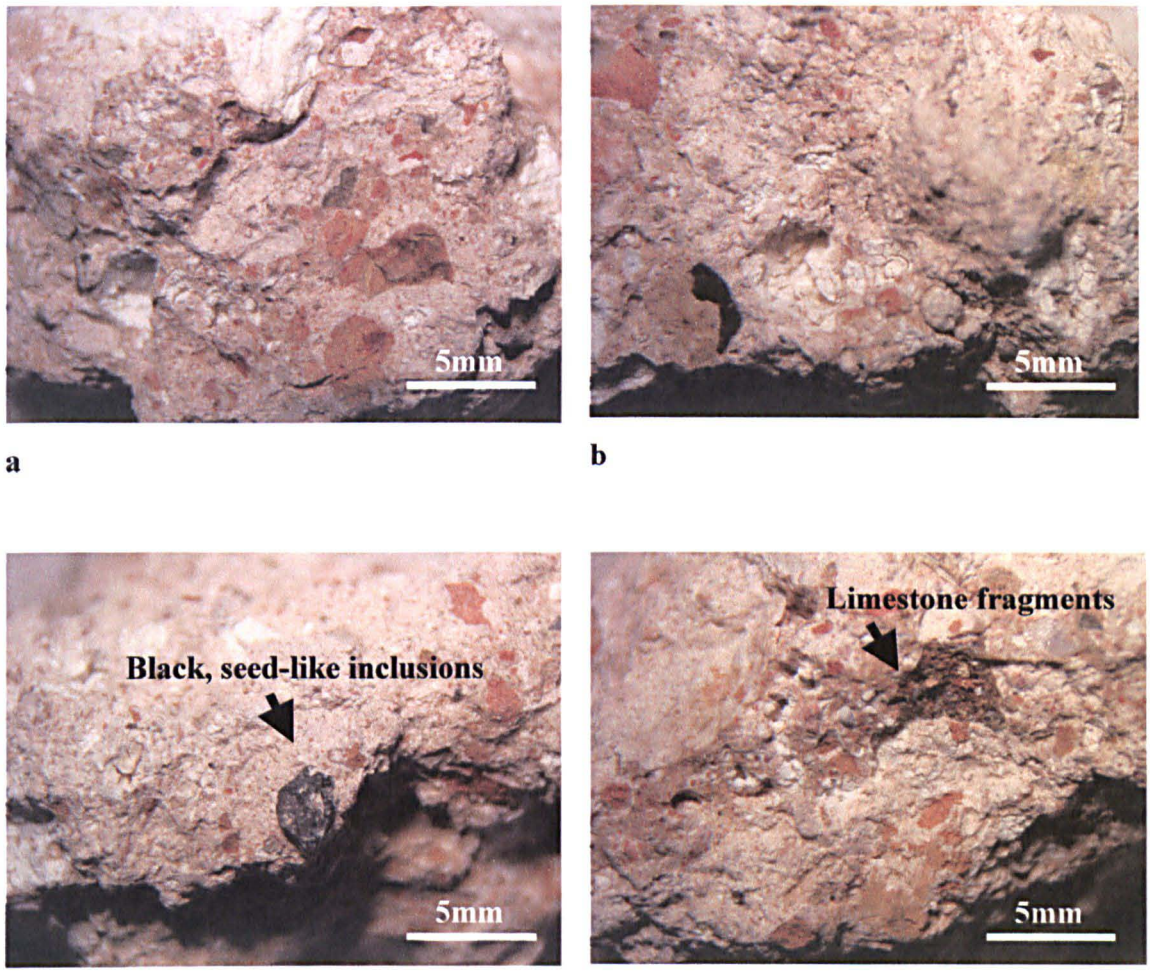

Figure 4.23: Sample TH-PIN. Examination of freshly fractured surfaces under a stereo-microscope. Mortar mass consists of slaked lime mixed with ceramic fragments and a small amount of limestone pieces. Small black inclusions and lime lumps are randomly observed within the mortar mass.

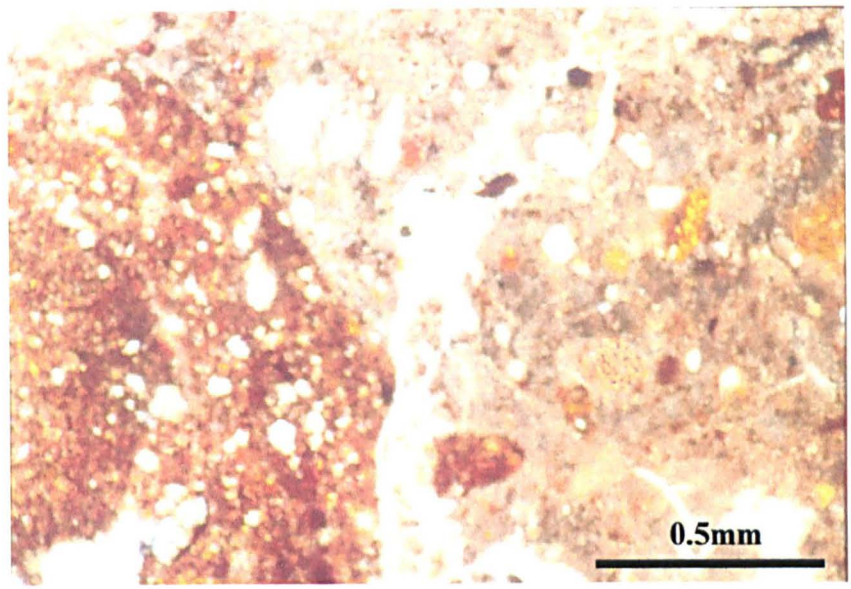

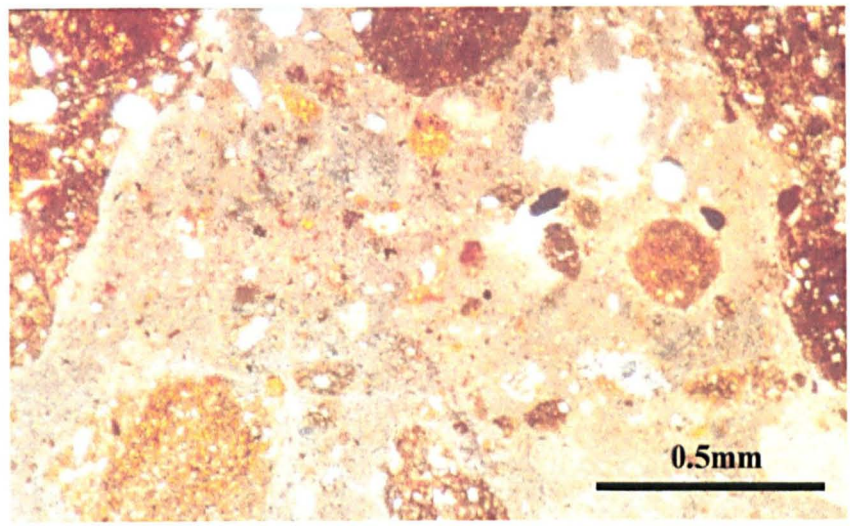

Figure 4.24: Sample TH-PIN. Examination of thin-sections in plane polarised light (PPL). Photomicrographs show different types and grain shapes of aggregates (ceramic and limestone fragments) within the mortar matrix. Shrinkage micro-cracks are also observed in the binding medium. Thin ceramic fragments are well distributed in the binder mass.

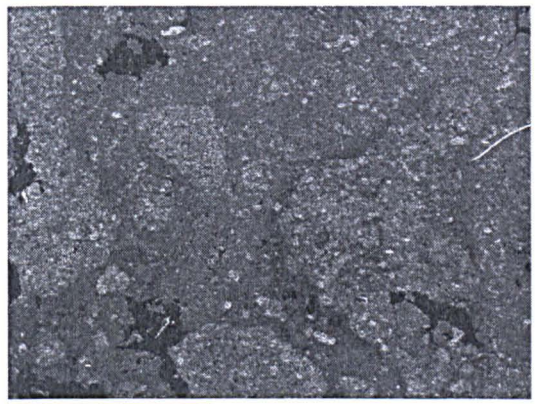

SE image (X50)

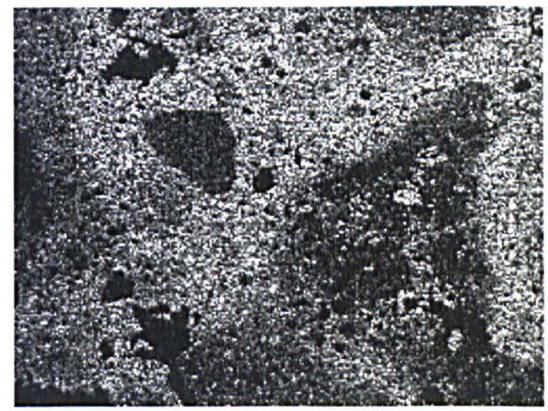

X-ray map: Ca

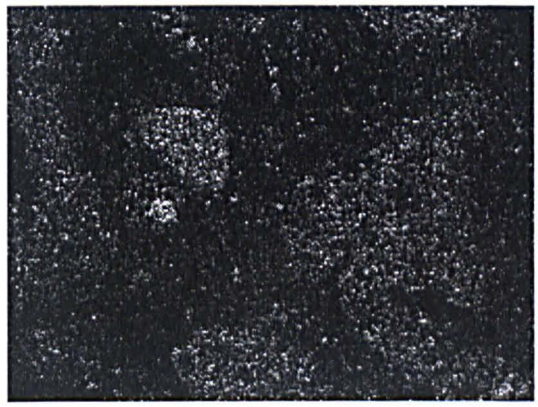

X-ray map: Al

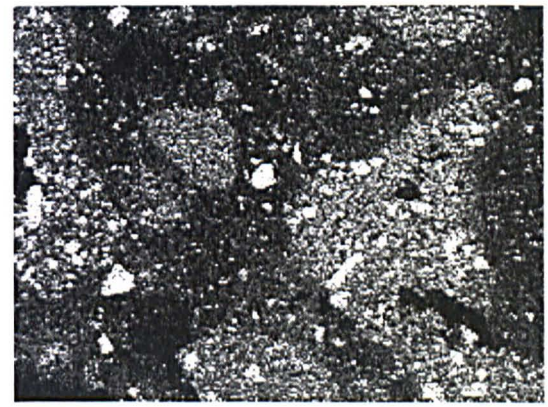

X-ray map: Si

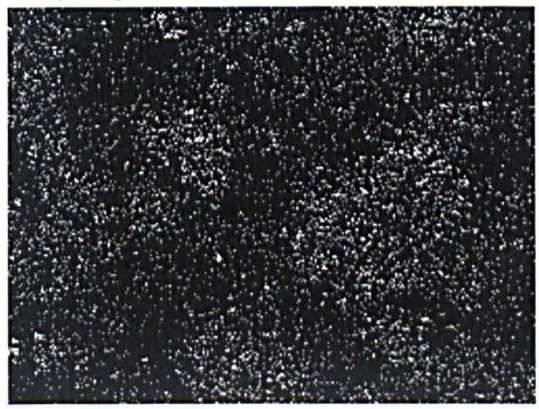

X-ray map: Fe

X-ray map: Mg

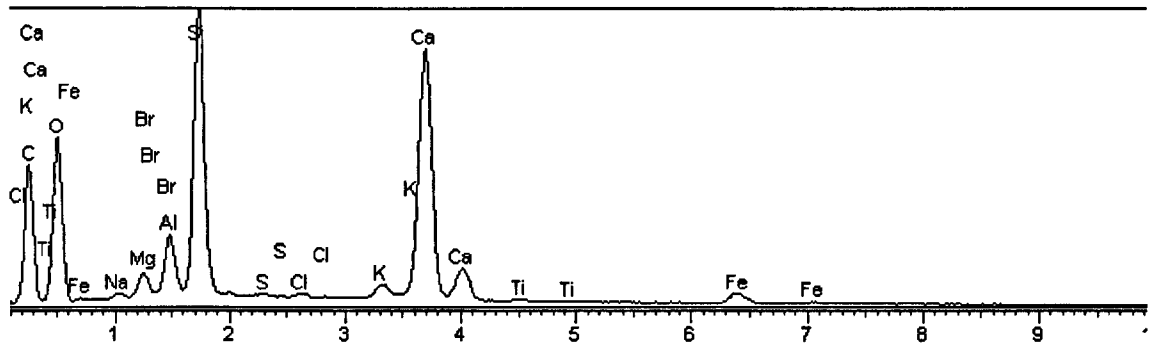

X-ray spectrum

Figure 4.25: Thin-section of TH-PIN sample examined under SEM. X-ray maps of elements provide data on the nature of aggregates within the mortar mass, as well as on the type of binding material.

4.2.2.2 Granulometric Distribution

The granulometric distribution of aggregates, the binder to aggregate ratio and the water content (or water to binder ratio) are the main parameters that control strength and pore space characteristics of hardened mortars, and consequently their behaviour with deterioration agents.

Figure 4.26 shows the grain-size distribution of mortar constituents after physical separation. The accumulative mass of the material passing through each sieve is expressed as a weight percentage (%) and is plotted on a logarithmic scale together with the sieve mesh size. The fraction below 0.063mm is considered to be the cementing material, although a considerable amount of cementing material remained in the larger fractions, either as lime lumps, or attached to the surface of the aggregates.

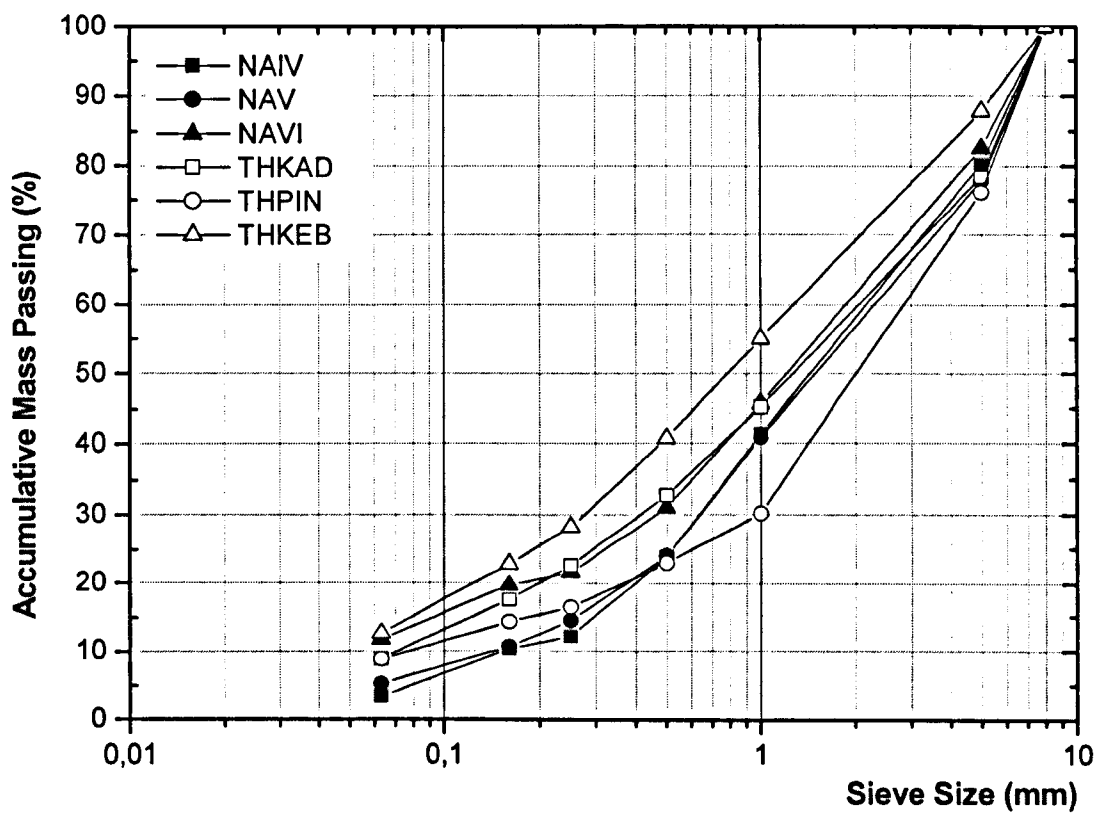

Figure 4.26: Granular distribution of mortar constituents, including the binder fraction.

The shape of the distribution is related to the production technology of the original mortars. It provides information about the mixing process and the wet properties of fresh mixtures such as the flow ability and the water content required to achieve the desired workability. Samples TH-KAD and TH-KEB formed the same type of curve which approaches, more or less, a straight line. Sample TH-PIN exhibited a larger slope in the range 0.25–1.0mm. Samples from Nea Anghialos (NA-samples) formed an S-like curve with 40% of the aggregates in the range 0.125–1.0mm.

There is a greater distinction between the constituents of different mortars in the range of 1mm and in the smaller fractions. A high content of aggregates larger than 1.0mm (sample TH-PIN) results in reduced workability, and the mixture requires more water, to ensure complete mixing. The presence of large aggregate fragments in the samples from Thebes, and the low amount of water, could be responsible for the poor mixing quality of mortar samples, as this was documented during microscopic examination.

4.2.3 Physical Properties

In addition to grain-size distribution, microstructure properties of different mortar mixtures have been measured, such as open porosity (%), total surface area, and apparent density. These results are summarised in Table 4.3.

Table 4.3: Mean values of microstructural properties of mortars determined by mercury porosimetry. Measurements were carried out in triplicate (n=3).

Sample	Pore radius range (nm)	Total surface area (m^2/g)	Apparent density (g/cc)	Open porosity (%)
NA-IV	2.21 – 4310.89	7.25 ± 0.21	2.08 ± 0.13	33.19 ± 2.92
NA-V		9.92 ± 0.32	2.23 ± 0.09	35.17 ± 2.29
NA-VI		10.06 ± 0.56	2.15 ± 0.12	21.04 ± 1.93
TH-KAD		22.27 ± 0.89	2.13 ± 0.07	30.8 ± 2.16
TH-KEB		12.79 ± 0.47	2.21 ± 0.09	28.12 ± 3.46
TH-PIN		19.19 ± 0.75	2.14 ± 0.10	25.46 ± 2.38

For the accurate evaluation of the results, the fact that the ceramic fragments present in the mortar are porous materials (and thus contribute to the total porosity) must be taken into account. Their contribution to the measured porosity in the samples is dependent upon the composition and the firing temperature of the ceramics. However, the values presented in Table 4.3 are useful for studying the deterioration mechanisms related to water absorption and the movement of aqueous solutions, as they contribute to the total open porosity.

Total open porosity values ranged from 21 to 35% by volume. These values are in accordance with those typical of the majority of historic lime mortars. Technological and micro-structural differences were more clearly seen in the pore-size distributions, given in Figures 4.27 and 4.28.

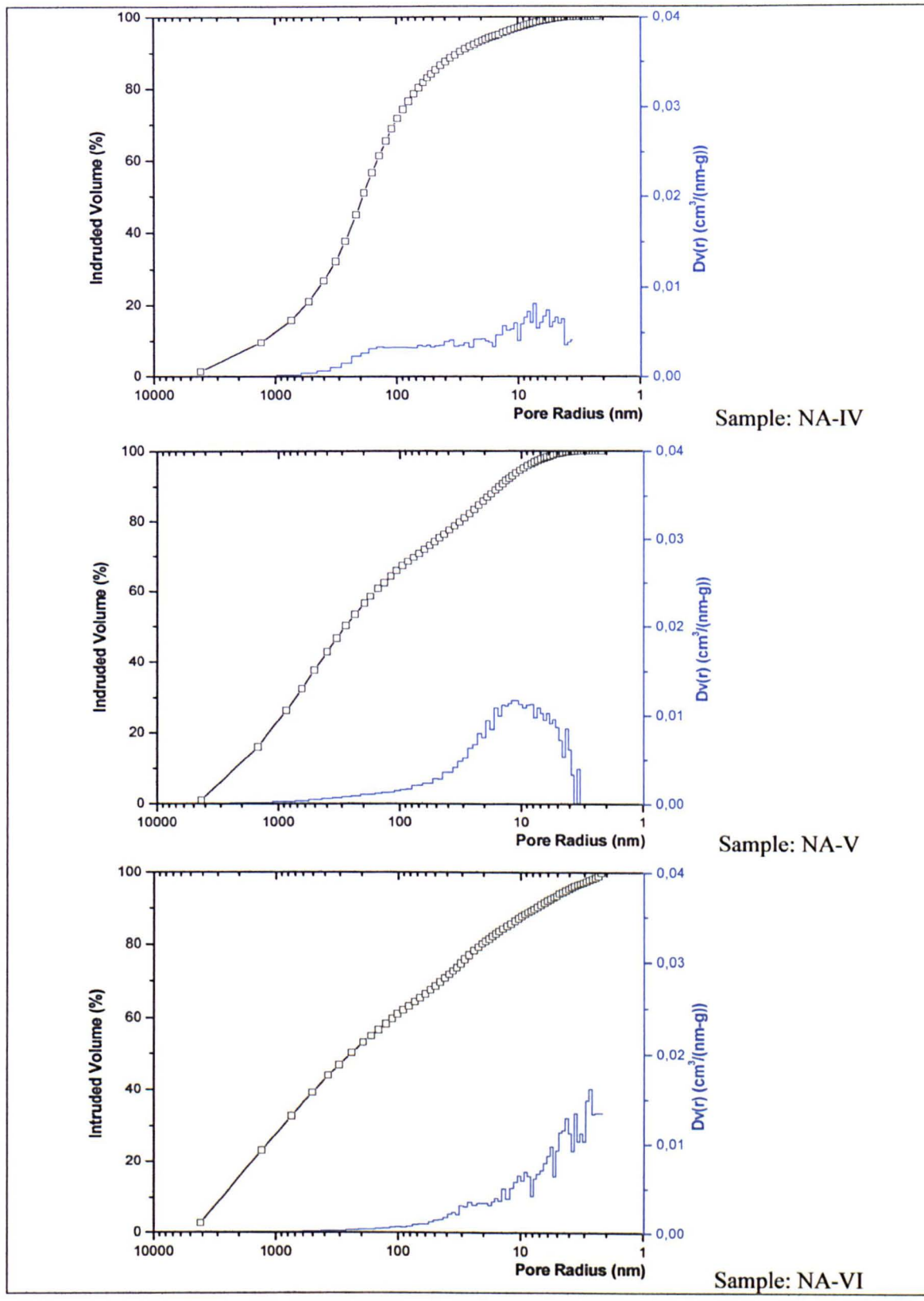

Figure 4.27: Representative graphs of mercury intrusion porosimetry measurements expressing the total intruded volume of mercury (%) and the pore-size distribution (Dv(r)) of the samples from Nea Anghialos.

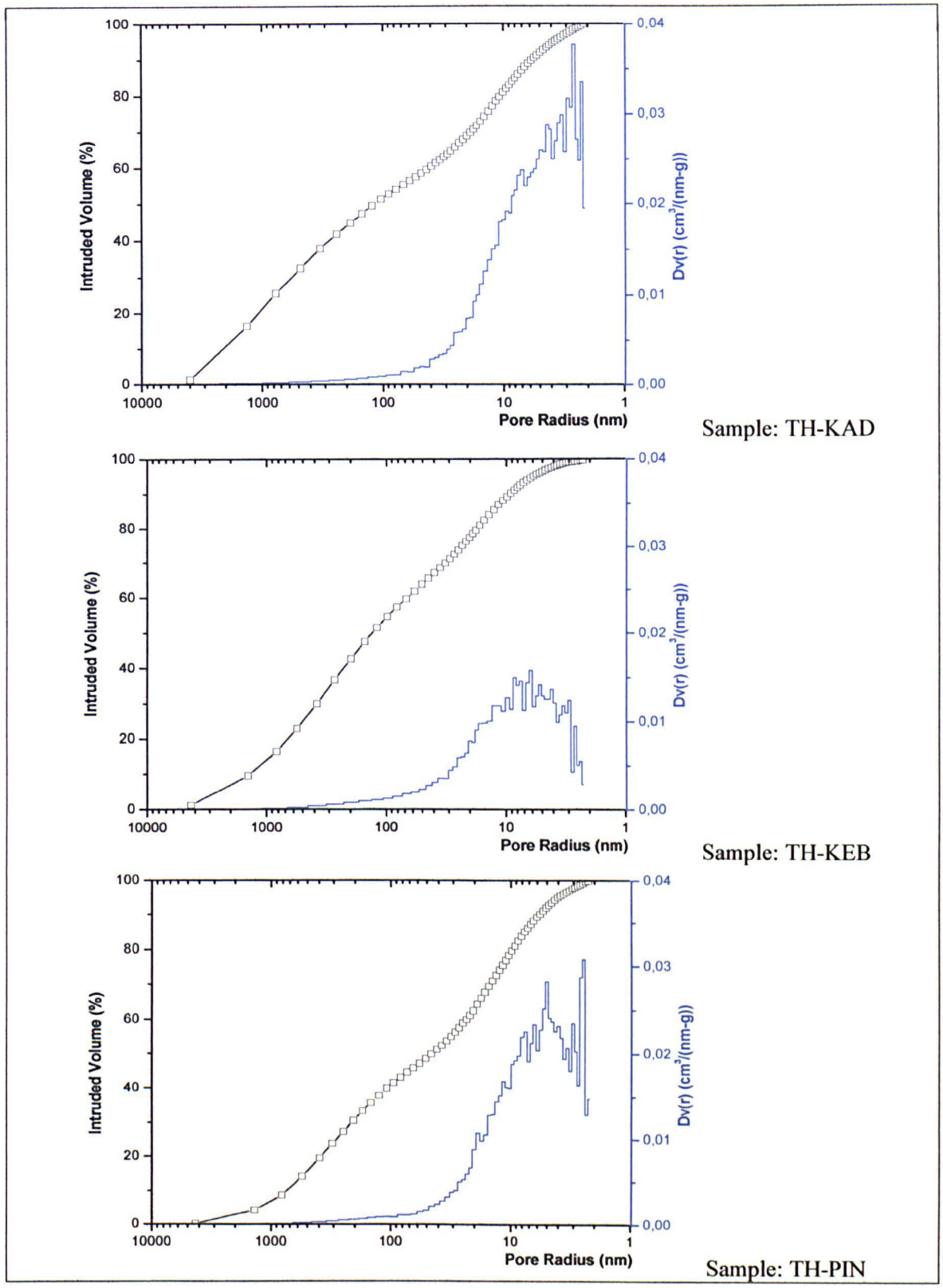

Figure 4.28: Representative graphs of mercury intrusion porosimetry measurements expressing the total intruded volume of mercury (%) and the pore-size distribution (Dv(r)) of the samples from Thebes.

4.2.4 Mineralogical and Chemical Analysis

From the results of the XRD analysis (Table 4.4 and Figure 4.29), it is evident that the binding material of the samples is calcitic, showing slight differences as far as aggregate fragments (quartz and plagioclase of various types) are concerned.

Table 4.4: Results of XRD analysis of the sample fractions less than 0.063mm: calcite (Cc), quartz (Qz), illite (Il), muscovite (Msc), albite (Alb), kaolonite (K), halite (H), and calcium silicate hydrate (CSH).

Sample	Cc	Qz	Il	Msc	Alb	CSH	K	H
NA-IV	****	***	**	**	*	-	*	*
NA-V	****	***	**	**	*	-	*	*
NA-VI	****	***	**	**	*	**	*	*
TH-KEB	****	***	**	**	*	-	*	-
TH-KAD	****	***	**	**	*	-	*	-
TH-PIN	****	***	**	**	*	-	*	-
**** very abundant		***abundant		** present		* traces		

In the XRD patterns (Figure 4.29), within the range 5–15°, there are some indications concerning the presence of hydrated, apparently amorphous, compounds (CAH, CSH), which give a cementitious character to the mortars. These amorphous compounds (calcium aluminate/silicate hydrate) are formed during the setting of mortars through a complicated chemical mechanism that involves the reaction of calcium ions with alumino-silicate phases of ceramic material. The formation of these hydraulic compounds is responsible for the essential properties of the mortars (Mishara, 1982).

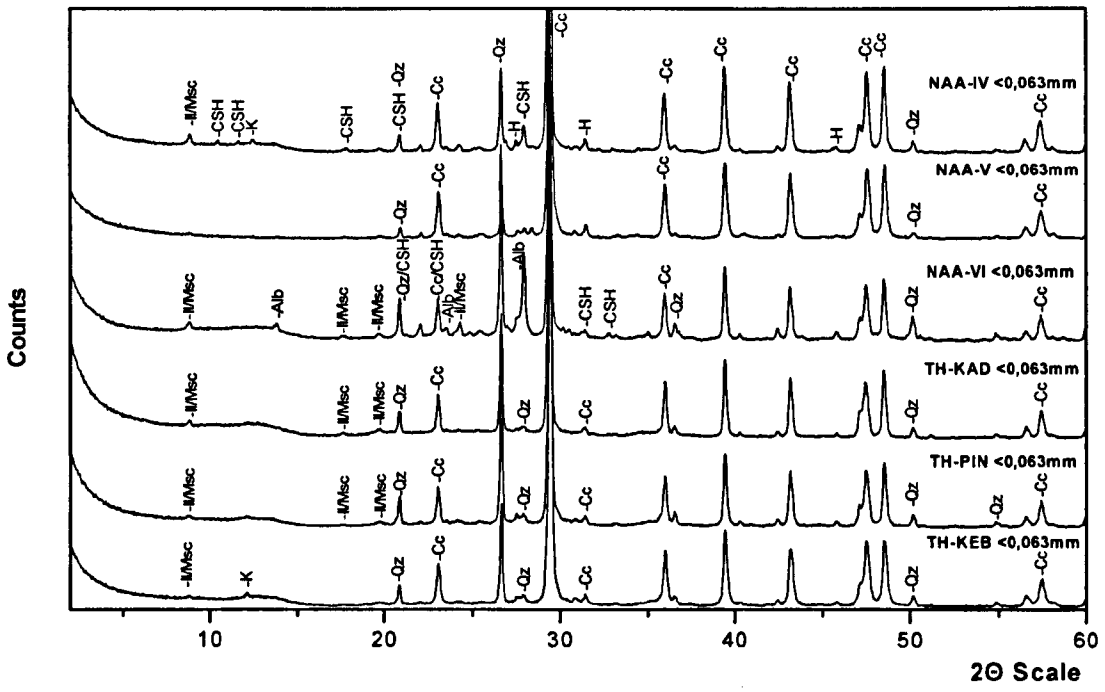

Figure 4.29: X-ray diffraction patterns corresponding to the cementing material fraction (<0.063 mm) of mortars.

The above results indicate that either interface reactions, between the lime and the finer fractions of ceramic, have occurred, or the origin of the lime is from argillaceous limestone.

The FT-IR analysis of the finest granulometric fraction (< 63μm) (Figure 4.30) indicates that the binding media is calcitic, as the peaks at 1430, 870, 780 and 720 cm^{-1} are attributed to CO_3^{2-} ($CaCO_3$) stretching and bending modes (Puertas et al, 1994). The peaks at 1170, 1084 and 798 cm^{-1} correspond to the vibration modes of SiO_4, whilst the band at 3400 cm^{-1} is attributed to water stretching vibration modes (Branda et al, 2000).

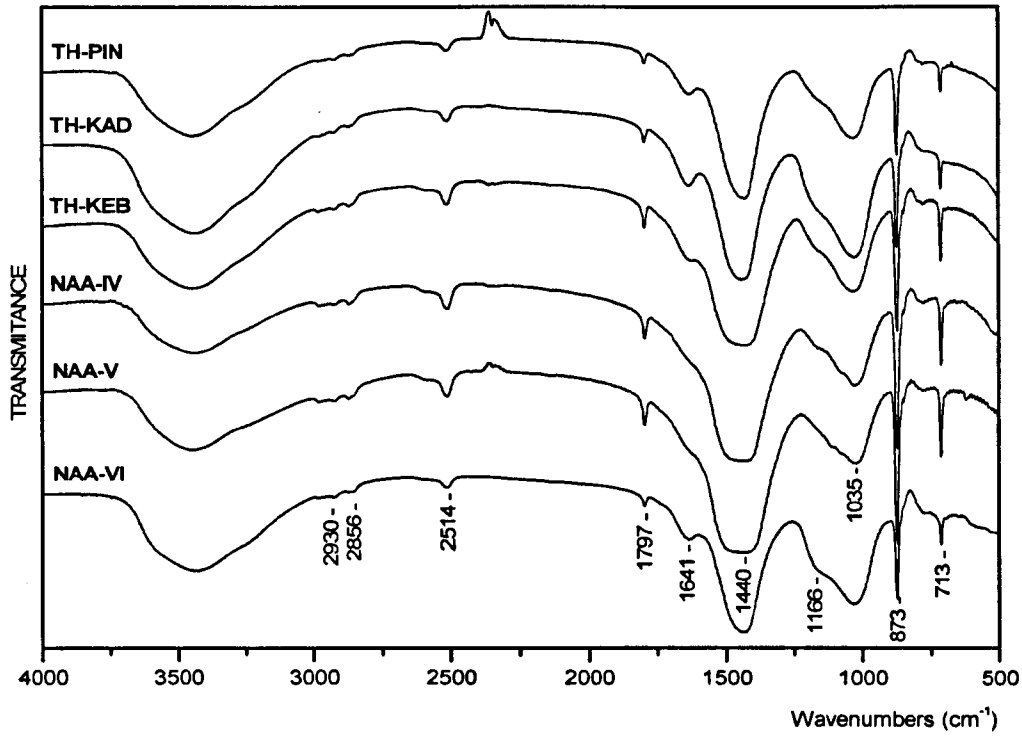

Figure 4.30: Infrared spectra corresponding to the cementing material fraction (<0.063 mm) of mortars.

The results of thermogravimetric analysis are presented in Table 4.5. Thermal analysis diagrams demonstrate a major peak between 760 °C and 820°C, indicating a weight loss (ranging from 18–28%) during the decomposition of calcite (Figure 4.31). Moreover, a weight loss between 1–2% was observed at about 80°C, due to the evaporation of the adsorbed water vapour (humidity).

Table 4.5: Weight loss of mortar samples during DSC/TGA analysis of the cementing material.

Sample	**Weight loss % per temperature range**					
Temp. (°C)	**<120**	**120–200**	**200–400**	**400–600**	**>600**	**total**
NA-IV	0.82	0.25	1.44	1.78	18.69	22.98
NA-V	0.91	0.80	1.82	4.01	28.96	36.48
NA-VI	1.91	1.59	1.74	2.08	16.75	24.07
TH-KAD	4.90	1.35	2.35	4.28	20.60	33.48
TH-KEB	1.25	0.60	1.20	2.76	25.48	31.29
TH-PIN	2.81	0.66	2.05	3.36	23.06	31.94

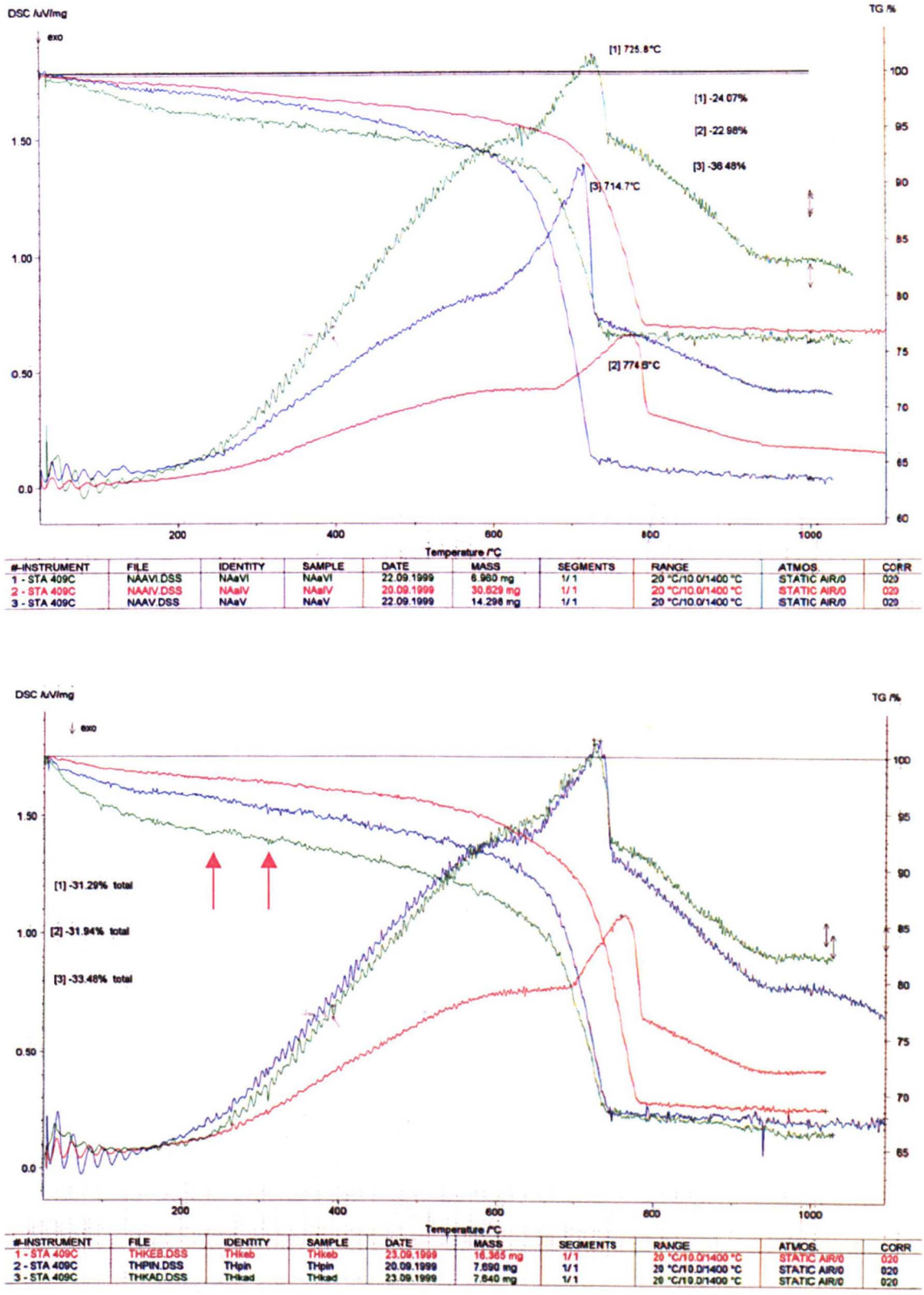

Figure 4.31: DSC/TG graphs of the cementing material fraction of mortars from Nea Anghialos (above) and Thebes (lower).

Chemical analysis by EDX (Table 4.6) has shown that the aggregate fraction within the mortars from Thebes consists of magnesian sandstone, which also contains some bioclastic inclusions. The aggregate fraction within the mortars from Nea Anghialos, the consists of alumino-silicate fragments. The analysis (line-scan) has been performed in areas of approximately 30X30μm, separately for binder medium and aggregate fragments.

Table 4.6: Chemical, semi-quantitative analysis of the mortar constituents by EDX.

Sample	Area	Elemental Analysis						
		Na	Mg	Al	Si	K	Ca	Fe
NA-IV	Binder	-	*	**	***	*	****	**
	Ceramic Fragments	-	*	**	****	**	***	***
	Natural aggregates	-	-	**	****	**	**	*
NA-V	Binder	-	*	**	***	*	****	**
	Ceramic Fragments	-	*	**	****	**	***	***
	Natural aggregates	-	-	**	****	**	**	*
NA-VI	Binder	-	*	**	***	*	****	**
	Ceramic Fragments	-	*	**	****	**	***	***
	Natural aggregates	-	-	**	****	**	**	*
TH-KAD	Binder	-	*	**	***	*	****	**
	Ceramic Fragments	-	**	***	****	**	***	**
	Natural aggregates	-	***	-	****	-	*	**
TH-KEB	Binder	-	*	*	***	-	****	**
	Ceramic Fragments	-	**	***	****	**	***	**
	Natural aggregates	-	***	-	****	-	*	**
TH-PIN	Binder	-	**	**	***	*	****	**
	Ceramic Fragments	*	**	***	****	**	**	**
	Natural aggregates	-	***	-	****	-	*	**
****** very abundant ***abundant ** present * traces**								

4.2.5 Mechanical Properties

The mechanical characteristics of historic mortars were studied by monitoring their deformability during continuous point loading (Vekinis and Kilikoglou, 1998). Load and displacement values were evaluated in order to produce a stress-strain diagram for each mortar. Diagrams are presented in Figures 4.32 and 4.33, grouped by provenance. Data provided from the above experimental procedure were mostly used to estimate the hardness of mortars and to better describe their mechanical behaviour and deformation.

Because the specimens prepared for the test had previously been mounted in resin, vertical deformation was limited. Horizontal deformation was affected by the population and the size of aggregates in contact with, and around, the steel ball. Therefore, it was decided not to calculate the modulus of elasticity (ε), but only to compare and describe the type of deformation. Stress-stain diagrams were described according to typical stress-strain curves of rocks in unconfined compression (Bell, 2000:231).

Curves of samples NA-IV and TH-PIN consisted of an initial part that is characterised by plastic deformation, followed by a straight-line behaviour, which is typical of brittle materials. Sample NA-VI presents a more brittle behaviour, characterised only by a straight line. Samples NA-V and TH-KAD are both quite soft, and exhibit a totally different behaviour. Sample NA-V presents a typical plastic deformation, characterised by a concave curve, whilst sample TH-KAD follows elastic-plastic behaviour. Similarly, the stress-strain curve of sample TH-KEB is characterised by three parts before failure, showing plastic-elastic-plastic deformation.

Plastic behaviour of mortar samples is caused by the compression of empty spaces between large pores, air voids and discontinuities. In contrast, a more brittle behaviour is typical of compact mixtures with enhanced strength, which usually contains pores of smaller diameter.

Plastic deformation in the initial part of stress-strain curves due to the bedding of the instrument has not been considered in the fracture mode characterisation.

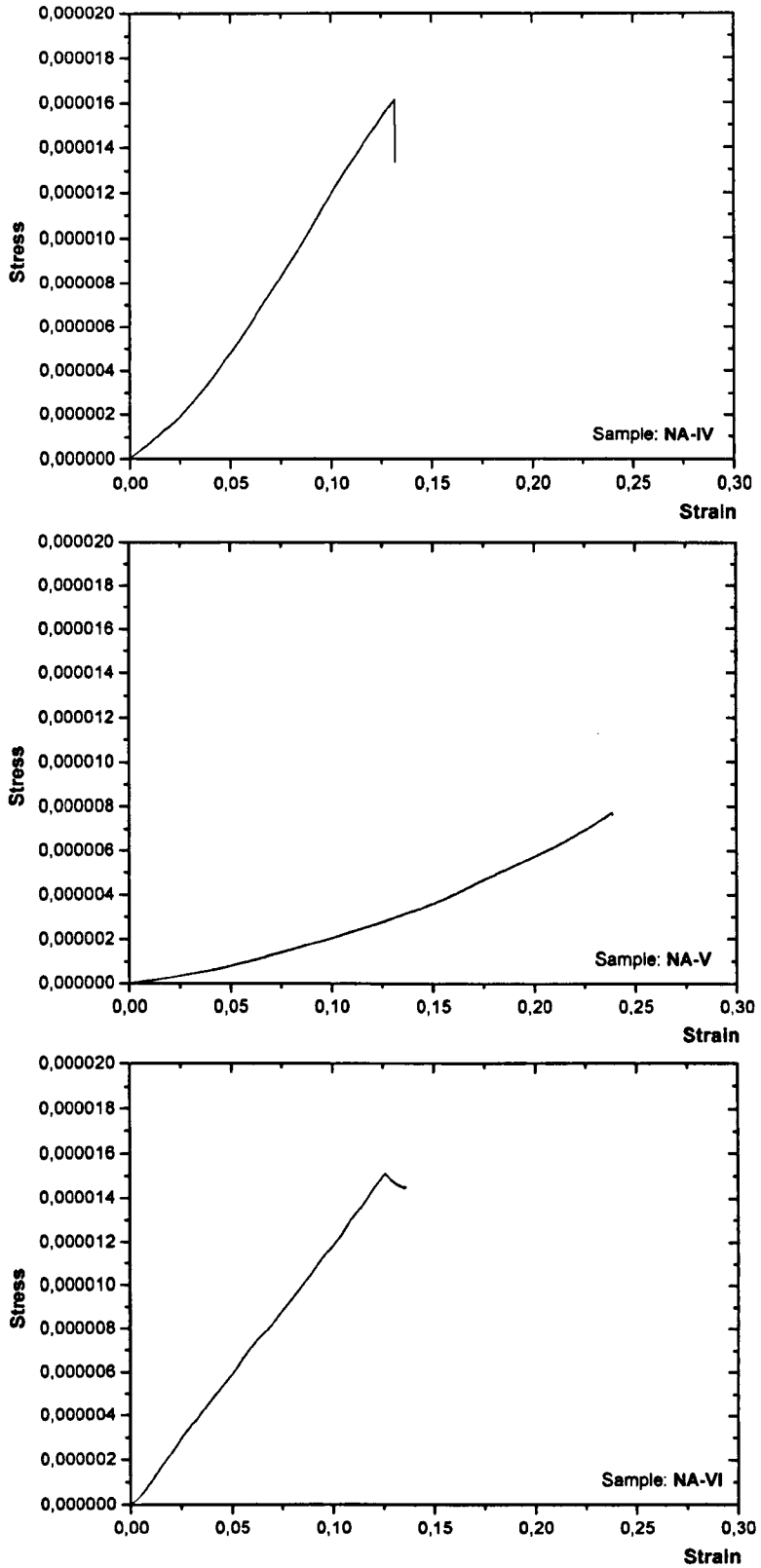

Figure 4.32: Stress-strain curves of NA-samples under continuous point loading.

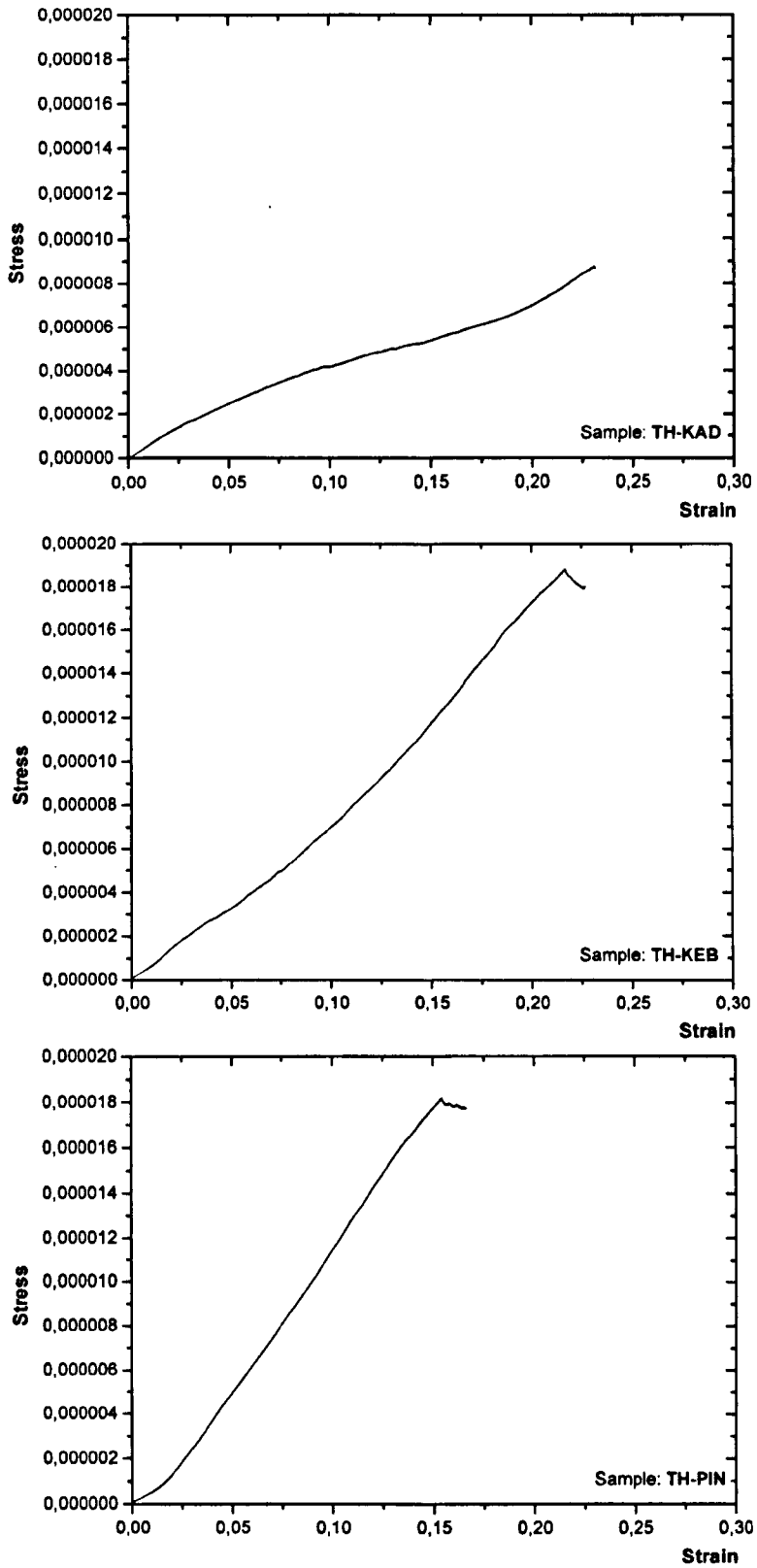

Figure 4.33: Stress-strain curves of TH-samples under continuous point loading.

4.3 DISCUSSION

4.3.1 Production Technology

Floor mosaics from both Nea Anghialos and Thebes were excavated at the ruins of the Byzantine cities of 'Fthiotides Thebes' in Magnesia, and 'Thebes' in Biotia. Both cities were destroyed by earthquakes in the Byzantine period. The mosaic pavements were buried under the ruins of buildings and covered with soil. From the analysis of the mortar samples, it seems that the bedding layer of the mosaic tesserae has not suffered any deterioration: the only damage that has occurred is the fragmentation of the pavements due to ground instability and the mechanical forces applied during burial.

The quality of the mortar reflects both the performance requirements and the importance of the monument on which they were used. This is clear in the case of Nea Anghialos, where the quality of floor mosaics improved between the forth and sixth centuries: the geometric motifs gave place to floral and animal designs, whilst the size of the tesserae was reduced from 2cm to 0.5mm (Ntina, 1990b). Consequently, the maximum grain size of the mortars was reduced from 6mm to 3mm diameter. This fact, together with the addition of a larger amount of ceramic fragments of less than 0.125mm diameter (Figure 4.26), and the use of smaller aggregates in general, resulted in the production of a mixture with better workability characteristics. The same technological evolution is not observed in the mosaic pavements from Thebes. The mosaics remained in geometric motifs with large stone tesserae, while the mortars contain more coarse aggregates (Table 4.2).

The analysis of the mortar samples gave information about the type of raw materials used, the size of aggregates, the compactness of the different mixtures, and their microstructure and preservation condition. From the evaluation of the analytical data, and from the examination of the samples under the polarising microscope, it was determined that there were no significant differences in the binder/aggregate ratio

between the different mixtures. The majority of samples contain a sufficient quantity of binder, with a binder/aggregate ratio of between 1:3 and 1:4 by volume.

The binding material of all of the samples was hydrated lime, which was mixed with fine- to medium-grained ceramic fragments. The aggregate fraction contained natural aggregates along with crushed ceramic fragments. The natural aggregates in the NA-mixtures consisted mostly of rounded-shape siliceous rock fragments, and some small fragments of calcareous limestone. The ceramic fragments were fired around 900°C and had low calcium (Ca) content. The natural aggregates of the TH-mixtures consisted of angular limestone fragments, containing random bioclastic fragments. Both limestone and ceramic fragments from Thebes showed a high magnesium (Mg) content (Table 4.6). The constant presence of a high concentration of magnesium in the ceramic and limestone aggregates of mixtures from Thebes (Table 4.6), in contrast to those of Nea Anghialos, supports the theory that the production of mortars was related to the availability and the type of local (or at least regional) raw materials (Dunbabin, 1999:280). Further petrographic examination of the thin sections and their interpretation with the petrography of local limestones may provide more data about the sources of lime production.

Medium- to large-size lime lumps were distributed within the mortar mass of all samples. The presence of lime lumps is connected to the preparation process of the mixtures. Craftsmen used to produce the required lime from local limestones, close to their working site. The presence of lime lumps in mortars may be safely attributed to the use of poorly-slaked lime, containing relict material, and the poor mixing of the raw materials (Hughes et al., 2001). Finally, the elongated voids observed in the mortar mass were probably formed during the preparation process, due to inappropriate mixing.

The microscopic examination of mortar samples revealed the identification of some reaction areas between the lime binder and the ceramic surface (Figure 4.34). These compact areas are attributed to calcium silicate formation at the interface between the brick fragment and lime. The formation of these areas is controlled by the dissolution of the siliceous phases in the aqueous solution that lead to the formation of the hydrated

phases of alumino-silicates (Gregerova and Pospisil, 2001; Moropoulou et al., 2004b). The surface of the ceramic fragments acts as the silicate source membrane, while the lime, which makes the interfacial surface alkaline, activates the hydraulic reactions (Moropoulou et al., 1998). The relevant reactions are described in detail in section 2.2.3.

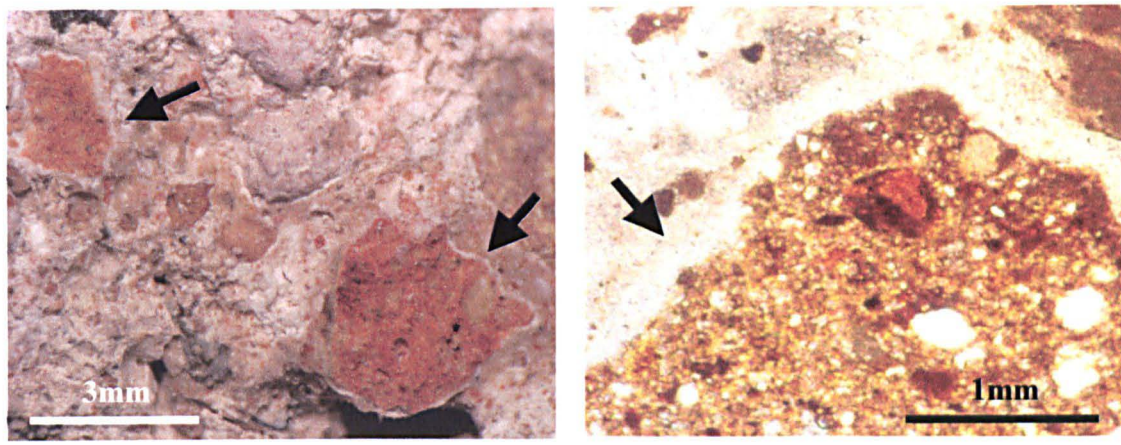

Figure 4.34: Reaction rims formed around the ceramic fragments indicating pozzolanic reactions. Photomicrographs of a freshly fractured surface of TH-KEB (left) under the stereomicroscope and thin-section of TH-KAD under the petrographic microscope (XPL).

The formation of calcium silicate is described schematically in Figure 4.35.

In an alkaline solution, the hydroxyl ions rapidly destroy the Si–O–Si bonds of the clay minerals present at the surface of ceramics fragments (Equation 4.1), putting all the compounds into solution (Verita, 2000).

$$\equiv Si–O–Si\equiv + OH^- \rightarrow \equiv Si–OH + O^-–Si\equiv \qquad \text{(congruent dissolution)} \qquad (4.1)$$

In this case, the alkaline solution can penetrate the ceramic body and continues to react, undisturbed. The amorphous, silica-rich mixture, so produced reacts with calcium hydrate to form the calcium silicate hydrate (CSH). The addition of small fragments of low-temperature ceramics makes the reaction between the lime and ceramic easier, and

leads to the formation of hydraulic phases in the binder (Charola and Henriques, 1999; Teutonico et al., 1999). The increased amount of hydraulic phases in the binder causes an increase in the compressive strength of the mortar.

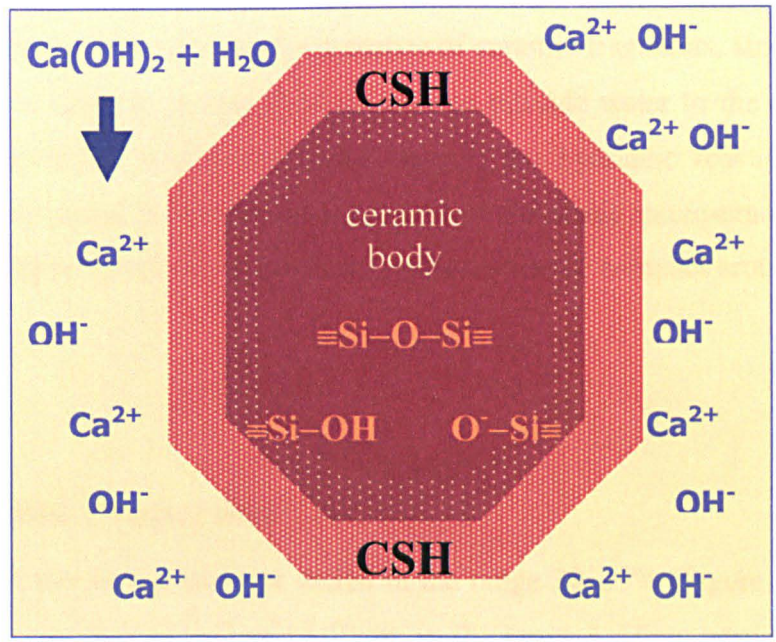

Figure 4.35: Schematic representation of the alteration and dissolution of the siliceous phases in the aqueous solution that lead to the formation of the hydrated phases of alumino-silicates.

The identification of the hydrated, apparently amorphous, compounds was achieved through XRD and DTA/TG analysis of the binder fraction. The identification of these phases is quite difficult even in fresh, laboratory-produced, mixtures (Charola and Henriques, 1999). However, the diffraction pattern of sample NA-VI showed peaks between 20° and 35° that may be attributed to the presence of CSH phases (Figure 4.29). Moreover, TG analysis of samples NA-VI and TH-KAD resulted in two small peaks in the range of 120–200°C (Figure 4.31), corresponding to weight loss of around 1.5% (Table 4.5). These are attributed to the presence of calcium silicate hydrate (CSH) (Moropoulou et al., 2004a).

The limited amount of hydraulic phases in the binder fraction is mainly attributed to the small amount of pozzolanic material present in the lime binder (<10%), and also to the rapid drying of the mixtures (due to the local climatic conditions): the fast evaporation of water blocks the hydraulic reactions that require an alkaline environment. Additionally, the reactions favour the presence of ceramic fragments, since their greater water absorption capacity means they are able to provide water to the ceramic-binder interface for a longer period, and hence support the hydraulic reactions. The latter assumption may partially explain the formation of shrinkage micro-cracks close to the siliceous aggregates, while the mortar mass appeared more compact around the ceramic fragments.

4.3.2 Physical Properties

The porosity of the mosaic mortars varied in the range 20–35% (Figure 4.36), with the majority of their pore volume around 10nm, in the range 3–50nm pore radius (Figures 4.27 and 4.28). Sample NA-IV had pores of up to 300nm radius, whilst samples TH-PIN and NAA-VI showed values similar to modern cement-lime mortars (in general 20–25% by volume). The other mortars had porosities similar to typical historic lime mortars in the range of 30–45% by volume (Schafer and Hilsdorf, 1993). However, it must be noted that the above values were limited to the measuring range of the mercury porosimeter, which measured pore radii of only 2.21–4310.89nm.

Differences between mortar samples were closely related to the production technology of the mortars, such as binder/aggregate ratio, water content, and aggregate type and size.

The differences in porosity observed between different mixtures could be attributed to the mixing parameters, such as binder/aggregate ratio, water content, aggregate type and size (Maurenbrecher et al., 2001; Henriques et al., 2004). From the grain-size distribution graphs (Figure 4.37) it is apparent that the different mixtures show very similar patterns and only exhibit significant differences in the aggregate fraction of maximum size above 0.5mm.

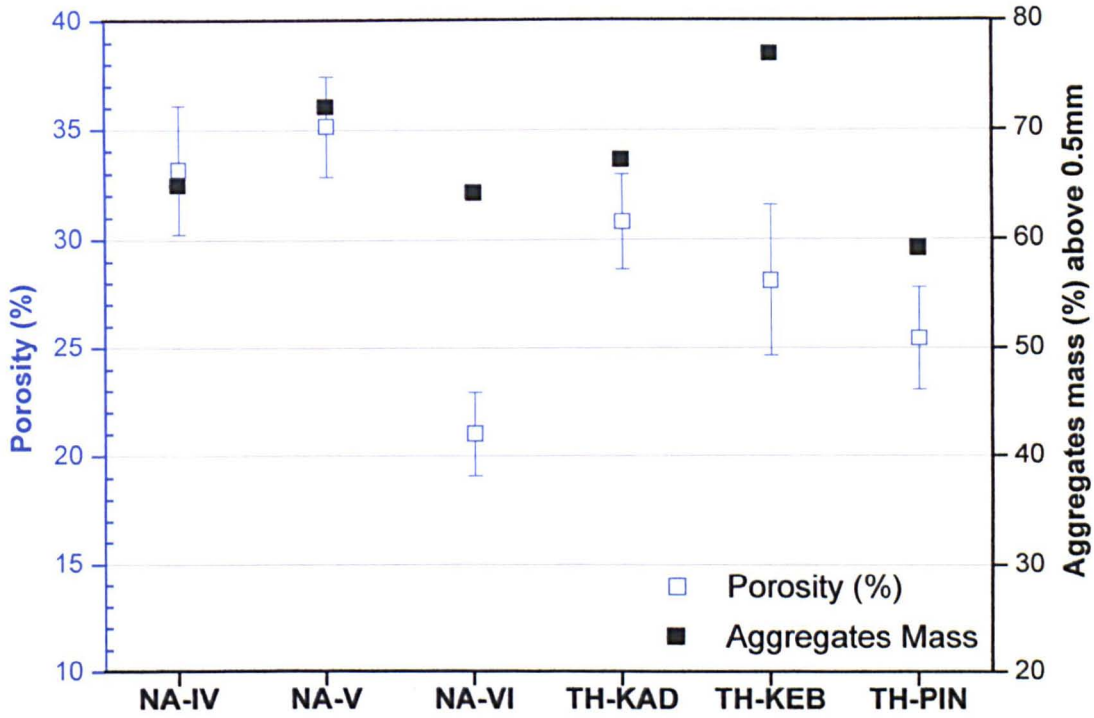

Figure 4.36: Total porosity values in comparison to the amount (%) of aggregates of diameter > 0.5mm (black marks).

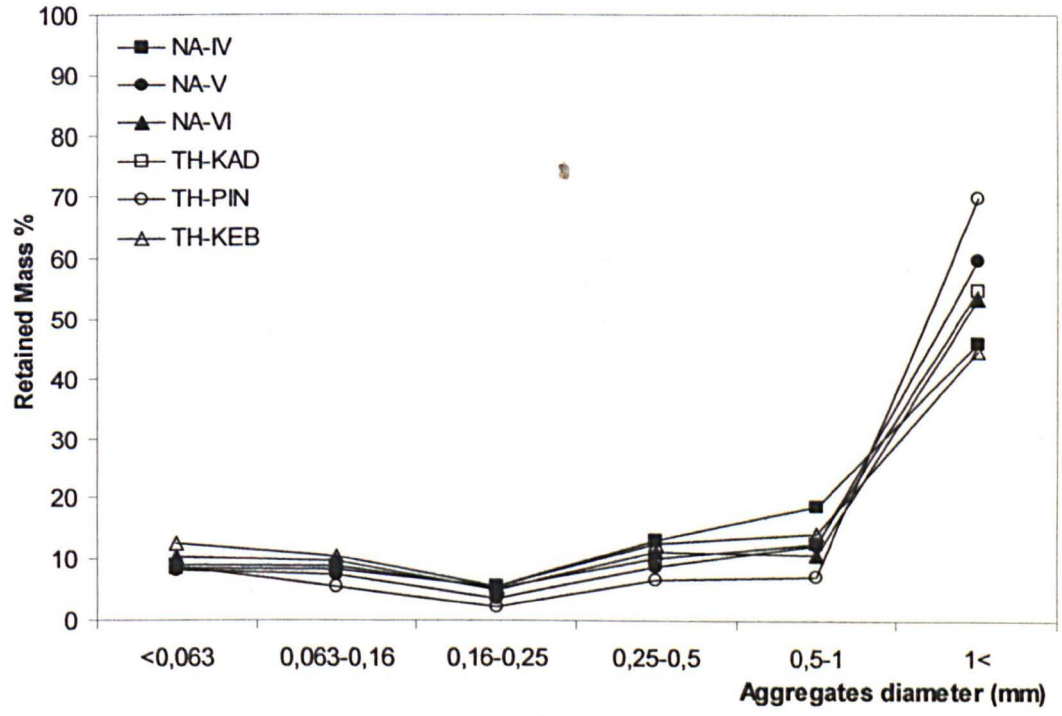

Figure 4.37: Grain-size distribution of aggregates present in the mosaic mortars.

Therefore, it could be assumed that differences in porosity were due to the grain-size distribution of the different mixtures. However, by plotting the amount of large aggregates (expressed as a mass percentage) together with the porosity, it is clear that there is no correlation between the two.

The observed differences in the pore-space structure and porosity could be related to the type of aggregate present in the mortar, and especially to the amount and microstructure of the ceramic fragments. The ceramics have a considerable amount of pore volume which is accessible by both mercury intrusion porosimetry and water.

The pore-space characteristics determined by mercury porosimetry arise from both the microstructure produced in the binder matrix during the evaporation of water and the carbonation process, and the aggregates present. Pores formed due to the partial dissolution of the binding material, shrinkage and mechanical stresses will also contribute to the measured pore volume (Fitzner, 1993) and should be taken into consideration.

In a simplified model, micro-porosity ($r<3.7nm$) and meso-porosity ($3.7nm<r<150\mu m$) are related to capillary rise phenomena (water and salt transportation) and durability of the mortar, while macro-porosity ($r>150\mu m$) is mainly related to the mechanical properties (Barsottelli et al., 1998; Meng, 1993). The mortar samples analysed were shown to have a great amount of capillary pores (Figures 4.27 and 4.28) and therefore are very susceptible to water. Sample NA-IV was shown to have a considerable amount of pores in the meso- to macro-pore range (Figure 4.27).

Microscopic examination of thin-sections of the mortars revealed that all samples contained a large amount of coarse and medium macro-pores.

4.3.3 Mechanical Behaviour

The determination of compressive and flexural strength of mosaic mortars with standard laboratory tests was not possible because of the limited quantity and volume of the

available samples. The mortar samples were classified according to the resistance that they exhibited against fracture by hand, and their modulus of elasticity (Table 4.7).

Table 4.7: Classification of mosaic mortars according to their strength characteristics. Values correspond to the mean of three measurements (n=3).

Sample	Strength estimation	Max. Load (N)	Elasticity (Stress/Strain) N ($x10^{-4}$)
NA-IV	Medium	3550 ± 155	1.28 ± 0.06
NA-V	Low	1487 ± 203	0.32 ± 0.06
NA-VI	High	3640 ± 180	1.25 ± 0.05
TH-KAD	Medium	1990 ± 118	0.30 ± 0.07
TH-KEB	High	4000 ± 190	0.85 ± 0.06
TH-PIN	Very high	4080 ± 185	1.28 ± 0.05

The modulus of elasticity is a very useful characteristic for understanding the mechanical performance of the mortar, and for comparing different materials. The slope of the stress/strain curve expresses the resistance of the material to deformation, and is a good tool for characterising a mixture as either weak or strong (Schafer and Hilsdorf, 1993).

The deformability of mortar depends upon the strength characteristics of its constituents. During continuous loading, through a steel ball on the polished surface of the mortar, the load is transferred from the harder constituents (i.e. siliceous aggregates, limestone and ceramic fragments) to the weaker lime binder. The binder is then compressed, the pore space is destroyed, and air voids and discontinuities are compacted. The specimen fails when there is no further empty space in the binder to be compacted. The shape and the slope of the stress/strain curves (Figures 4.32 and 4.33) are therefore related to the amount of binder available between aggregate particles and the extent of compactness.

The weaker, and more porous, samples result in a flatter slope (samples NA-V and Th-KAD), which is typical of high deformability.

The modulus of elasticity measurements show that the mosaic mortars fall roughly into two groups – the weak group, containing samples NA-V and TH-KAD with elasticity values around 0.30×10^{-4}N; and a more brittle group with elasticity values around 1.25×10^{-4}N.

4.4 CONCLUSIONS

From the analysis of the original mosaic mortars from Thebes and Nea Anghialos, it was determined that there were no significant differences in the binder/aggregate ratio between the different mixtures. The majority of samples contained a sufficient quantity of binder, with a binder/aggregate ratio of between 1:3 and 1:4 by volume. The binding material in all mixtures was hydrated lime, which was mixed with fine-grained ceramic powder. The fraction of aggregates contained both natural aggregates and crushed ceramic fragments. The presence of lime lumps in their matrix was connected to the preparation process of the mixtures and may be safely attributed to both the use of poorly-slaked lime containing relict material, and poor mixing.

The study of original mosaic mortars showed that, historically, mortars were produced from local raw materials. The quality of the mortar was depended on the availability and quality of the raw materials, the importance of the building/monument, and their use and performance requirements. Mortars of the same period, and made for the same use, presented similar composition and mix proportions.

The analysis of the mortars should be regarded on the basis of developing a methodology which was able to provide answers on specific archaeological, technological and conservation questions, along with information concerning the durability and the deterioration mechanisms of historic mortars.

Special care must be given to the sampling procedure, in order to obtain reliable and representative results. It has been found that the majority of answers to the above questions can be provided by microscopic examination under petrographic and scanning electron microscope, mineralogical analysis of both the binder and aggregates, and the determination of the binder/aggregate ratio (by weight) and grain-size distribution.

5 EXPERIMENTAL

5.1 STUDY OF BARIUM HYDROXIDE MORTARS

The experimental procedure followed to assess the effect of barium hydroxide on the durability of different mortar mixtures against sulphate action, is described in this chapter.

The project focuses on the effect of barium hydroxide, as an additive material, to both the physicochemical properties and the durability of conservation mortars against sulphate solutions. Therefore, compatibility and durability (in terms of performance characteristics) are regarded between barium mixtures and a reference, lime-mixture.

The mixtures prepared were not based on the analytical results of mosaic mortars. The laboratory mixtures were synthesised based on the directives described in British standards for testing cement (BS EN 196, 1995). Only the types of raw materials used in laboratory mixtures were selected according to those identified in mosaic mortars.

In order to study and evaluate new synthesized mortar mixtures, a number of laboratory tests and experiments need to be carried out to determine their physicochemical properties, evaluate their durability against different decay agents, and determine their applicability in the field (BS 4551, 1998a,b). During the development of the methodology, the requirements for the preparation of mortar samples to be tested, and the tests to be performed were taken into account in order to select test procedures applicable to the study of lime-based mortars (Charola and Henriques, 1998).

As the proposed repair mortars must be reproducible, special care is needed to ensure compatibility to other structural units, preparation instructions and application procedure directives (Holmstrom, 1981; Bouineau, 1981; Zacharopoulou, 1998).

The methodology followed is based on the standard test methods described in the British Standards and other tests, which have been used in similar research and experimental projects. Moreover, a modified testing procedure was developed aiming to estimate the performance and durability of different mortar mixtures.

In this project, durability of mortars is considered to be their relative resistance to degradation and especially to the deterioration caused by the attack of sulphate solutions, i.e. crystallization of soluble salts, dissolution and leaching out of the binding material.

Both binary pastes and mortar mixtures containing different portions of barium hydroxide have been prepared for studying the effect of barium hydroxide on conservation mortars. Their physicochemical properties and durability were compared to those of a reference mixture that did not contain any barium hydroxide.

Quality control of raw materials to be used was carried out in a preliminary cycle, where, additionally, a number of parameters that control the performance of the new synthesized mortars such as workability, formation of setting products, microstructure, internal cohesion, movement of water solutions and weathering resistance have also been measured.

Durability of mortars was focused on sulphate action and was carried out through the monitoring of their behaviour during crystallisation of soluble salts tests, electrochemically accelerated degradation, sulphate fixation ability and resistance on the leaching of their cementing material. The results have been considered along with the physical properties of the mortars that also influence their durability.

5.2 QUALITY CONTROL OF RAW MATERIALS

The raw materials selected for preparing mortar mixtures consisted of: a) calcium hydroxide [$Ca(OH)_2$]; b) barium hydroxide octahydrate [$Ba(OH)_2 \cdot 8H_2O$]; c) medium fraction of ceramic fragments containing granules of diameter 0.125–2mm and; d) calcitic sand containing fragments in the range of 0.125–2mm.

The selection of the raw materials was based on the type of materials originally used in the mosaic mortars analysed, as well as on the majority of Roman and Byzantine mortars and plasters.

Calcium hydroxide and barium hydroxide were pure chemical products, provided by FLUKA and MERCK, respectively. Calcitic sand and ceramic fragments were commercially available materials and were obtained from local builders' supply firms in Greece.

Laboratory-prepared lime putty from the chemical $Ca(OH)_2$ powder was chosen, rather than hydrated lime powder or commercially-available lime putty, in order to ensure lime quality, be in accordance with traditional craft-persons practice and provide greater repeatability of future experimental tests and field applications.

Hydrated lime (calcium hydroxide) powder, from different manufacturers, usually has different bulk densities due to variation in particle size. This leads to different weights of lime being added when volume batching and hence, mortars with different proportions (Maurenbrecher et al., 2001). The particle size of hydrated lime powder also influences workability, porosity and the long-term strength of the produced mortars as it is closely related to the amount of water required (Rodriguez-Navarro et al., 1998; Cazzalla et al., 2000).

Lime putty, on the other hand, usually contains more lime than an equivalent volume of dry hydrated lime. This amount also varies in commercial limes produced by different manufacturers in the range of 10–50% (Phillips, 1994; Maurenbrecher et al., 2000).

Moreover, commercial lime putty is matured (storing slaked lime under excess water) for different lengths of time. This has been shown to strongly affect the quality of lime-based mortars (Ashurst, 1990:79). Upon aging, portlandite crystals undergo a considerable crystal size reduction, with the generation of plate-like, nanometer-scale, portlandite crystals that contribute to an overall surface area increase. These changes explain the reported increase in plasticity, water retentivity, and workability of lime-putty-based mortars if they are compared with hydrated lime powder, or fresh lime putty (Rodriguez-Navarro et al., 1998; Elert et al., 2000).

In order to minimize factors that may result in differentiations of mortar properties in future reproduction, pure, chemical calcium hydroxide and barium hydroxide were mixed individually with equal portions of water in order to produce homogeneous fat putty. Hydrated lime powder was mixed with water in a ratio of 1:1 by weight, in order to produce fat putty, having specific weight between 1350–1400 kg/m^3. The mixture was placed in plastic containers, covered with 2 cm of deionised water, sealed and left to mature for a period of 3 months.

Chemical and mineralogical composition of all raw materials were studied in the solid (air-dried) state along with their microstructure. Chemical composition of raw materials studied together with their microstructure examination under SEM equipped with EDX. Additionally, the ceramic fraction was analysed with FT-IR spectroscopy in order to get more information about their chemical composition and structure (Russell, 1987:144). Micro-morphology of raw material fragments was also examined under stereomicroscope. Mineralogical composition was carried out by mean of XRD analysis in the range of 2–60° 2θ.

5.3 PREPARATION AND CURING OF TEST SPECIMENS

The test specimens studied were divided into two large groups:

i. Binary pastes, containing mixtures of lime putty with varying proportions of barium hydroxide ($Ba(OH)_2$) and water, as well as mixtures of each of these components with a very fine fraction (<0.063 mm) of calcium carbonate ($CaCO_3$) and ceramic powder; and

ii. Mortar mixtures, containing mixtures of lime putty with aggregates, barium hydroxide and water.

Based on the assumption that the role of the required binder in mortar mixtures is to fill the voids between aggregate grains (TAN 1, 2003:19; Hayen et al., 2001), it was chosen to present all mix proportions for Binary pastes and Mortar mixtures in terms of volumes. However, all laboratory specimens were prepared by weighting the required amounts of raw materials. The specific weight of raw materials is given in Table 5.1.

Curing conditions were based on the directives described in BS standards (196-1, 1995) for testing lime mortars. Storage periods were modified in order to be able to de-mould the specimens without causing any damage to them (plastic deformations, cracking).

Table 5.1: Specific weight values of raw materials used in Binary pastes and Mortar mixtures.

Raw Materials	Symbol	Specific weight (Kg/m^3)
Lime putty	CaH	1400
Barium hydroxide	BaH	1360
Fraction of Aggregates	Aggr	2350
Fine calcium carbonate powder	Cc	1760
Fine ceramic powder	Cer	1620

5.3.1 Binary Pastes

The paste mixtures were prepared initially in order to:

i. Determine the optimum amount of barium hydroxide that could be added to mortars; and
ii. Study the new products formed during the setting and hardening of the lime binder, containing different amounts of barium hydroxide.

Moreover, the potential ability of barium hydroxide to act as a binding material on its own was investigated by preparing a set of different binary mixtures of barium hydroxide with ceramic and calcium carbonate powder.

The binary pastes prepared, together with their mix proportions, are given in Table 5.2.

Cubic (50mm X 50mm X 50mm) and cylindrical shape specimens of 60mm height and 30mm diameter were prepared. The specimens were initially stored inside a polyethylene box at a temperature of 20°C ± 2°C and relative humidity of 90% ± 5%. The specimens were removed from the moulds and the box after 7 days, placed on a thick plastic grid and stored for further curing at a temperature of 20°C ± 2°C and relative humidity of 65% ± 5% for a period of 28 days. After this period, the specimens were removed from the moulds and stored in the laboratory room, at a temperature of 20°C ± 2°C and relative humidity of 50% ± 5%.

The relative humidity inside the polyethylene box was fixed and controlled by a saturated solution of potassium nitrate (KNO_3) and ammonium nitrate (NH_4NO_3). Their equilibrium relative humidities (ERH) at 20°C are 94% and 66%, respectively.

Table 5.2: Mix proportions, expressed in parts per volume, of binary pastes, prepared by mixing barium hydroxide (Ba), with lime putty (Ca), fine calcium carbonate (Cc) and ceramic (Cer) powder in different portions.

No	Mixture Code Name	Mix Proportions by volume				Water:binder ratio	Amount (%) of binder being replaced
		CaH	BaH	Cc	Cer		
1	Ca	1	-	-	-	0.5	0
2	Ca3Ba1	3	1	-	-	0.5	25
3	Ca2Ba2	1	1	-	-	0.5	50
4	Ca1Ba3	1	3	-	-	0.5	75
5	Ba	-	1	-	-	0.5	100
6	BaCc10	-	9	1	-	0.5	10
7	BaCc25	-	3	1	-	0.5	25
8	BaCc50	-	1	1	-	0.5	50
9	BaCer10	-	9	-	1	0.5	10
10	BaCer25	-	3	-	1	0.5	25
11	BaCer50	-	1	-	1	0.5	50

5.3.2 Mortar Mixtures

Mortar mixtures were prepared after evaluation of the results obtained from both the analysis of the original mosaic mortars and the study of the binary pastes. Careful consideration was given to the critical parameters that control the physical and mechanical properties of mortars, such as the binder:aggregate ratio, the maximum aggregates size and their grain-size distribution, the water:binder ratio, along with the maximum amount and particle size of barium hydroxide that could be added to mortars without causing any defect to their microstructure or internal cohesion.

Type and gradation of aggregates

Two different types of aggregates were used for the production of mortar mixtures:

i. Calcitic sand and;
ii. Medium fraction (0.125–2.00 mm) of ceramic fragments.

Separate fractions of the aggregates were mixed individually in a ratio of 1:1 by volume. The grain-size distribution of the aggregates is given in Figure 5.1. The distribution chosen is based on the recommendations proposed by BS EN 196-1 standard (1995) but, it has been slightly modified due to the analytical results of the original mosaic mortars.

Binder:aggregate ratio

The optimum amount of binder for the granular distribution of aggregates given above, can be calculated on the assumption that the binder should completely fill the voids between aggregate grains (TAN 1, 2003:19; Hayen et al., 2001). The amount of required binder was determined by means of the density of the lime putty and the volumetric porosity of the sand skeleton. The volume of air voids between aggregate grains was determined by calculating the water volume required to fill a cylinder that contains 1L of water-saturated aggregates.

The calculated binder:aggregate ratio ranged from 1:2.95–1:3.1 by volume. The ratio finally chosen was 1:3 for practical reasons.

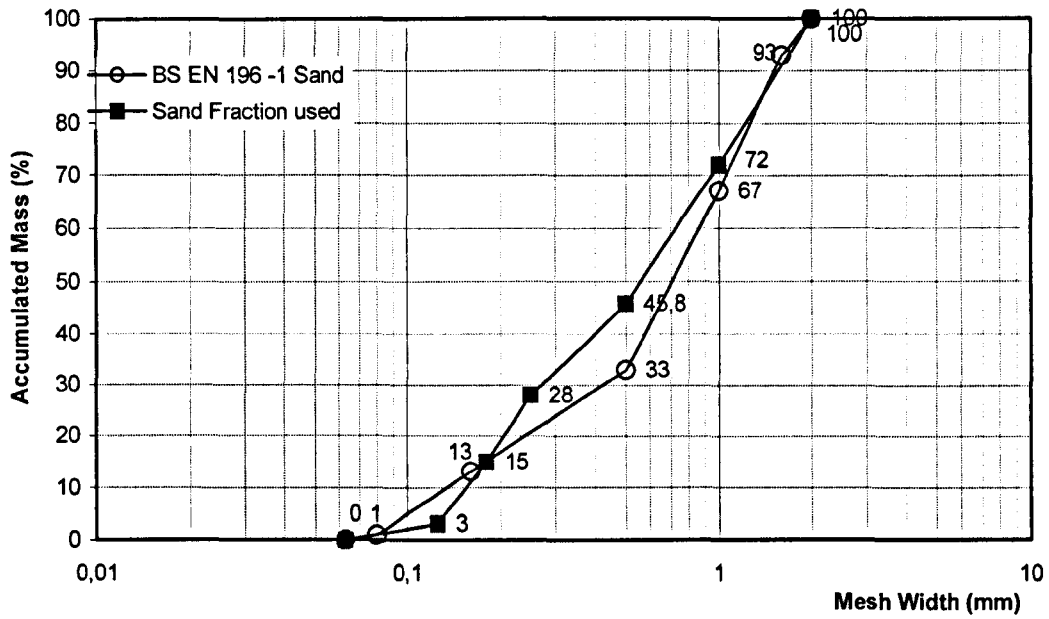

Figure 5.1: Grain-size distribution of aggregates used in the mortar mixtures. Each fraction consists of calcitic sand and ceramic fragments mixed in a ratio of 1:1 by volume.

Water:binder ratio

The amount of water added to the mixture of binder and aggregates strongly affects the consistency of freshly mixed mortars as well as those properties that are used to characterise them after setting (e.g. porosity, pore-size distribution, compression and flexural strength). The optimum amount of water required for the mixtures was determined through the measurement of the consistency of three different fresh mortar mixtures (LM-01, LM-02 and LM-03) containing different amounts of water, by flow test (BS EN 1015-3, 1999) (See Table 5.3).

Consistency is a measure of the fluidity and/or wetness of the fresh mortar and gives a measure of the deformability of the freshly mixed mortar when subjected to a certain type of stress.

The binder in all the above mixtures was pure hydrated lime putty.

Table 5.3: Flow values of mixtures of the same mix proportions containing different amounts of water, according to the procedure described in BS EN 1015-3 (1999).

MIXTURE	Aggregates		Binder	Binder: aggregate ratio	Water: binder ratio	Flow value (mm)
	Calcitic sand	Ceramic fragments				
LM-01	1	1	Lime	1/3	0.40	155±9
LM-02	1	1	Lime	1/3	0.80	>250
LM-03	1	1	Lime	1/3	0.55	200±15

The flow value was measured by the mean diameter of a test sample of the fresh mortar, which was placed on a defined flow table disk (Figure 5.2) by means of a defined mould and given a number of vertical impacts by raising the flow table and allowing it to fall freely through a given height (BS EN 1015-3, 1999). The mean flow values of each mixture are presented in Table 5.3.

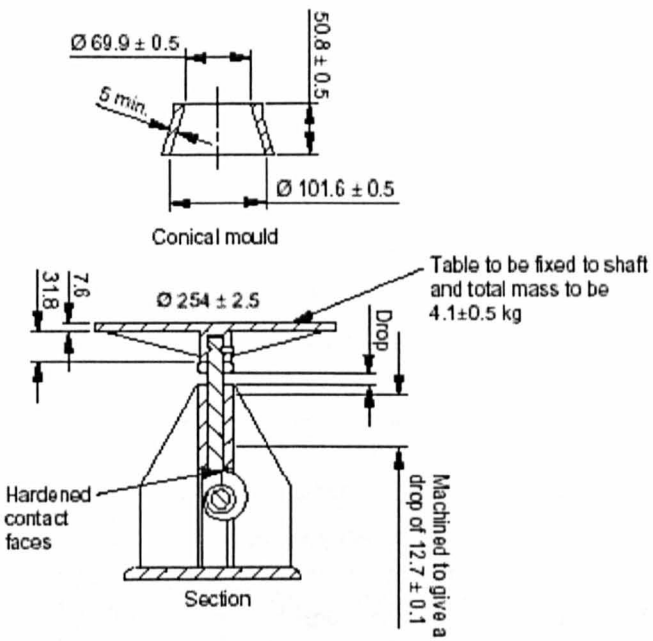

Figure 5.2: Schematic representation of the flow table and conical mould used for the measurement of the fluidity and/or wetness of the fresh mortar mixtures.

A water: binder ratio of 0.55 was finally selected, which gave a mean flow value of 200 mm (LM-03 mixture). At this ratio, the mixture achieves a workability typical to that used on site.

Barium hydroxide

The effect of barium hydroxide on the properties of lime-based mortars relating to microstructure and durability was studied by comparing and contrasting different mixtures containing barium hydroxide with a typical lime-mortar mixture. Mortar mixtures were prepared after the binary pastes were studied. The maximum amount of barium hydroxide that could be added to mortars without causing any defect was determined by the evaluation of the above results and, after this optimisation, the final mixtures were prepared (see Table 5.4).

Table 5.4: Mix proportions of mortar mixtures synthesized. The amount of barium hydroxide that is presented on the table represents the amount of hydrated lime putty being replaced. All values in the table refer to volumes.

MIXTURE	Aggregates		Binder	Binder: aggregate ratio	Amount of $Ba(OH)_2$ (%)	Water: binder ratio
	Calcitic sand	Ceramic fragments				
LM-01	1	1	Lime	1/3	0	0.40
LM-02	1	1	Lime	1/3	0	0.80
LM-03	1	1	Lime	1/3	0	0.55
LM-04	1	1	Lime + barium hydroxide	1/3	10	0.55
LM-05	1	1	Lime + barium hydroxide	1/3	25	0.55
LM-06	1	1	Lime + barium hydroxide	1/3	~15% (saturated solution)	0.55 (BaH saturated solution)

Barium hydroxide was added to mortars in three different amounts. In the first two mixtures (LM-04, LM-05) barium hydroxide constituted 10% and 25%, respectively, in the total volume of binder, by replacing equal amounts of lime putty. In the third mixture (LM-06), the water was replaced by an equal volume of a saturated solution of barium hydroxide at a temperature of 80°C. At this temperature, barium hydroxide octahydrate reaches its maximum solubility (DiBello et al., 1992). The amount of barium hydroxide added to the mixture in this way was calculated as 15% v/v. The composition of the mixtures that were studied are presented in Table 5.4.

Cubic (50mm X 50mm X 50mm), prismatic (40mm X 40mm X 160mm) and cylindrical specimens of 60 mm height and 30 mm diameter were also prepared at this stage. The specimens were initially stored in their moulds inside a polyethylene box at a temperature of 20°C ± 2°C and relative humidity of 90% ± 5% for 7 days and then, at a temperature of 20°C ± 2°C and relative humidity of 65% ± 5% for a period of one month. Steel moulds were used for cubic and prismatic specimens, while cylindrical specimens were moulded in PVC. The specimens were removed from the moulds and the box after the above period and were stored in the laboratory, at a temperature of 20°C ± 2°C and relative humidity of 50% ± 5% until tested, after three and twelve month's period of setting and natural carbonation.

Relative humidity inside the polyethylene box was fixed and controlled by a saturated solution of potassium nitrate (KNO_3) and ammonium nitrate (NH_4NO_3). Their equilibrium relative hymidities (ERH) at 20°C are 94% and 66%, respectively.

5.3.3 Monitoring of Setting Process

During the setting period, mortar mixtures harden over time and gradually achieve their final physical characteristics, strength and durability. The evaporation of water has a strong effect on the above processes as the amount of water that remains in mortars controls the diffusion of carbon dioxide into the mortar and its dissolution in the water present in pores, as well as all reactions that take place in the liquid phase.

Mineralogical analysis of the binary pastes and mortar mixtures was carried out by XRD after one- and twelve months setting time, in order to determine the setting products that are formed in each case, as a function of time.

The specimens were drilled and the samples (0.9-1.2g) were collected from a surface layer of 1–1.5 cm thickness. Measurements were carried out in triplicate (n=3).

X-ray diffraction analysis of the samples was performed in on a Siemens D-500 diffractometer using the Cu-K_α radiation (λ=1.5406 Å) with a graphite monochromator in the diffraction beam, at 1.2kW (40kV, 30mA). Spectra were collected in the range of 2–60° 2θ, with a step of 0.03°/sec. The identification of setting products was performed in Siemens Diffract, EVA-1 software.

The setting process was also monitored by studying the mixtures under a JEOL 5310 SEM, coupled to an Oxford EDX analyser. Analysis was performed using Link ISIS software. Freshly fractured surfaces of both binary and mortar mixtures, as well as thin-sections of the mortar mixtures cured for one year, were examined. Thin sections were prepared according to the methodology described in chapter 4.1.3. The analysis details are described in chapter 4.1.6.

Thermogravimetric analysis was additionally used to determine the phases formed in the binary pastes and mortar mixtures after a one year setting and hardening period. Analysis was carried out in a Perkin-Elmer Diamond TG/DTA unit, in representative samples of the binding material (20μg) taken from a batch (4-5g) collected from a surface layer of 1–1.5 cm thickness. Measurements were performed in powder samples, in static air with a heating rate of 10°C/min in the range 30–1000°C, in triplicate (n=3).

Finally, the depth of carbonation was estimated in the fractured surface of prismatic specimens after a curing period of three months, by spraying a solution of phenolphthalein indicator (1% wt) dissolved in alcohol. Phenolphthalein becomes violet when the pH is higher than 8.3 and it is indicative of the amount of free, unreacted, hydroxyl ions.

5.3.4 Properties Defining the Microstructure

The microstructure of mortars refers to the way that the binder is distributed within their mass, the total amount of pores formed in the mixture and, the way that these pores are interconnected. The study of pore structure is of great interest as it has a direct influence on the absorption, movement and evaporation of water solutions through the mortar mass (Meng, 1996; Quenard et al., 1998).

Pores are formed during setting, as moisture evaporates and the mixture is passing from the liquid to the solid state. Their total amount and structure is dependent upon the amount of water initially added to the mixture, the manner in which the water evaporates over time, as well as on changes in the crystal volume during carbonation, and the air enclosed during the mixing process.

Microstructure properties of both the binary pastes and mortar mixtures was determined according to the test procedures described in BS standards, as well as by evaluating the data derived from mercury intrusion porosimetry (MIP). Moreover, the microstructure of mixtures was studied under stereomicroscope, petrographic and scanning electron microscope, by examining both freshly-fractured surfaces and thin-sections of the samples.

5.3.4.1 Shrinkage upon Setting

Dimensional changes of mortar mixtures during setting are caused due to water evaporation and molecular volume changes during the formation of setting products. Deformations of different mixtures due to shrinkage were measured in cubic specimens after been cured for three and twelve months respectively. The dimensions of their three directions were measured using a Vernier calliper of 0.02mm accuracy and the difference was expressed as percentage of their initial dimensions.

5.3.4.2 Porosity and Pore Size Distribution

Total and open porosity, pore-size distribution, surface area, bulk density and real density were used for the description of the pore space of different mortar mixtures. Measurements were carried out on specimens cured for 3 and 12 months respectively, by means of both mercury intrusion porosimetry and water absorption by total immersion as the two methods have different measuring ranges (Figure 5.3). Pore space characteristics of binary pastes have also been determined in specimens matured for three months.

MIP results are expressed in terms of the total open pores volume (p_o) and the surface area (A) values measured in the range given below, as well as in diagrams representing the pore-size distribution ($DV(r)$ vs. log r) and the percentage of the cumulative pore volume (P_{mo}) versus the pore radius (log r). The maximum pressure of the porosimeter was 18980 MPa and the measurable pore size (radius r) was between 2.21nm to 4310.89nm.

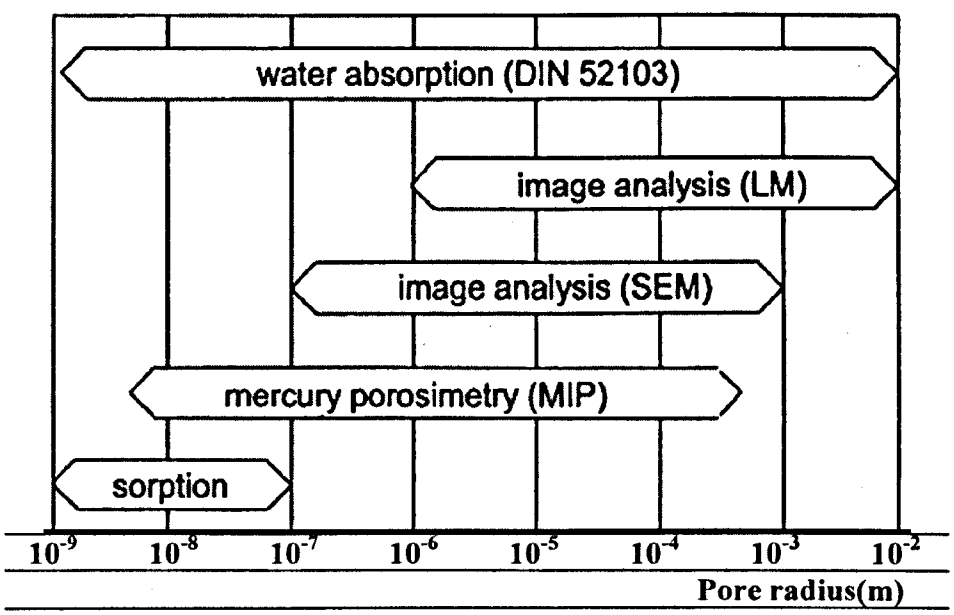

Figure 5.3: Measuring range of pore radius accessible by different methods (Meng, 1996).

Total porosity (p), open porosity (p_o) accessible to water, apparent (bulk) density (ρ_b) and real density (ρ_r) of mortar mixtures were determined on cubic specimens according to the procedure described in the BS EN 1936-1 (1999) standard.

After drying of specimens at 70 ± 5°C to constant mass, their dry mass (m_d) was determined and the specimens were placed in an evacuation vessel. The pressure was gradually lowered to (2.0 ± 0.7)kPa = (15 ± 5)mmHg and then de-mineralized water at (20 ± 5)°C was slowly introduced into the vessel, until the specimens were completely immersed. After this time, the vessel was returned to atmospheric pressure and the specimens were left under water for another 24h.

Next, the specimens were weighed under water (hydrostatic weighing) and the mass of the sample immersed in water (m_h) was determined. After this, the mass of water-saturated specimens was also determined (m_s). Finally, the apparent (bulk) volume was calculated by measuring the dimensions of the specimens. Mass values are expressed in grams (g) and volume values in milliliters (ml).

The volume of the open pores (ml) was calculated by the equation:

$$V_o = \frac{m_s - m_d}{\rho_{rh}} x1000 \qquad (5.1)$$

Where:
m_d mass of the dry specimen (g);
m_s mass of the saturated specimen (g);
ρ_{rh} density of water at 20 °C (998 kg/m^3).

The apparent density (in kg/m^3) was calculated by the ratio of the mass of the dry specimen and its apparent volume, by the equation:

$$\rho_b = \frac{m_d}{V_b} \qquad (5.2)$$

Where:

m_d mass of the dry specimen (g);

V_b volume of the specimen (ml);

The open porosity was calculated by the ratio (as a percentage) of the volume of open pores and the apparent volume of the specimen, by the equation:

$$p_o = \frac{V_o}{V_b} x100 \tag{5.3}$$

Where:

V_o volume of open pores (ml);

V_b apparent volume of the specimen (ml);

The real density (in kg/m^3) was calculated by the ratio of the mass of the dry specimen and its real volume, by the equation:

$$\rho_b = \frac{m_d}{V_b - V_o} \tag{5.4}$$

Where:

m_d mass of the dry specimen (g);

V_b volume of the specimen (ml);

V_o volume of open pores (ml);

The total porosity was calculated by the ratio (as a percentage) of the volume of pores (open and closed) and the apparent volume of the specimen, by the equation:

$$p = \frac{\frac{1}{\rho_b} - \frac{1}{\rho_r}}{\frac{1}{\rho_b}} \chi 100 = (1 - \frac{\rho_b}{\rho_r}) x100 \tag{5.5}$$

Where:

ρ_d apparent density of the specimen (kg/m^3);

ρ_r real density of the specimen (kg/m^3).

5.3.5 Properties Describing the Movement of Aqueous Solutions

5.3.5.1 Water Absorption Coefficient by Capillarity

Many of the problems that commonly occur in mortars are associated with the presence and movement of moisture through their mass. The most common route for the ingress of water in porous materials is by capillarity (Vos, 1975; Blanco et al., 1989; Meng, 1996; Quenard et al., 1998; Krus and Kieβl, 1998). The extent to which water is admitted and retained by mortars, as well as other building materials, depends not only on the amount of water that is incident from the exterior, but also on their pore space characteristics, such as pore-size distribution and interconnection of voids and pores (Taylor, 2000:142-145). Thus, the efficiency of different types of mortars to absorb water is described through the determination of the water absorption coefficient (C).

The test procedure followed was based on BS EN 1015-18 (2002) and BS EN 1925 (1999) standards for determining the water absorption coefficient of hardened mortar and natural stone, respectively. The water absorption coefficient was measured using the mortar prism specimens, under prescribed conditions, at atmospheric pressure (Figure 5.4).

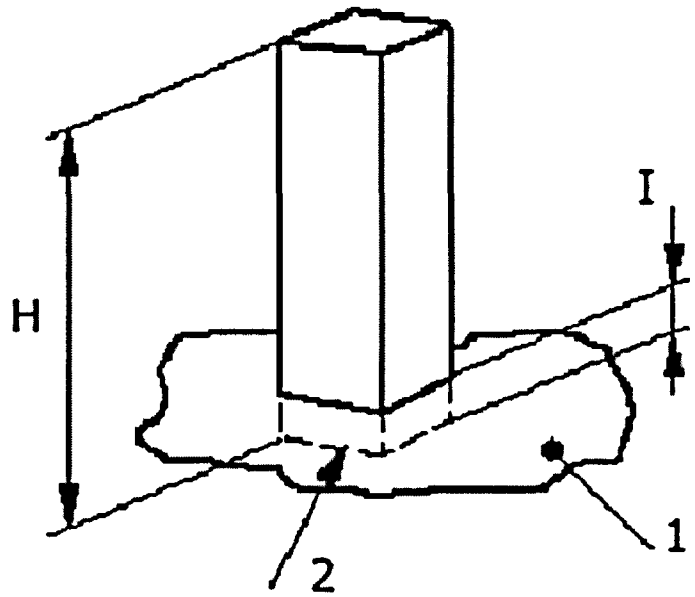

Figure 5.4: Experimental setup for measuring the water absorption coefficient using prismatic specimens. 1= water level, 2= filter paper, H = prism specimen 160 mm height, I= immersion depth 3 to 5 mm (after BS EN 1015-18, 2002).

Test prism specimens, with dimensions 160 mm X 40 mm X 40 mm, were prepared according to the BS EN 1015-11 (2002) standard. A layer of filter paper was placed on the surface of the mortars base and test specimens were cured under the conditions described in chapter 4.3.2. After the end of the curing period, specimens were dried to constant mass at a temperature of 70 °C ± 5 °C and weighed (m_d). The area of the base to be immersed (A) was calculated and expressed in square metres (m^2).

Specimens were immersed in the water to a depth of (3 ± 1) mm, maintaining a constant water level throughout the test. At time intervals, initially very short and then longer, each specimen was removed in succession, lightly dried using a damp cloth and weighed immediately to the nearest 0.01 g. Then they were replaced in the container. The time elapsed since the start of the test until the time of each weighing was recorded and, finally, a graph, representing the mass of water absorbed (in grams) divided by the

area of the immersed base of the specimen (in square metres) as a function of the square root of time (in seconds) was obtained (Equation 4.6).

$$\frac{m_i - m_d}{A} = C\sqrt{t_i} \tag{5.6}$$

Where:

m_d mass of the dry specimen (g);

m_i successive masses of the specimen during testing (g);

A area of the side immersed in water (m^2);

t_i time elapsed from the beginning of the test until the times at which the successive masses mi were measured (s);

C water absorption coefficient by capillarity

The coefficient of water absorption by capillarity C (in $gm^{-2}s^{-½}$) was calculated from the slope of the first half of the graph.

5.3.5.2 Water Vapour Permeability

Another property, which is also related to the pore structure of mortars, is water vapour permeability. The laboratory measurement of water vapour permeability describes the ability of different types of mortars to permit the diffusion, movement and evaporation of water vapours and/or other water solutions through their mass, under isothermal conditions. Permeability of porous materials, like mortar, controls the movement and evaporation of water, which in turn, controls a number of setting and deterioration mechanisms, such as carbonation of binding material, salt crystallization and frost action.

Determination of the steady state water vapour permeability was carried out according to the BS EN 1015-19 standard (1999), at the upper part of the hygroscopic range. According to this test, the water vapour flux passing through a unit area under

equilibrium conditions, per unit difference in water vapour pressure between the two sides of the material, is calculated.

Specimens to be tested are sealed on the open mouth of circular cups in which the water vapour pressure is maintained constant at appropriate levels by means of saturated salt solutions. The cups are placed in a temperature-controlled environment with a constant water vapour pressure, different from that inside the cups. The rate of moisture transfer is determined from the change in the weight of the cups under steady state conditions.

The cups were placed in a temperature-controlled environment with a constant water vapour pressure, controlled by a saturated solution of calcium chloride ($CaCl_2$).

Circular, disc-shaped specimens (10 cm diameter) of uniform thickness (10 mm) were placed in test cups and their edges sealed. The water vapour pressure within the cup was maintained constant by means of a saturated solution of potassium nitrate (KNO_3), for the upper hygroscopic range. This provides a relative humidity of 93.2 % at a temperature of 20°C. An air-gap of 20 mm between the specimen and the surface of the solution was left in each cup (Figure 5.5). The test cups were placed in a storage box, at 20°C ±2°C and relative humidity of 50 % ±5 %, and weighed at normal time intervals.

A graph of the mass of the cup was plotted against time and the water vapour flux, $\Delta G/\Delta t$ was calculated. The water vapour permeance (Λ) for each specimen was then determined using the following equation:

$$\Lambda = \frac{1}{A \cdot \Delta_p / (\Delta G / \Delta t) - R_A} \text{ (kg/m}^2 \text{ s Pa)} \qquad (5.7)$$

Where:

A is the area of the open mouth of the test cup (m^2)

Δ_p is the difference in water vapour pressure between the ambient air and the salt solution (Pa)

$\Delta G/\Delta t$ is the water vapour flux (kg/s)

R_A is the water vapour resistance of the air gap between the specimen and the salt solution (0.048 X 10^9 Pa m^2s/kg, per 10 mm air gap).

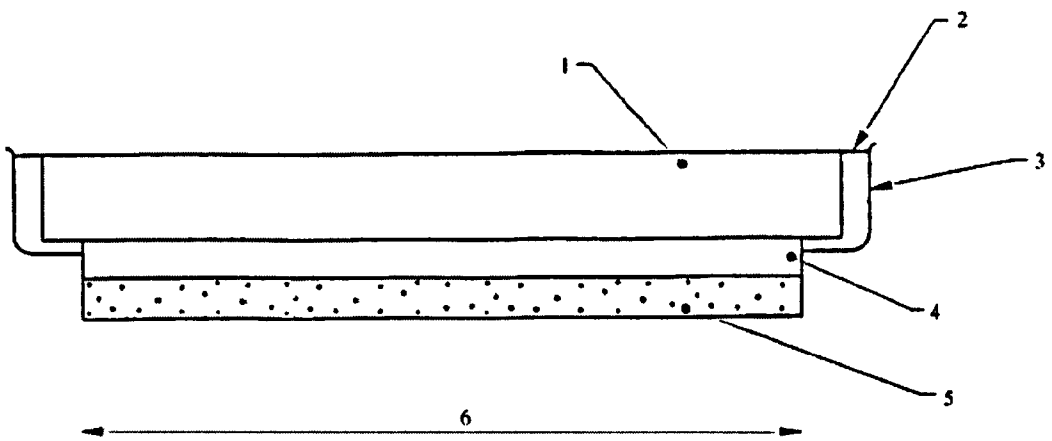

1 Specimen
2 Sealant
3 Circular test cup
4 Air gap (≈ 10 m)
5 Saturated salt solution
6 Area (≈ 0,02 m^2)

Figure 5.5: Test cup with test specimen used for determining water vapour permeability (BS EN 1015-19, 1999).

The mean water vapour permeance was calculated from the values of the five individual specimens and, finally, the water vapour permeability for every mixture was calculated from the mean value for the water vapour permeance by multiplying this by the specimen thickness.

The difference in water vapour pressure (Δ_p) between the air within the testing cup and the air in the storage box was determined using the equations defining relative humidity (4.8, 4.9), since in both cases the relative humidity of the air was in equilibrium with one of the saturated salt solutions used (Price, 2000:4). This means that:

$$RH_{KNO_3} = \frac{p_1}{p_o} x100\% \Leftrightarrow p_1 = \frac{RH_{KNO_3} \cdot p_o}{100} \qquad (5.8)$$

$$RH_{CaCl_2} = \frac{p_2}{p_o} x100\% \Leftrightarrow p_2 = \frac{RH_{CaCl_2} \cdot p_o}{100} \qquad (5.9)$$

where p_1 and p_2 are the vapour pressures of the salt solutions and p_o is the vapour pressure of water at the same temperature, in (Pa).

Table 4.5 presents the vapour pressure of water at different temperatures.

By replacing Δ_p in formula (4.7) this becomes:

$$\Lambda = \frac{1}{A \cdot \frac{p_o}{100}(RH_{KNO_3} - RH_{CaCl_2})/(\Delta G / \Delta t) - R_A} \text{ (kg/m}^2\text{ s Pa)} \qquad (5.10)$$

Table 5.5: Vapour pressure of liquid water (Perry and Green, 1984:45)

T (°C)	P_w (mmHg)	P_w (Pa)
18	5.219	35.984
19	5.256	36.239
20	5.294	36.501
21	5.332	36.763
22	5.370	37.025
23	5.408	37.287
24	5.447	37.556

5.3.6 Tests Defining the Mechanical Performance

The strength of mortars and their behaviour under external mechanical forces define the mechanical performance. This is due to the resistance that the binder achieves during setting and hardening, the independent components (aggregates) present, and the adhesion bonds developed between the binding material and the external surface of the

aggregates. This behaviour is expressed by the critical stress causing failure or cracking of a specimen (RILEM, 1980).

5.3.6.1 Compressive Strength

The compressive strength of mortar mixtures was determined in moulded cubic specimens of 50 mm, according to the procedure described in British Standard (BS EN 1015-11:1999). Three specimens from each mixture, cured for 90 and 365 days respectively, were tested, using a displacement rate of 109 μm/min.

The specimens were carefully aligned to the centre of the testing machine so that the load was applied to the whole width of the faces in contact with the plates. The load values (in N) and the displacement of the plates (in mm) were continuously recorded during the test.

The compression strength of each specimen (f_c) was calculated as the maximum load (F_{max}) carried by the specimen divided by its cross-sectional area (S). The strength of each specimen was recorded to the nearest 0.05 N/mm^2 and then, the mean value for each mixture was calculated to the nearest 0.1 MPa (N/mm^2). Finally, axial deformation of specimens during loading was described through a stress-strain curve.

5.3.6.2 Static Modulus of Elasticity

Data recorded during the monitoring of the behavior of specimens tested in unconfined compression were also used to determine the static modulus of elasticity (E_c) of the mortar mixtures. The static modulus of elasticity in compression E_c, in MPa (N/mm^2) is defined as the ratio of the differences in stress and strain between a basic loading level of 0.5 MPa and an upper loading level of one-third the compressive strength of the specimen.

The stress-strain curves of specimens previously plotted were used for the determination of the static modulus of elasticity of the mixtures according to Equation 5.11. Test

specimens used were cubes of 50 mm, although the test procedure described in BS 1881-121 (1983) applies to cylindrical specimens.

$$E_c = \frac{\Delta_\sigma}{\Delta_\varepsilon} = \frac{\sigma_a - \sigma_b}{\varepsilon_a - \varepsilon_b} \tag{5.11}$$

where:

σ_a is the upper loading stress, in MPa, ($\sigma_a = f_c/3$);

σ_b is the basic stress (0.5 MPa);

ε_a is the mean strain under the upper loading stress;

ε_b is the mean strain under the basic stress.

5.3.6.3 Flexural Strength

The flexural strength of mixtures was determined through three point loading test, using moulded mortar prisms 160 mm X 40 mm X 40 mm. The test carried out in specimens previously cured for 3 and 12 months, using 3 samples from each mixture. A displacement rate of 109μm/ min was used during loading. The flexural strength f was calculated, in N/mm^2 using the following equation:

$$f = 1.5\frac{Fl}{bd^2} \tag{5.12}$$

where:

F is the maximun load applied to the specimen (N);

l is the distance between the axes of the support rollers (mm);

b is the width of specimen (mm);

d is the depth of the specimen (mm).

The flexural strength of each specimen was recorded to the nearest 0.05 N/mm^2 and then, the mean value was calculated to the nearest 0.1 MPa (N/mm^2). Figure 5.6 gives

the setup of the testing machine for the three point loading test, and shows the distance between rollers.

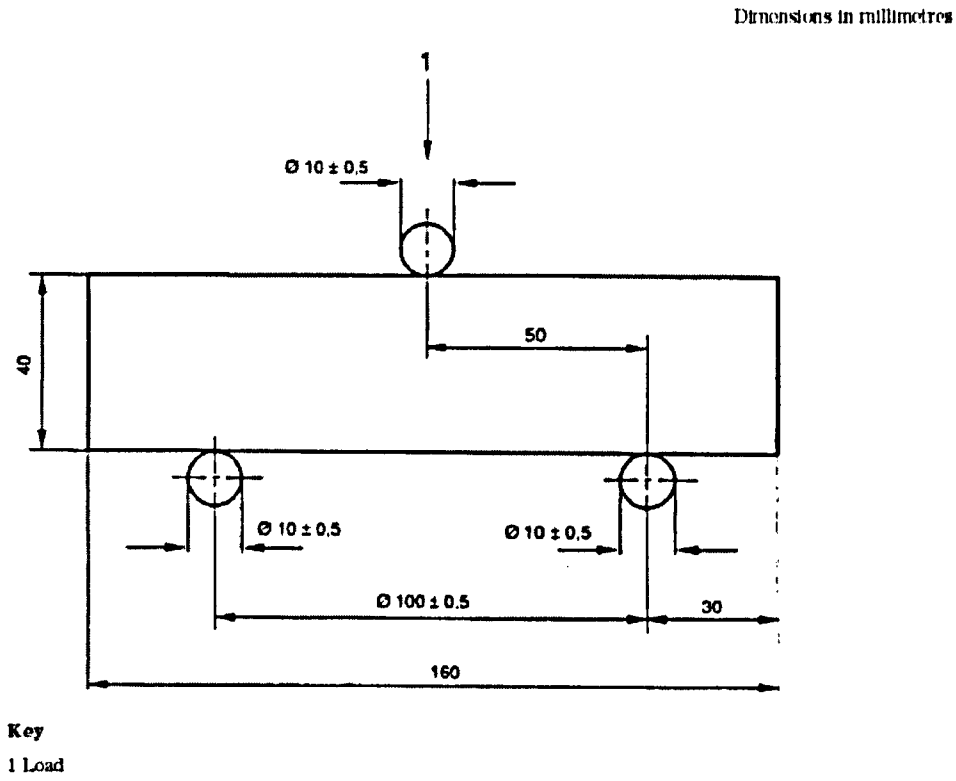

Figure 5.6: Graphical representation of the flexural strength test (after BS EN 1015-11, 1999).

5.3.7 Accelerated Aging – Durability Monitoring Tests

In order to assess the relative resistance of different mixtures to deterioration, and especially to the damage caused by sulphate action, a number of accelerated aging tests were carried out. The aim of these tests was to clarify if the addition of barium hydroxide had any effect on the durability of those mixtures and if so, to describe the parameters and the conditions that could result optimum performance.

Accelerated aging tests were carried out on mortar mixtures which had been cured for 3 and 12 months, respectively. They were supported by a number of experiments, where samples taken from the binary pastes were used in order to study and monitor the

reactions that take place between the cementing paste of the mortars and the sulphate ions in aquatic environment. Four accelerated aging tests were carried out:

i. Crystallisation of salts by total immersion;
ii. Deterioration caused by sulphate attack
iii. Electrochemical degradation; and
iv. Fixation of sulphate ions.

Prior to the accelerated aging tests, the microstructural properties and the mineralogical composition of the various mixtures were determined. Scanning electron microscopy, mercury porosimetry, X-ray diffraction analysis and thermo-gravimetric analysis were used for this purpose, according to the procedures already described previously.

5.3.7.1 Crystallisation of Salts by Total Immersion

This is an accelerated weathering test that simulates the deterioration mechanisms that occur when crystallisation of soluble salts occurs under natural environmental conditions. The test contributes to the monitoring of the behaviour of mortars over time and in the assessment of their relevant resistance against salt crystallisation.

According to the procedure described in BS EN 12370 (1999), three cubic specimens of 50 mm side were used from each mixture. The specimens were dried at 80 ± 5°C until constant mass. They were then allowed to cool at room temperature and weighed to ±0.01g (M_d).

The specimens were immersed in a polyethylene container and covered with a 14% w/w solution of sodium sulphate decahydrate ($Na_2SO_4 \cdot 10H_2O$). The container was covered to reduce evaporation and the specimens were left to soak for two hours. After immersion the specimens were removed from the solution and dried in the oven at 80 ± 5 °C. The oven was arranged to provide high levels of relative humidity, at least in the early stages of drying, by placing a tray of water in it 30 minutes before the specimens.

The specimens were left in the oven to dry for 22 hours and then allowed to cool to room temperature and weighed to ±0.01g (M_i) before re-soaking in a fresh sodium sulphate solution. The cycle of operation was carried out 15 times, or until the specimens broke up.

After each cycle, the weight difference of the samples (ΔM) was calculated, using the following equation:

$$\Delta M = \frac{M_i - M_d}{M_d} \times 100 \qquad (5.13)$$

where:

M_d the dry weight of the sample before the first immersion in the salts solution;

M_i the dry weight of the sample after *i* accelerating weathering cycles.

In order to obtain more information about the behaviour of different mixtures, a graph of the mean value of the (%) weight difference of the samples after every aging cycle, against the respective number of test cycles, was plotted. A photographic record of the initial and final condition of the samples was also kept.

The above results were finally considered with other physical properties and tests of mortars in order to assess their durability and relevant resistance to salt crystallisation.

5.3.7.2 Deterioration Caused by Sulphate Attack

This test aims to simulate the deterioration of mortars exposed to external conditions, due to acid rain and other atmospheric pollutants. In order to examine the performance of lime mortars and the effect of barium hydroxide on their durability, an artificial weathering test was designed, aiming to subject the specimens to sulphate attack. The test is based on the experimental procedure described by Martinez and Thompson (1999), and Rendell and Jauberthie (1999).

Three cylindrical specimens of 30mm diameter and 60mm height were used from each mixture. The specimens were dried at 80 ± 5°C until constant mass, then allowed to cool at room temperature and weighed to ±0.01 g (M_{d1}). Then, the specimens were placed in plastic tubes, allowing 1 mm free space around their surface, and solution was introduced at the top of the tube, flowing over the surface of the specimen and exiting at the bottom.

The exposure protocol involved dry and wet cycling, with the addition of a dilute solution of sulphuric acid (0.05M) for 2 hours, followed by drying at room temperature for 22 hours. A solution flow rate of 0.5L/h was employed, for an exposure period of 50 days.

Collecting tubes and vessels were arranged beneath the samples to collect the run-off solution from the surface of the mortars (Figure 5.7). The run-off solutions were collected regularly during the cycles and the accumulative concentration of calcium (Ca^{2+}) and barium (Ba^{2+}) ions was determined by inductively coupled plasma spectroscopy (ICP). Additionally, compositional and structural changes of mortars were determined by SEM/EDX and XRD.

After the completion of the exposure time, the specimens were dried at 80°C and weighed to ±0.01g (M_{d2}). Weight changes were determined as a percentage (%), using the following equation and then the mean value for each mixture was calculated to the nearest 0.1g.

$$\Delta M = \frac{M_{d2} - M_{d1}}{M_{d1}} \times 100 \qquad (5.14)$$

where:

M_d the dry weight of the sample before the acid attack;

M_i the dry weight of the sample after the final aging cycle.

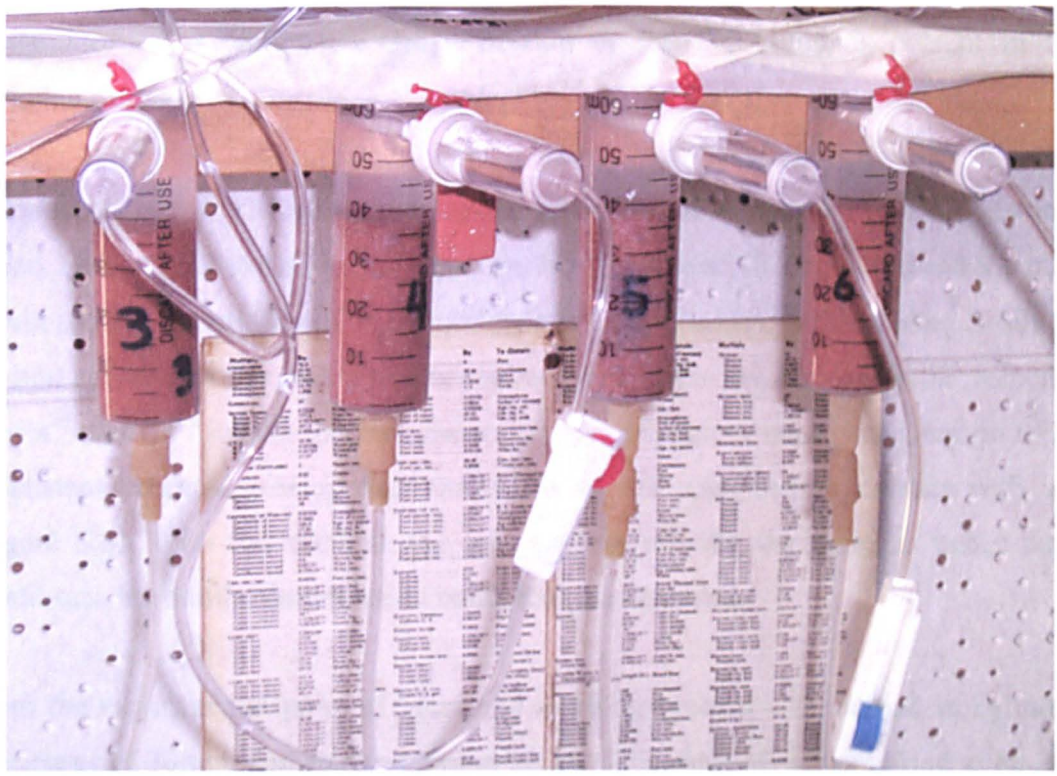

Figure 5.7: Experimental setup for simulating the flow of acid rain solution over the surface of mortars.

5.3.7.3 Electrochemical Degradation

The aim of this test is to study the behaviour of mortars in contact with water and to investigate the deterioration mechanisms of mortars relating to the dissolution of the binding material and the decalcification of the matrix.

Leaching of the binding material leads, in a simplified model, to an increase of porosity and a decrease of mechanical properties (Carde and Francois, 1997). Studies concerning physicochemical and prediction models describing the leaching process are mainly focused on cement pastes (Ademot and Buil, 1992; Carde et al., 1996; Maingury et al., 2000; Ryu et al., 2002).

The phenomenon is more aggressive in lime and lime-pozzolan mortars as the Ca^{2+} bond in $Ca(OH)_2$ and C-S-H products is more vulnerable, resulting in leaching of

portlandite and a progressive decalcification of the C-S-H bonds present in lime-pozzolan mortars.

Because of the slow leaching kinetics of lime mortars obtained by using de-ionized water, an electrochemical acceleration method was used to degrade different mortar specimens by dissolution of their binding material (Faucon, 1998; Saito, 2000). The method accelerates the dissolution of binder from mortar by increasing the velocity of the Ca^{2+} and Ba^{2+} ions in the pore water. In order to achieve speed acceleration of ions, a constant potential was applied across the mortar specimen in contact with water (Figure 5.8). With this method, the ions are not moving the same as under natural conditions, but similar deterioration conditions are obtained.

From the experimental point of view, the leaching process was studied in cylindrical specimens of 30mm diameter and 25mm height. The specimens were dried at 80 ± 5°C until constant mass; they were allowed to cool at room temperature and weighed to ±0.01g.

The specimen was placed between two Plexiglas (Perspex) vessels, each one containing 1.5L of de-ionized water, and shielded inside a PVC tube with Teflon tape. Each vessel also had a small pipe for exhausting the gas produced by electrolysis. One vessel contained the anode (Pt) and the other the cathode (stainless steel). The electrodes were connected to a DC power source to provide a voltage of 30V across the specimen.

The leaching acceleration tests were carried out in an air-conditioned room at 25±2°C. Random monitoring of the temperature in the solution at the cathode indicated that occasionally changes of about 2°C occurred, but for most of the test period, it was maintained at 25°C. Test periods were fixed to about 2500 min until the specimens started to fail and small fragments passed on the cathode due to deterioration.

The concentration of Ca^{2+} and Ba^{2+} ions at the cathode was measured by ICP, in samples collected at prescribed times. Moreover, the conductivity values of the solutions and the current (mA) created by the movement of ions through the mortar

were monitored as a function of time (min) during the test. After the acceleration test, the specimens were removed from the apparatus, dried at 80 ± 5°C until constant mass, and weighed to ±0.01g. Finally, the deterioration morphology of the specimens was documented under stereomicroscope.

The potential effect of water electrolysis on the current values recorded during the test was investigated prior to the leaching test by monitoring the current values of de-ionized water at the same voltage (30V).

According to electrochemical principles, ions in solution move towards opposite electrodes under a direct-current potential gradient, i.e., cations move toward the cathode and anions move toward the anode. Ca^{2+} and Ba^{2+} ions in the pore solution move rapidly to the cathode, and thus hasten calcium hydroxide and calcium carbonate (formed during setting) dissolution. In this electrochemical reaction, cations in the pore solution, such as Na^{+}, K^{+}, Ca^{2+} and Ba^{2+} move toward the cathode, whilst anions, such as OH^{-}, move towards the anode. Under natural conditions, Ca^{2+} and OH^{-} ions resulting from dissolution move in the same direction. Thus, with this experimental arrangement, the OH^{-} ions move in the wrong direction.

Furthermore, a small current (of some mA) may flow during the test, produced by water electrolysis at both electrodes, forming H^{+} and OH^{-} ions and H_2 and O_2 gases. This also does not occur under natural conditions. Nevertheless, these differences do not affect the dissolution mechanism, only the ion transport efficiency and solubility because of the different pH conditions. Consequently, this method of acceleration with an electric field produces leached samples in a short time without altering the assumed degradation mechanism (Saito and Deguchi, 2000).

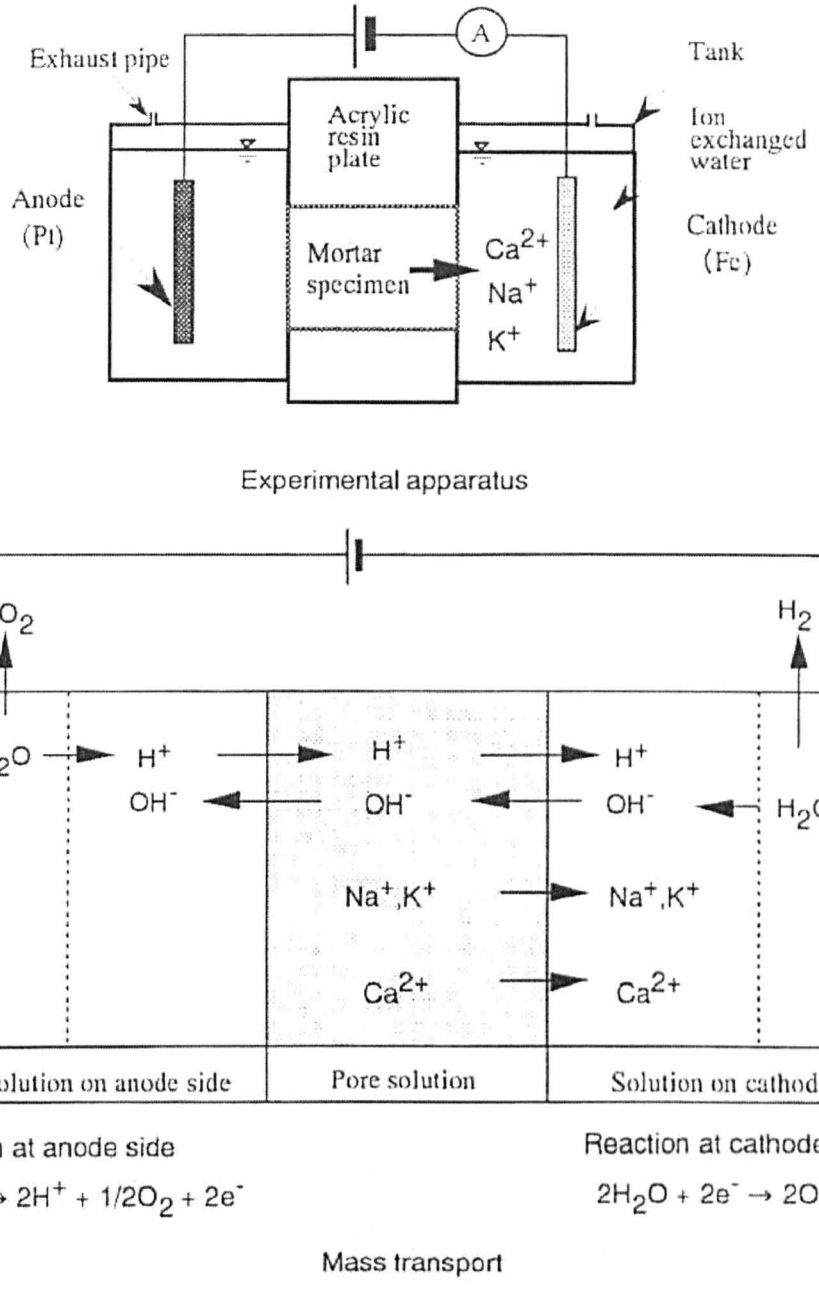

Figure 5.8: Schematic representation of the experimental apparatus used in the electrochemical degradation test and the mass transport concept.

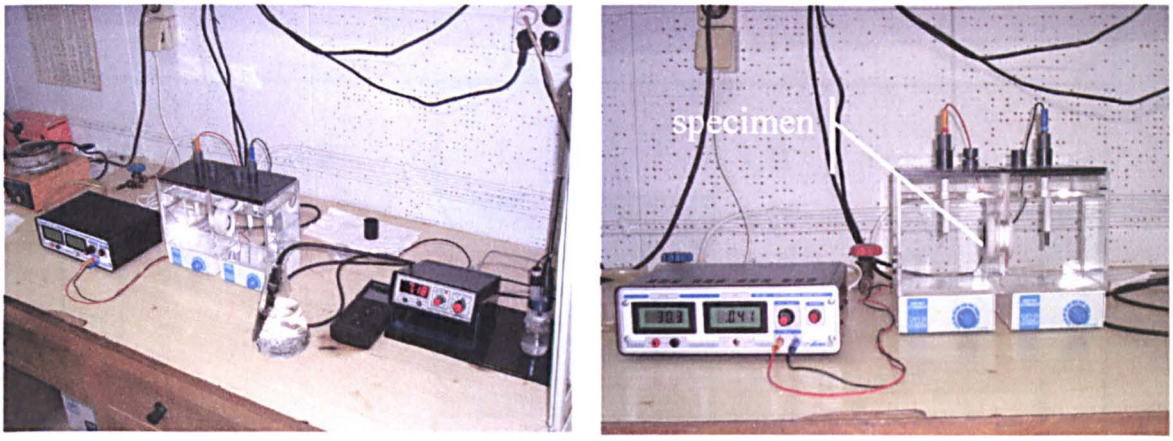

Figure 5.9: Photographs of the instrumentation developed for the leaching test.

5.3.7.4 Fixation of Sulphate Ions

The effect of barium hydroxide on the fixation of sulphate ions was studied using a diffusion cell. In this test, sulphate ions are forced to pass through the body of the mortar mixture by applying a constant potential gradient across the specimen in contact with water. Fixation of sulphates may affect durability and performance of lime-mortars by preventing deterioration caused by acid rain or soluble salt crystallization. The test is based on the experimental procedure described by Tsuyuki et al. (2000).

Sulphate fixation was studied in cylindrical specimens of 30mm diameter and 25mm height. The specimens were dried at 80 ± 5°C until constant mass, allowed to cool at room temperature and weighed to ±0.01g.

The small cylinders were placed between two Plexiglas vessels and shielded inside a PVC tube with Teflon tape. Each vessel also contained a small pipe for exhausting the gas produced by electrolysis. The anode electrode (Pt) was placed in the vessel containing de-ionized water. The cathode (stainless steel) was placed in the vessel containing a 10% w/w solution of sodium sulphate. The electrodes were connected to a DC power source to provide a potential of 30V across the specimen (Figure 5.10).

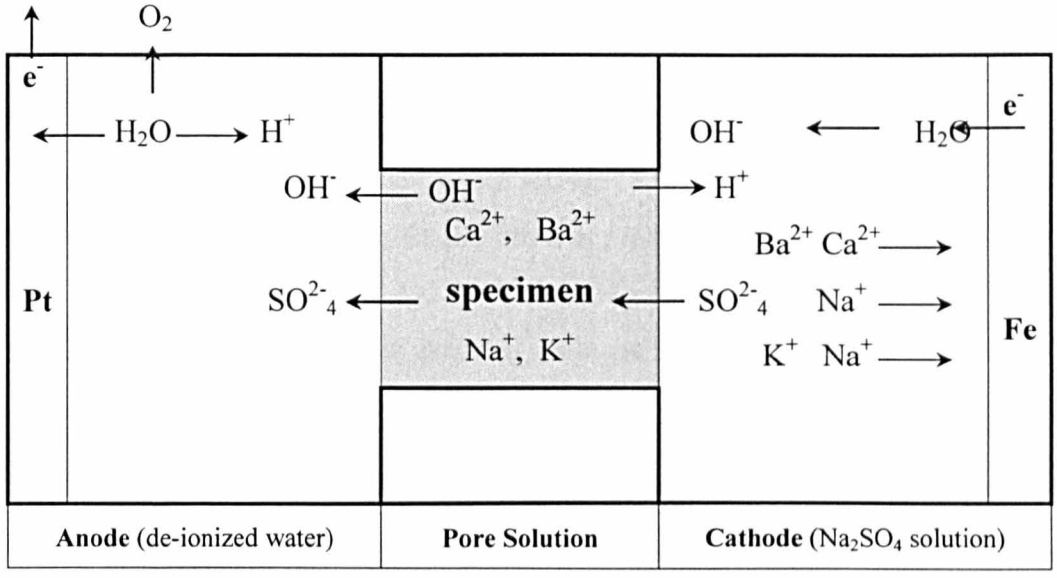

Figure 5.10: Schematic representation of the mass transport concept during the sulphate fixation test.

The fixation test was carried out in an air-conditioned room at 25 ± 2°C. The test period was set at about 4000 min, until conductivity values in the anode solution were constant.

The concentration of Ca^{2+} and Ba^{2+} ions at the anode was determined in samples collected at preset time periods by means of inductively plasma spectroscopy (ICP), whilst SO_4^{2-} concentration at the cathode was determined by a MERCK strip-test (Merckoquant Test Strips for Sulphates). Moreover, the conductivity values of the solutions and the current (mA) created by the movement of ions through the mortar were monitored as a function of time (min) during the test.

5.3.7.5 Monitoring of Reactions in Sulphate Solutions

Throughout this procedure, the reactions between the binding material of the mortars and the sulphate solutions were monitored, both in salt and acid solutions. Ten grams from each binary paste and each mortar mixture were collected and ground to produce a fine powder. All mixtures were twelve months old. Two grams of the above powder

were dispersed in 100ml of sodium sulphate decahydrate ($Na_2SO_4 \cdot 10H_2O$, 14% w/w) and stirred for 60 min at a temperature of 40°C. Another two grams of the powder was dispersed in 100ml of sulphuric acid (H_2SO_4, 0.1M) and stirred for 60 min at a temperature of 40°C. The solid and liquid phases of the above solutions were separated by filtration. The solid phase was finally dried in the oven at 80 ± 5°C.

Mineralogical composition of the reaction products in the solid phase was determined by XRD. SEM/EDX was additionally used for studying the micro-morphology of the phases formed.

5.3.8 Pilot Evaluation of Performance

Evaluation of the properties of the mortars containing barium hydroxide was carried out with mosaic fragments, by students in the conservation laboratories of the Department of Conservation of Antiquities and Works of Art, TEI of Athens. The evaluation concerned the determination of any problems occurring during preparation and application of the mixtures, their wet properties, and monitoring of performance after application and curing.

6 EXPERIMENTAL RESULTS

6.1 QUALITY CONTROL OF RAW MATERIALS

Raw materials were analysed prior to the preparation of mortar mixtures in order to identify any potential impurities or contamination that could cause problems in their use. Moreover, the initial mineralogical composition and texture of raw materials was necessary for monitoring the setting process and changes in the mineralogical composition of mixtures.

The results of the chemical analysis of the raw materials, by EDX, are given in Table 6.1.

Table 6.1: Chemical analysis of raw materials carried out by EDX. Analysis was performed in pellets of 1cm diameter.

MATERIAL		$Ca(OH)_2$	$Ba(OH)_2 \cdot 8H_2O$	Ca-Sand	Ceramic Fraction	
					0–500μm	500μm – 2mm
Element	**Formula**	**Oxide Weight %**				
Ba	BaO	nd	99.90	nd	nd	nd
Ca K	CaO	99.80	0.03	98.40	4.14	7.17
Mg K	MgO	0.03	0.02	0.03	3.75	3.57
Fe L	FeO	0.04	nd	0.05	12.04	15.57
K K	K_2O	0.01	nd	0.06	5.68	4.07
Na K	Na_2O	nd	nd	0.03	0.94	0.26
Al K	Al_2O_3	nd	nd	0.43	15.96	16.64
Si K	SiO_2	0.07	nd	0.84	56.23	50.14
Mn L	MnO	nd	0.02	0.07	nd	0.32
S K	SO_3	nd	nd	0.03	0.23	1.13
Cl K		0.05	nd	0.04	nd	0.13
Ti K	TiO_2	nd	0.03	0.02	1.03	1.00
Totals		100.00	100.00	100.00	100.00	100.00

Chemical analysis of the calcium hydroxide powder used to produce the lime putty showed no impurities were present that could affect the quality and performance of the produced lime putty (Table 6.1). The X-ray diffraction analysis of the same powder showed only crystalline portlandite [$Ca(OH)_2$] was present, with no indications of any other crystalline or amorphous material (Figure 6.1). The scanning electron photomicrographs (Figure 6.2) of the material showed irregularly shaped masses of portlandite crystallites. The maximum dimensions of these did not exceed 3-5μm.

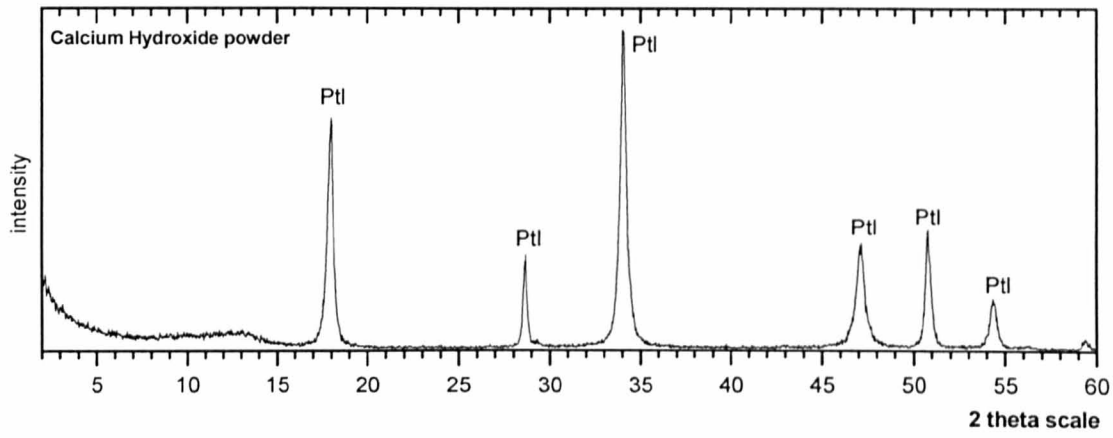

Figure 6.1: Diffraction pattern of calcium hydroxide powder. All the peaks correspond to portlandite (Ptl) crystals.

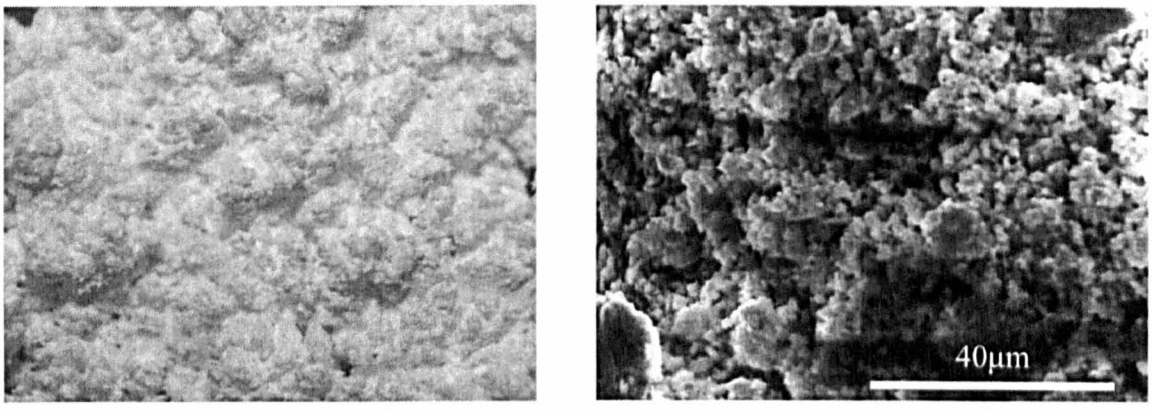

Figure 6.2: Calcium hydroxide powder photomicrographs under stereo-microscope (left) and scanning electron microscope (right). SEM photomicrograph shows more clearly the irregularly shaped masses of $Ca(OH)_2$ crystallites.

The chemical analysis of barium hydroxide octahydrate powder (Table 6.1) showed the material to be very pure in barium compounds (>99%). Its diffraction pattern (Figure 6.3) gave the crystalline form of barium hydroxide octahydrate [$Ba(OH)_2 \cdot 8H_2O$] as the predominant mineral. The anhydrous form of barium hydroxide and the barium carbonate were also identified as secondary minerals, albeit in a very low amount. According to the chemical sheet of the material, carbonates do not exceed 2%. Examination by SEM proved that the size of barium hydroxide crystals varied between 5-300μm. The crystals were well formed in the monoclinic system (Figure 6.4).

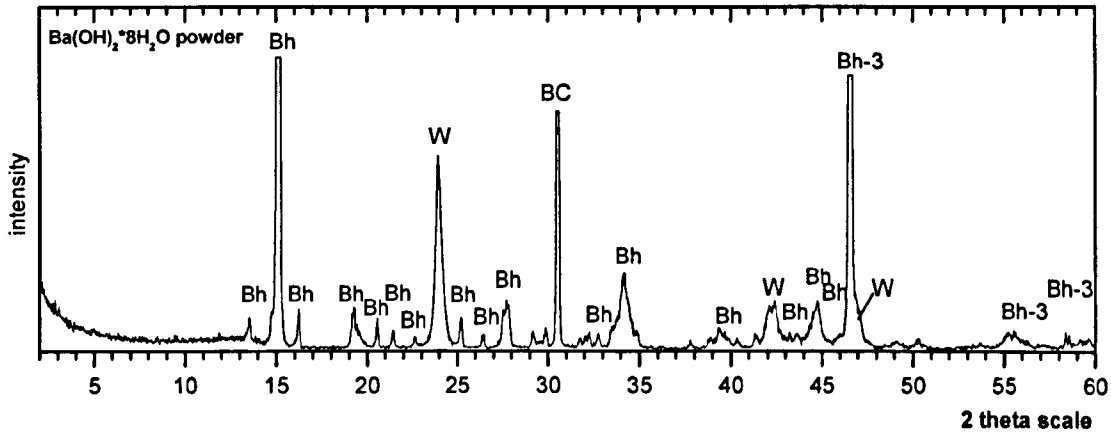

Figure 6.3: Diffraction pattern of barium hydroxide powder. The majority of the peaks correspond to barium hydrate forms, crystallized with 8 and 3 water molecules (Bh) and (Bh-3) respectively. Carbonate phases of barium in the crystalline forms of witherite (W) and barium carbonate (BC) were also detected.

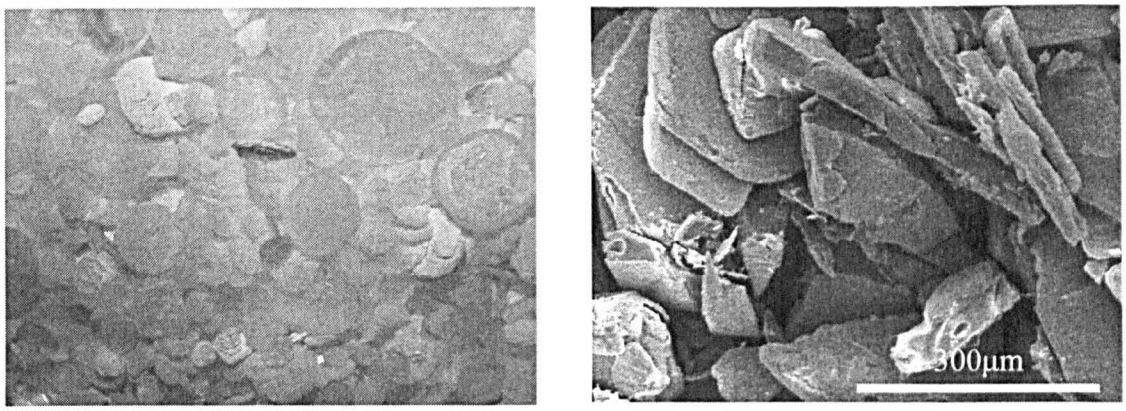

Figure 6.4: Barium hydroxide powder photomicrographs under stereo-microscope (left) and scanning electron microscope (right). SEM photomicrograph shows barium hydroxide crystals of maximum size 300μm and of about 25μm thickness.

The only phase identified in the diffraction pattern of the calcareous sand was calcite (Figure 6.5). Chemical analysis showed that silicon (Si) and aluminium (Al), most probably in the form of alumino-silicate impurities, were present in the sand fraction to a maximum percentage of 2% (Table 6.1). Examination of the fraction between 500μm and 1mm by SEM showed that the sand particles consisted of angular, partially elongated, rock fragments (Figure 6.6).

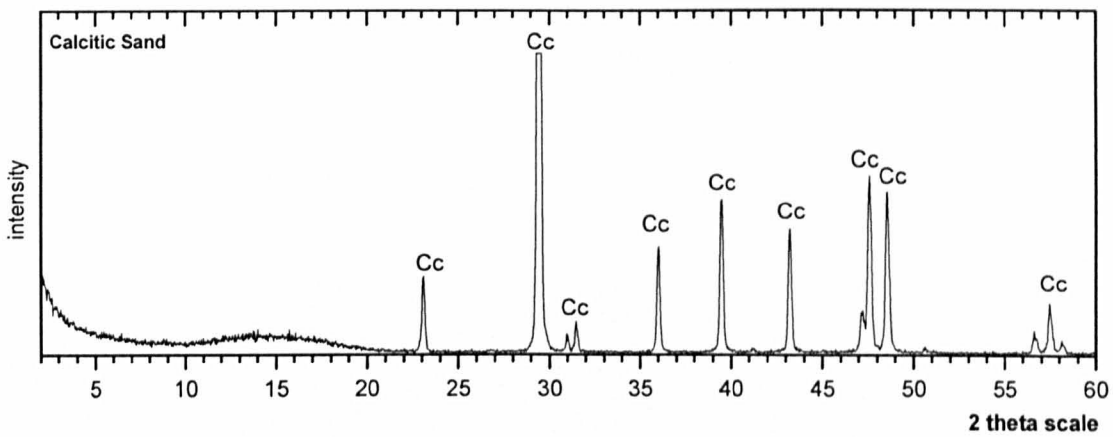

Figure 6.5: Diffraction pattern of calcitic sand. All the peaks correspond to calcium carbonate (Cc) crystals.

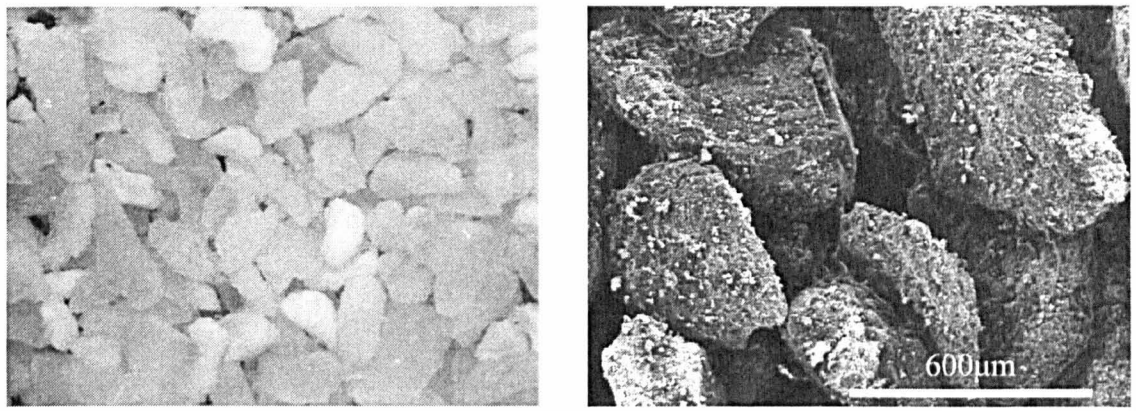

Figure 6.6: Calcitic aggregates under stereo-microscope (left) and scanning electron microscope (right). The granules of aggregates are angular and elongated.

Examination of the ceramic particles used as aggregates by SEM showed that the ceramic mass was vitrified (Figure 6.7), resulting in an extensive network of glass filaments. The above structure is representative of ceramics that have been fired over 900°C (900-950°C) (Maniatis and Tite, 1981; Kilikoglou, 1994). The granules were angular and the ceramic mass contained a small portion (5-10%) of quartz inclusions, with maximum dimension 300–500µm. Chemical analysis of the ceramic fractions between 0–500µm (Ceramic fraction 1) and 500µm–2mm (Table 6.1) showed that the ceramic mass was slightly calcareous and potassium rich. Quartz (Q), plagioclase (P), illite-montmorillonite (I-M), K-feldspars (Kf) and hematite (H) were the main minerals matched in the diffraction pattern of the ceramic fragments (Figure 6.8).

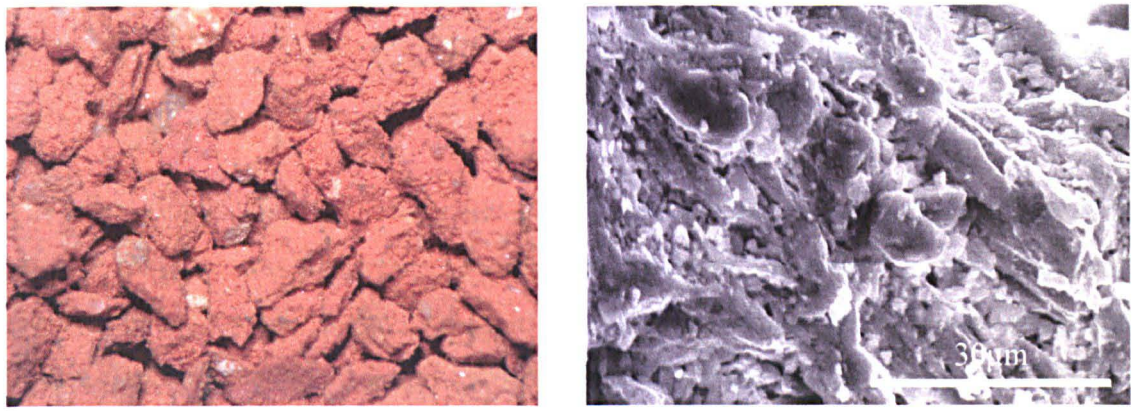

Figure 6.7: Ceramic aggregates under stereo-microscope (left) and scanning electron microscope (right). The extensive network of glass filaments observed in the SEM photomicrograph is typical of the ceramic mass vitrification. The stereo-microscopic picture indicates quartz inclusions of maximum size about 300μm.

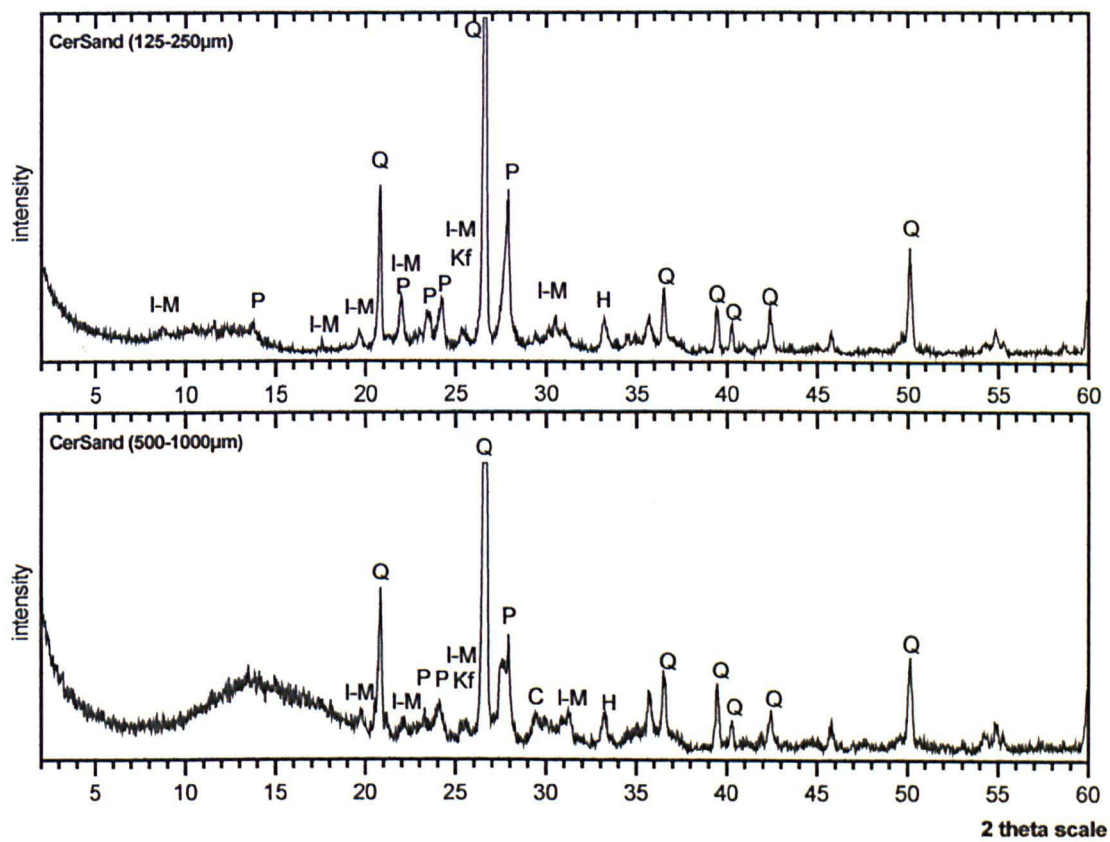

Figure 6.8: Diffraction patterns of the ceramic fragments. Quartz (Q), plagioclase (P), illite-montmorillonite (I-M), K-feldspars (Kf) and hematite (H) were the main minerals identified in the ceramic mass.

6.2 MICROSTRUCTURE OF THE BINARY PASTES

The effect of barium hydroxide on the setting process and the physical properties of the binding material was determined through the study of the binary pastes. The partial replacement of slaked lime by barium hydroxide was found to affect the microstructure of the produced material after hardening. The effects on microstructure that are discussed in this section are dependent upon, and controlled by, the granular size of the barium hydroxide crystals and the amount present in the cementing mass.

The results of the mercury intrusion porosimetry (Table 6.2) and SEM examination of the pastes showed that as the amount of barium hydroxide in the binding material was increased, a coarser microstructure was formed. Even though the open porosity of the binary pastes was around 50%, the total surface area was strongly influenced by the presence of barium hydroxide. The replacement of 10, 25 and 75% per volume of lime putty resulted in a 44, 47 and 67% reduction in the total surface area, respectively.

Table 6.2: Mean values of microstructural properties of binary pastes determined by mercury porosimetry. Measurements were carried out in triplicate (n=3).

Sample	Pore radius range (nm)	Total surface area (m^2/kg)	Apparent density (kg/m^3)	Open porosity (%)
Ca	2.21 – 4310.89	19034.3 ± 524.3	2233.5 ± 67.3	52.38 ± 2.85
Ca3Ba1		10667.2 ± 541.5	2871.8 ± 82.6	49.41 ± 3.16
Ca2Ba2		10061.4 ± 656.7	3587.3 ± 73.2	53.27 ± 2.69
Ca1Ba3		6290.6 ± 687.2	3360.5 ± 95.8	47.17 ± 3.32
Ba		n.d.	n.d.	n.d.

Surface areas correspond to the adhesion ability of the binding material, and consequently the strength of the mixture. Pastes consisting only of barium hydroxide, did not achieve a compact and coherent mass, and could not withstand even a small load. Therefore, the physical properties of the Ba-pastes could not be determined.

The influence of barium hydroxide on the microstructure of the binary pastes was confirmed by the examination of the fractured surfaces under the SEM (Figure 6.9).

The SEM photomicrographs show that a coarser and more porous structure is observed as the barium content is increased. Small amounts of spherical air voids of around 100μm diameter are randomly distributed within the Ca-paste, while pastes Ca2Ba2 and Ca1Ba3 exhibit large amounts of macro-pores and air voids. The structure of the Ca3Ba1 paste appears to be the less affected, and the one closer to pure slaked lime (Ca-paste).

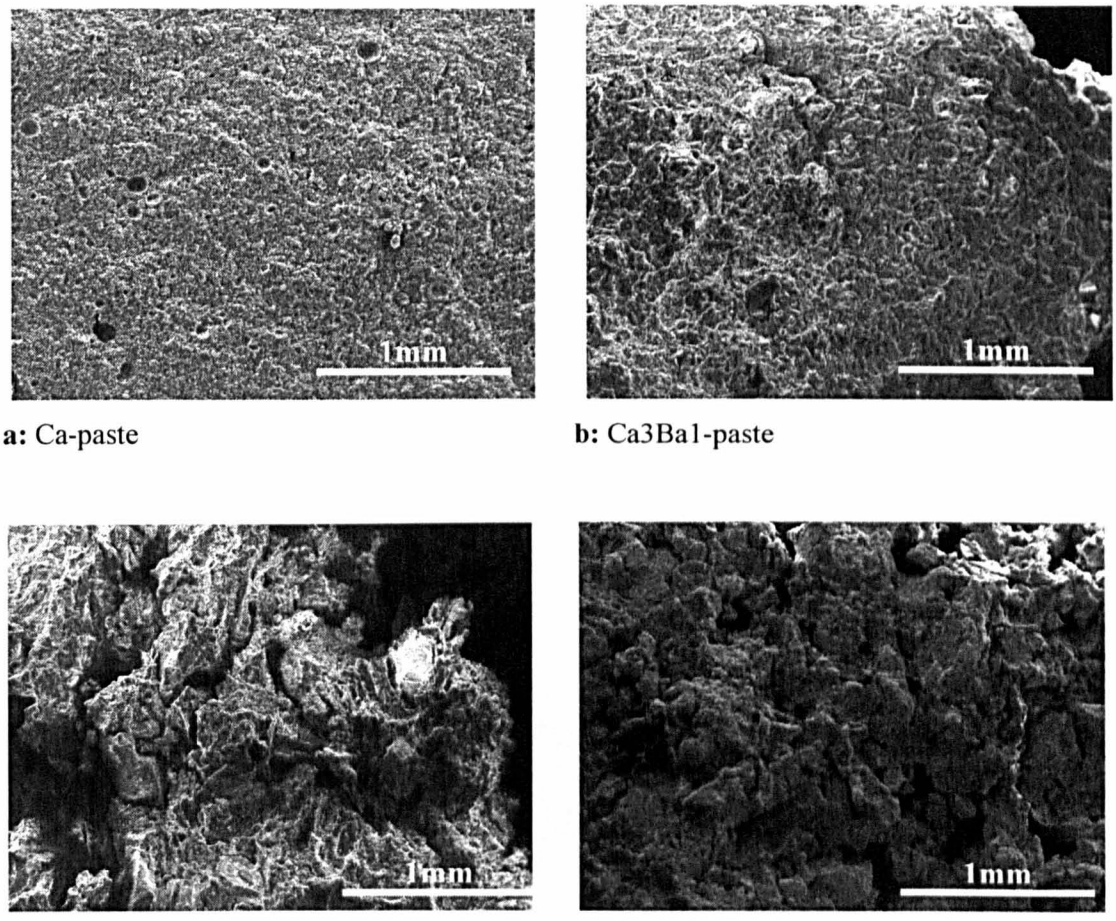

a: Ca-paste

b: Ca3Ba1-paste

c: Ca2Ba2-paste

d: Ca1Ba3-paste

Figure 6.9: Scanning electron microscope photomicrographs of fractured surfaces showing the microstructure of binary pastes after setting for three months.

Pore-size distribution diagrams are given in Figures 6.10–6.13.

In the reference sample (Ca-paste), the pore population is distributed between two peaks: the larger peak at pore radius 100nm, and a second, much smaller peak, at 3000nm (Figure 6.10). As the barium hydroxide concentration is increased, the pore population at these two peaks is gradually reduced, and a new peak formed at about 600nm (Figure 6.11). The peak at 3000nm has disappeared in sample Ca2Ba2, with pores being distributed between two peaks at around 800nm and 100nm (Figure 6.12). Finally, in sample Ca1Ba3, the majority of the pores are concentrated at a radius around 800nm (Figure 6.13).

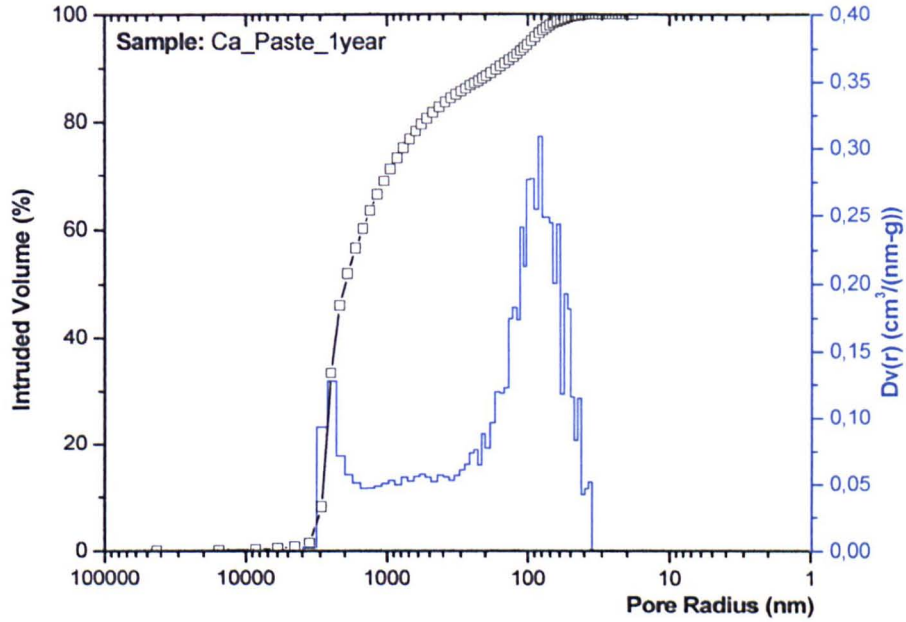

Figure 6.10: Porosity (intruded volume %) and pore-size distribution (Dv(r)) diagrams of Ca-paste.

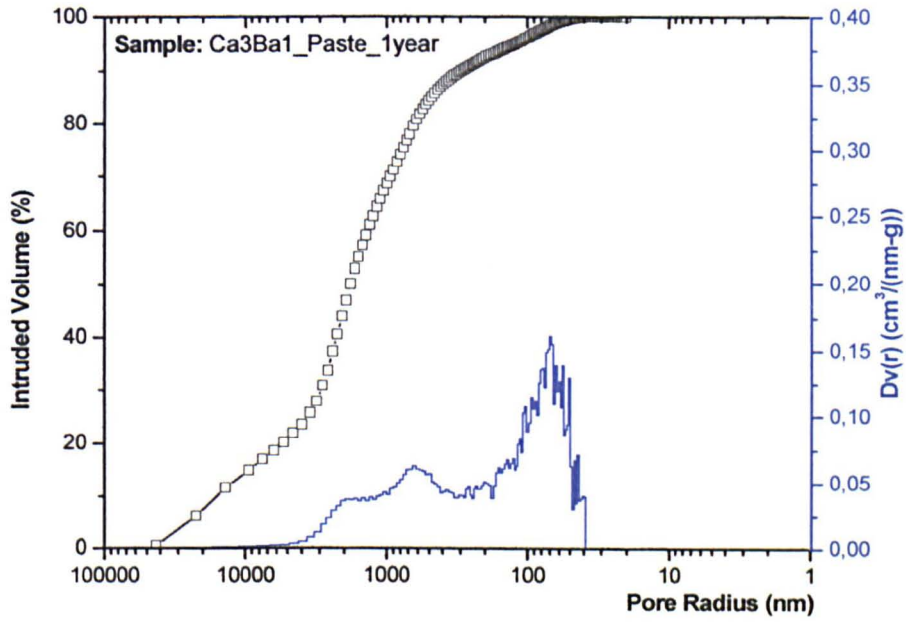

Figure 6.11: Porosity (intruded volume %) and pore-size distribution (Dv(r)) diagrams of Ca3Ba1-paste.

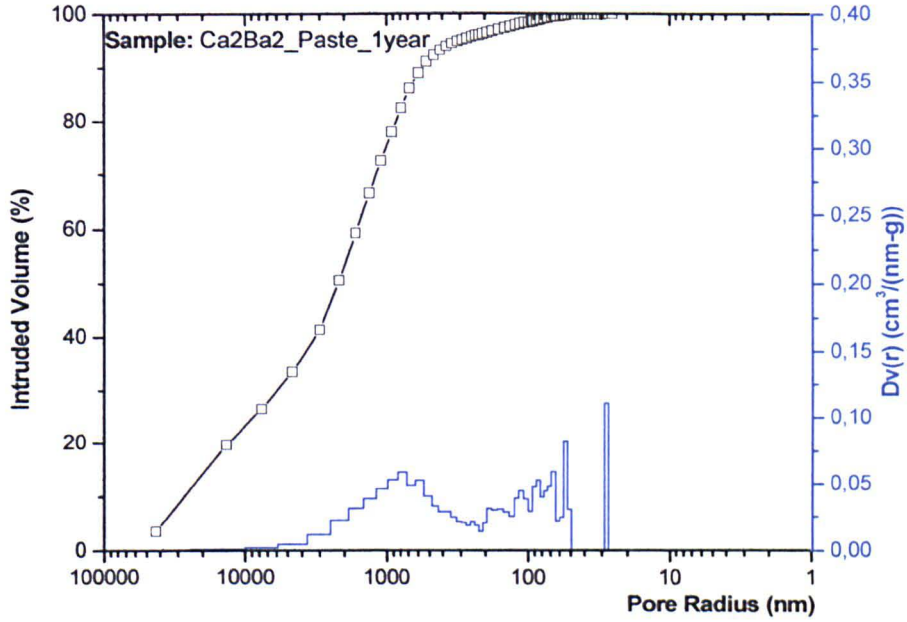

Figure 6.12: Porosity (intruded volume %) and pore-size distribution (Dv(r)) diagrams of Ca2Ba2-paste.

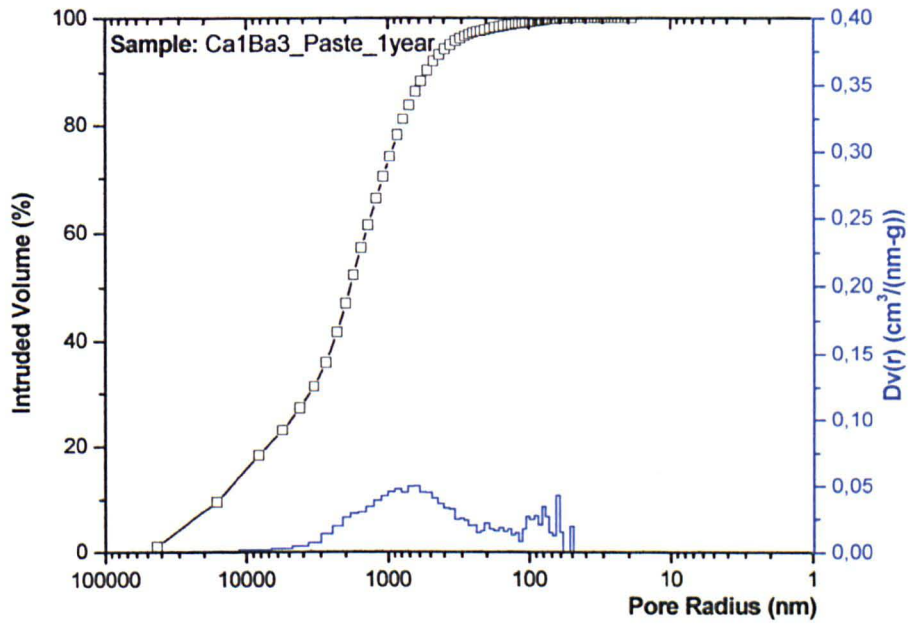

Figure 6.13: Porosity (intruded volume %) and pore-size distribution (Dv(r)) diagrams of Ca1Ba3-paste.

From the examination of the binary pastes under SEM and the results of the mercury intrusion porosimetry, it was determined that the optimum amount of barium hydroxide in the binding medium was 25% per volume (v/v).

6.3 SETTING OF BINARY PASTES

The carbonation process of the binary pastes, and the determination of the new phases formed during their setting, was studied by XRD and thermal analysis (DTA/TG). The XRD diffraction patterns of the setting products were analysed using the Search-Match software (2003) in order to extract semi-quantitative data on each crystal phase present in the sample. The diffraction patterns of the different pastes are presented in Figures 6.14–6.18. The relative concentrations (%) of the phases identified in the binary pastes at different setting periods are given in Table 6.3. These values are only semi-quantitative, as the precision of the results is reduced when strong peaks overlap weaker peaks of other phases.

Calcite, and a small portion of aragonite, are the two carbonate phases ($CaCO_3$) formed during the carbonation of lime putty. A considerable amount of portlandite [$Ca(OH)_2$] was identified in all of the samples containing lime, even those with a setting period of 12 months (Table 6.3).

In contrast, non-carbonated barium hydroxide was identified only in those samples analysed after a setting period of one month. Witherite ($BaCO_3$), formed by the carbonation of barium hydroxide, is the main product in the binary pastes.

Finally, barium-calcium carbonate [$BaCa(CO_3)_2$] crystals were also identified, especially in the Ca2Ba2 sample. However, its main peaks have the same 2-theta position as those of witherite.

Table 6.3: Semi-quantitative results calculated from the XRD patterns of binary pastes at twelve months using Crystallographica Search-Match software. The mineral phases identified are portlandite (Ptl), calcite (Cc), barium hydroxide hydrate (Bh), witherite (W) and aragonite (A).

Samples	**Relative concentration of phases (%)**									
Phases	Ptl		Bh		Cc		W		A	
Setting Period (months)	1	12	1	12	1	12	1	12	1	12
Ca	44	26	-	-	51	70	-	-	5	4
Ca3Ba1	37	22	3	-	3	7	57	71	-	-
Ca2Ba2	39	18	4	-	1	3	56	79	-	-
Ca1Ba3	16	9	4	-	-	-	80	91	-	-
Ba	-	-	4	-	-	-	96	100	-	-

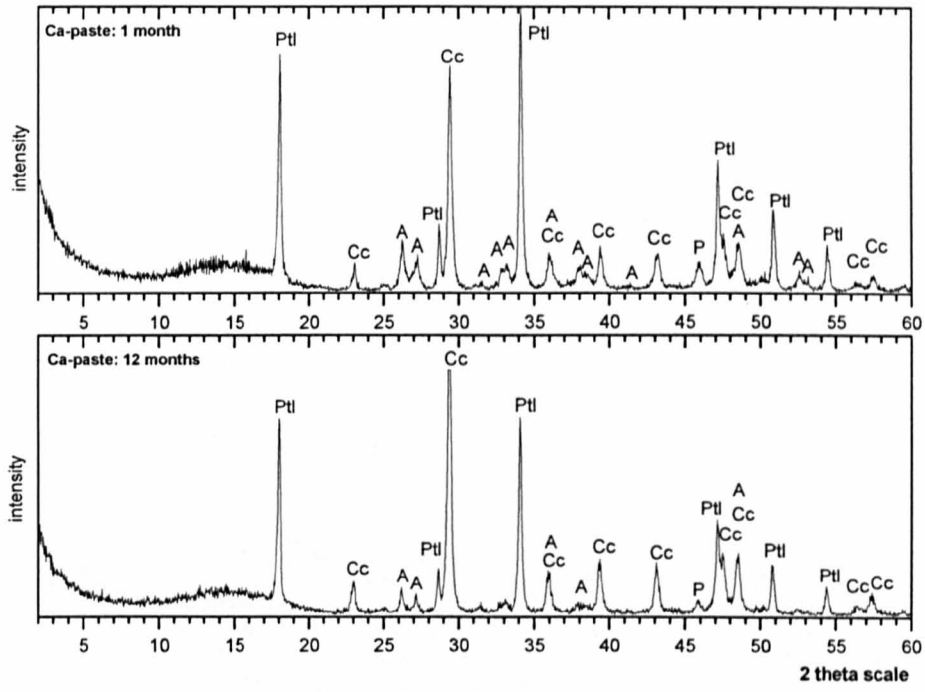

Figure 6.14: Representative diffraction patterns of Ca-paste after a one- and twelve-month setting period. Identified peaks correspond to portlandite (Ptl), aragonite (A) and calcite (Cc) mineral phases.

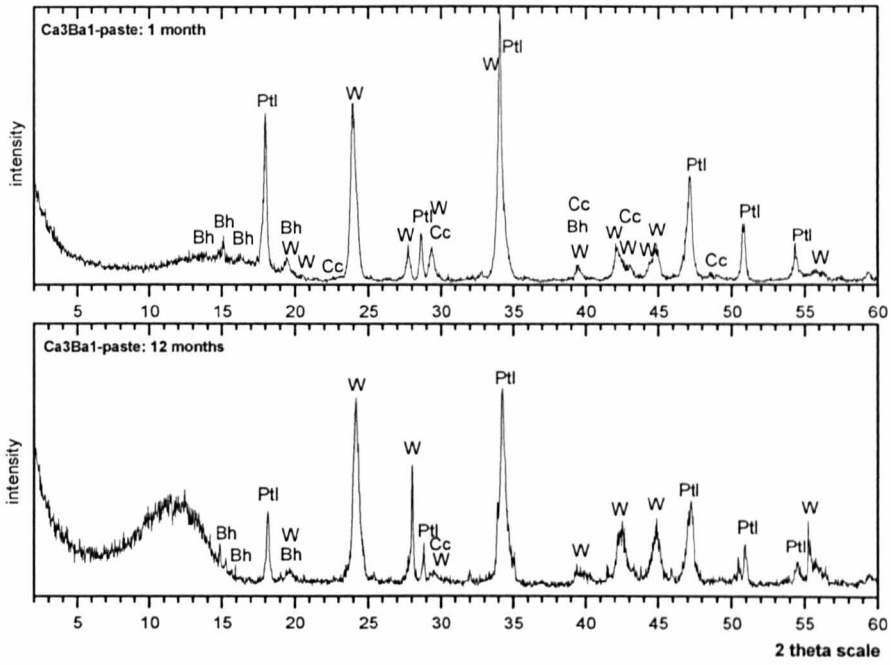

Figure 6.15: Representative diffraction patterns of Ca3Ba1-paste after a one- and twelve-month setting period. Identified peaks correspond to portlandite (Ptl), barium hydroxide hydrate (Bh), calcite (Cc) and witherite (W) mineral phases.

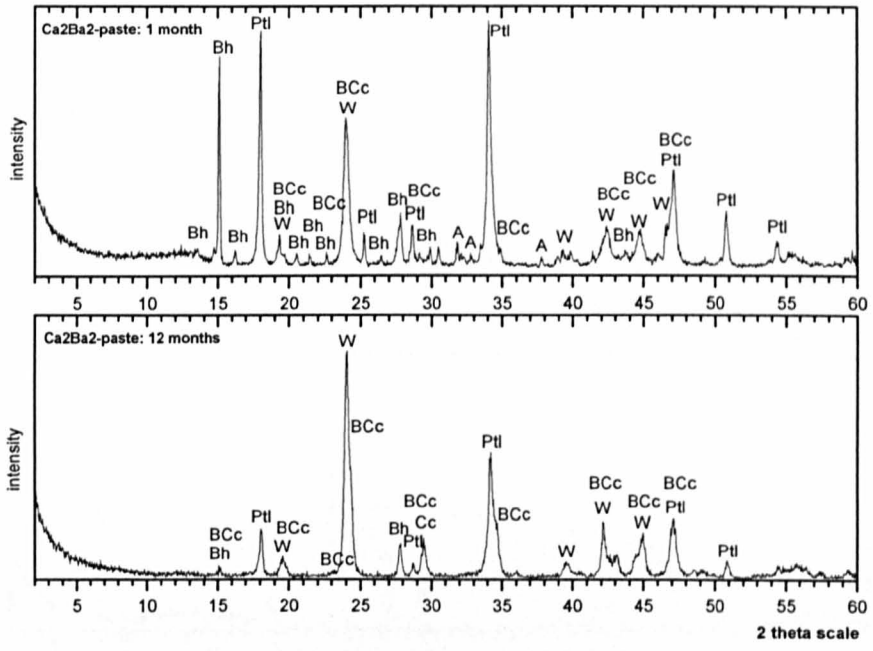

Figure 6.16: Representative diffraction patterns of Ca2Ba2-paste after a one- and twelve-month setting period. Identified peaks correspond to portlandite (Ptl), barium hydroxide hydrate (Bh), calcite (Cc) aragonite (A), witherite (W) and barium-calcium carbonate (BCc) phases.

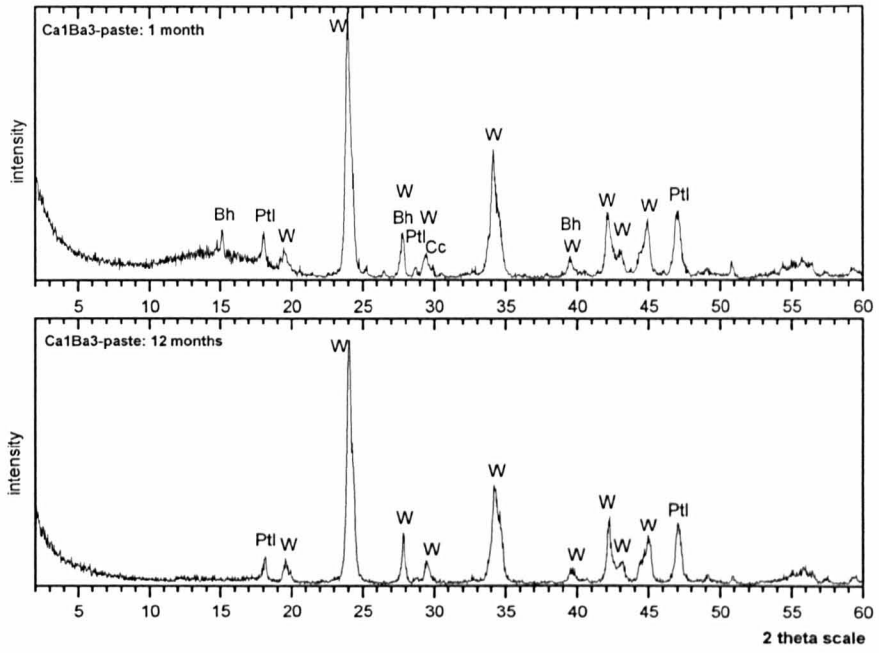

Figure 6.17: Representative diffraction patterns of Ca1Ba3-paste after a one- and twelve-month setting period. Identified peaks correspond to portlandite (Ptl), barium hydroxide hydrate (Bh), calcite (Cc) and witherite (W) phases.

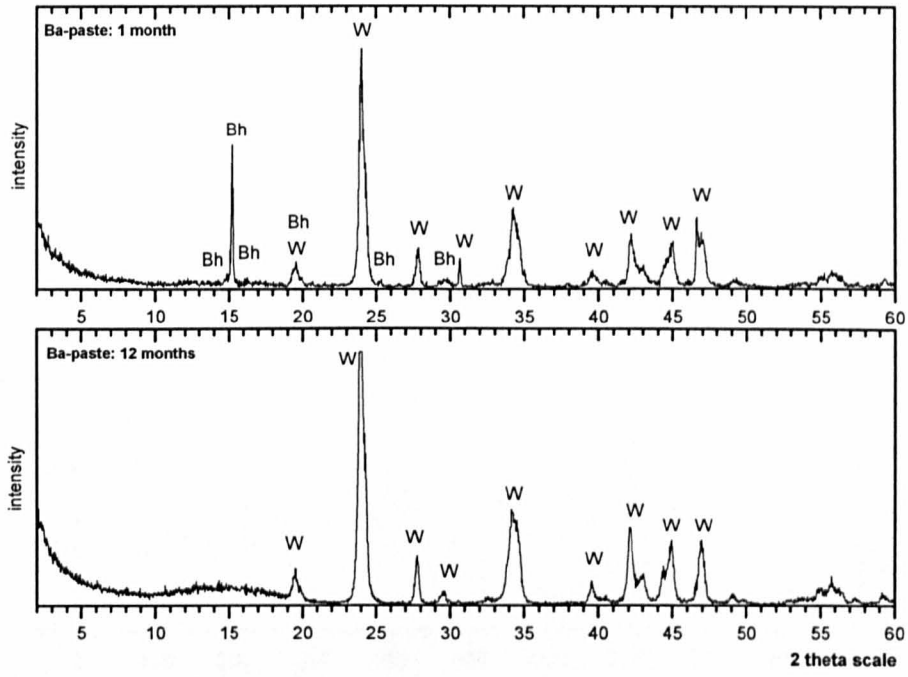

Figure 6.18: Representative diffraction patterns of Ba-paste after one and twelve months setting period. Identified peaks correspond to barium hydroxide hydrate (Bh) and witherite (W) phases.

The thermal analysis diagrams, given in Figures 6.19–6.23, describe the thermal transformations (μV) and weight changes (%) attributed to the dehydration, dehydroxylation and decarboxylation reactions that are taking place during continuous heating of the samples. The weight loss values (%) of the binary pastes, at different temperature ranges, are summarised in Table 6.4.

Table 6.4: Thermal analysis (DTA/TG) results of binary pastes at twelve months. Values correspond to the weight loss (%) of samples at different temperature ranges.

Temperature range (°C)	<80	80-120	120-450	450-750	750-950	
Samples	**Weight loss (%)**					Total
Ca	0.58	0.22	7.70	30.13	nd	38.63
Ca3Ba1	2.21	0.24	7.32	15.60	3.86	29.23
Ca2Ba2	9.77	1.55	5.48	6.50	4.68	27.98
Ca1Ba3	10.26	1.46	3.01	4.11	4.72	23.56
Ba	24.03	3.00	0.51	nd	4.22	31.76

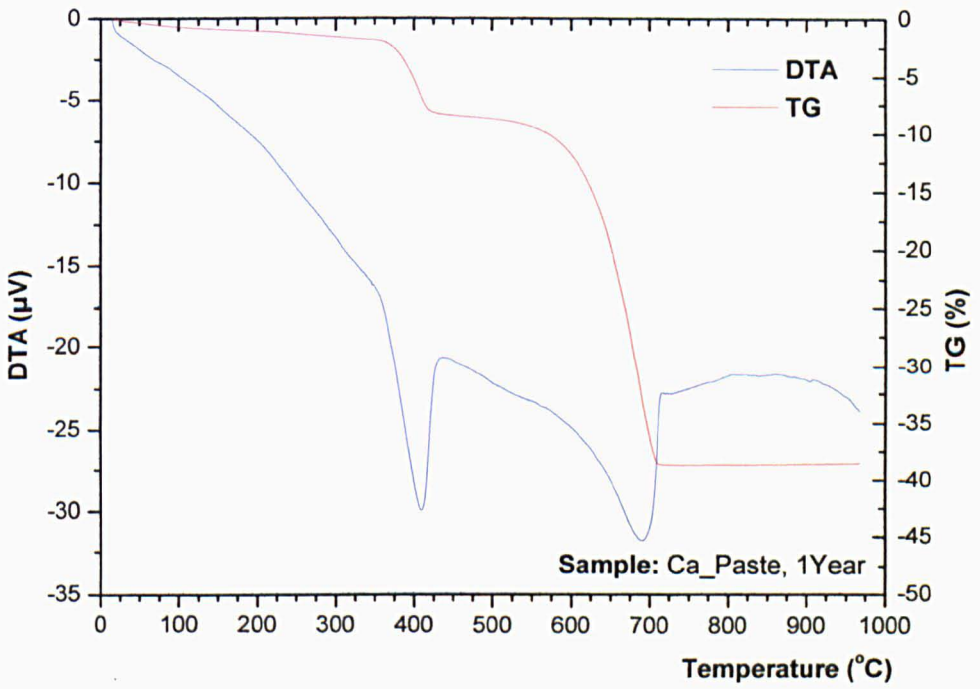

Figure 6.19: Representative diagrams of thermal analysis of Ca-paste cured for 12 months.

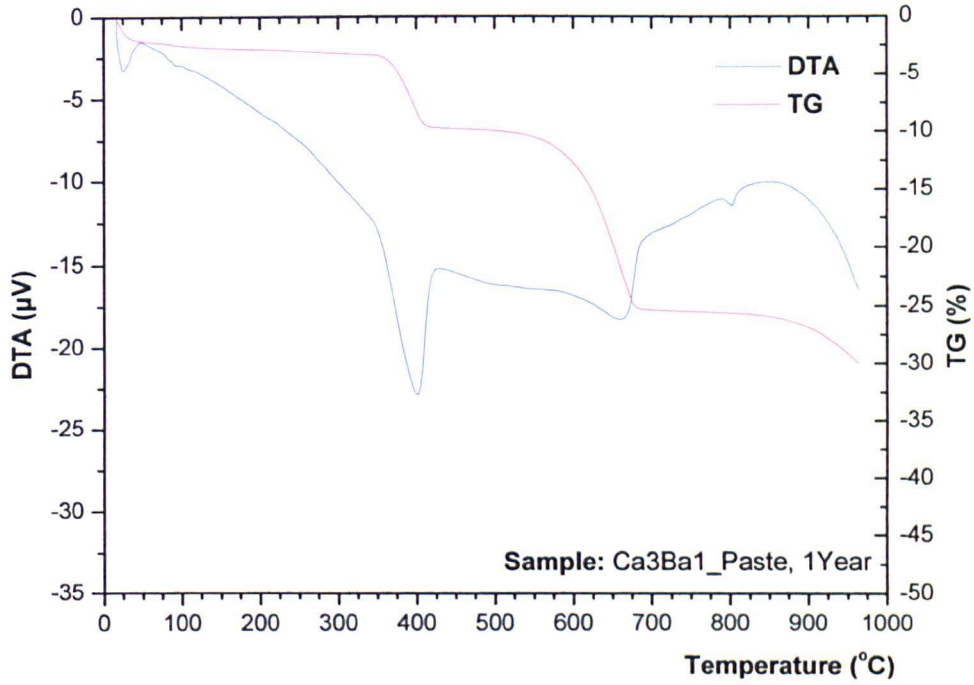

Figure 6.20: Representative diagrams of thermal analysis of Ca3Ba1-paste cured for 12 months.

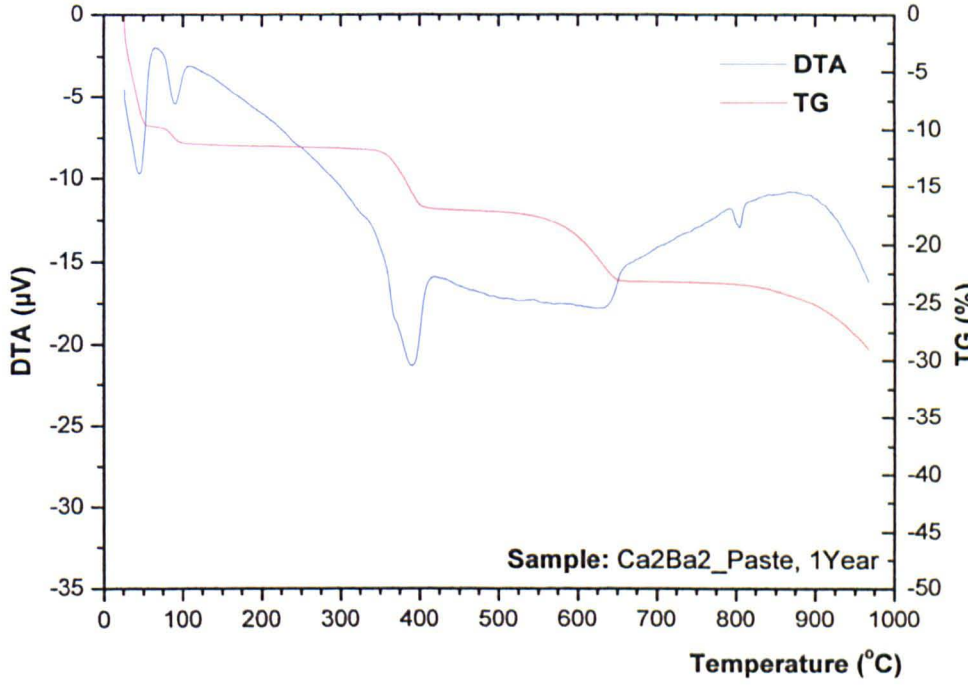

Figure 6.21: Representative diagrams of thermal analysis of Ca2Ba2-paste cured for 12 months.

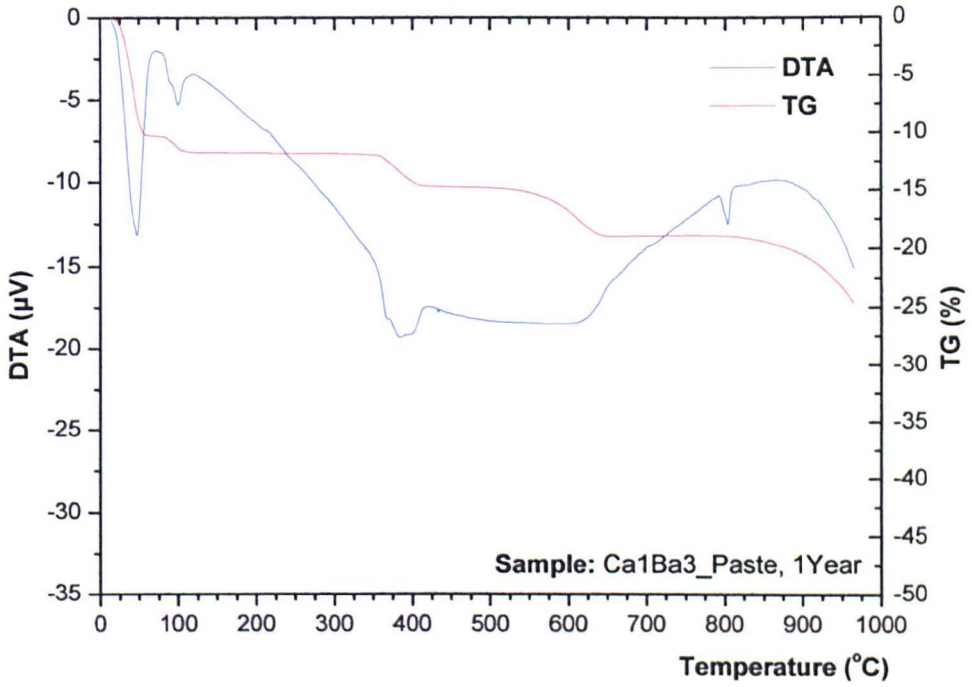

Figure 6.22: Representative diagrams of thermal analysis of Ca1Ba3-paste cured for 12 months.

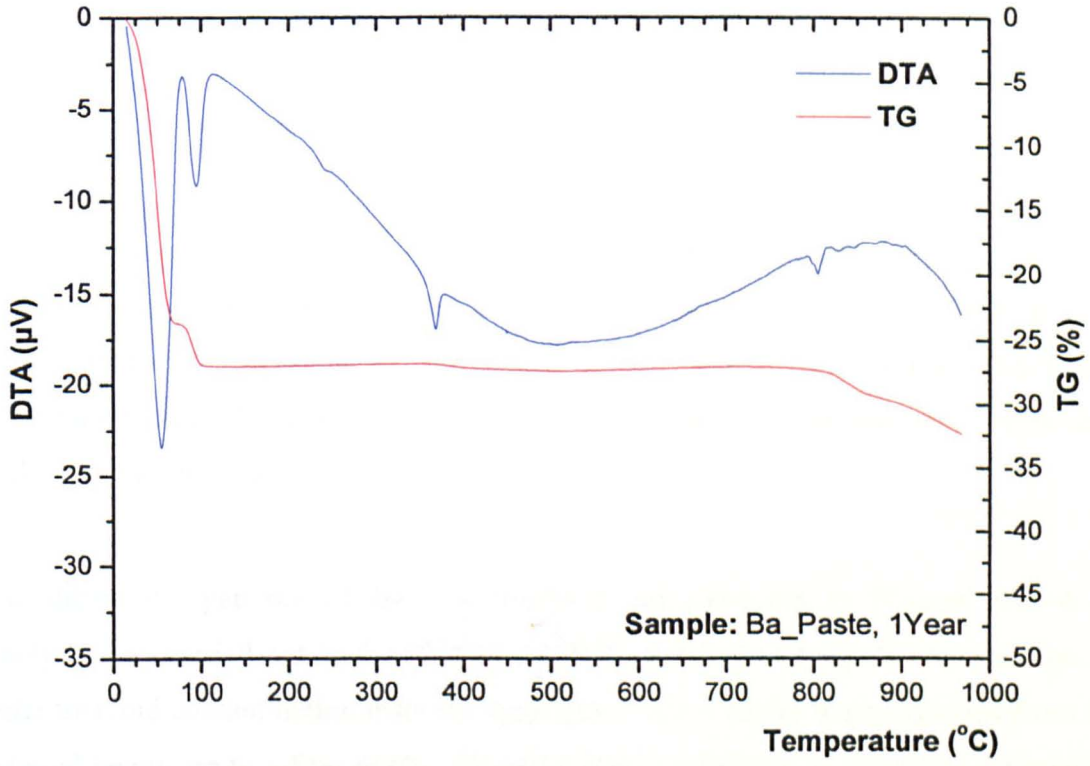

Figure 6.23: Representative diagrams of thermal analysis of Ba-paste cured for 12 months.

The peaks in the range of 80–120°C correspond to the evaporation of the absorbed water, humidity and the melting of barium hydroxide hydrate [$Ba(OH)_2 \cdot 8H_2O$] in its water of crystallisation (DiBello, 1992). The faint peak at 250°C is attributed to the dehydration of chemically-bound water in the barium hydroxide [$Ba(OH)_2$] phases. Dehydroxylation reactions for barium hydroxide and calcium hydroxide take place at 350°C and 400°C, respectively. Finally, decarboxylation of the carbonate phases is observed at 700°C for calcite ($CaCO_3$) and at 800°C for witherite ($BaCO_3$).

6.4 SETTING PRODUCTS OF MORTAR MIXTURES

Mortar mixtures were produced according to the results derived from the study of the binary pastes. The maximum content of barium hydroxide hydrate was found to be 25% per volume. Accordingly, three mixtures containing different amounts of barium hydroxide were produced and their properties compared to those of a reference mixture (LM-03), containing no barium. The mixture LM-04 contain 10% barium hydroxide hydrate, LM-05, 25%, while in LM-06 a saturated solution of barium hydroxide (at 80°C) replaced the water in the mixture.

The mineralogical composition of the phases formed during the setting of the LM mixtures was monitored by means of XRD and thermal analysis (DTA/TG). The examination of thin-sections and fractured surfaces using SEM-EDX provided further information about the setting process and the distribution of barium (Ba) compounds within the mortars mass.

The diffraction patterns of the LM mixtures are presented in Figures 6.24–6.27. Analysis was carried out in the binding material of the specimens, after separation, in order to avoid contamination from the aggregates. The samples were collected from the external layers, up to 1.5cm depth. The main phases identified in the reference mixture (LM-03) were calcite ($CaCO_3$), portlandite [$Ca(OH)_2$] and a small amount of quartz

(Figure 5.51). Calcite is produced by the carbonation of the lime binder while portlandite is attributed to the non-carbonated lime putty. Calcite and witherite ($BaCO_3$) were the main products identified in the mixtures that contain barium hydroxide hydrate (LM-04, LM-05 and LM-06), along with portlandite and some small amounts of quartz or clay minerals. Moreover, there are also indications about the formation of pozzolanic compounds, such as gismondine ($CaAl_2Si_2O_8{\cdot}4H_2O$) in all mixtures, and the presence of barium-calcium carbonate [$BaCa(CO_3)_2$] in sample LM-05. The interaction between barium and calcium is also evident under the SEM (Figure 6.28).

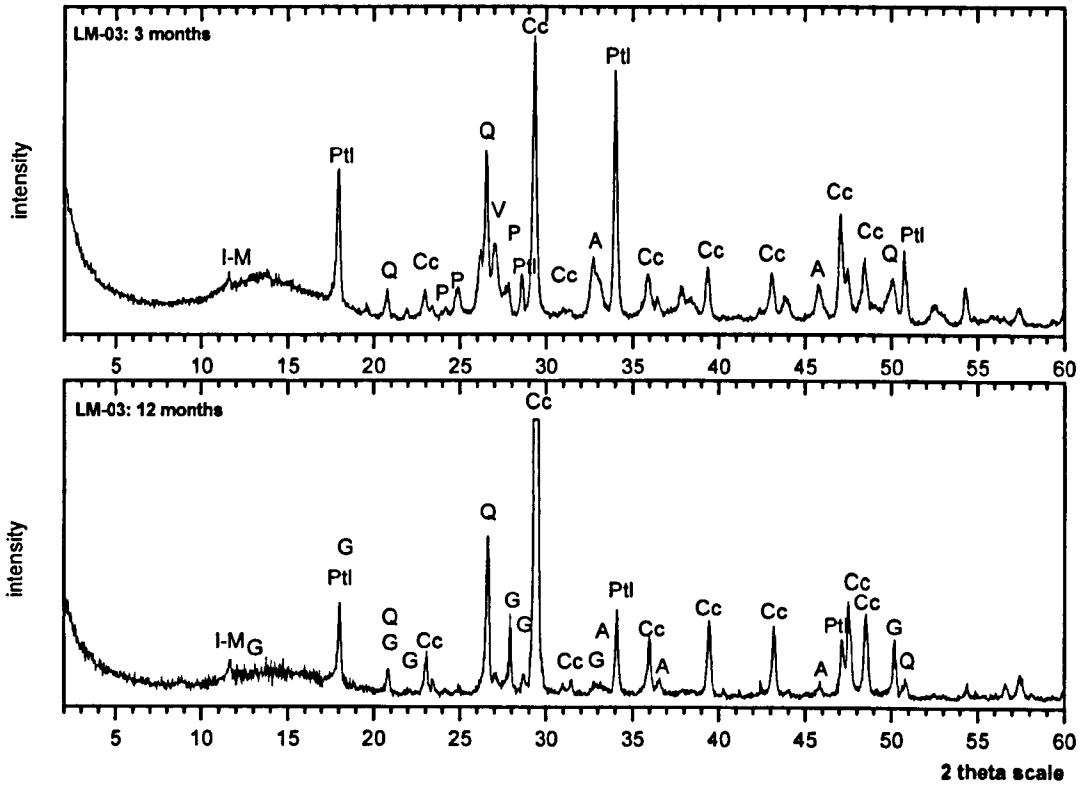

Figure 6.24: Representative diffraction patterns of LM-03 mixture after a three- and twelve-month setting period. Identified peaks correspond to portlandite (Ptl), quartz (Q), illite-montmorilonite (I-M), plagioclase (P), calcite (Cc), vaterite (V), aragonite (A) and gismondine (G) phases.

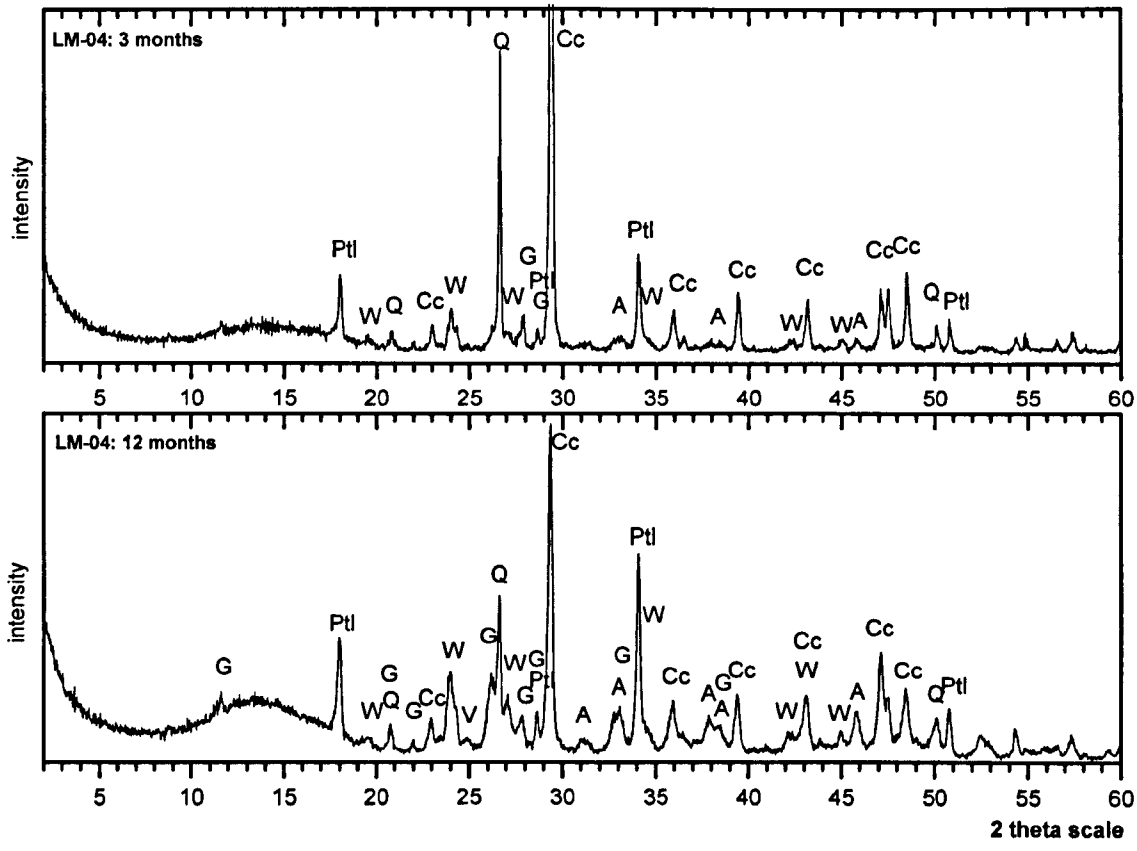

Figure 6.25: Representative diffraction patterns of LM-04 mixture after a three- and twelve-month setting period. Identified peaks correspond to portlandite (Ptl), quartz (Q), witherite (W), calcite (Cc), aragonite (A) and gismondine (G) phases.

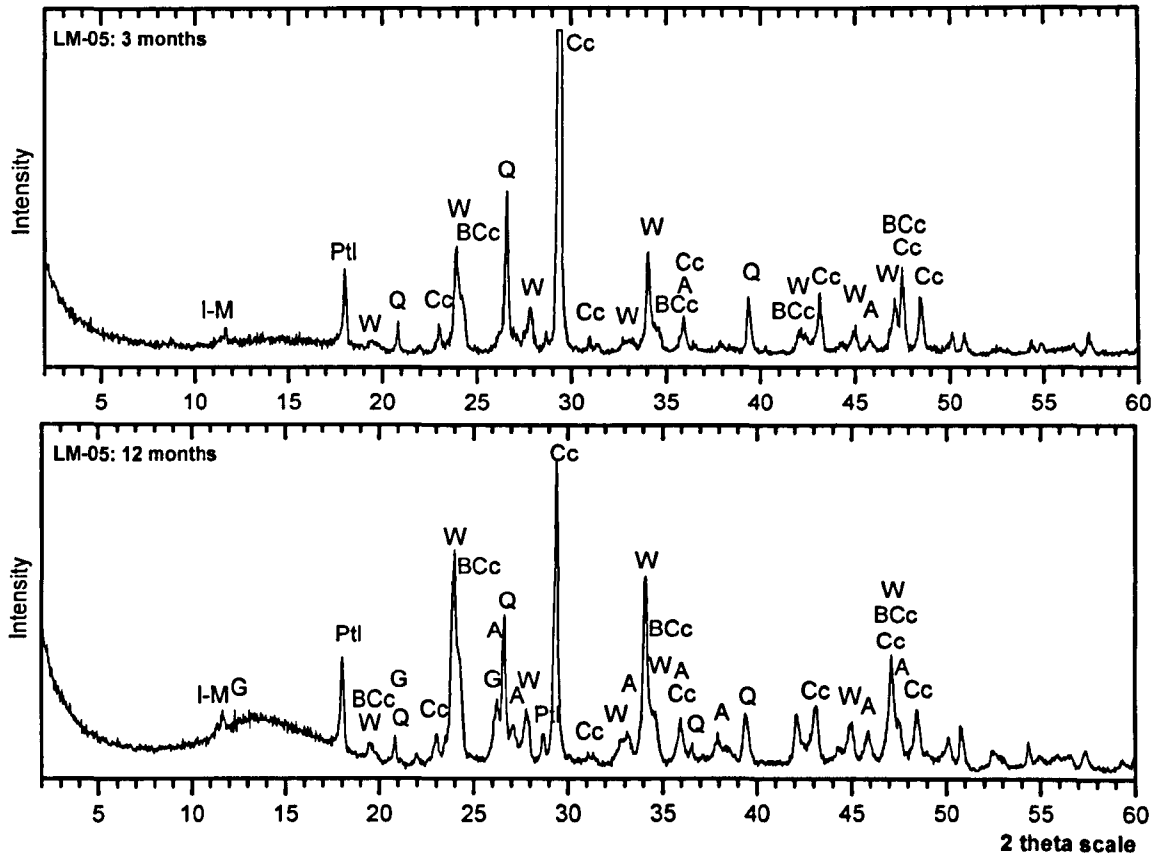

Figure 6.26: Representative diffraction patterns of LM-05 mixture after three- and twelve-month setting period. Identified peaks correspond to portlandite (Ptl), quartz (Q), illite-montmorilonite (I-M), witherite (W), calcite (Cc), barium-calcium carbonate (BCc), aragonite (A) and gismondine (G) phases.

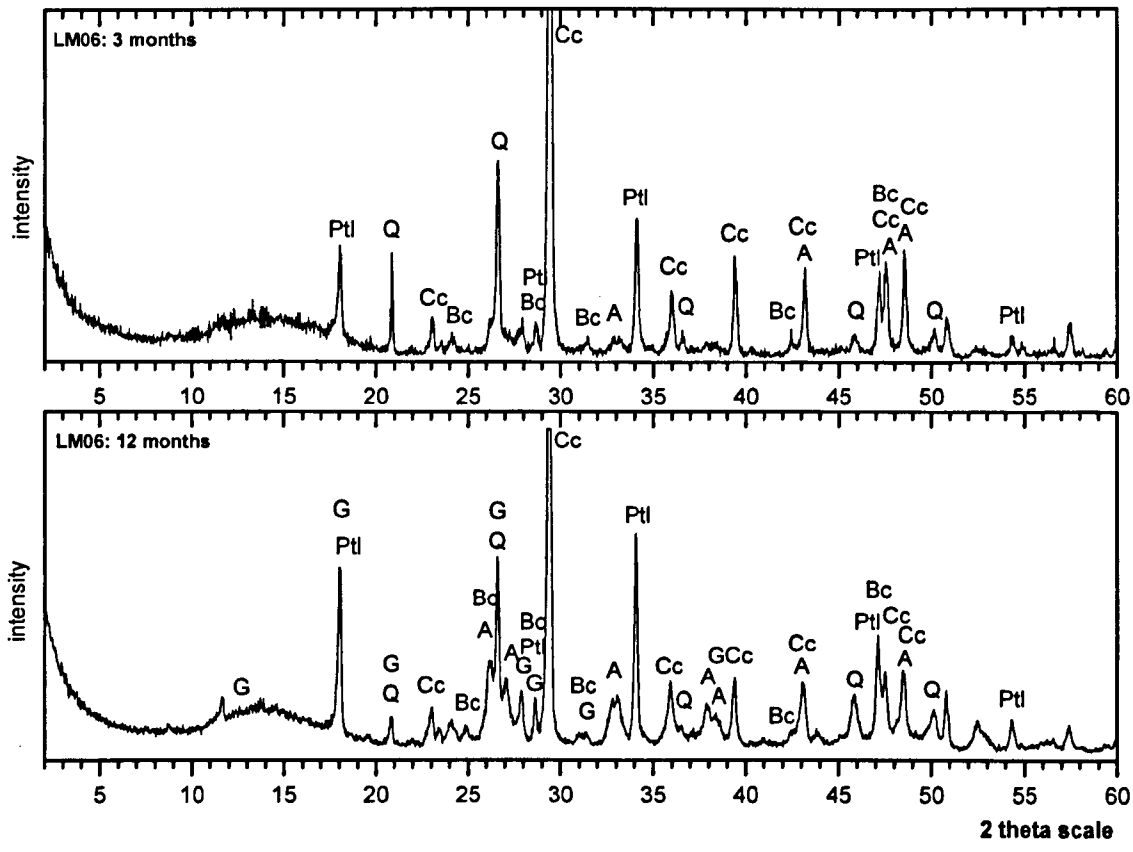

Figure 6.27: Representative diffraction patterns of LM-06 mixture after a three- and twelve-month setting period. Identified peaks correspond to portlandite (Ptl), quartz (Q), barium carbonate (Bc), calcite (Cc), aragonite (A) and gismondine (G) phases.

Examination of the mixtures under SEM verified that pozzolanic reactions had taken place between lime and the ceramic material, which resulted in the formation of hydrated phases (CSH), with the typical needle-like shape (Figure 6.29). The size and the shape of the other phases formed during the setting of the LM-mixtures are given in Figures 6.30 to 6.33.

X-ray mapping of elements present in the LM-mixtures (Figures 6.34–6.36) showed that barium (Ba) was homogeneously distributed through the mortars containing barium hydroxide, and concentrated around the calcite grains (Figures 6.35 and 6.36).

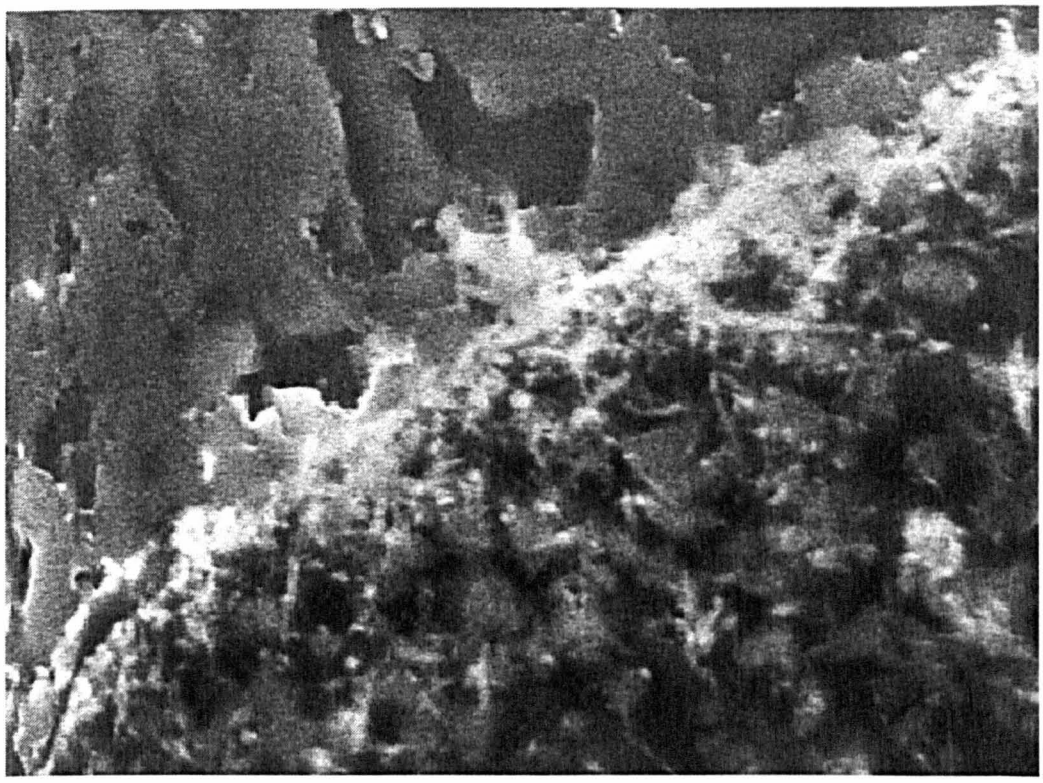

SE image

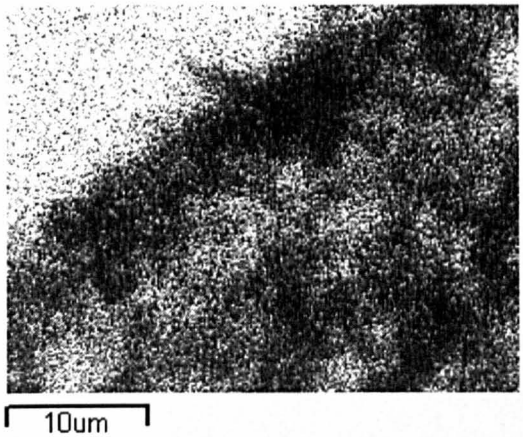

X-ray map: Ca

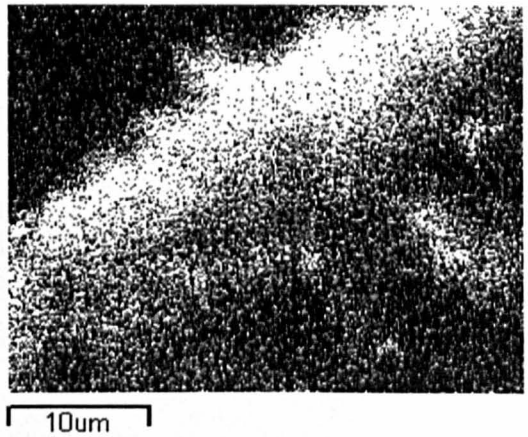

X-ray map: Ba

Figure 6.28: Thin-section of mixture LM-05 under SEM after curing for twelve months. X-ray maps indicate the interaction between barium and calcium compounds which leads to the formation of a mixed area with compact structure.

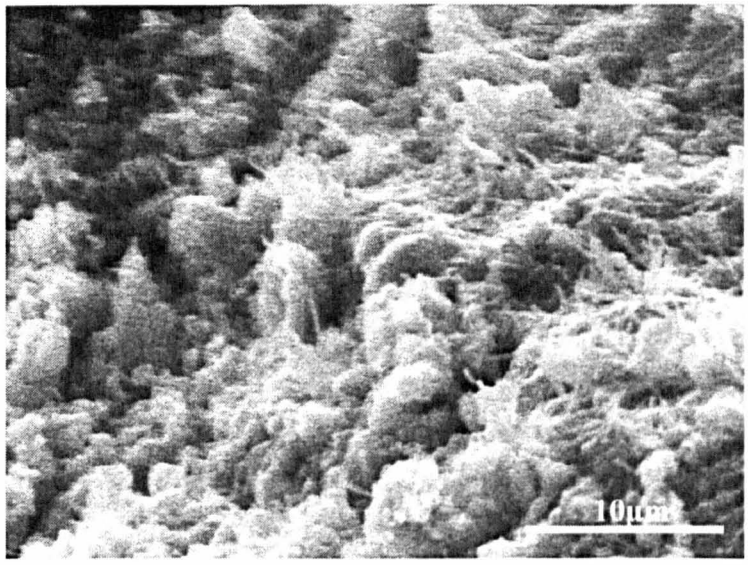

Figure 6.29: Mixture LM-03 under the SEM. Initial stage of the development of hydrated phases (CSH), which were produced by the reaction of lime with the pozzolanic material (ceramic).

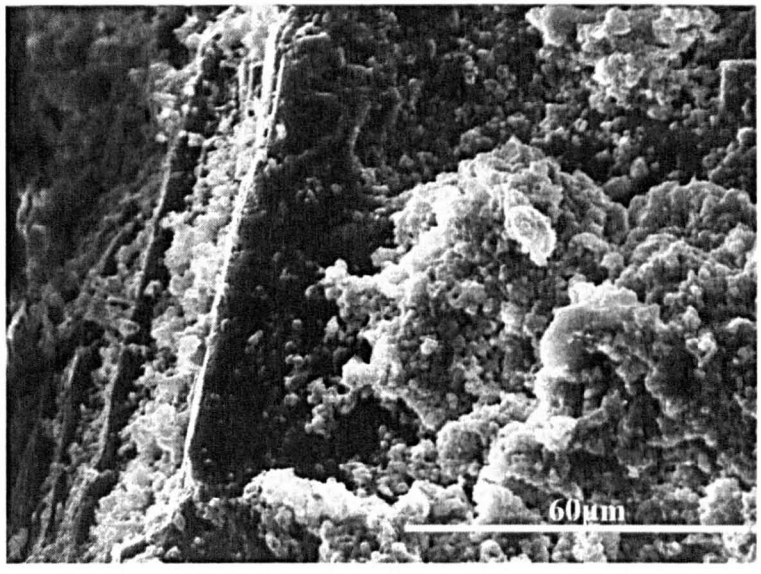

Figure 6.30: Fractured surface of LM-03 mixture under SEM after curing for three months, showing the surface of a large ceramic grain covered with irregularly shaped calcite crystals.

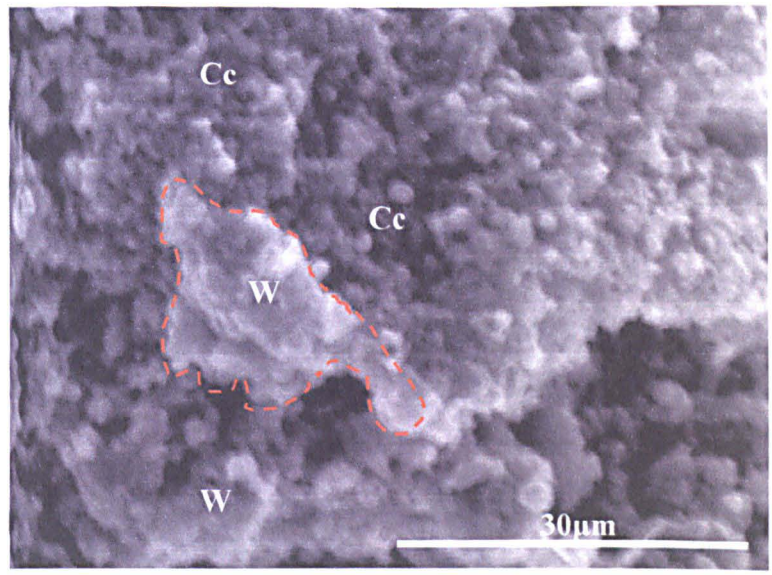

Figure 6.31: Mixture LM-05 under SEM after curing for three months. Spherical calcite crystals are partially covered with witherite.

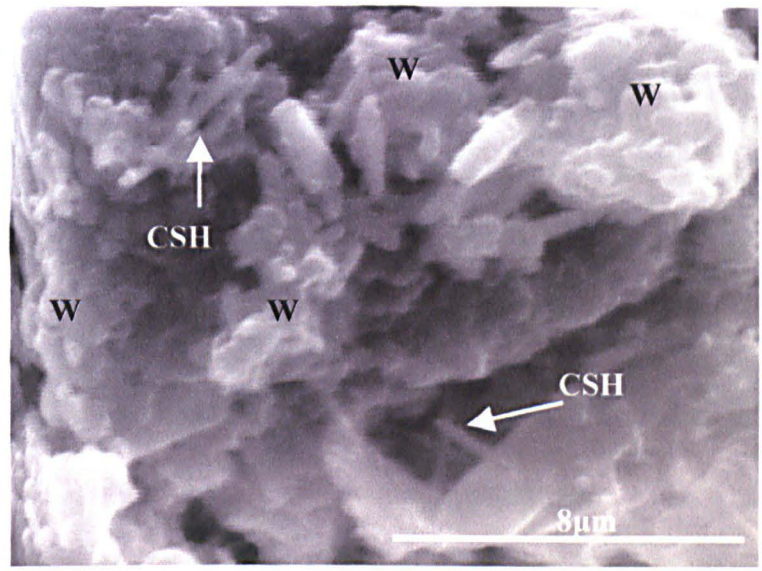

Figure 6.32: Mixture LM-05 after curing for three months. Scanning electron photomicrograph of witherite crystals. Traces of needle-like, hydrated (CSH) phases are also observed.

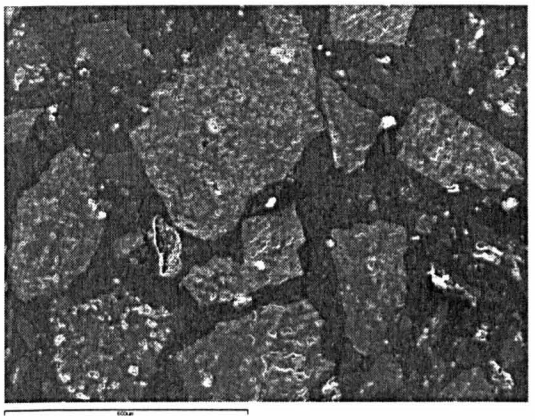

SE image (X100)

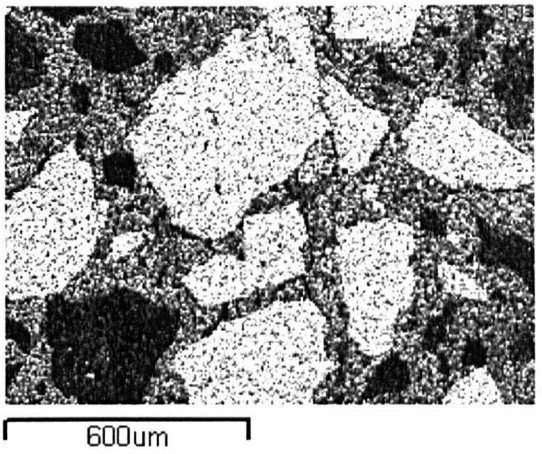

X-ray map: Ca

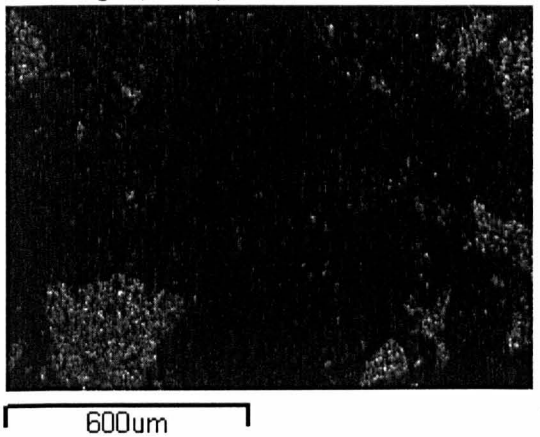

X-ray map: Al

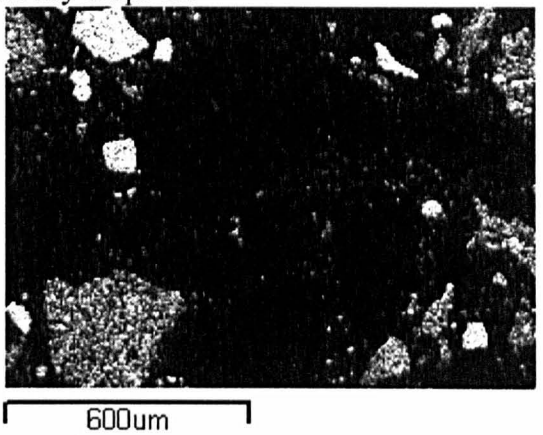

X-ray map: Si

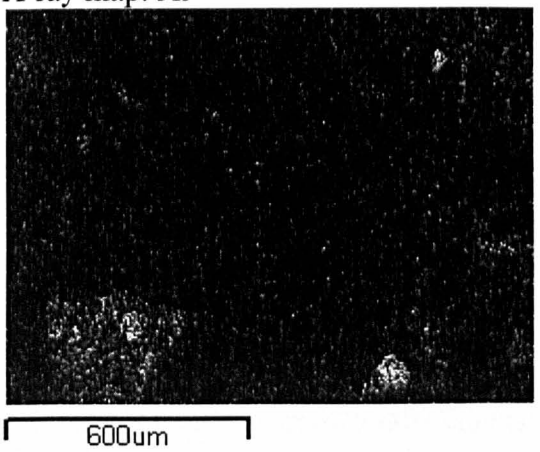

X-ray map: K

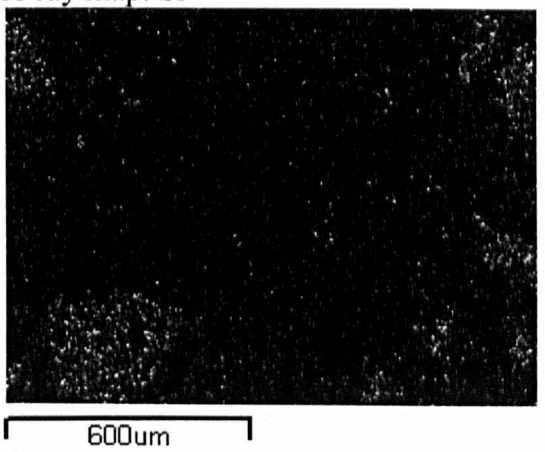

X-ray map: Fe

Figure 6.33: Thin-section of mixture LM-03 (reference) under SEM after curing for twelve months. X-ray maps help to distinguish between calcitic and ceramic aggregate fragments.

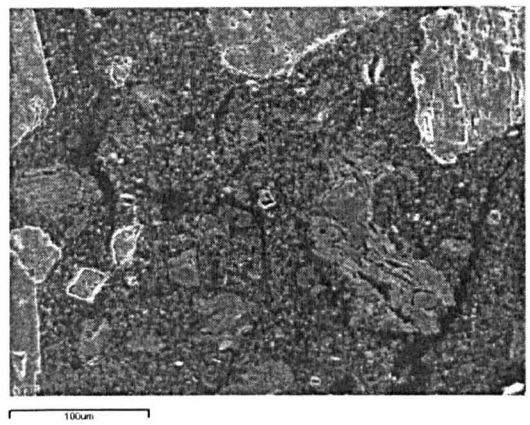

SE image (X50)

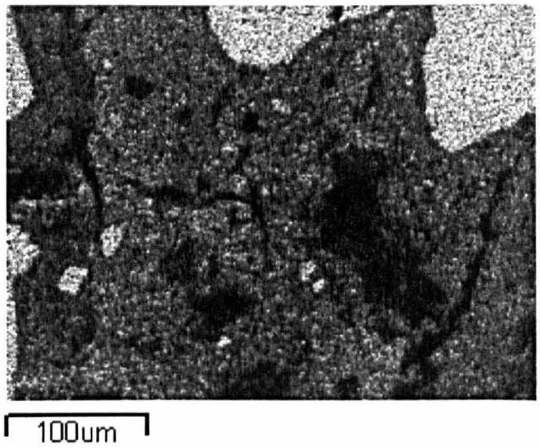

X-ray map: Ca

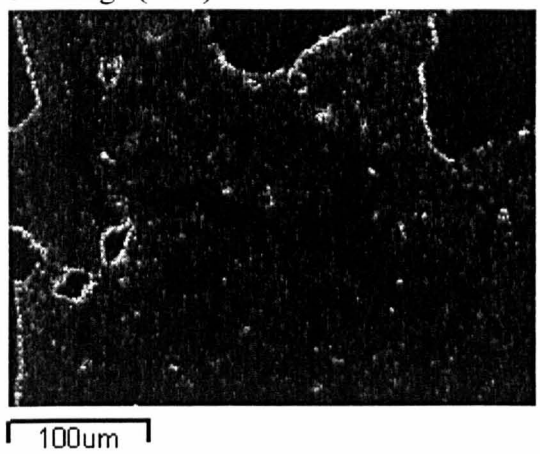

X-ray map: Ba

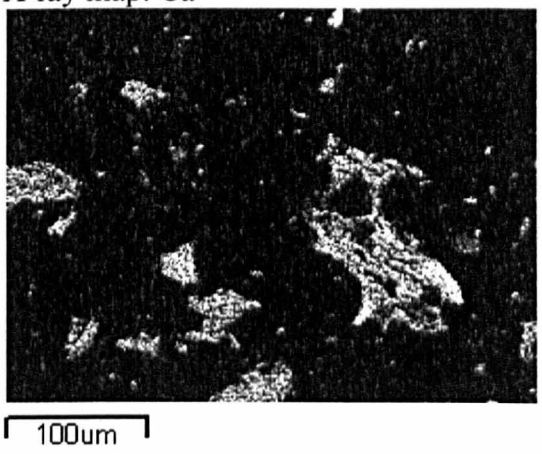

X-ray map: Al

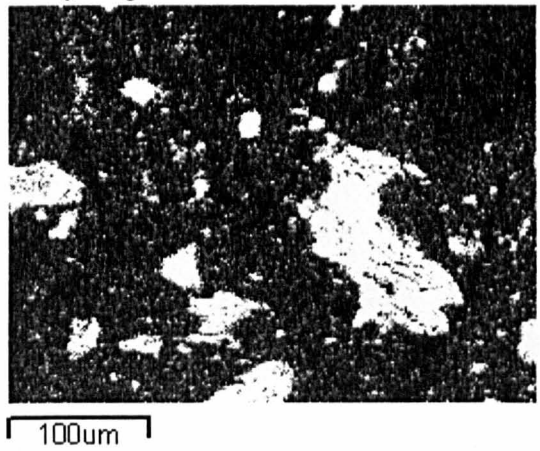

X-ray map: Si

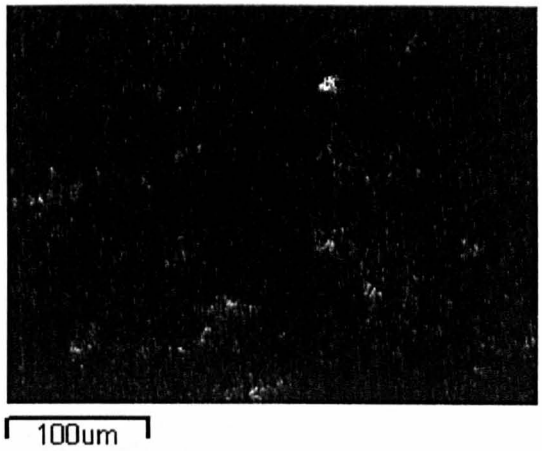

X-ray map: K

Figure 6.34: Thin-section of mixture LM-05 under SEM after curing for twelve months. X-ray mapping of elements present in the mortar indicates an increased concentration of barium around calcitic grains.

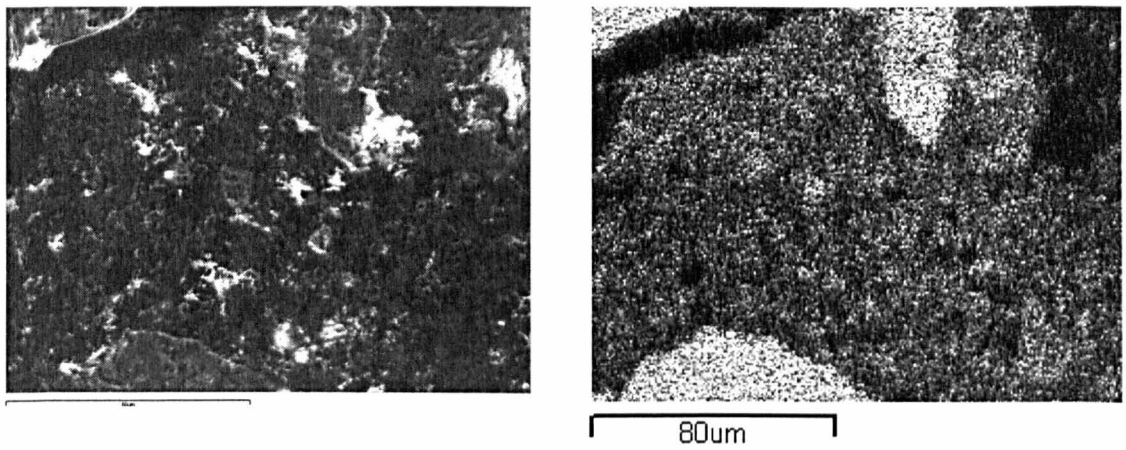

SE image (X750)

X-ray map: Ca

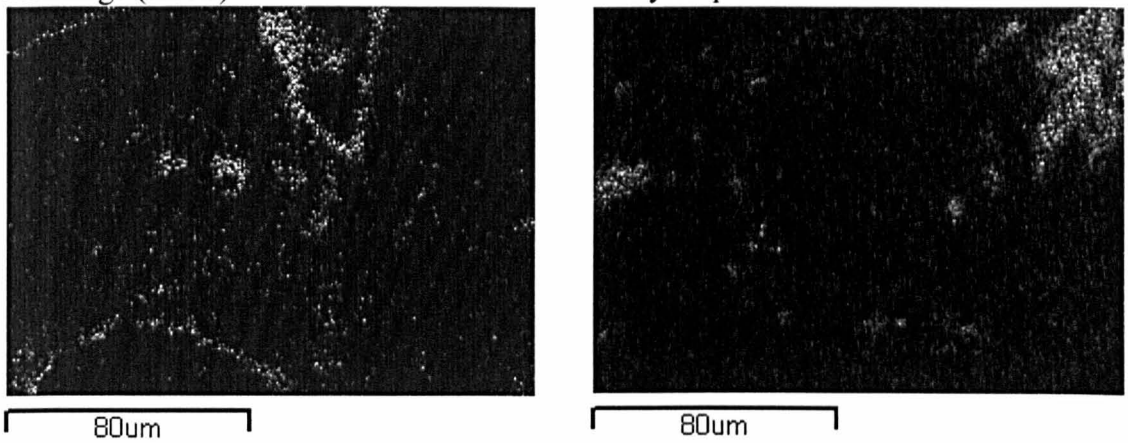

X-ray map: Ba

X-ray map: Al

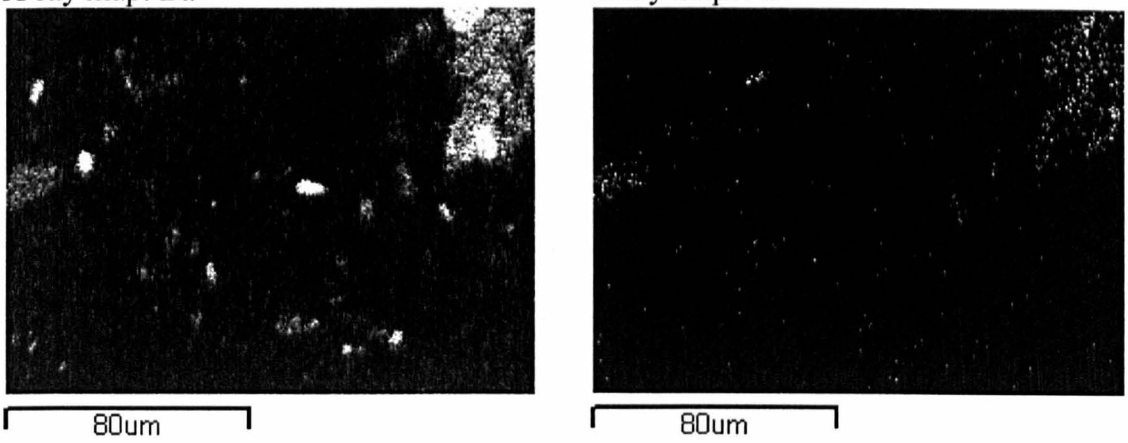

X-ray map: Si

X-ray map: Fe

Figure 6.35: Thin-section of mixture LM-06 under SEM after curing for twelve months. X-ray mapping of elements present in the mortar indicates an increased concentration of barium around calcitic grains.

Thermal analysis diagrams, given in Figures 6.36–6.39, describe the thermal transformations (μV) and weight changes (%) taking place in the binding material of the mortar mixtures after a twelve-month setting period. The weight loss values (%) of LM-mixtures, at different temperature ranges, are summarised in Table 6.5.

Table 6.5: Weight loss (%) of LM-mixtures cured for twelve months, at different temperature ranges, during thermal analysis (DTA/TG).

Temperature range (°C)	<120	120-400	400-500	500-750	750-900	
Samples	**Weight loss (%)**					Total
LM-03	1.13	2.26	1.97	25.55	0.49	31.42
LM-04	0.97	2.46	2.02	25.52	0.86	31.82
LM-05	0.94	2.44	2.02	23.11	0.96	29.48
LM-06	0.97	2.23	1.89	27.54	0.59	33.23

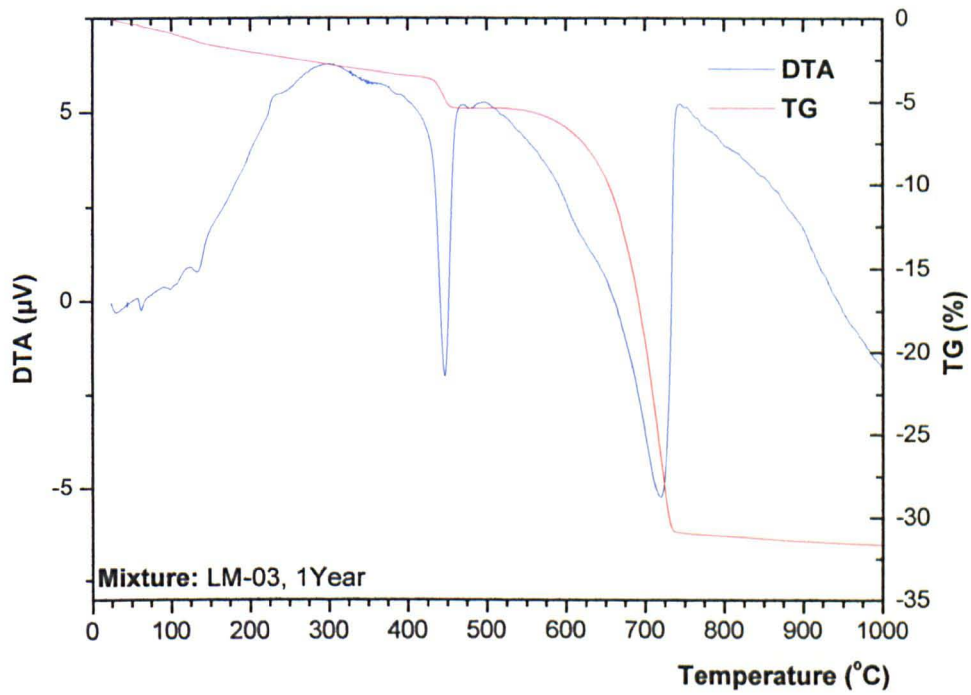

Figure 6.36: Representative thermal analysis diagrams of LM-03 mixture after a 12-month setting period.

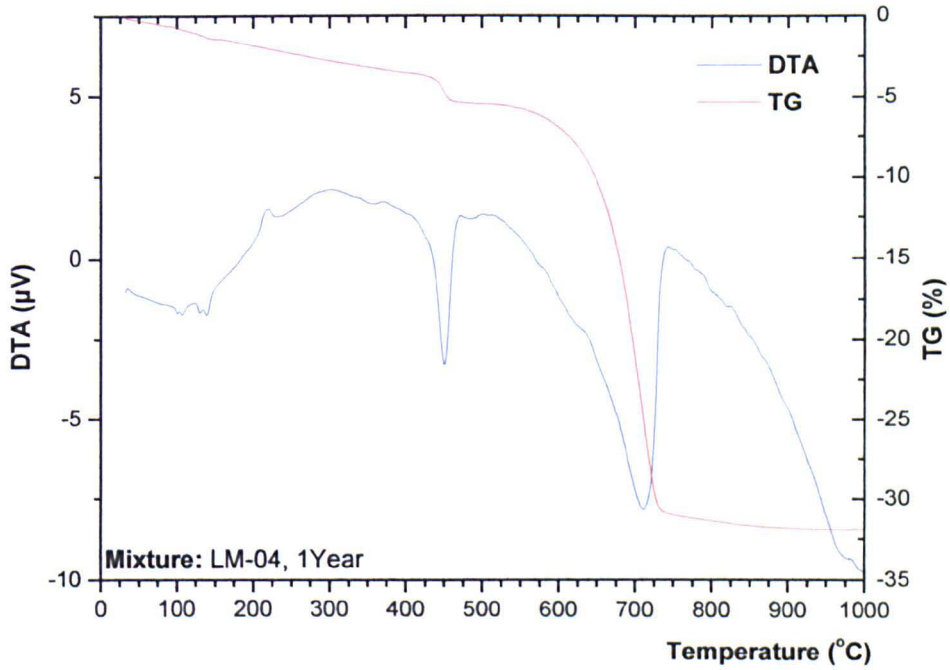

Figure 6.37: Representative thermal analysis diagrams of LM-04 mixture after a 12-month setting period.

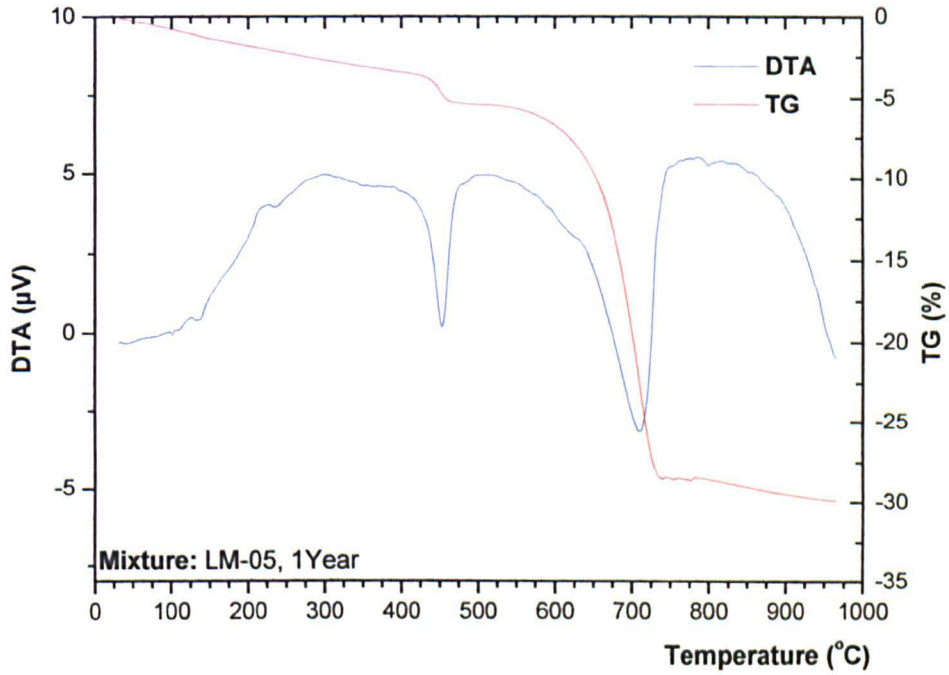

Figure 6.38: Representative thermal analysis diagrams of LM-05 mixture after a 12-month setting period.

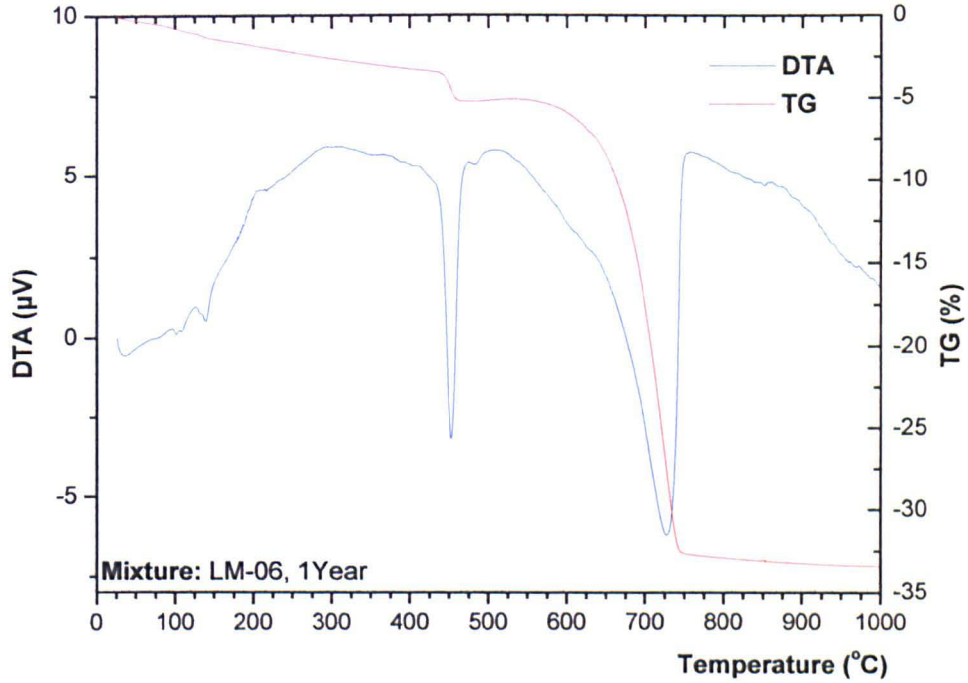

Figure 6.39: Representative thermal analysis diagrams of LM-06 mixture after a 12-month setting period.

The peaks which occurred in the temperature range between 80–200°C corresponded, in general, to the evaporation of physically-absorbed or hydroscopic water (Rice, 1987:103). However, peaks around 120°C indicated the presence of hydraulic phases (CSH), formed by the reaction of lime with the ceramic powder (Moropoulou et al., 2004a). The small peaks in the range of 200–250°C were due to the loss of water chemically bound to the aluminosilicate phases (dehydration). The very small endothermic peaks in the area around 500°C characterise the dehydroxylation of the clay minerals present in the binder fraction (Moropoulou et al., 1995). The peak at 450°C is attributed to the dehydroxylation of the non-carbonated portlandite [$Ca(OH)_2$], while the main peak at 700°C is due to the transformation of calcite ($CaCO_3$) to calcium oxide (CaO) and water (H_2O). The small peak at 800°C in samples LM-05 and LM-06 is attributed to the decarboxylation of witherite ($BaCO_3$). In LM-04, this peak is not clearly evident. Above 900°C, CaO reacts with clays forming calcium silicates (Rice, 1987: 103).

The carbonation depth of LM-mixtures after a three-month setting period was estimated between 0.5cm and 1cm (Figure 6.40). A fractured surface of the four different mortar mixtures was sprayed with a solution of phenolphthalein indicator (1% wt) dissolved in alcohol. The area coloured violet indicates the non-carbonated surface of the specimens.

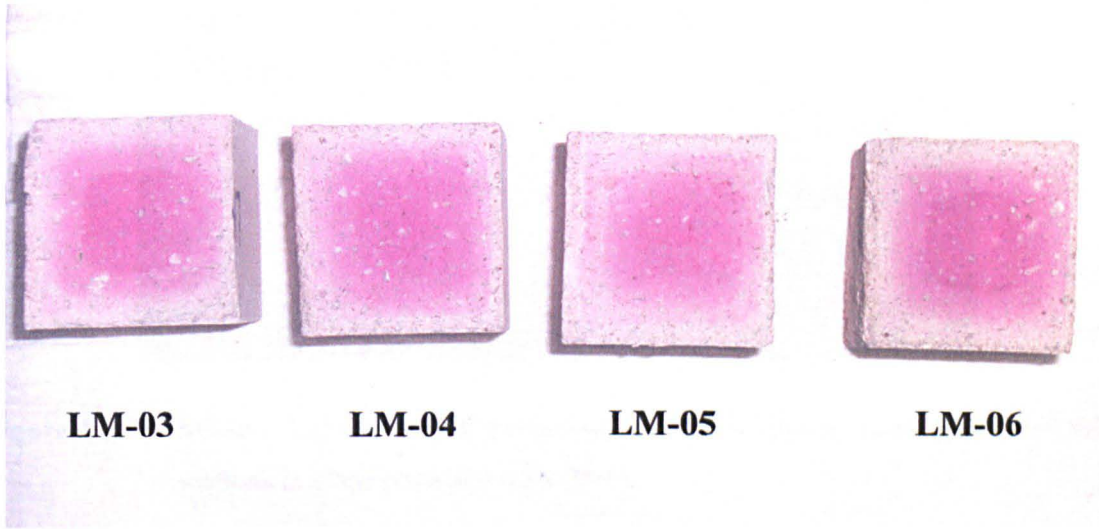

Figure 6.40: Fractured surfaces of the four LM-mixtures after a three-month setting period. The surfaces were sprayed with a phenolphthalein indicator solution. The area coloured violet indicates the non-carbonated portlandite.

6.5 MICROSTRUCTURE OF MORTAR MIXTURES

In order to study the microstructure, thin-sections of LM-mixtures were examined under the petrographic and scanning electron microscope. The photomicrographs of the different mixtures are given in Figures 6.41–6.48.

All of the mixtures exhibited a homogenous matrix, with rich binding material and very good aggregate distribution. A network of micro-cracks was formed during setting. Shrinkage micro-cracks in all mixtures were mainly located around the angular calcitic fragments. This may be attributed to the faster evaporation of water from sedimentary aggregates and the water retention by the ceramic fragments for a longer period. Spherical air voids were randomly distributed throughout the mortar. Air voids were created by the air which is encapsulated in the wet mixture during the mixing procedure.

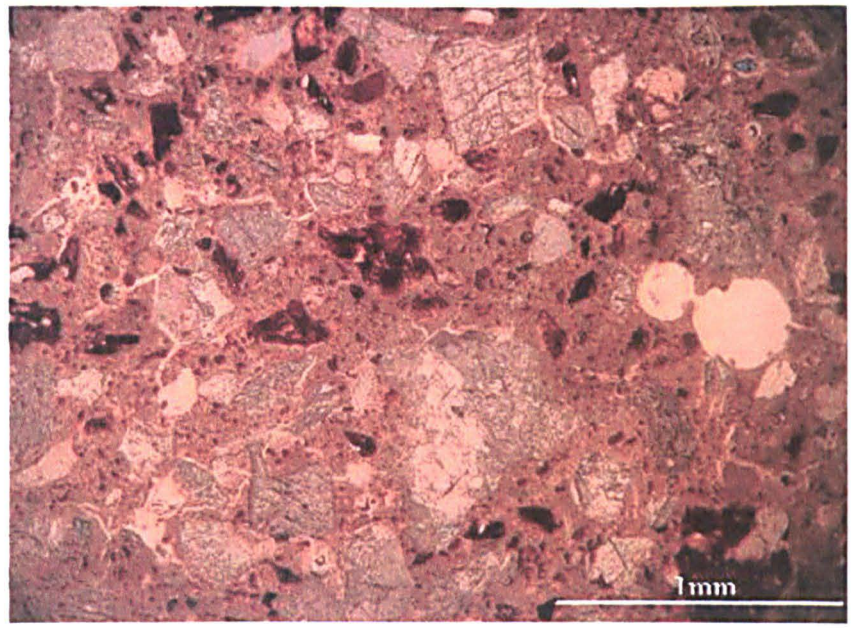

Figure 6.41: Mixture LM-03 after a twelve-month setting period. Examination of thin-sections in plane polarised light (PPL).

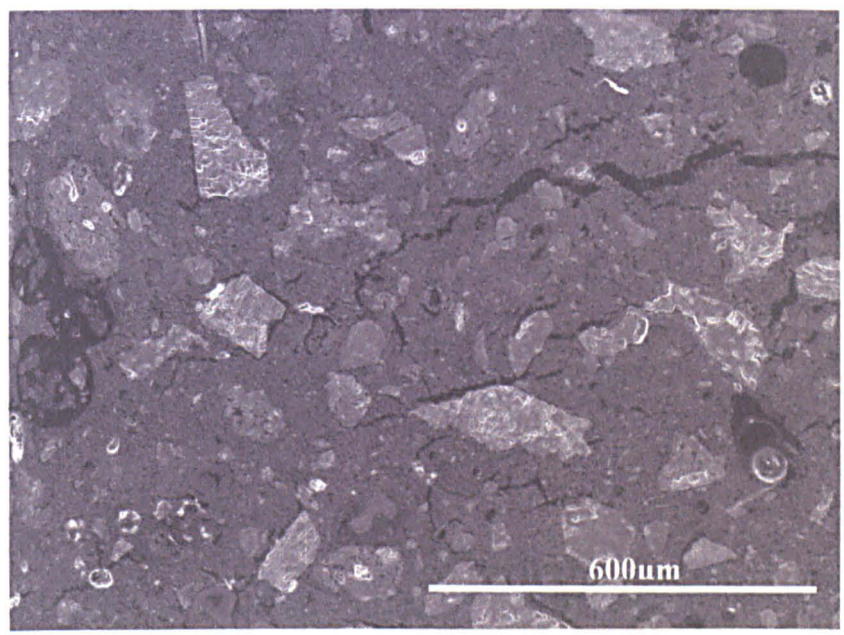

Figure 6.42: Mixture LM-03 after a twelve-month setting period. Photomicrograph of thin-section under SEM, indicating the network of shrinkage cracks and air voids.

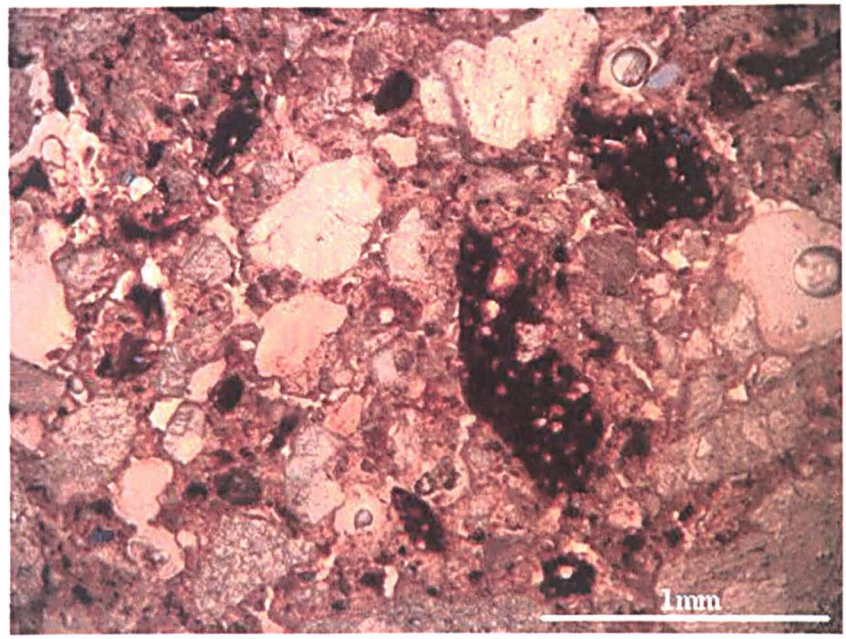

Figure 6.43: Mixture LM-04 after a twelve-month setting period. Examination of thin-sections in plane polarised light (PPL).

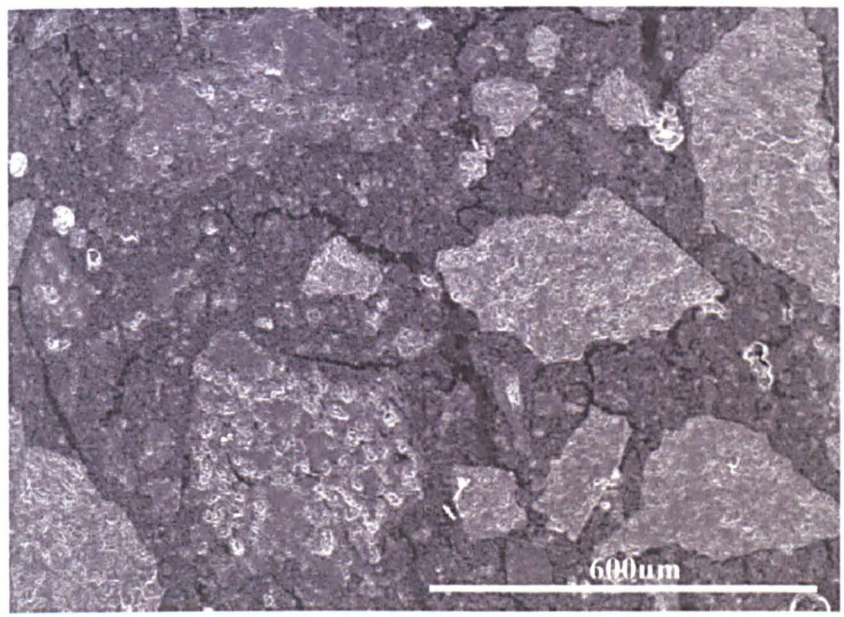

Figure 6.44: Mixture LM-04 after a twelve-month setting period. Photomicrograph of thin-section under SEM, indicating the network of shrinkage cracks and air voids.

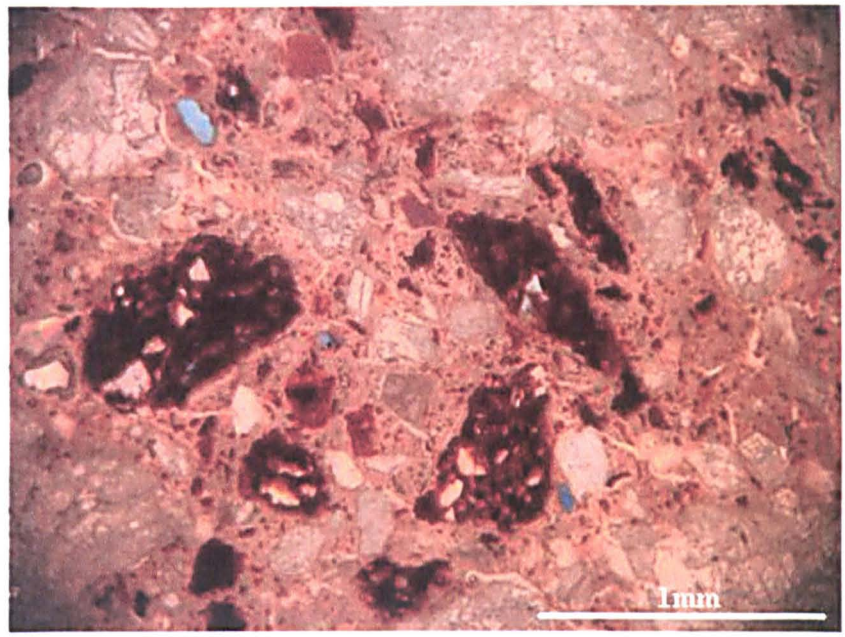

Figure 6.45: Mixture LM-05 after a twelve-month setting period. Examination of thin-section in plane polarized light (PPL).

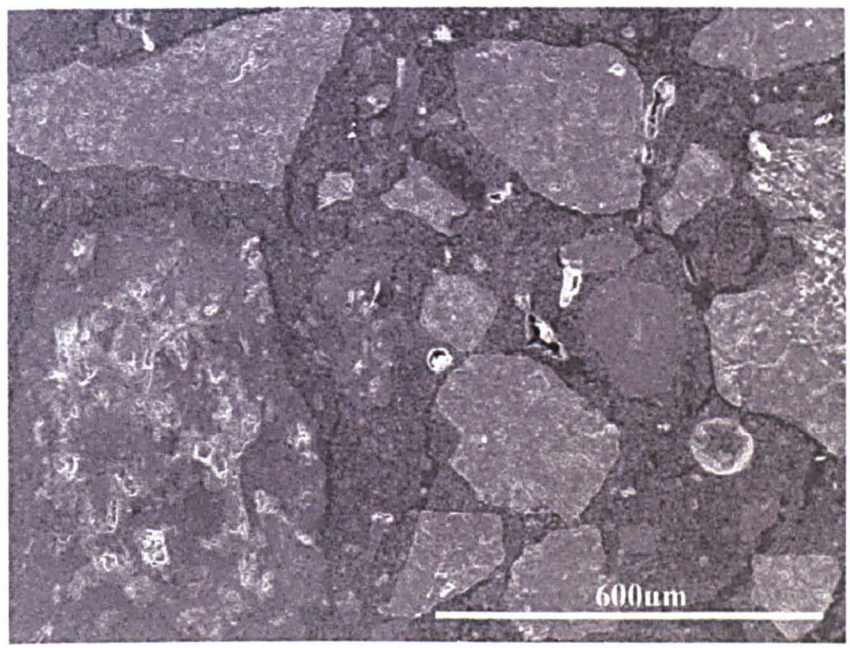

Figure 6.46: Mixture LM-05 after a twelve-month setting period. Photomicrograph of thin-section under SEM, indicating the network of shrinkage cracks and air voids.

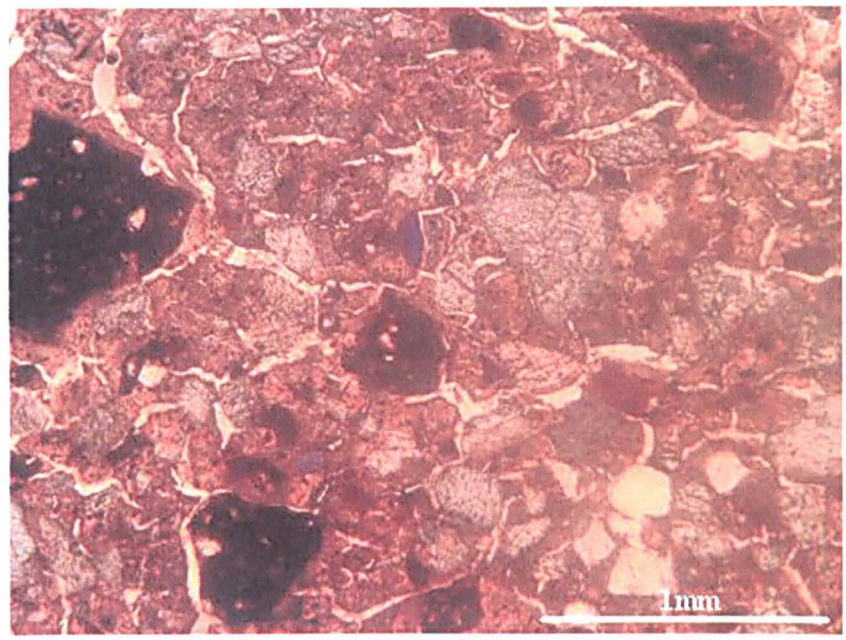

Figure 6.47: Mixture LM-06 after a twelve-month setting period. Examination of thin-section in plane polarised light (PPL).

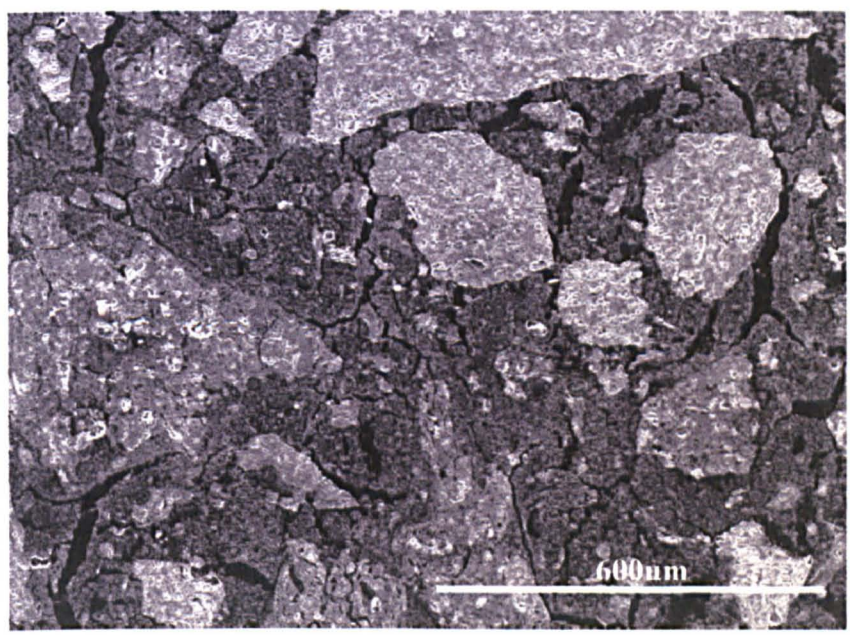

Figure 6.48: Mixture LM-06 after a twelve-month setting period. Photomicrograph of thin-section under SEM, indicating the network of shrinkage cracks and air voids.

6.5.1 Physical Properties

The main physical properties that describe the microstructure of the LM-mixtures are summarised in Tables 6.6 and 6.7. Shrinkage upon setting, open porosity, solid and apparent density were determined according to the procedure described BS EN 1936-1 (1999) standard and by mercury intrusion porosimetry. The values correspond to specimens of the mixtures cured for three and twelve months.

Table 6.6: Volume changes and pore-space properties of LM-mixtures determined by water absorption and mercury intrusion porosimetry. Measurements were carried out in triplicate (n=3).

	Volume Change (%)		**Total surface area (m^2/kg)**		**Apparent density (kg/m^3)**		**Solid density (kg/m^3)**
Setting Time (months)	**3**	**12**	**3**	**12**	**3**	**12**	**12**
Specimens							
LM-03	-4.92 ± 0.51	-5.12 ± 0.43	8924.7 ± 455.2	5311.9 ± 329.3	2629.3 ± 134.6	2623.3 ± 72.8	2410.5 ± 95.3
LM-04	-4.64 ± 0.46	-4.80 ± 0.40	8513.6 ± 583.5	4612.0 ± 284.4	2538.0 ± 125.3	2.4303 ± 121.1	2381.3 ± 101.2
LM-05	-4.21 ± 0.42	-4. 43 ± 0.41	5886.2 ± 383.5	5692.6 ± 355.3	2572.1 ± 117.6	2610.0 ± 102.4	2337.8 ± 92.4
LM-06	-4.96 ± 0.55	-5.26 ± 0.52	6372.9 ± 371.2	5083.6 ± 306.4	2626.8 ± 143.1	2546.2 ± 134.5	2354.9 ± 105.1

Table 6.7: Mean open porosity of LM-mixtures determined both by water absorption and mercury intrusion porosimetry. Measurements were carried out in triplicate (n=3).

Specimens	OPEN POROSITY (%)		
	Mercury accessible (2.21 – 4310.89)nm		Water accessible ($1 - 10^7$)nm
Setting Time (months)	3	12	12
LM-03	34.73 ± 2.07	32.90 ± 1.87	36.06 ± 1.33
LM-04	33.85 ± 1.51	32.79 ± 1.75	37.12 ± 1.63
LM-05	38.78 ± 1.81	36.40 ± 1.05	37.21 ± 1.55
LM-06	31.55 ± 1.25	28.96 ± 1.96	36.11 ± 1.47

Shrinkage of the mortars during their setting caused a volume change of around 5% in all mixtures (Table 6.6). Mixture LM-06 was slightly modified and presented a volume change of around 6%.

Volume changes of mortars are usually caused by water evaporation and shrinkage of the binding material. Lime mortars that contain ceramic fragments are usually more vulnerable to this procedure since the ceramic fragments will absorb water until they become saturated. A small network of micro-cracks is, therefore, usually formed in this type of mortar, and hydrated, pozzolanic phases are formed. The higher values (around 6%) recorded in LM-06 mixtures may be partially attributed to the precipitation of the barium hydroxide hydrate crystals during the cooling of the saturated solution. During precipitation, each molecule of barium hydroxide 'traps' eight molecules of water [$Ba(OH)_2 \cdot 8H_2O$] (Figure 6.18).

Total surface area, apparent density, solid density and open porosity values (Table 6.6) were calculated from the data provided by mercury intrusion porosimetry. However, a

considerable amount of the large pores, air voids and micro-cracks formed during setting are not accessed by mercury porosimetry as their dimensions are outside the detection limits. Therefore, in order to extend the measuring range from the μm to the mm scale, the open porosity values were additionally calculated by water absorption.

The comparison of open porosity values after the setting period of twelve months, showed that the main differences between the LM-mixtures fell within the data determined by mercury intrusion. These pores are clustered in pore radii between 2nm and 4300nm. In this range, open porosity values vary almost 10 units, from 28.96% (LM-06) to 38.78% (LM-05). The values of the reference mixture (LM-03) appeared in the middle of this range (34.73%), very close to those of LM-04 (32.79%).

Porosity values calculated by water absorption do not present any wide fluctuations and are concentrated between 36% and 37% (Table 6.7).

Representative pore-size distributions diagrams of the LM-mixtures are given in Figures 6.49–6.56. Diagrams correspond to measurements carried out in specimens cured for three and twelve months, respectively.

Mixtures LM-03, LM-04 and LM-05 followed the same type of pore-volume distribution, with 50% of their total pore volume in the range 1000–3000nm, while almost 20% of their pores are concentrated between 50nm and 300nm. The pore-size distribution curve of LM-06 shows a peak in the range of 700–2000nm which represents almost 70% of the total pore volume. A second peak was observed between 50nm and 300nm corresponded to 10% of the total pore volume.

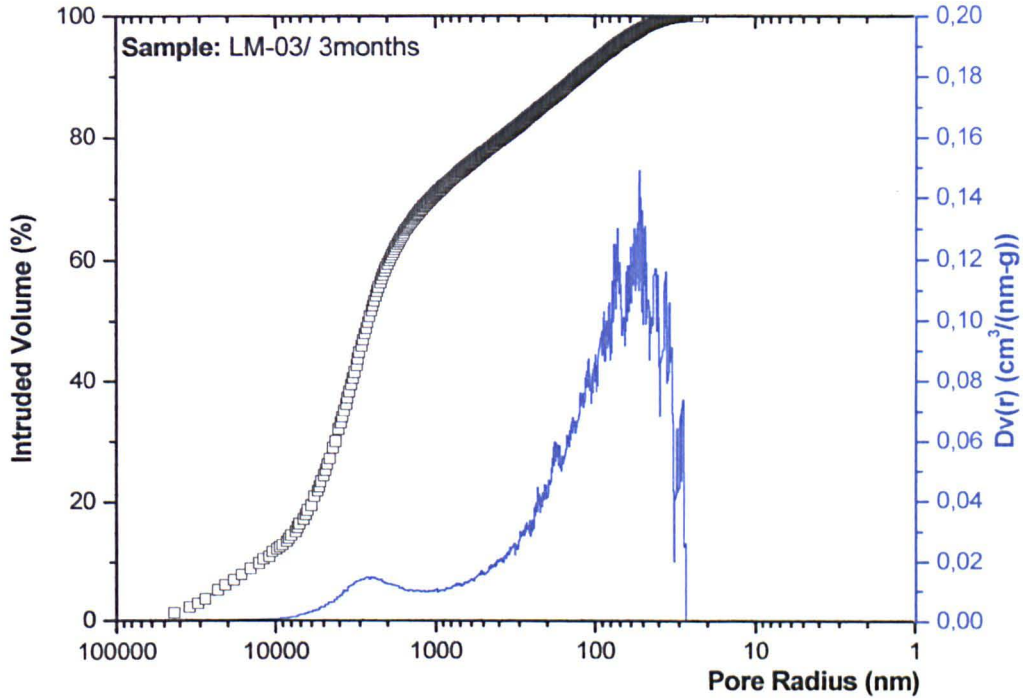

Figure 6.49: Porosity (intruded volume %) and pore-size distribution (Dv(r)) diagrams of LM-03 after a three-month setting period.

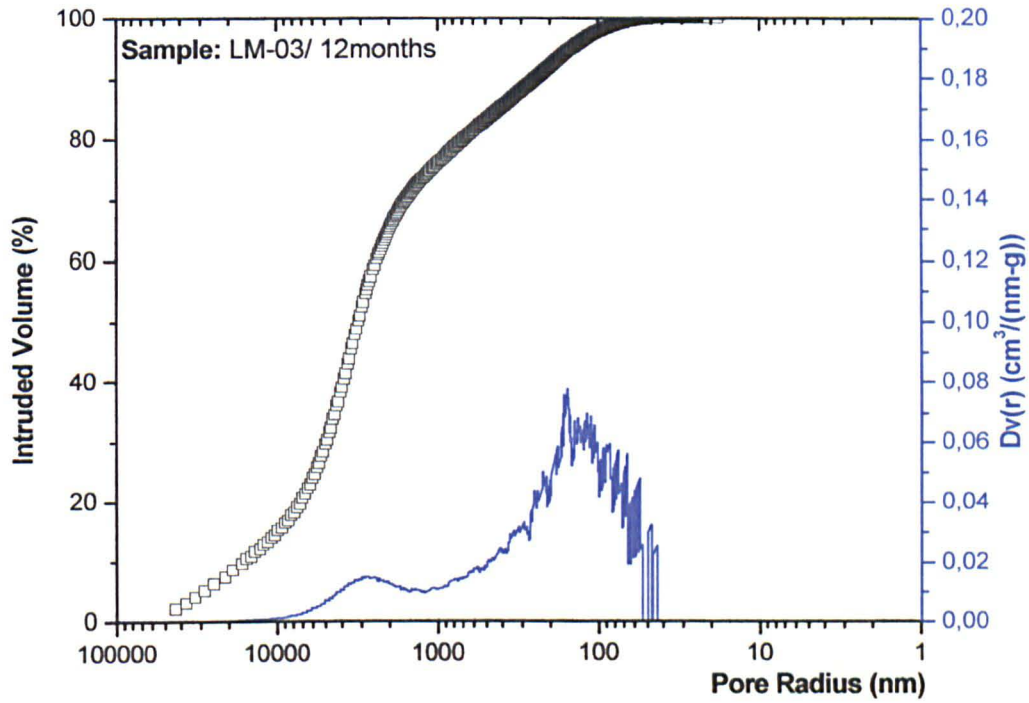

Figure 6.50: Porosity (intruded volume %) and pore-size distribution (Dv(r)) diagrams of LM-03 after a twelve-month setting period.

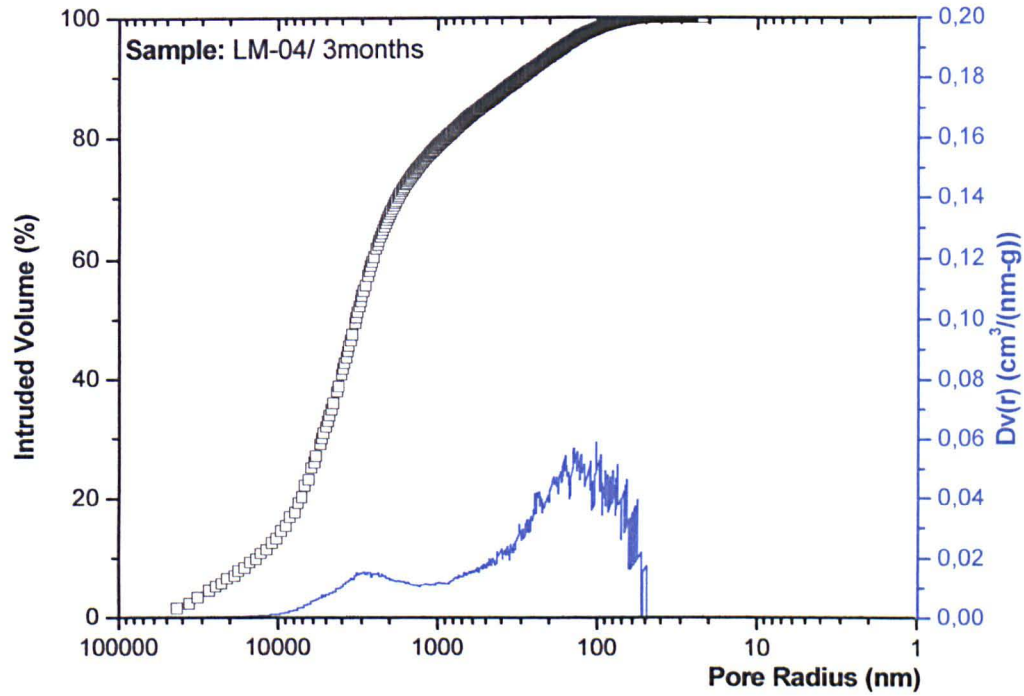

Figure 6.51: Porosity (intruded volume %) and pore-size distribution (Dv(r)) diagrams of LM-04 after a three-month setting period.

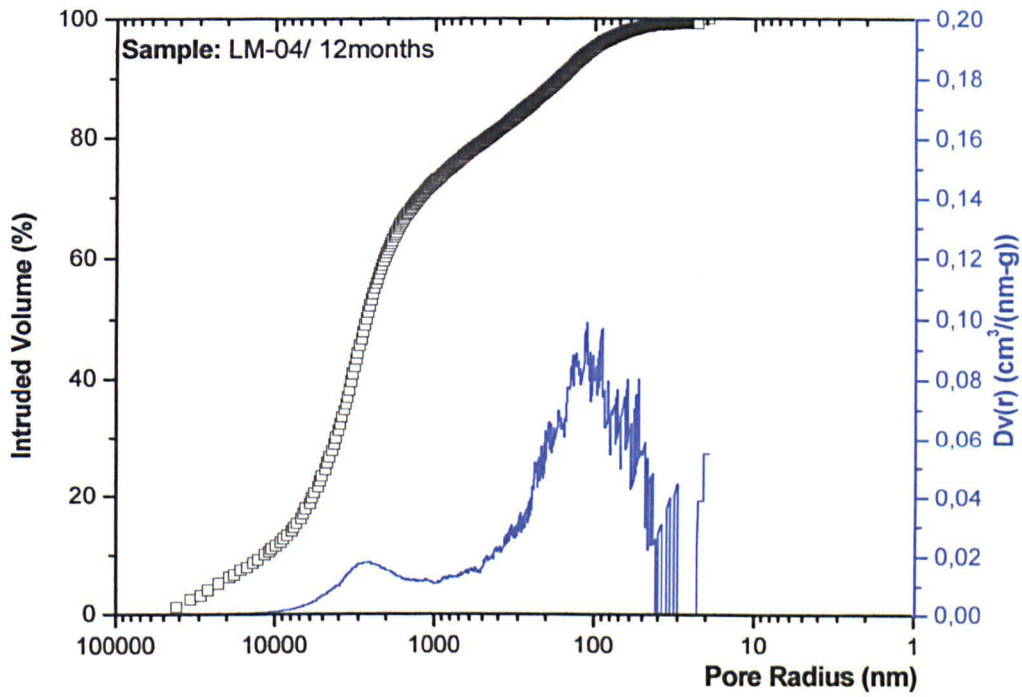

Figure 6.52: Porosity (intruded volume %) and pore-size distribution (Dv(r)) diagrams of LM-04 after a twelve-month setting period.

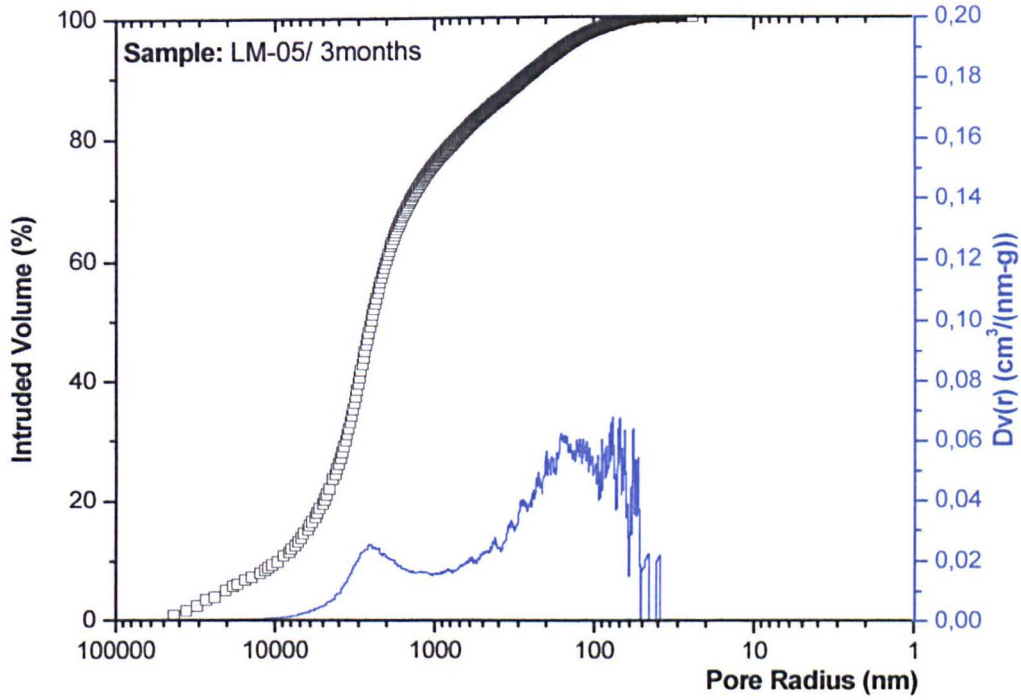

Figure 6.53: Porosity (intruded volume %) and pore-size distribution (Dv(r)) diagrams of LM-05 after a three-month setting period.

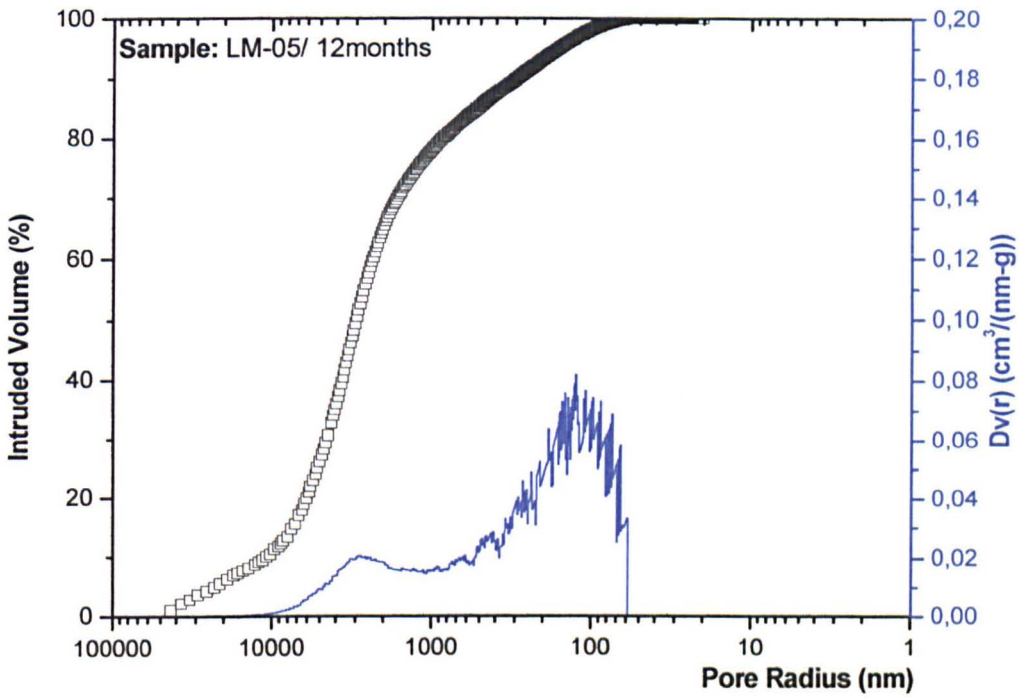

Figure 6.54: Porosity (intruded volume %) and pore-size distribution (Dv(r)) diagrams of LM-05 after a twelve-month setting period.

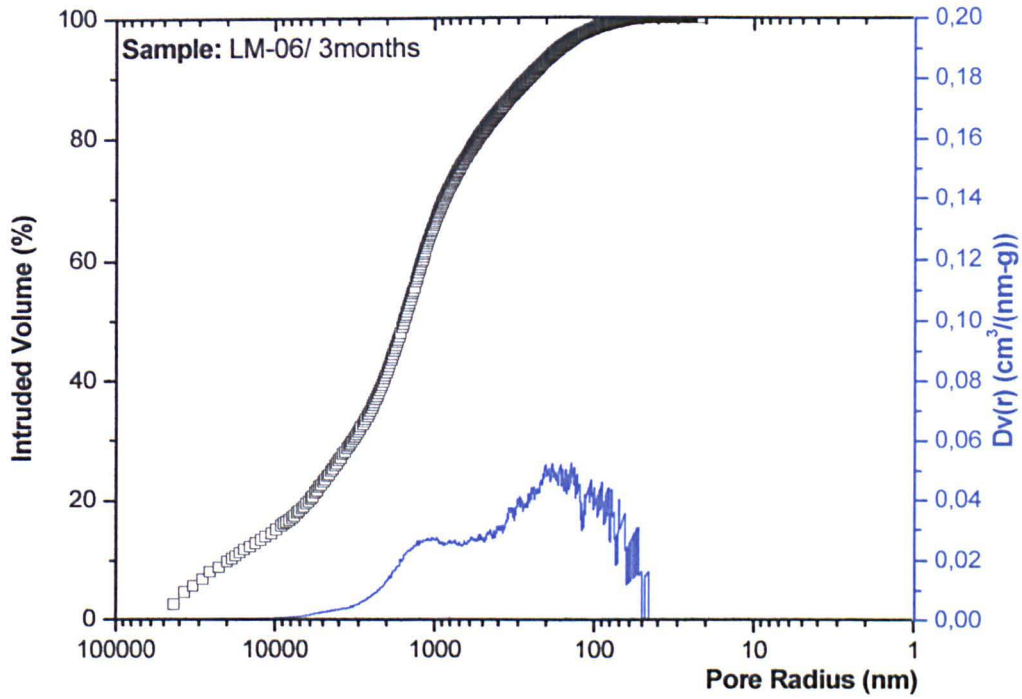

Figure 6.55: Porosity (intruded volume %) and pore-size distribution (Dv(r)) diagrams of LM-06 after a three-month setting period.

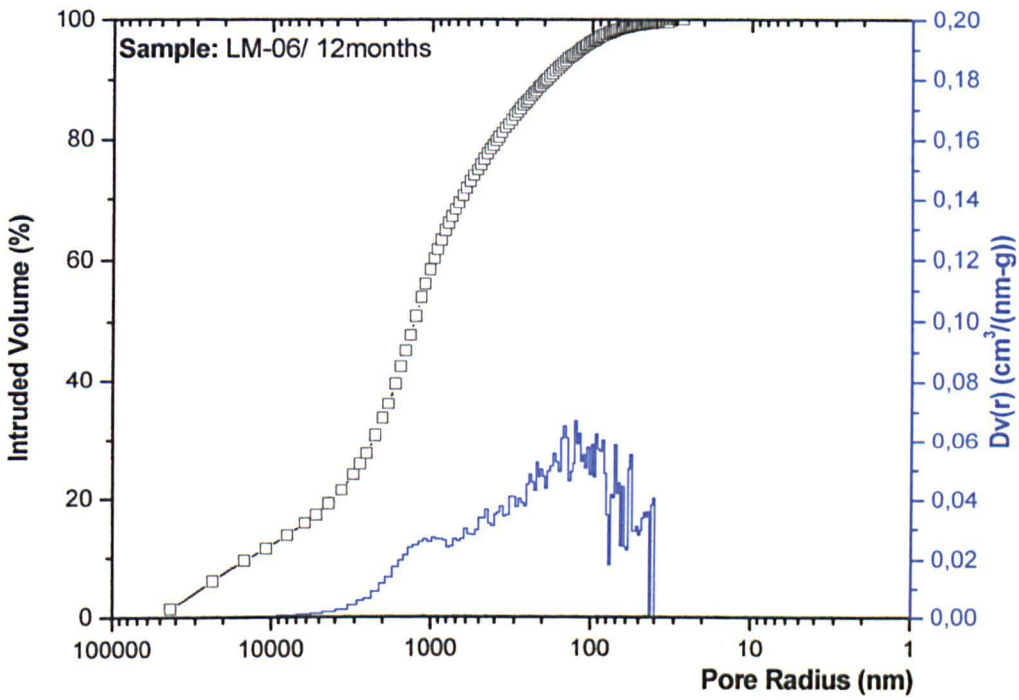

Figure 6.56: Porosity (intruded volume %) and pore-size distribution (Dv(r)) diagrams of LM-06 after a twelve-month setting period.

Further to the pore-space characteristics of the LM-mixtures, the movement of aqueous solutions and water vapour within their mass was studied through the determination of the water absorption coefficient by capillarity and the water vapour permeability.

Representative diagrams of the LM-mixtures describing the absorption of water are given in Figure 6.57, while Figure 6.58 shows representative diagrams of the water vapour flux through the mass of the four different LM-mixtures. A summary of the water absorption coefficient and the water vapour permeability values is given in Table 6.8, with volume changes (%) given in reference to mixture LM-03.

Table 6.8: Mean values of water absorption coefficient by capillarity, rate of water absorption and water vapour permeability of the LM-mixtures. Measurements were carried out in triplicate (n=3).

Specimens	**Water Vapour Permeability** ($kg/m^2 \cdot s \cdot Pa$)	**Water Absorption Coefficient**	**Rate of Water Absorption**
Setting Time (months)	**12**	**12**	**12**
		C_1 (kg/m^2)	C_2 ($g/m^2\ s^{0.5}$)
LM-03	$-1.45 \cdot 10^{-11} \pm 5.41 \cdot 10^{-13}$	0.054 ± 0.002	483.1 ± 14.2
LM-04	$-1.54 \cdot 10^{-11} \pm 6.72 \cdot 10^{-13}$	0.062 ± 0.003	595.1 ± 13.5
LM-05	$-1.66 \cdot 10^{-11} \pm 4.32 \cdot 10^{-13}$	0.065 ± 0.003	527.5 ± 15.6
LM-06	$-1.84 \cdot 10^{-11} \pm 5.73 \cdot 10^{-13}$	0.055 ± 0.004	798.6 ± 15.2

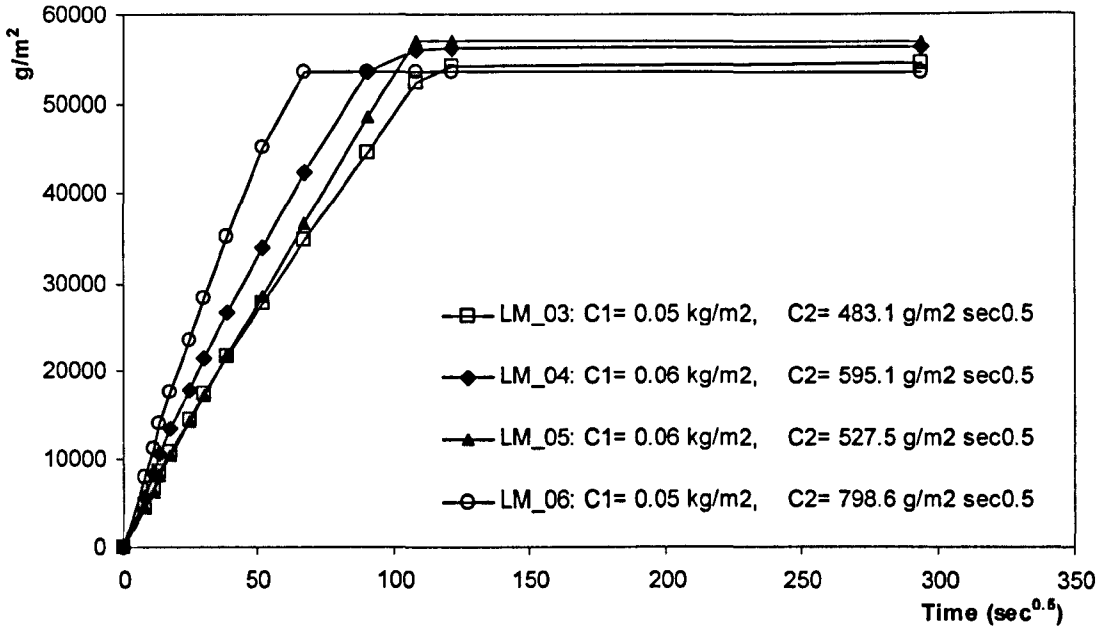

Figure 6.57: Representative diagrams of the LM-mixtures concerning water absorption by capillarity. The water absorption coefficient values for each specimen are presented in the diagram.

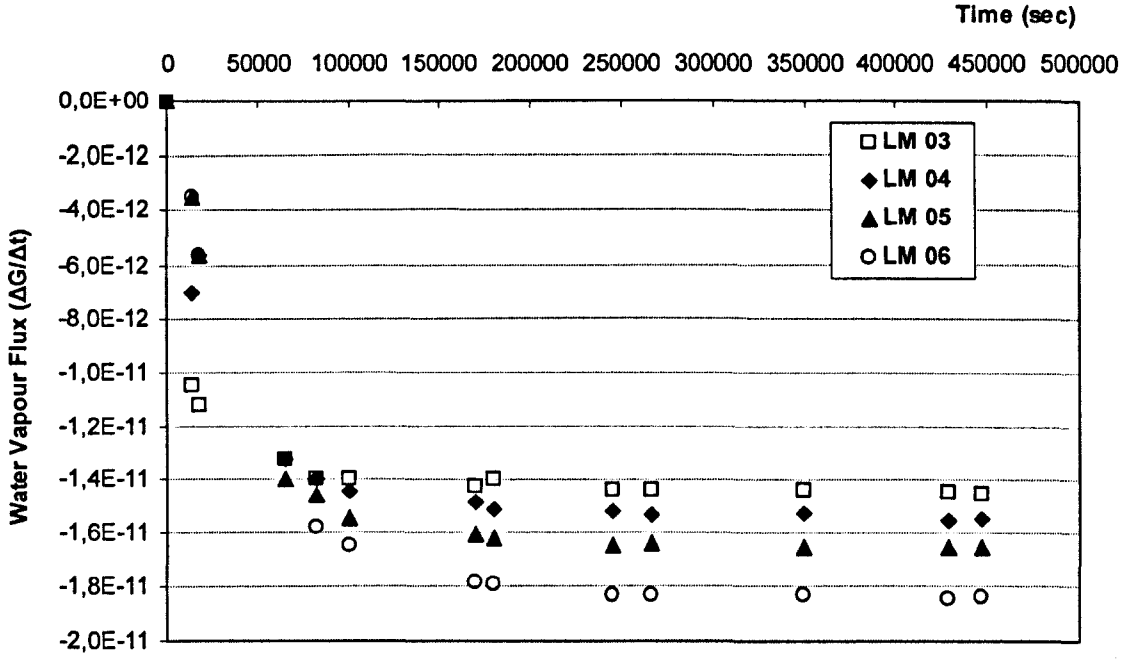

Figure 6.58: Representative diagrams of the water vapour flux for LM-mixtures against time.

All four LM-mixtures exhibited similar water absorption graphs, reflecting homogenous structures, with no discontinuities. However, the interpretation of the water absorption values showed that the addition of barium hydroxide hydrate increases the amount of capillary pores. Thus, mixtures LM-04 and LM-05 increased the water absorption coefficient (kg/m^2) by 14.8% and 20.1%, respectively. Mixture LM-06, however, showed the smallest increase (1.8%), although it showed the highest increase (65%) in the rate of the water absorption ($g/m^2 \cdot s^{0.5}$).

The water vapour flux that is given in Figure 6.58 reflects the quantity of water vapour passing through the mass of the specimens as a function of time. At the beginning of the curves the values are low, since the majority of the water evaporating from the salt solution is retained in the mass of the specimens until their pore space becomes saturated. After this point, the conditions equilibrate and the water vapour flux presents no further variations. The water vapour permeability, calculated for this time period corresponds to the last value of each curve.

All four mixtures exhibited similar curves in their water vapour diagrams (Figure 6.58), although a correlation between the water vapour permeability and the barium hydroxide concentration was apparent, with LM-06 showing the highest increase (26.9%). The water vapour permeabilities are directly proportional to the open pore volume, since this type of porosity allows the easy circulation of water. Mixtures LM-04 and LM-05 showed smaller increases in the permeability values (6.2% and 14.4%, respectively).

6.5.2 Mechanical Properties

Compressive and flexural strength measurements were carried out in the mortar mixtures in order to study their internal cohesion, and hence development of strength, during their setting. The measurements were carried out in specimens cured for three and twelve months. The mechanical properties determined are given in Table 6.9, whilst representative stress-strain graphs of all four mixtures, in unconfined compression, are given in Figures 6.59–6.62.

Table 6.9: Mean values of the mechanical properties of LM-mixtures. The static modulus of elasticity has been calculated from the compressive strength graphs. Loading rate for all tests was set at 0.1mm/min. (n=3).

Sample	Maximum Load P (N)		Compressive Strength F_c (MPa)		Static Modulus of Elasticity E (MPa)		Flexural Strength F_f (MPa)	
Setting Time (months)	3	12	3	12	3	12	3	12
LM-03	2182	2552	0.87 ± 0.07	1.06 ± 0.04	37.53 ± 1.44	41.35 ± 1.82	1.24 ± 0.07	0.78 ± 0.08
LM-04	1626	1771	0.68 ± 0.06	0.77 ± 0.05	35.47 ± 2.11	38.91 ± 2.35	0.78 ± 0.08	0.37 ± 0.08
LM-05	1362	1602	0.57 ± 0.06	0.70 ± 0.04	27.15 ± 3.42	36.75 ± 3.93	0.78 ± 0.05	0.75 ± 0.07
LM-06	1605	1892	0.67 ± 0.05	0.79 ± 0.06	33.35 ± 2.65	41.21 ± 2.20	1.23 ± 0.08	0.38 ± 0.09

All the specimens tested in unconfined compression exhibited a satisfactory type of failure, showing uniform damage and cracking on all four exposed faces. All of the mixtures increased their compressive strength values (15-21%) between three and twelve months. The reference mixture (LM-03) exhibited a 30% higher strength at twelve months (1.06 MPa) than the mixtures containing barium hydroxide. Mixture LM-05, which contained the highest amount of barium hydroxide, showed the lowest strength at twelve months (0.70 MPa). However, these values are still acceptable for lime-based mortars.

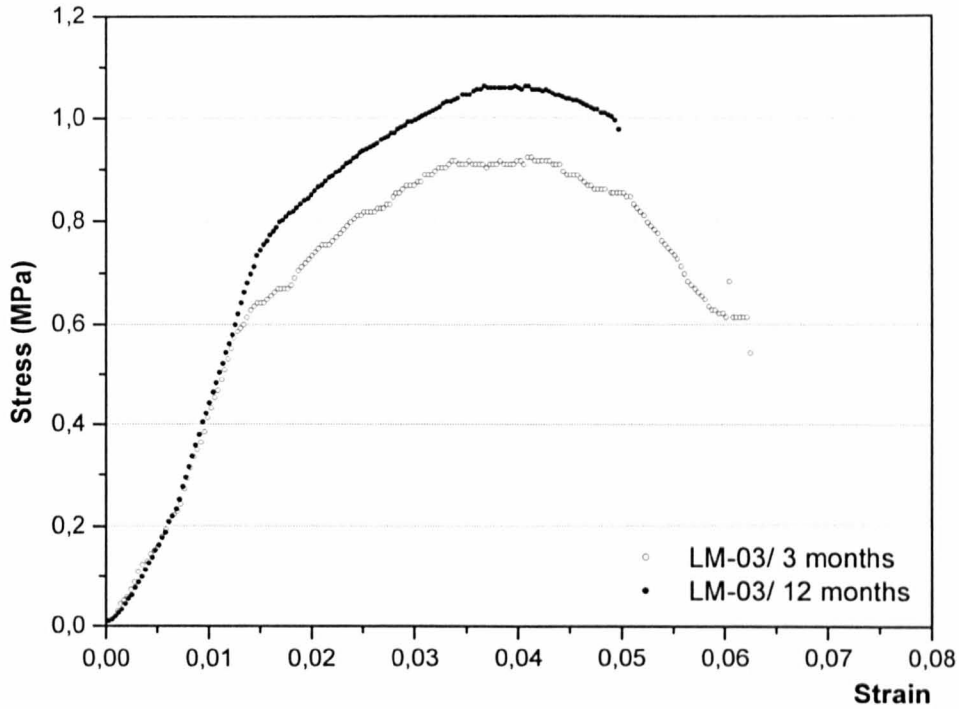

Figure 6.59: Representative stress-strain curves of LM-03 mixtures in unconfined compressive strength, at three and twelve months.

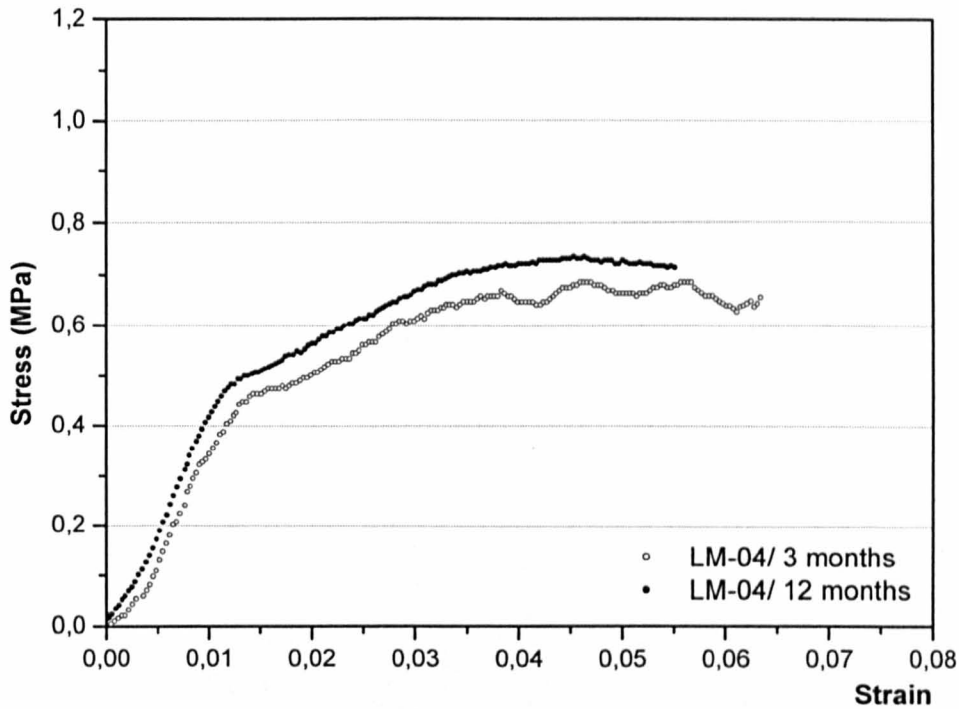

Figure 6.60: Representative stress-strain curves of LM-04 mixtures in unconfined compressive strength, at three and twelve months.

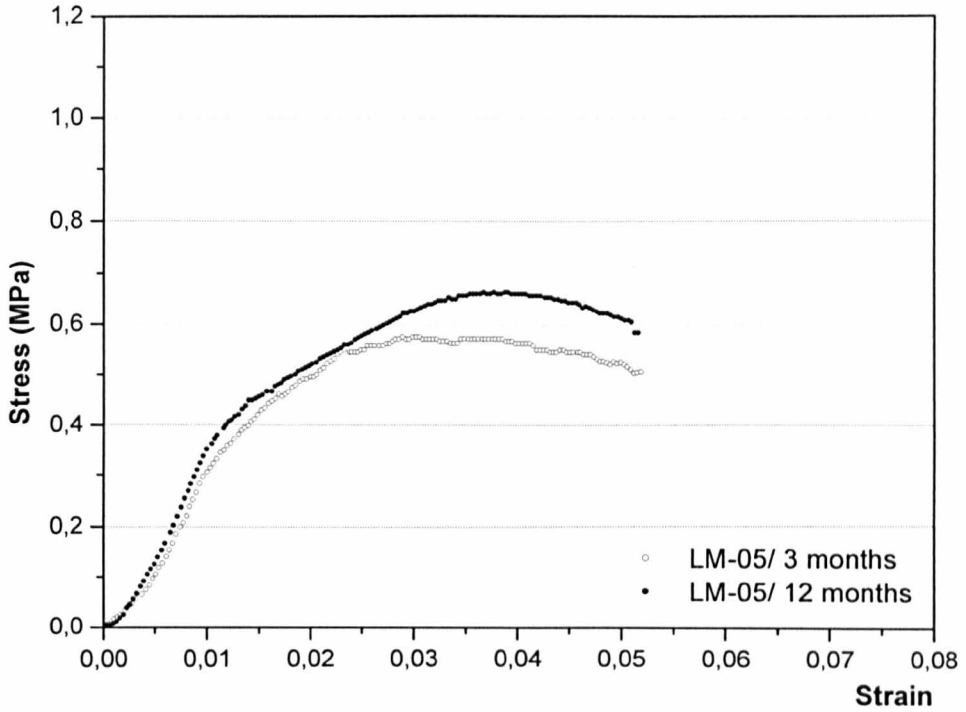

Figure 6.61: Representative stress-strain curves of LM-05 mixtures in unconfined compressive strength, at three and twelve months.

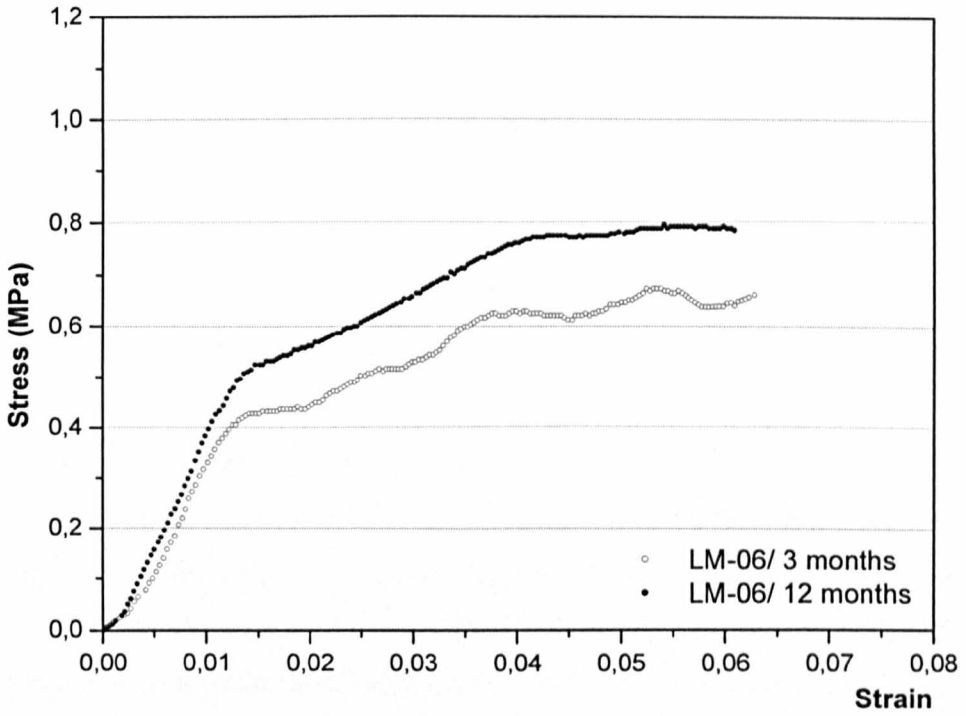

Figure 6.62: Representative stress-strain curves of LM-06 mixtures in unconfined compressive strength, at three and twelve months.

The stress-strain graphs given in Figures 6.59–6.62 describe the deformation of the cube specimens under continuous loading until failure. The shape of the graphs is representative of the mechanical behaviour of the materials.

In the case of the LM-mixtures, the stress-strain graph consists of three parts:

1. At the beginning, the mortar follows a brittle behaviour and the shape of the graph is described by a straight line (elastic behaviour;
2. At the end of the straight line, the shape of the curve changes, increasing until maximum load is reached. Up to this point the stress values increase continuously and specimens exhibit a plastic behaviour; and
3. Finally, the slope of the graph changes totally and a continuous reduction in stress occurs until total failure. This type of graph is due to presence of micro-cracks.

The mixtures exhibit more plastic behaviour at three months, when they are still fresh, and gradually become harder and more brittle. The setting time affects both the compressive strength and the stress-strain behaviour. The time influence on the deformability of mixtures is more clearly seen in the second part of the graph.

In contrast to the compressive strength, flexural strength of the mixtures is reduced at twelve months. At three months, mixtures LM-03 and LM-06 exhibit 1.2MPa flexural strength, whilst mixtures LM-04 and LM-05 are 0.78MPa. At twelve months, mixture LM-05 remains relatively unchanged (0.75MPa), whilst LM-03 falls to 0.78MPa, LM-04 to 0.37MPa and LM-06 to 0.38MPa.

The reduction in flexural strength is attributed to the micro-cracks that form in the external layers of the specimens during hardening. This is due to the difference in rates of setting between the core and external layers of the specimens. This phenomenon was recorded using the three point loading test. When the fractured surfaces of the mixtures were sprayed with a phenolphthalein solution, the core of the specimens was coloured violet (pH>8.3), whilst the external layers were not affected (Figure 6.40).The gradual development of these micro-cracks leads to the total failure of the specimens.

6.6 ACCELERATING AGING – DURABILITY MONITORING TESTS

6.6.1 Crystallisation of Soluble Salts

Accelerated aging of the LM-mixtures through the crystallisation tests was carried out in mortar specimens cured for three and twelve months, in a 10% w/w sodium sulphate solution. Figure 6.63 shows a photographic record of the condition of representative specimens during the crystallisation tests.

The results of the crystallisation tests are given in Figures 6.64 and 6.65 respectively, as the percentage of the weight change for each specimen, after each aging cycle.

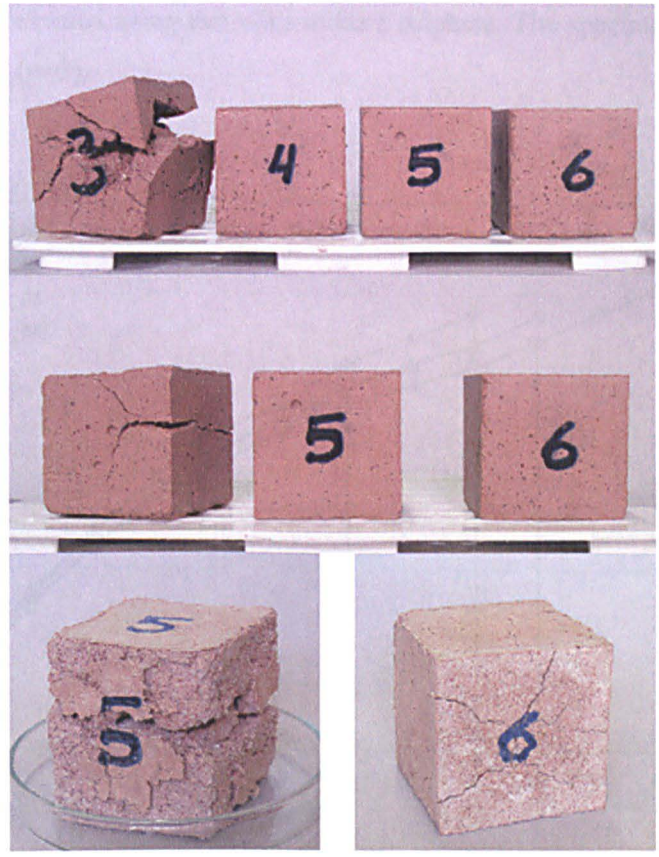

Figure 6.63: Representative photographs of mortar specimens exhibiting the type and order of their failure during the crystallisation test.

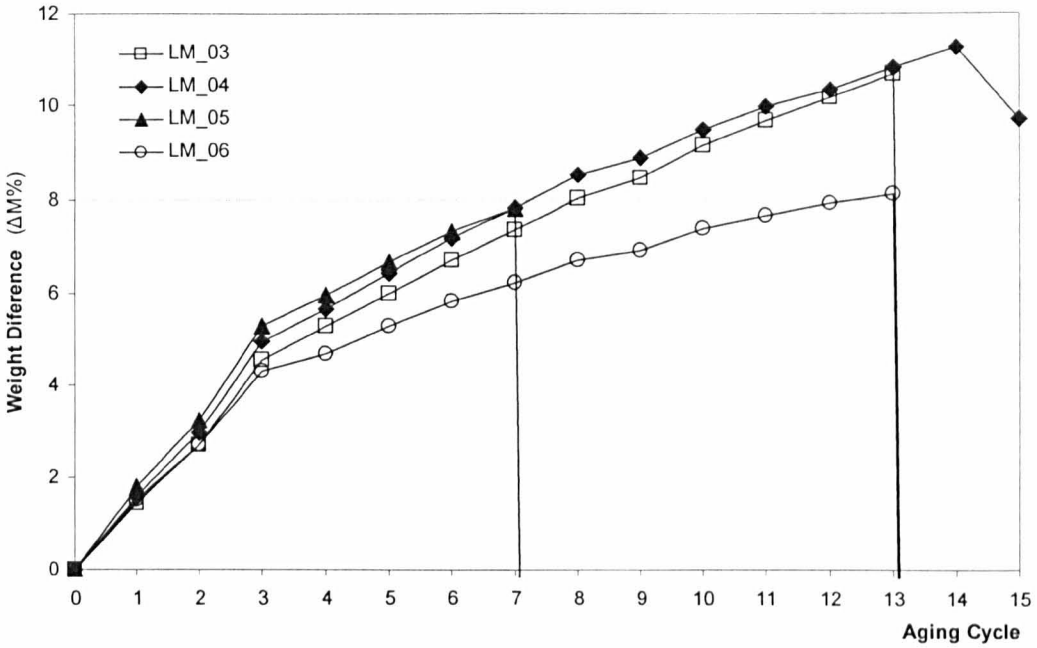

Figure 6.64: Representative diagrams of the LM-mixtures showing the weight change during accelerated aging test with sodium sulphate. The specimens were three months old (n=3).

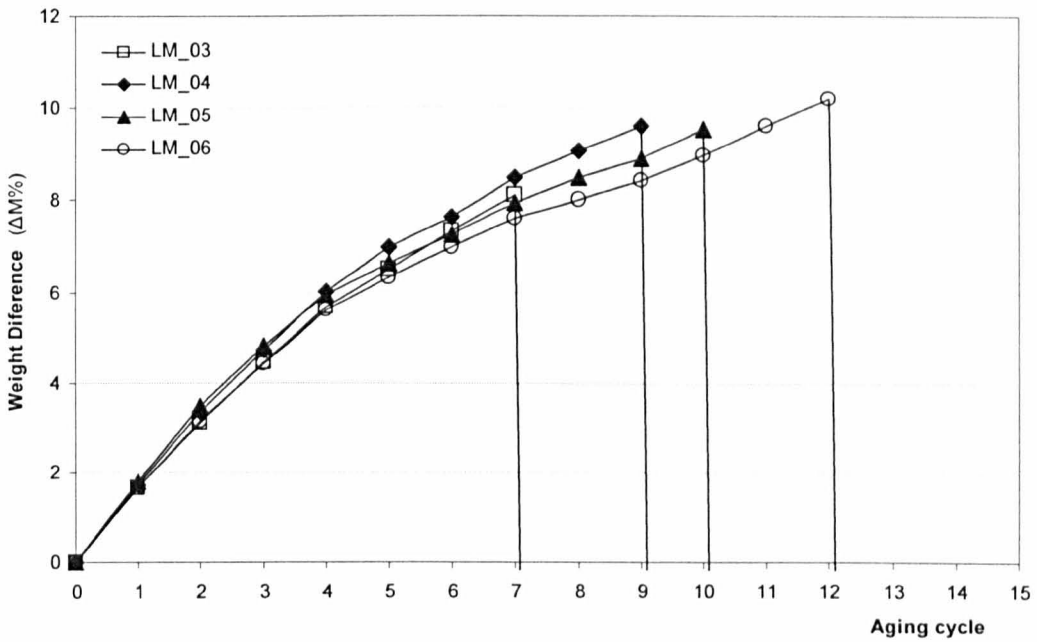

Figure 6.65: Representative diagrams of the LM-mixtures showing the weight change during accelerated aging test with sodium sulphate. The specimens were twelve months old (n=3).

Conclusions were drawn by comparing the behaviour of the mixtures containing barium hydroxide with those of the reference mixture (LM-03), as well as from the evaluation of the XRD diffraction patterns and the data provided by the examination of mortar samples under the SEM.

Examination of the specimens under the SEM during the accelerated aging cycles provided data about the crystal growth of phases formed inside the pores. The photomicrographs, given in Figures 6.66–6.78, were captured after the 3rd, 6th and final aging cycle.

The photomicrographs were captured from freshly fractured surfaces, after drying at 80°C for 22 hours. The identification of the phases was based in the interpretation of XRD analysis, X-rays mapping of elements during SEM examination and, EDX spot analysis. XRD was performed in samples pure of aggregates. For elements maps, 700-800 frames per image were captured, which corresponds to 900.000-1.200.000 counts per image. Finally, the resolution of pictures was set at 1024X768, while 3 frames per image were collected. The charging of images is attributed to the hydroscopic nature of the samples and the rough surface of samples.

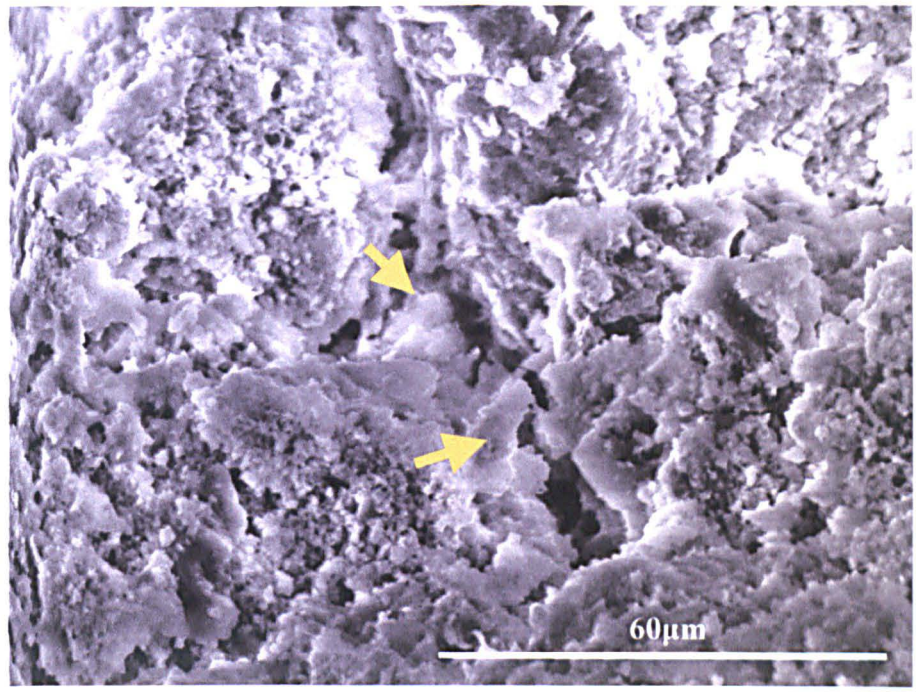

Figure 6.66: SEM photomicrograph of LM-03 after the 3rd cycle. Sodium sulphate is precipitated inside the pores and the micro-cracks of the specimen.

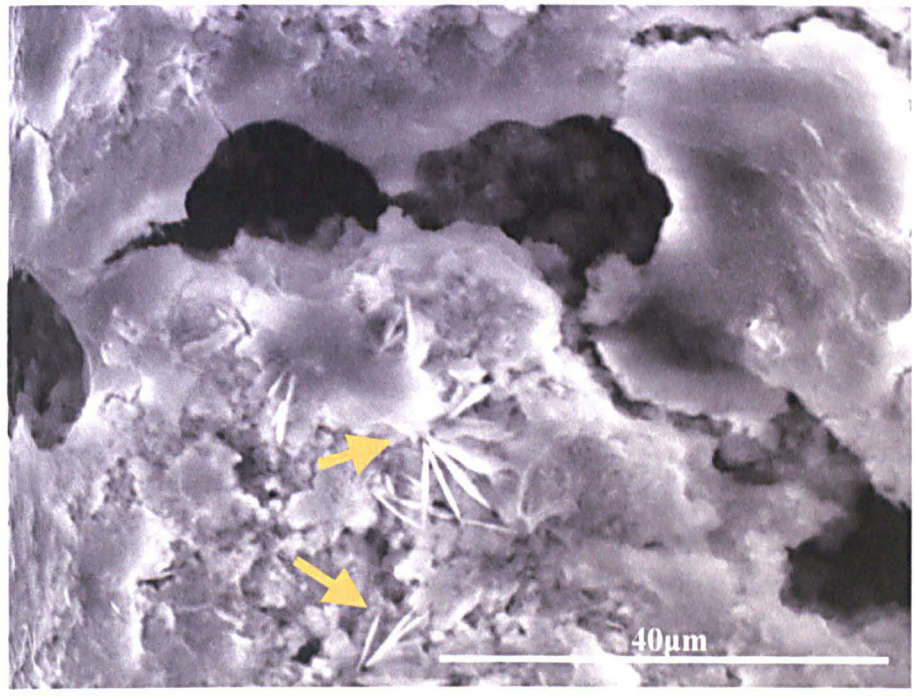

Figure 6.67: SEM photomicrograph of LM-03 after the 3rd cycle. Development of gypsum crystals, formed during the re-crystallisation of the non-carbonated lime in the sulphate solution.

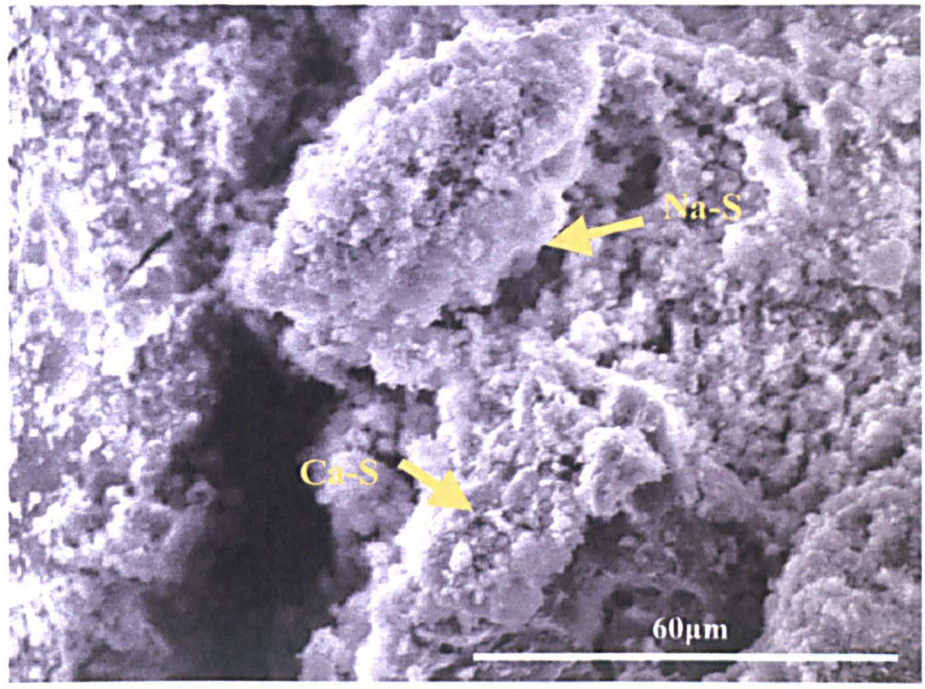

Figure 6.68: SEM photomicrograph of LM-03 after the 6th cycle. Development of sodium sulphate crystals in the pore space of the mixture and, precipitation of micro-crystalline calcium sulphate.

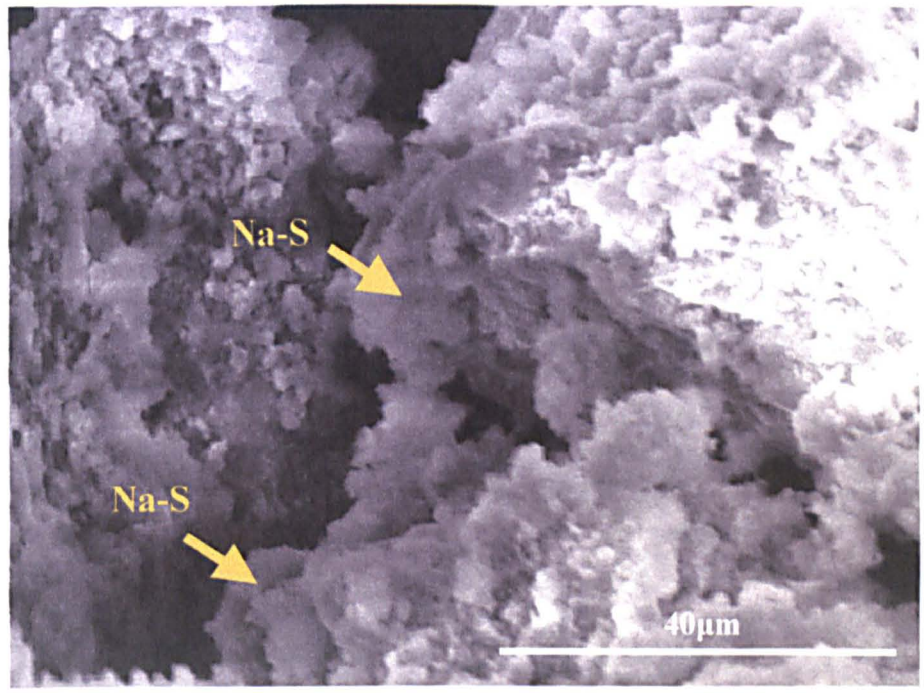

Figure 6.69: SEM photomicrograph of LM-03 after the 6th cycle. Development of sodium sulphate phases inside the pore network.

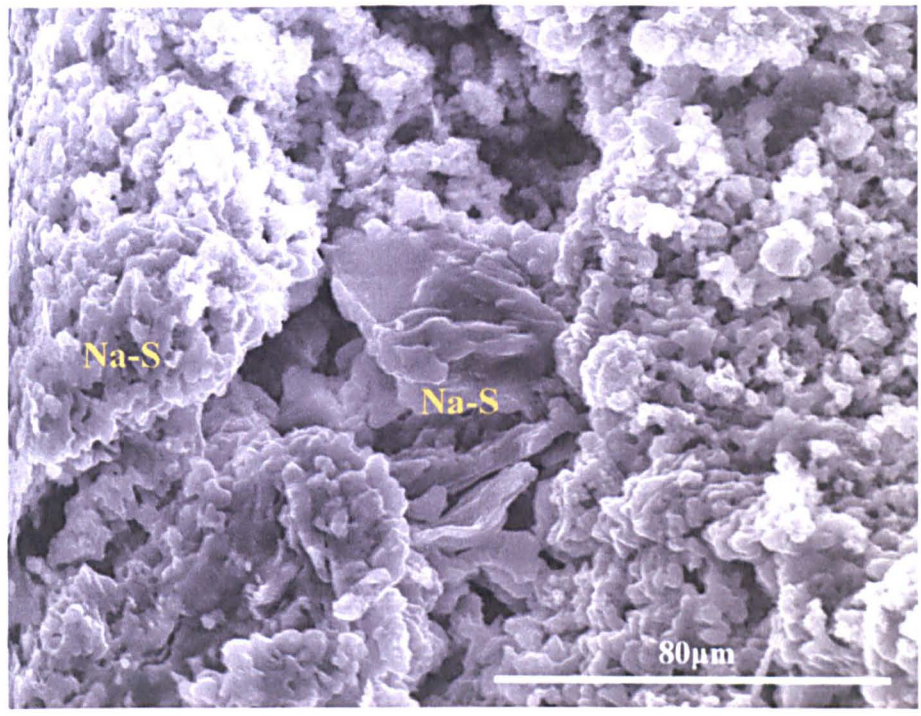

Figure 6.70: SEM photomicrograph of LM-03 after failure (7th cycle). Sodium sulphate crystals fill all the available space inside the mortar mass.

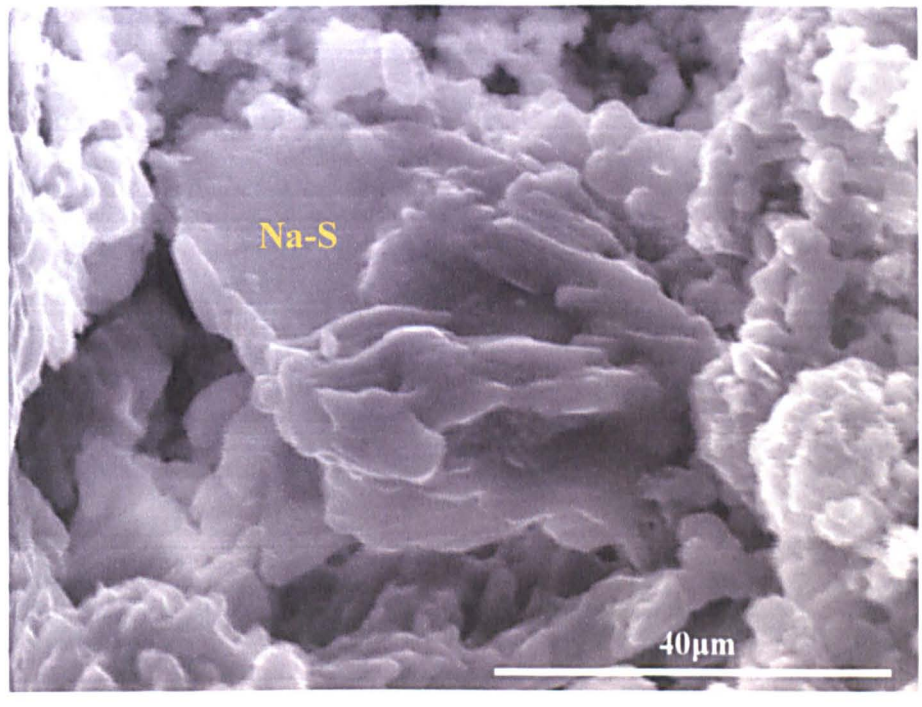

Figure 6.71: SEM photomicrograph of LM-03 after failure (7th cycle). Development of well-crystallised, free-shaped sodium sulphate crystals.

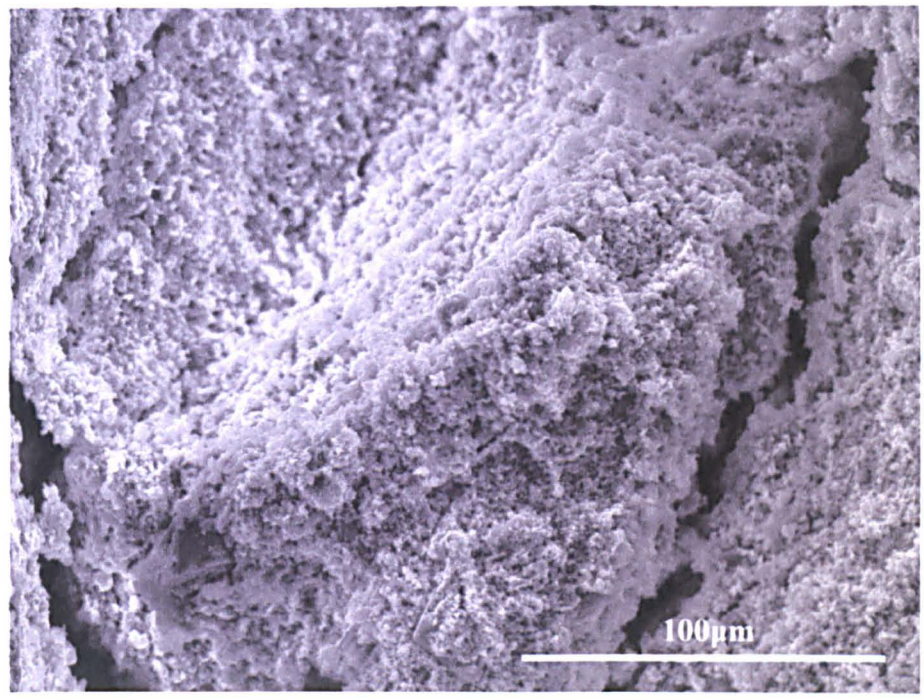

Figure 6.72: SEM photomicrograph of LM-05 after the 3rd cycle. Precipitation of sulphate compounds on the pore's surface.

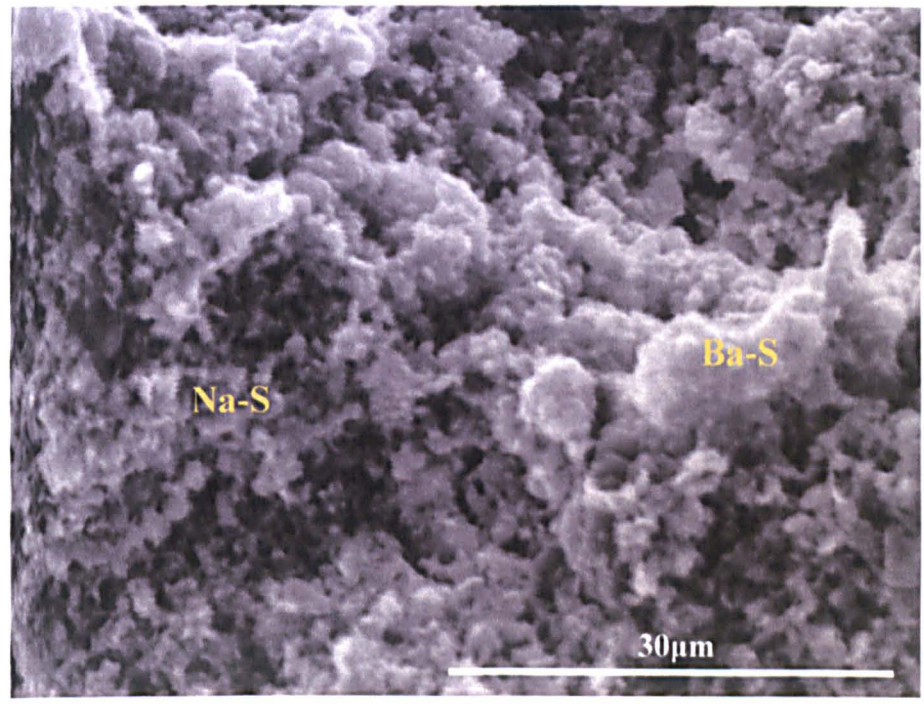

Figure 6.73: SEM photomicrograph of LM-05 after the 3rd cycle. Precipitation of sodium sulphate and formation of barite and gypsum crystals inside the pores.

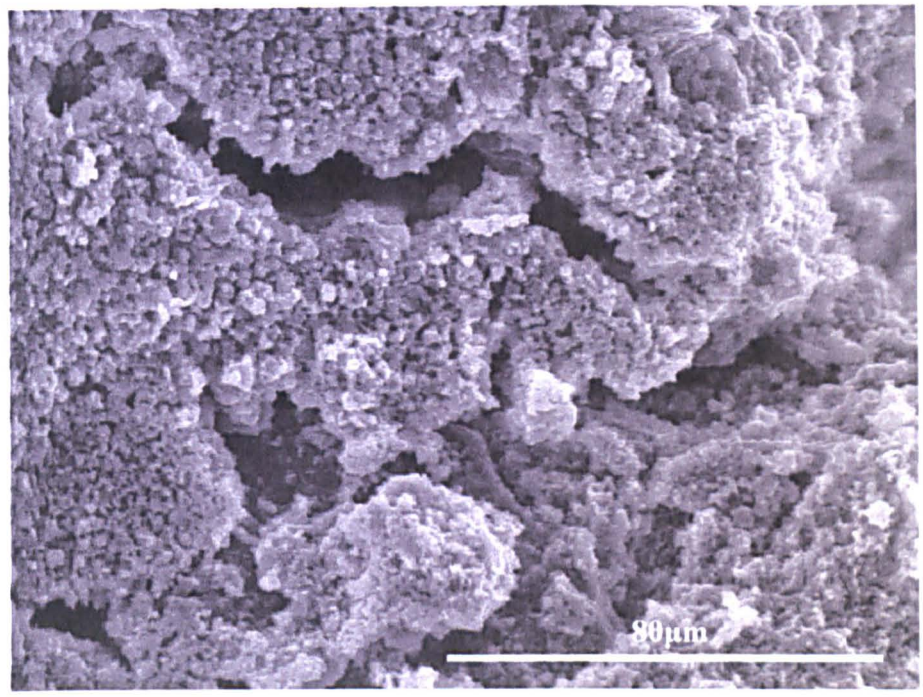

Figure 6.74: SEM photomicrograph of LM-05 after the 6th cycle. Precipitation of sulphate compounds on the surface of a ceramic granule.

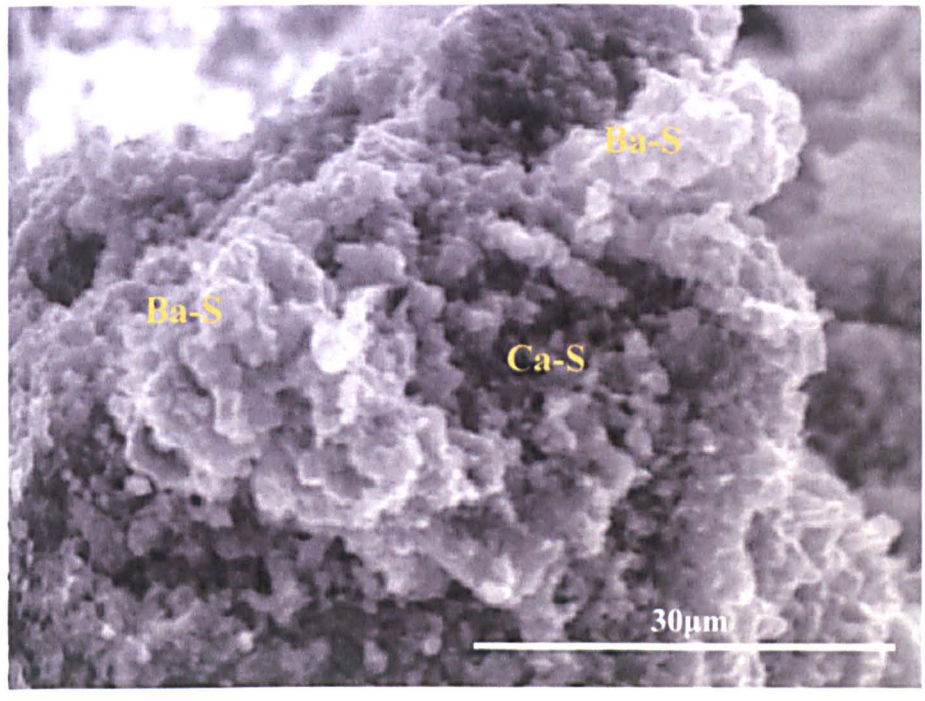

Figure 6.75: SEM photomicrograph of LM-05 after the 6th cycle. Formation of calcium and barium sulphate phases, along with the precipitation of sodium sulphate.

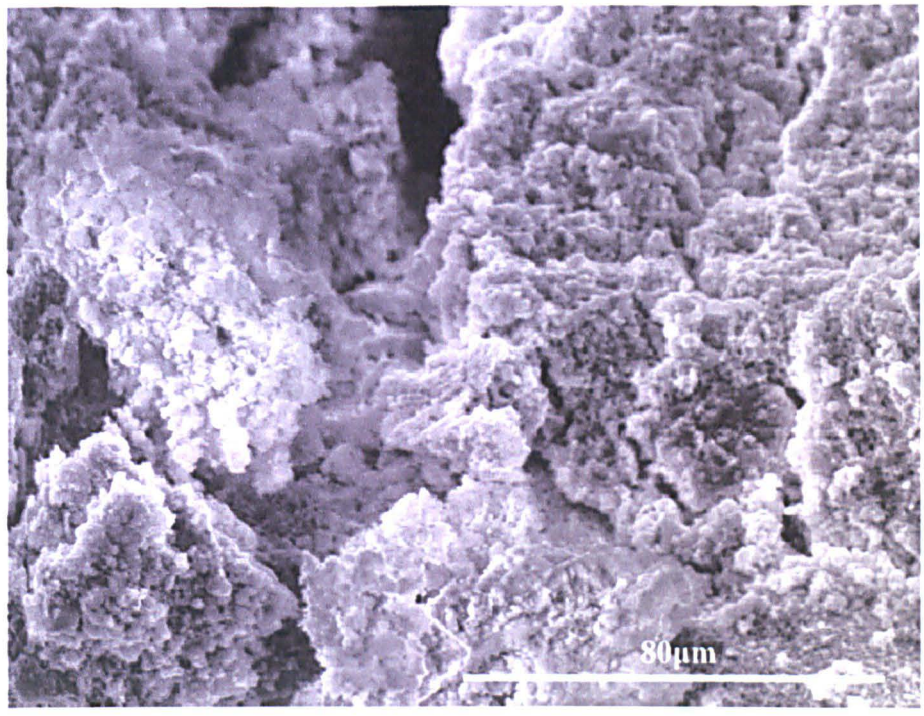

Figure 6.76: SEM photomicrograph of LM-05 after failure (10th cycle). Micro-cracks and pore space is filled by sulphate salts.

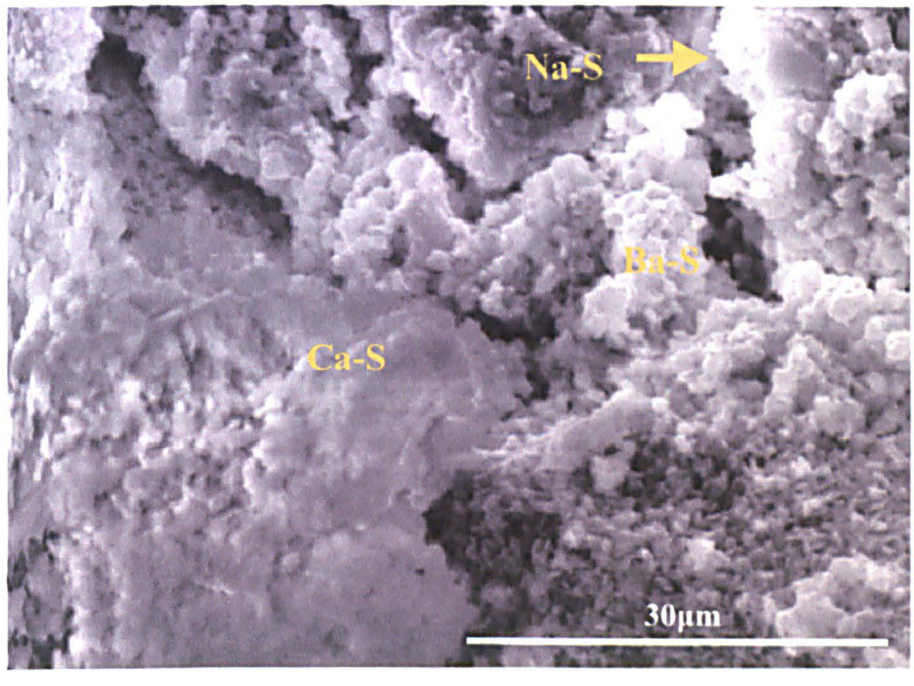

Figure 6.77: SEM photomicrograph of LM-05 after failure (10th cycle). Calcium sulphate and barium sulphate crystals are filling the pores of the specimen, along with the precipitated sodium sulphate crystals.

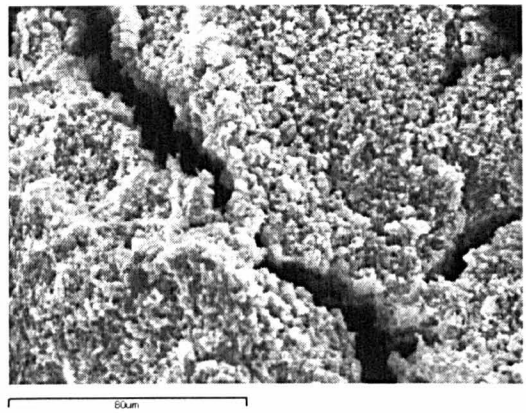

SE image

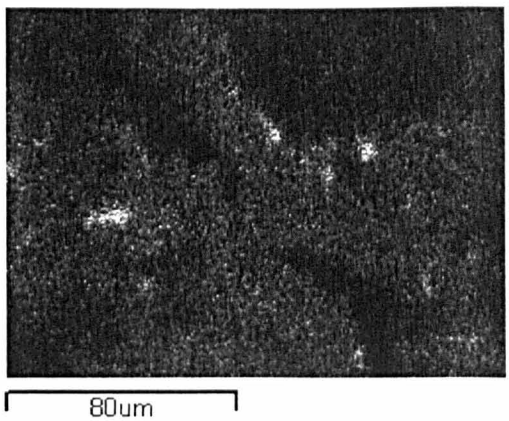

X-ray map: Al

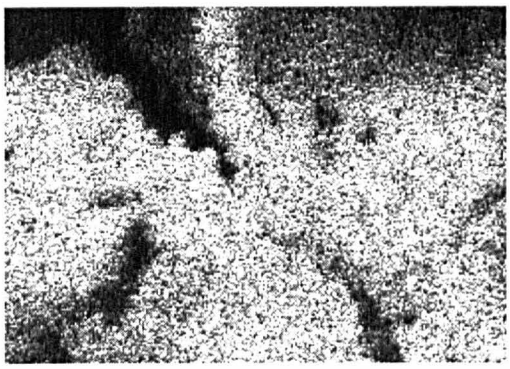

X-ray map: Ca

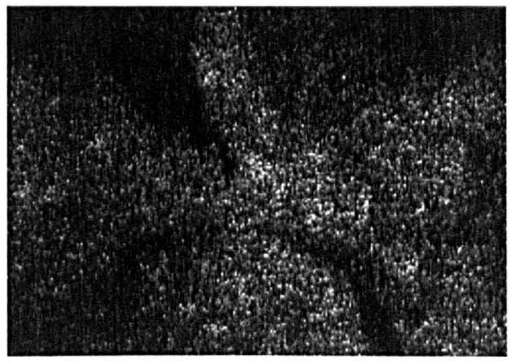

X-ray map: Ba

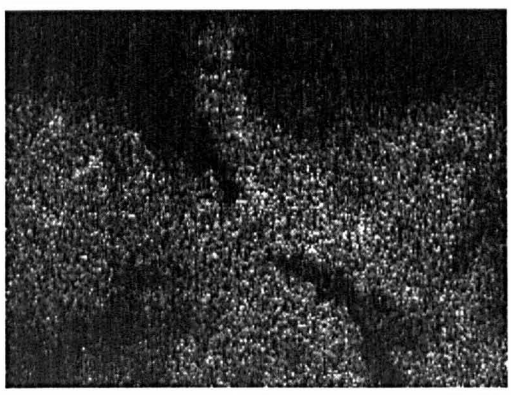

X-ray map: S

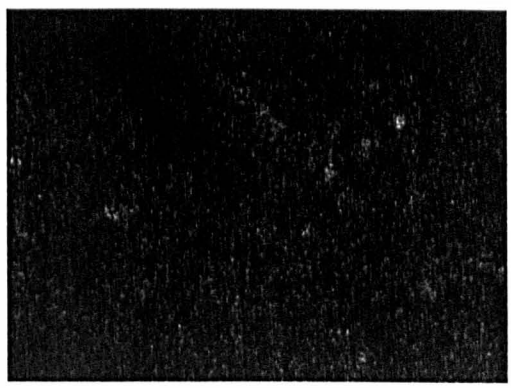

X-ray map: Na

Figure 6.78: SEM photomicrograph of LM-05 **after** failure (10th cycle). X-ray map presents the distribution of elements **on** the surface of the sample and provides information on the type of phases **formed** during the accelerated aging test.

The comparison of the results of the specimens of three and twelve months showed that fresh mixtures were, in general, more durable against the crystallisation of soluble salts than specimens cured for longer time periods. This may be attributed to the more plastic behaviour of lime mixtures in their initial stage of setting.

In the first test, at three months, LM-04 failed after the fifteenth cycle, LM-03 and LM-06 after the thirteenth cycle and LM-05 after the seventh cycle.

In the second test, after twelve months, the maximum durability of mixtures was reduced from fifteen to twelve cycles. Mixture LM-06 exhibited the better performance against crystallisation of sodium sulphate, failing after the twelfth cycle. LM-05 failed after the tenth cycle, and LM-04 after the ninth. LM-03 exhibited the lowest durability, failing after the seventh cycle.

The crystallisation tests have shown that the durability of mortars towards the crystallisation of soluble salts is mainly dependent upon their age (setting period), their mechanical behaviour, as this is defined by their setting period (plastic or elastic deformability), and their pore-space characteristics (such as air voids, discontinuities, total open porosity and pore-space distribution).

The diffraction patterns of samples analysed after their failure showed that, apart from sodium sulphate phases, barite ($BaSO_4$), gypsum ($CaSO_4 \cdot 2H_2O$) and other calcium sulphate phases were formed in the mortar. The amount of these phases is increased in mixtures cured for three months. This observation strengthens the assumption that calcium and barium sulphates are formed by the partial dissolution of the binder compounds in the pore solution and their re-crystallisation in the sulphate form.

6.6.2 Leaching Test

The electrochemically accelerated leaching test was carried out on twelve-month old specimens. The test provided information on the stability of products formed in the mortar during the setting period. According to their solubility product, calcium

hydroxide and barium hydroxide are the main products leached into the pore water. Decalcification of the CSH and the carbonate phases are secondary reactions that are also taking place. The correlation of the amount of calcium and barium ions leached during the test is representative of the chemical stability of those compounds against alteration.

The variation of current in the electrochemical cell as a function of time (Figure 6.79) describes the movement of ions between the two electrodes. In the initial stage, when the de-ionized water contains no ions from the specimens, the only current produced is due to the electrolysis of water. Gradually, the setting products in the binder either dissolve or are leached into the water filling the pores due to the applied voltage. The current increases as long as the water in the two cells has a low concentration of leached ions. When the solutions become saturated, the speed of the ions is reduced, resulting in a continuous reduction in current. The alteration of the mortar, however, continues, due to the constant potential applied in the electrodes. This is illustrated better in the conductivity diagram (Figure 6.80), where the conductivity is observed to continuously increase. The amount of ions leached into the pore water primarily depends upon the chemical stability of the compounds/phases formed during the setting. The total amount of ions that pass to both the anode and cathode solutions is, however, also dependent upon the pore-space characteristics of the specimens (Bagel et al., 1997).

The accumulative concentration of cations leached from the mortars is given in Figures 6.81 and 6.82. The maximum concentration of barium ions leached (moles/g of specimen) was five times lower than that of the calcium ions. The increased concentration of Ca^{2+} ions must be correlated to the considerable quantities of portlandite remaining in the mixtures after twelve months of setting. The correlation between the ion concentrations in the different mortar mixtures is difficult to determine, however, since other parameters, such as porosity and the diffusion coefficient, also play a part.

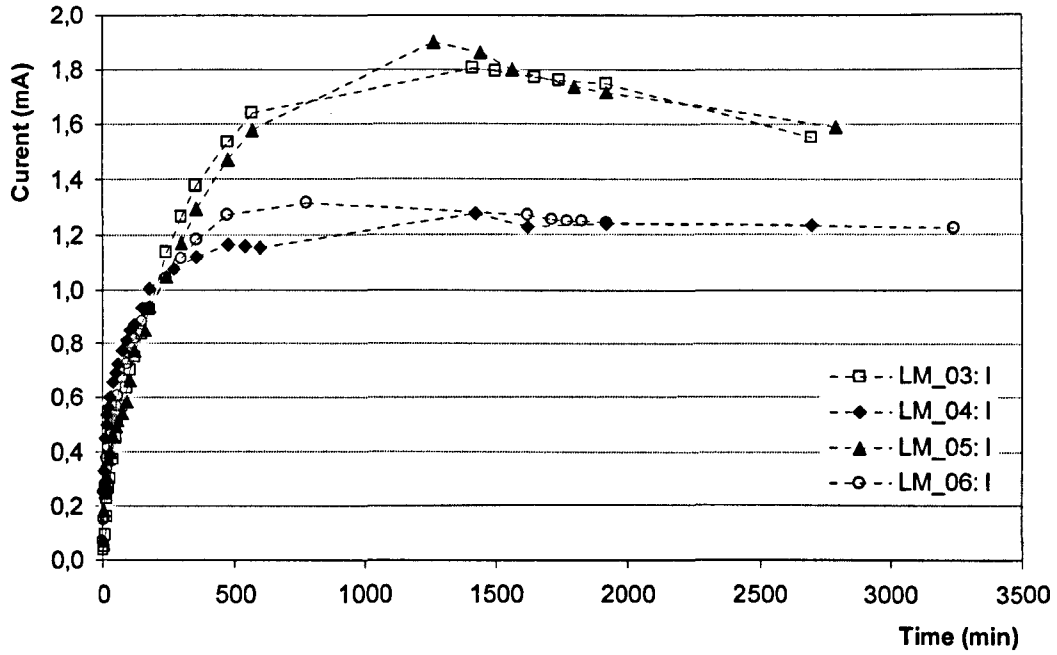

Figure 6.79: Variation in current across the specimens during the electrochemically accelerated leaching test.

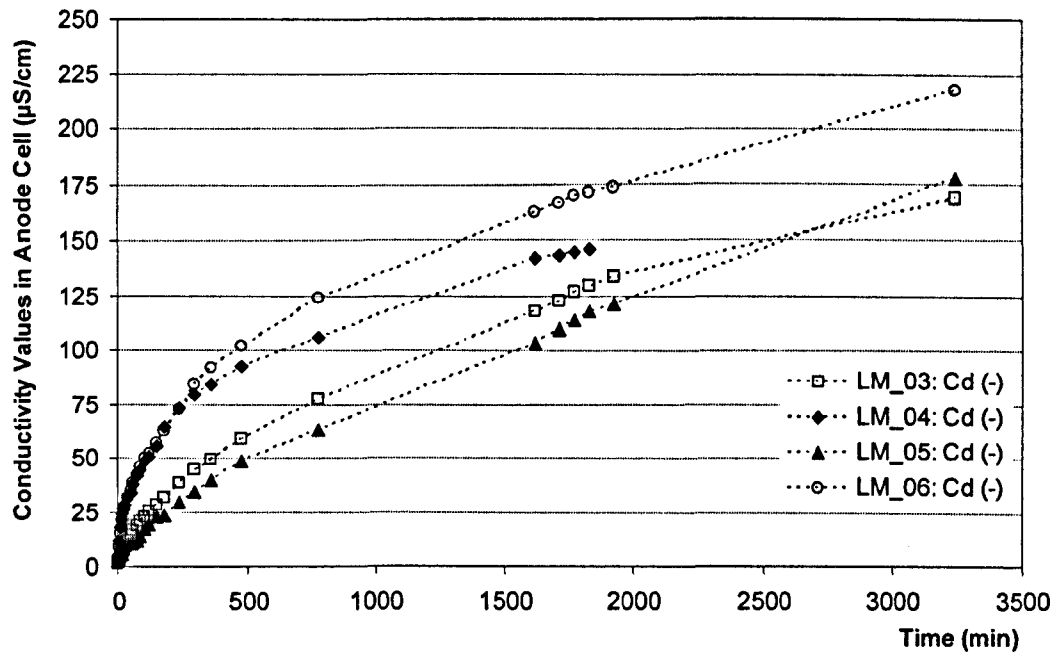

Figure 6.80: Variation in conductivity in the anode cell during the electrochemically accelerated leaching test.

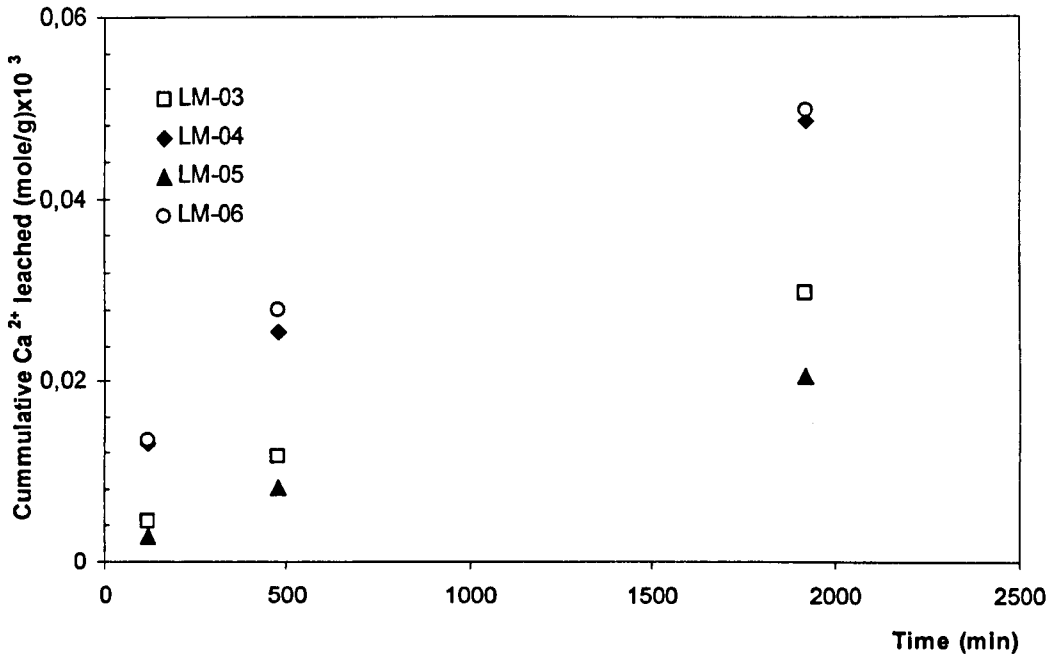

Figure 6.81: Accumulative concentration of calcium ions (moles/g of specimen) during the electrochemically accelerated leaching test.

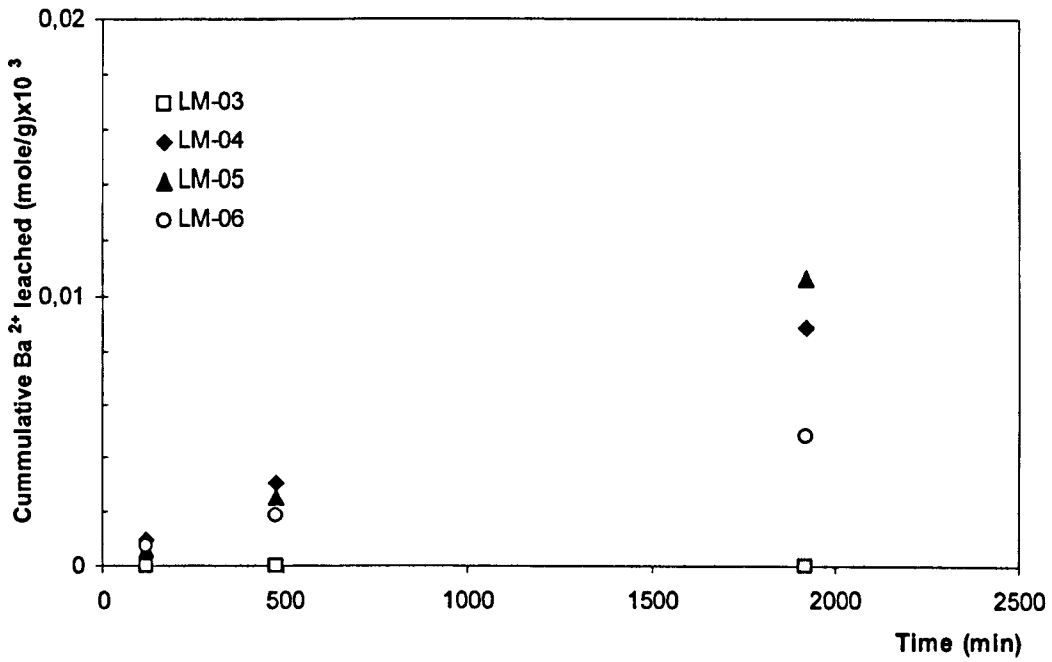

Figure 6.82: Accumulative concentration of barium ions (moles/g of specimen) during the electrochemically accelerated leaching test.

6.6.3 Sulphate Resistance

The aim of the sulphate resistance test was to simulate the deterioration of mortars in contact with acid rain. The action of acid rain, over time, leads to the loss of a significant quantity of the original material from the mortar. The phenomenon is mainly described by surface reactions between the acid solution and the binding material of the mortar, without incorporating microstructure parameters such as porosity, diffusion and permeability.

The concentration of ions dissolved from the mixtures was determined by inductively-coupled plasma spectroscopy (ICP) at preset time periods. The results, given in Figure 6.83, are expressed in moles of ions per gram of the specimen.

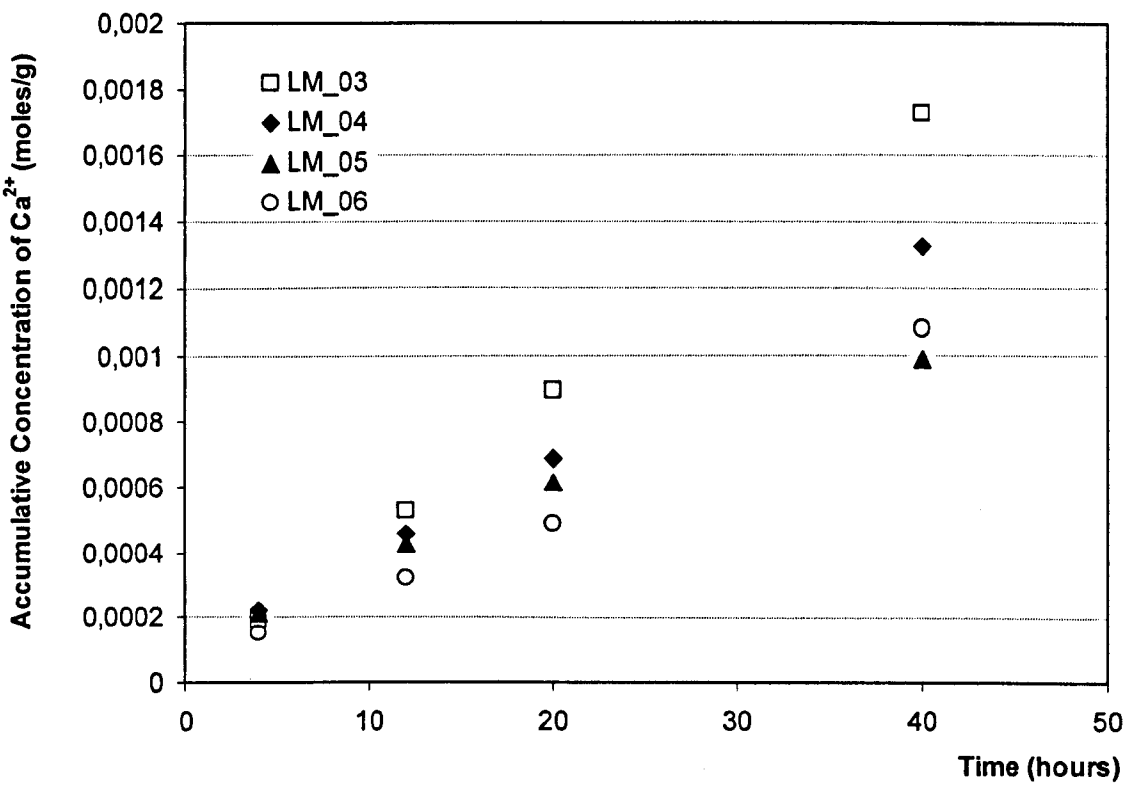

Figure 6.83: Accumulative concentration of calcium ions (moles/g of specimen) leached form the LM mixtures during the acid rain simulation test.

Examination of fractured surfaces in SEM provided information about the morphology and the depth of the weathering layers. Representative photomicrographs are given in Figures 6.84–6.91.

Both the graph describing the cumulative amount of calcium washed out and the SEM pictures of the external surface of the specimens showed that the addition of barium hydroxide reduces the deterioration rate of mortars specimens.

The sulphuric acid flowing over the surface of the LM-mixtures reacted with the calcium carbonate and barium carbonate in the external layers, forming calcium sulphate and barium sulphate, respectively. Barium sulphate is insoluble and remains on the surface of the mortars, whilst calcium sulphate is more soluble and is washed out by the run-off solution. After forty hours, LM-03 showed the highest concentration of calcium ions in the run-off solution (0.0017 moles/g), followed, in decreasing order, by LM-04 and LM-06. Mixture LM-05, which contained the maximum amount of barium hydroxide, showed the lowest calcium ion concentrations (0.001 moles/g).

The barium ion concentrations were found to be negligible. All values were around 0.05μg/ml, which is considered to be zero. In practice, this was expected, as sulphate ions strongly react with the barium ions to form the insoluble barium sulphate, which precipitates.

Examination of the external layers of the specimens subjected to the acid rain simulation test under the SEM showed there was a clear correlation between the depth of alteration and the amount of barium participating in the mixture.

After 25 aging cycles, the depth of the altered layer of the specimens containing 25% barium hydroxide (LM-05) was 100–150μm (Figure 6.91). For the same period, the altered layer of the reference mixtures (LM-03) was 450–500μm (Figure 6.88). The loss of signal in X-ray maps is attributed to the rough morphology (cavities) of the surface close to the altered area. Moulding under vacuum and polishing of the surface could provide better quality images.

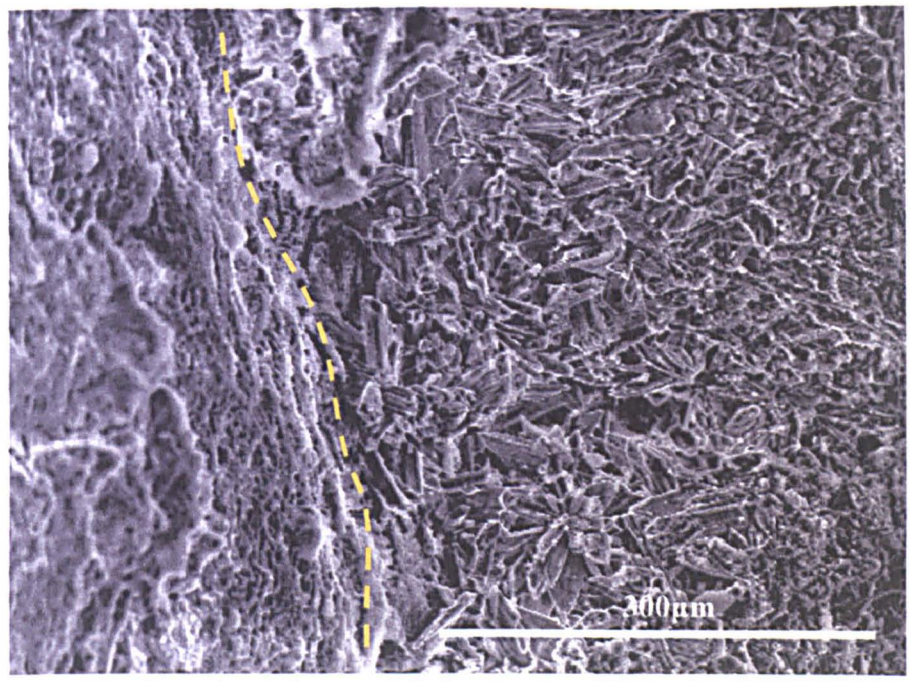

Figure 6.84: SEM photomicrograph of LM-03 after the acid rain simulation test. Fractured surface of the specimen showing the texture of the altered layer. The line indicates the limit between altered and unaffected material.

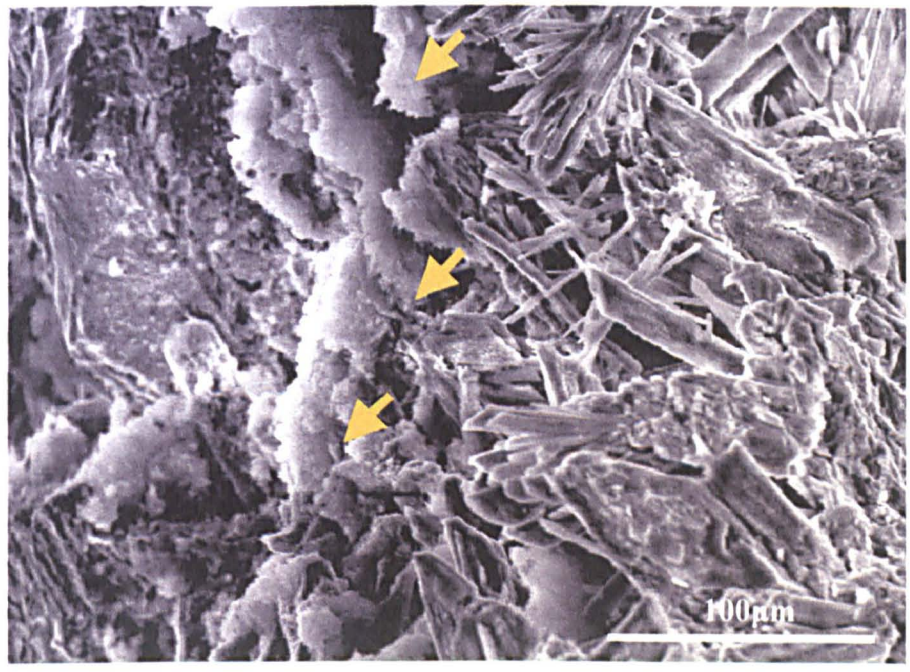

Figure 6.85: SEM photomicrograph of LM-03 after the acid rain simulation test. A thin layer with plate-shaped crystals of calcium sulphate is observed between the main mass and the altered layer of the mortar.

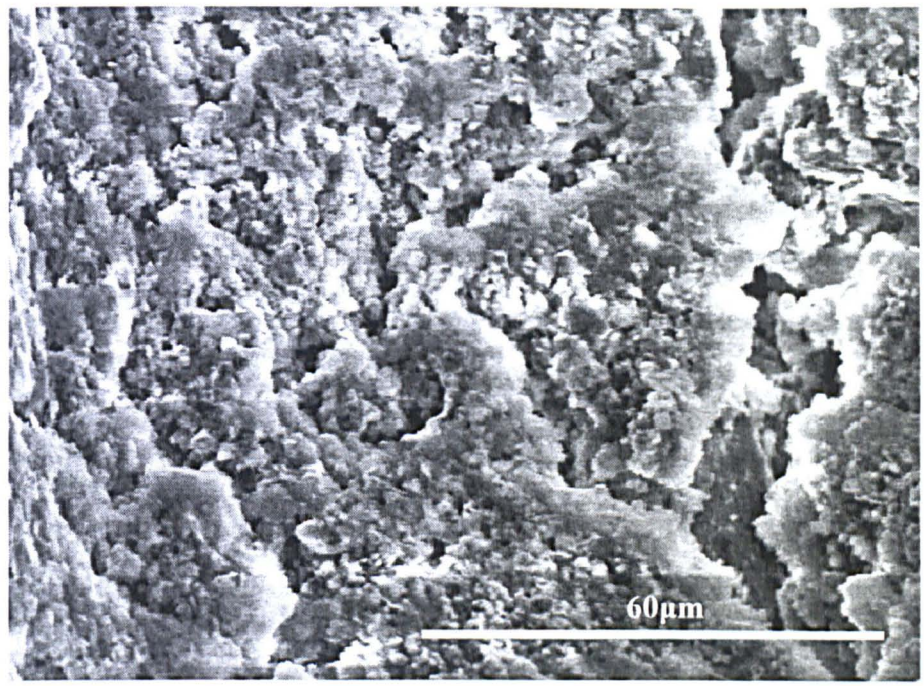

Figure 6.86: SEM photomicrograph of LM-03 after the acid rain simulation test. Typical texture of the non-altered mass of the specimen.

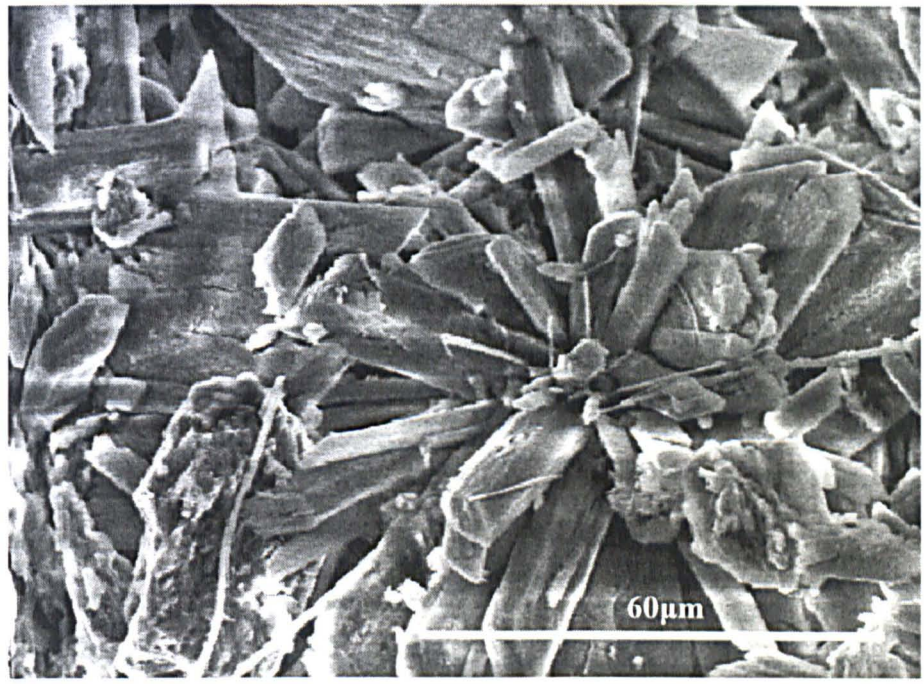

Figure 6.87: SEM photomicrograph of LM-03 after the acid rain simulation test. Elongated crystals of re-crystallised calcium sulphate formed in the external layer of the specimen.

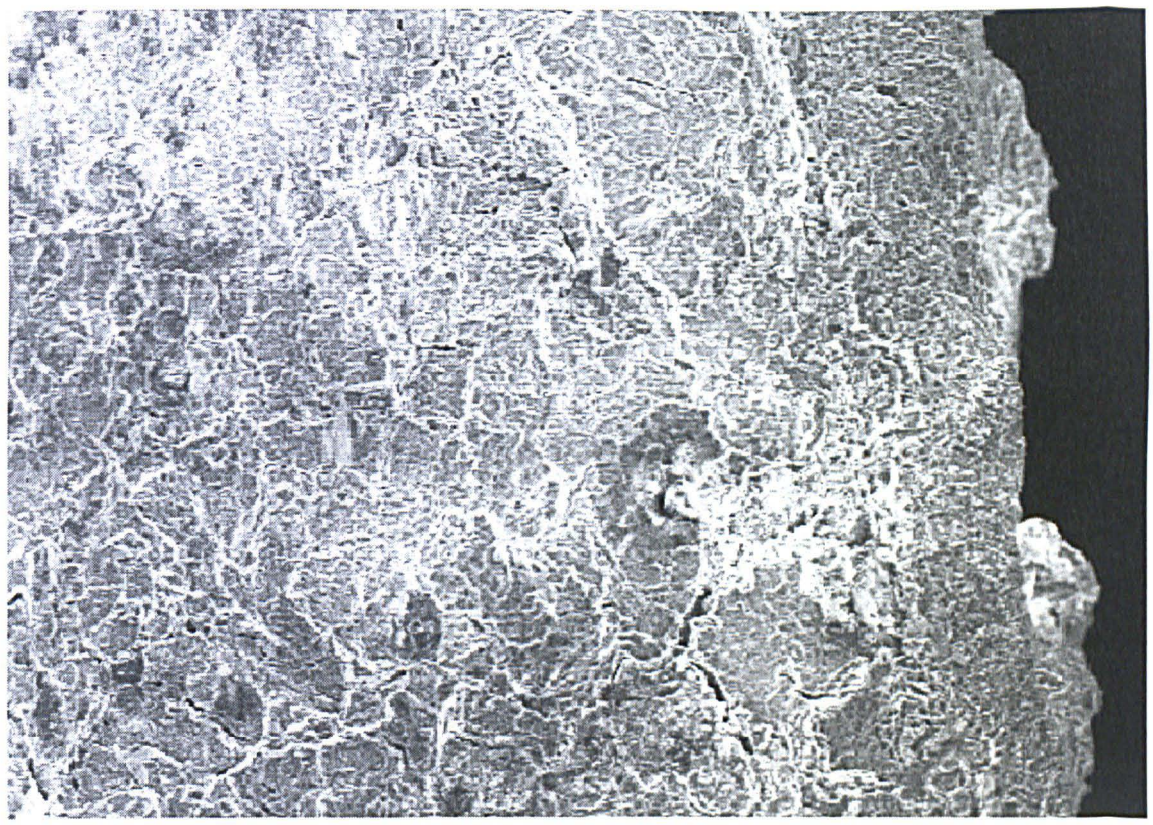

SE Image

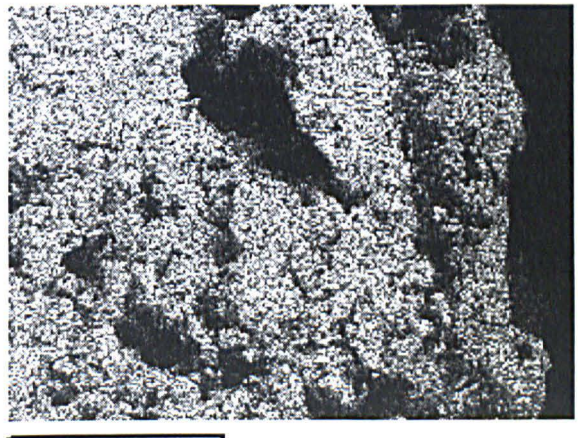

X-ray map: Ca

X-ray map: S

Figure 6.88: SEM photomicrograph of a freshly fractured surface from LM-03 after the acid rain simulation test. Secondary electron image and X-ray maps showing the sulphated area of the specimen. The depth of the altered layer is approximately 500μm.

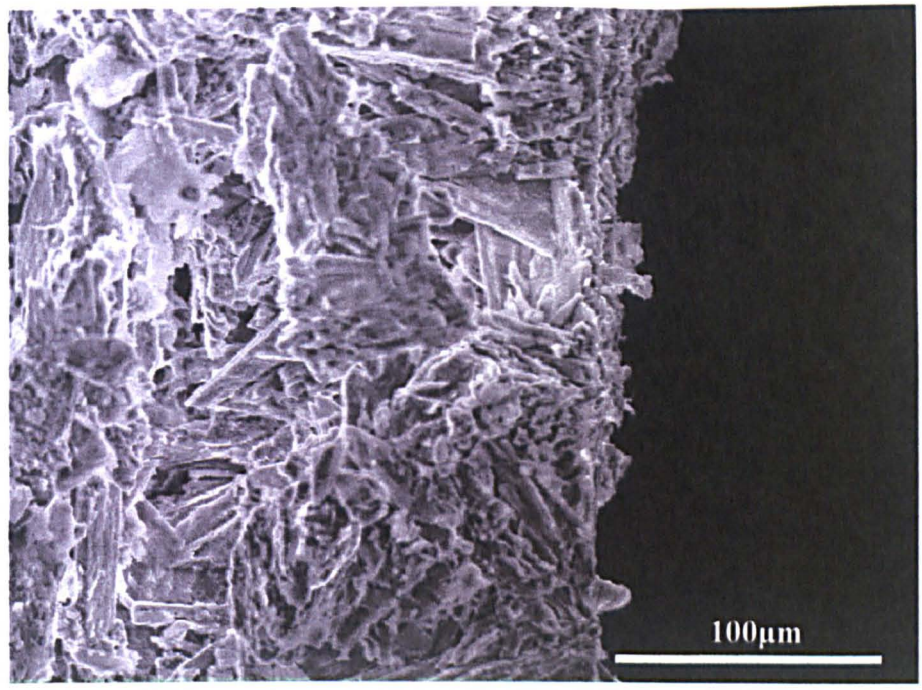

Figure 6.89: SEM photomicrograph of LM-05 after the acid rain simulation test. The altered layer of the specimen presents the same texture as the reference mixture (LM-03).

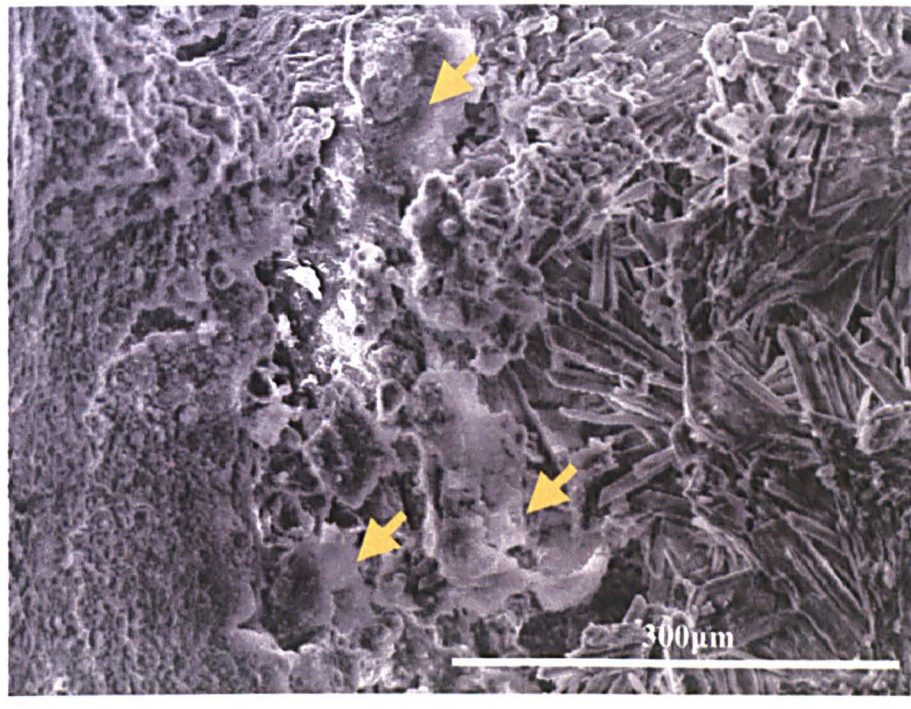

Figure 6.90: SEM photomicrograph of LM-05 after the acid rain simulation test. A barrier layer of barium sulphate is observed between the altered and the non-affected mass.

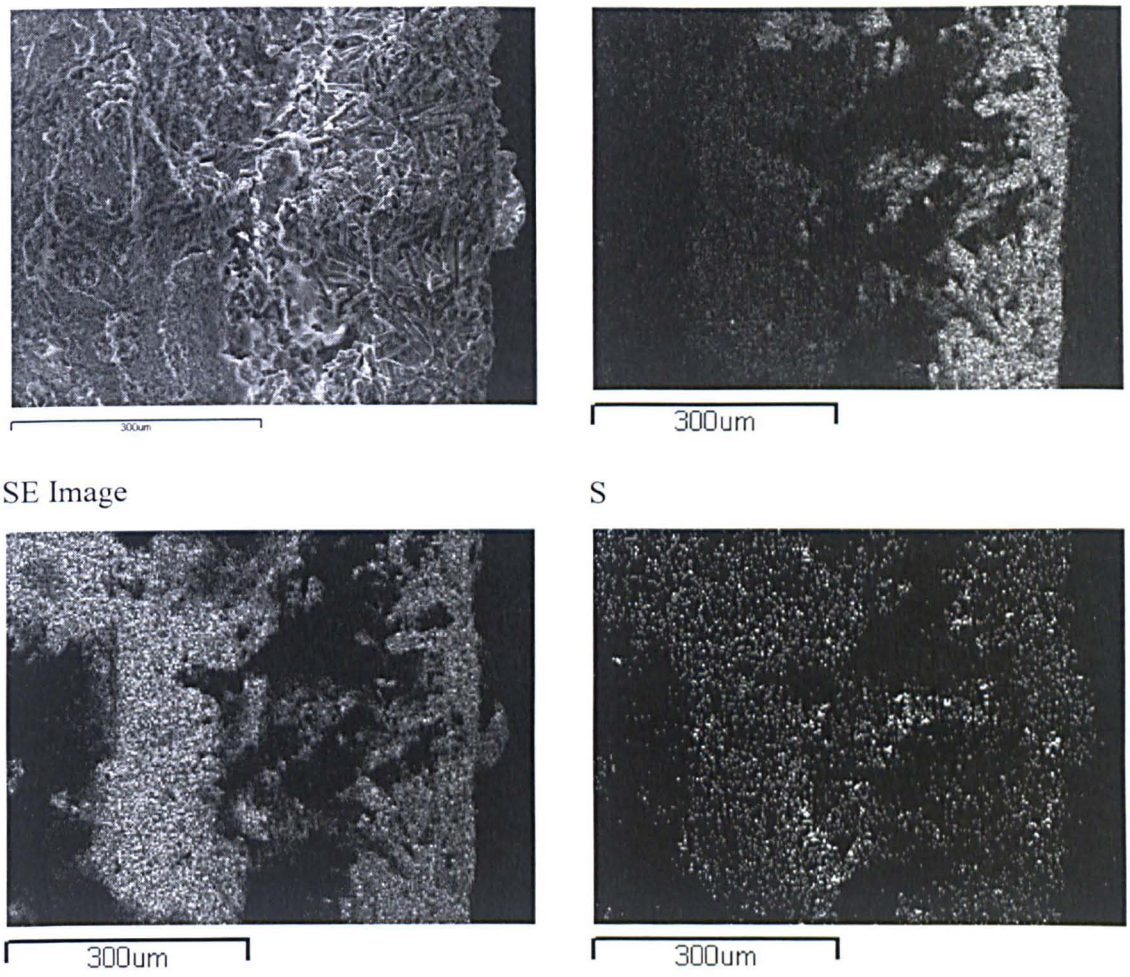

Figure 6.91: SEM photomicrograph of a fractured surface from LM-05 after the acid rain simulation test. Secondary electron image and X-ray maps showing the sulphated area of the specimen. The depth of the altered layer is approximately 150μm. The loss of signal in X-ray maps is attributed to the rough morphology of the surface.

6.6.4 Fixation of Sulphate Ions

The sulphate fixation test was carried out in twelve-month old specimens. The test provided information on the ability of different mixtures to fix sulphate ions and reduce the amount of material that could be washed out. According to the experimental setup, results corresponded to the sulphate ions that passed through the mass of the specimens. Therefore, the results are influenced by both the chemical composition of the

specimens, and its permeability. Concentrations of sulphate ions in the cathode solution, for every LM-mixture, are given in Figure 6.92.

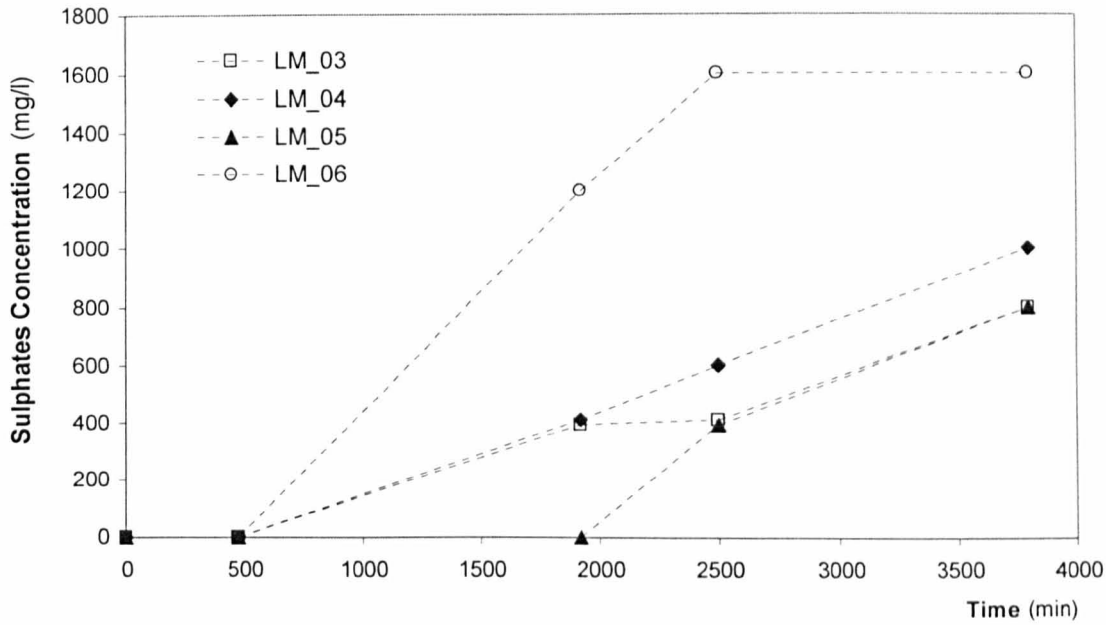

Figure 6.92: Concentration of sulphate ions passed through the specimen during the sulphate fixation test.

Calcium hydroxide, barium hydroxide, CSH phases, and the carbonate phases present in the mixtures are all dissolved in the pore water, providing a considerable source of calcium and barium ions. The accumulative concentration of the Ca^{2+} ions (moles/g of specimen) leached from the mixtures is given in Figure 6.93.

Concentrations of Ba^{2+} ions leached were below the detection limit, and are therefore not presented.

Mixture LM-05 showed the lowest amounts of calcium ions leached and the lowest sulphate concentration, followed, in increasing order, by LM-03 and LM-04, respectively. Mixture LM-06 showed the highest rate of decomposition and the highest concentration of sulphates. This must be attributed to the extensive network of micro-cracks in its mass, leading to easy access and circulation of weathering solutions.

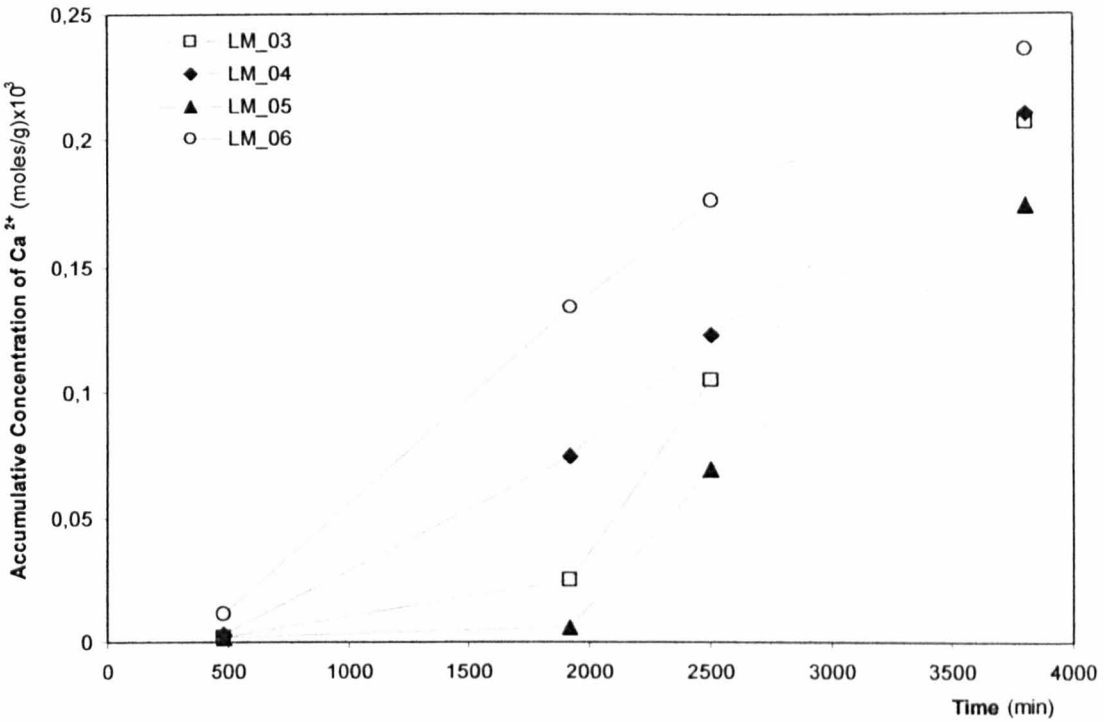

Figure 6.93: Concentration of calcium ions leached from the mortar due to the voltage applied across the specimen during the sulphate fixation test.

The barium ions produced by the dissolution of barium carbonate rapidly react with the sulphate ions and form the insoluble barium sulphate (barite) that precipitates from the pore solutions. This mechanism, along with the low permeability of the specimens, may explain the delay in the detection of sulphates in the case of LM-05 and LM-03 (Figure 6.92). The presence of barium compounds should, however, be considered the main reason for this delay in mixture LM-05, as the barium compounds have led to a less compact microstructure and more permeable pore space than in mixture LM-03.

6.6.5 Formation of Sulphate Weathering Products in Binary Pastes

The aim of this test was to monitor the micro-morphology of the weathering products formed when the binding material of the mortar was subjected to weathering by sulphate solutions. Sodium sulphate (14% w/w) and sulphuric acid (0.1M) solutions were used for this purpose. The weathering products were studied under the SEM, while their mineralogical composition was identified by XRD. Prior to the aging test, the lime-paste consisted of calcite ($CaCO_3$), aragonite ($CaCO_3$) and portlandite [$Ca(OH)_2$]. Calcite, portlandite and $BaCO_3$ were the main constituents of the binary-pastes, while witherite was the only constituent of the barium-paste.

After dispersion in the sulphuric acid solution, gypsum ($CaSO_4 \cdot 2H_2O$) was the only product identified in the pure lime paste (Ca-paste). Calcite, bassanite ($CaSO_4 \cdot 0.5H_2O$), calcium sulphate hydrate ($CaSO_4 \cdot XH_2O$) and thenardite (Na_2SO_4) were identified in the solid material filtered from the sodium sulphate solution. Witherite formed barite ($BaSO_4$) in both solutions. The above products were identified in the binary pastes in different proportions, depending upon the composition of the initial mixture. Diffraction patterns of binary pastes, filtered from the sulphuric acid solution, showed that barite ($BaSO_4$) and gypsum ($CaSO_4 \cdot 2H_2O$) were the only products precipitated in the solution.

The diffraction patterns of the binary-pastes dissolved in the sulphate solutions are presented on Figures 6.94 and 6.95. Moreover, the micro-morphology of the products formed in both the binary-pastes and the LM-mixtures are presented in Figures 6.96–6.103.

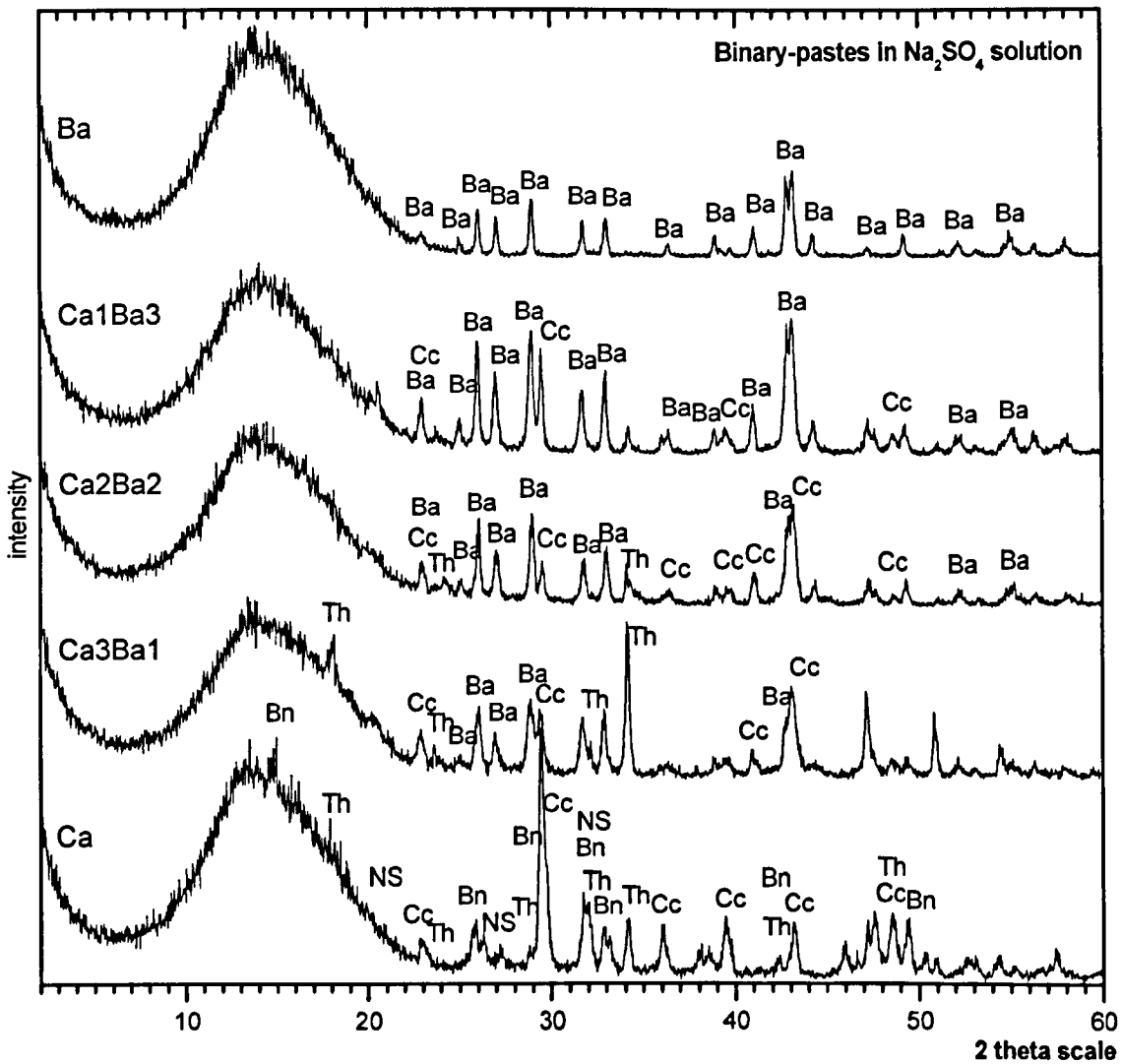

Figure 6.94: Diffraction patterns of the solid material filtered from sodium sulphate solution after the dissolution of binary pastes. Calcite (Cc), bassanite (Bn), calcium sulphate hydrate (NS), barite (Ba) and thenardite (Th) were identified in the solid material filtrated from the sodium sulphate solution.

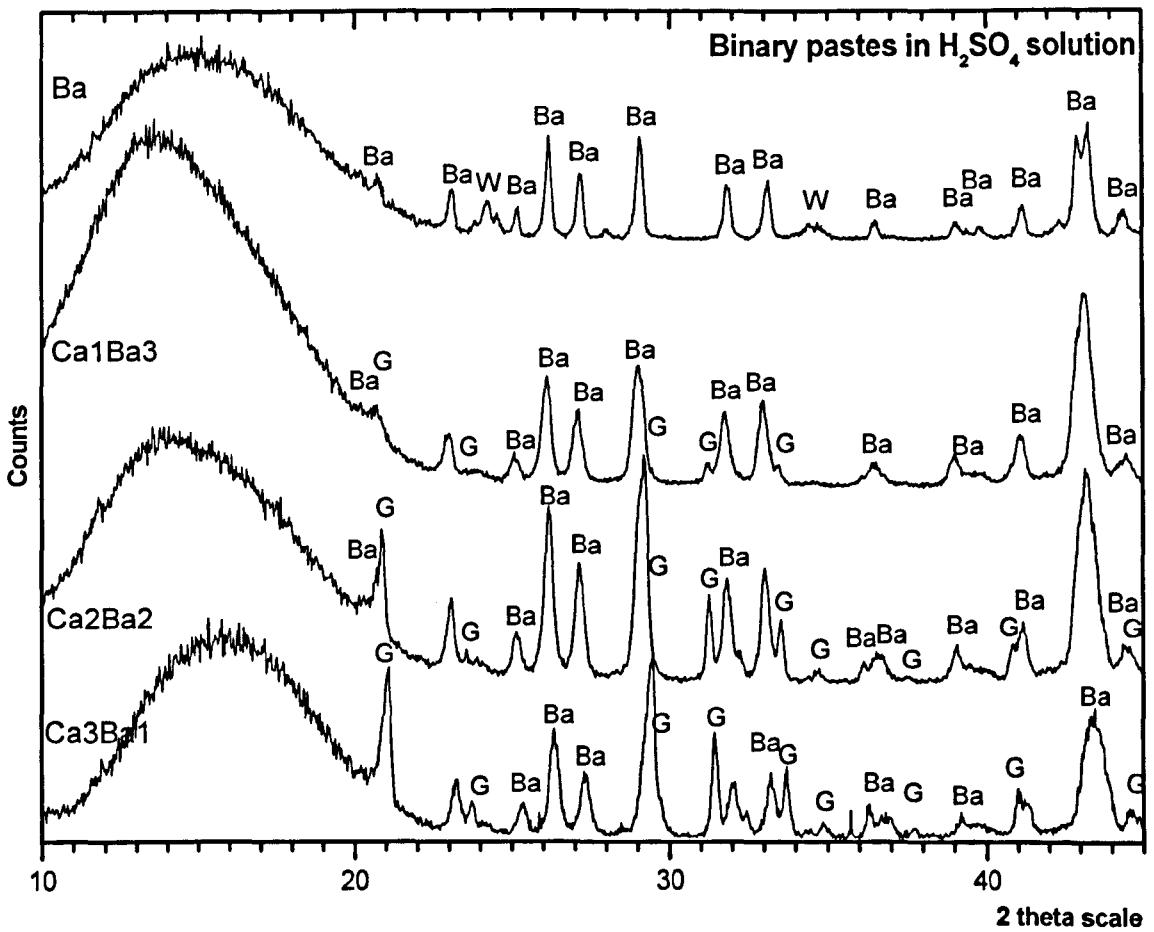

Figure 6.95: Diffraction patterns of the solid material filtered from sulphuric acid solution after the dissolution of the binary pastes. Barite (Ba) and gypsum (G) were the only phases identified.

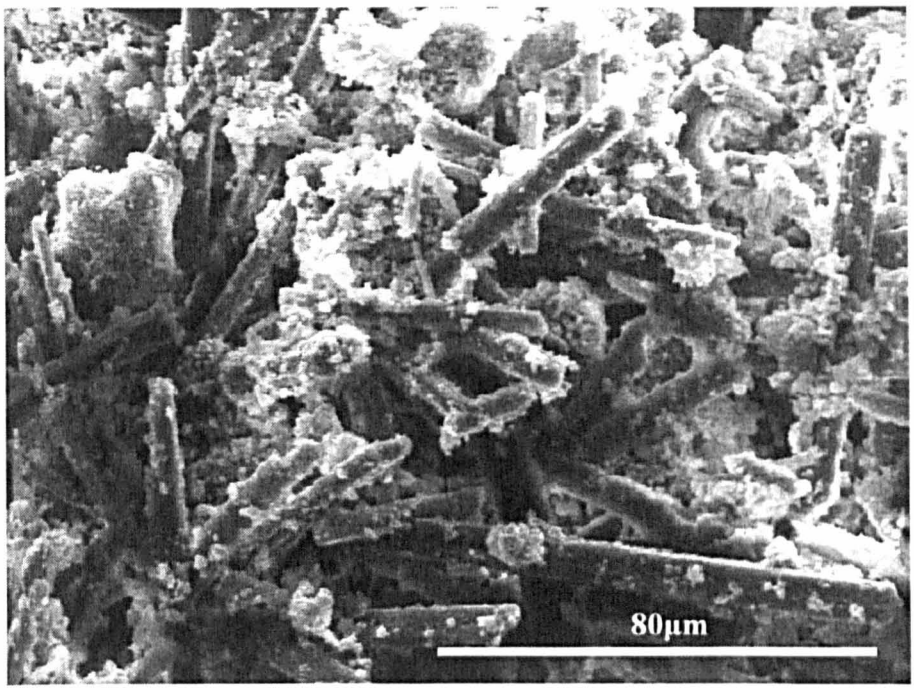

Figure 6.96: SEM photomicrograph of the solid material filtered after the dissolution of Ca-paste in sodium sulphate solution. Elongated calcium sulphate hydrate crystals are the main weathering products formed.

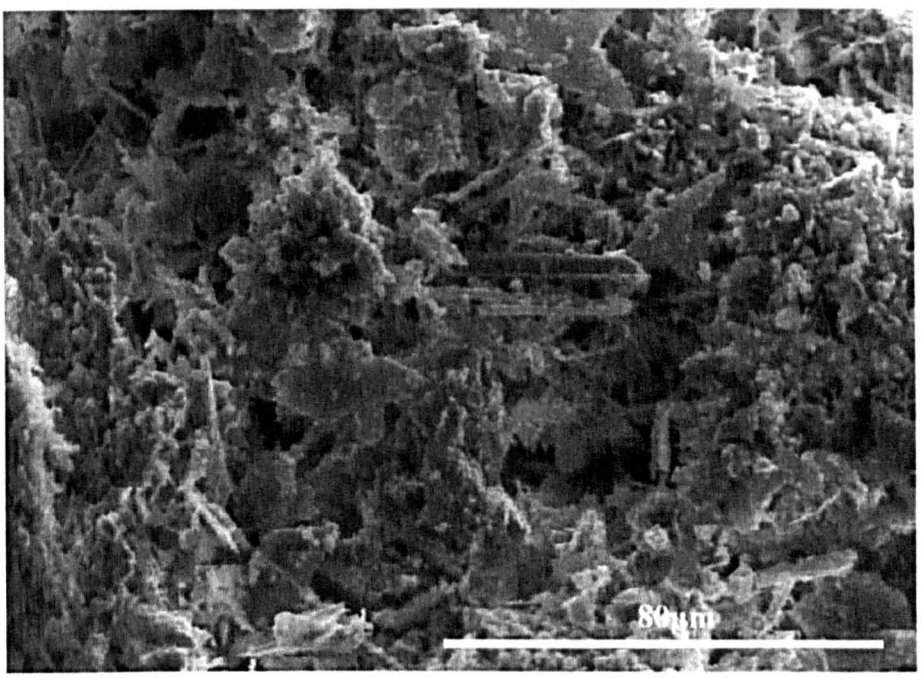

Figure 6.97: SEM photomicrograph of the solid material filtered after the dissolution of Ca-paste in sulphuric acid solution. Small plate-shaped gypsum crystals are formed mainly.

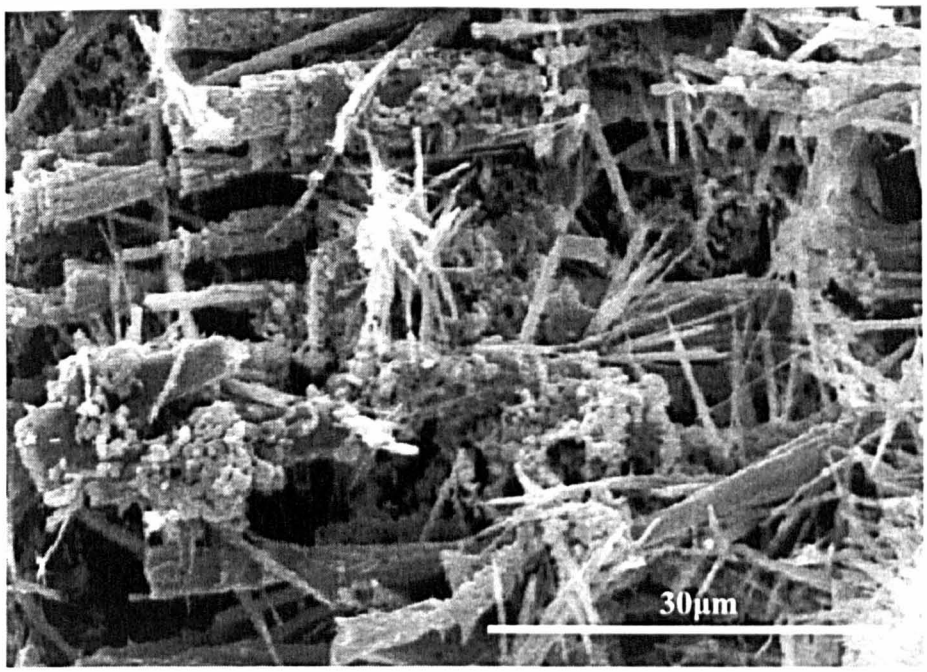

Figure 6.98: SEM photomicrograph of the solid material filtered after the dissolution of Ba-paste in sodium sulphate solution. Needle-like barite crystals are formed.

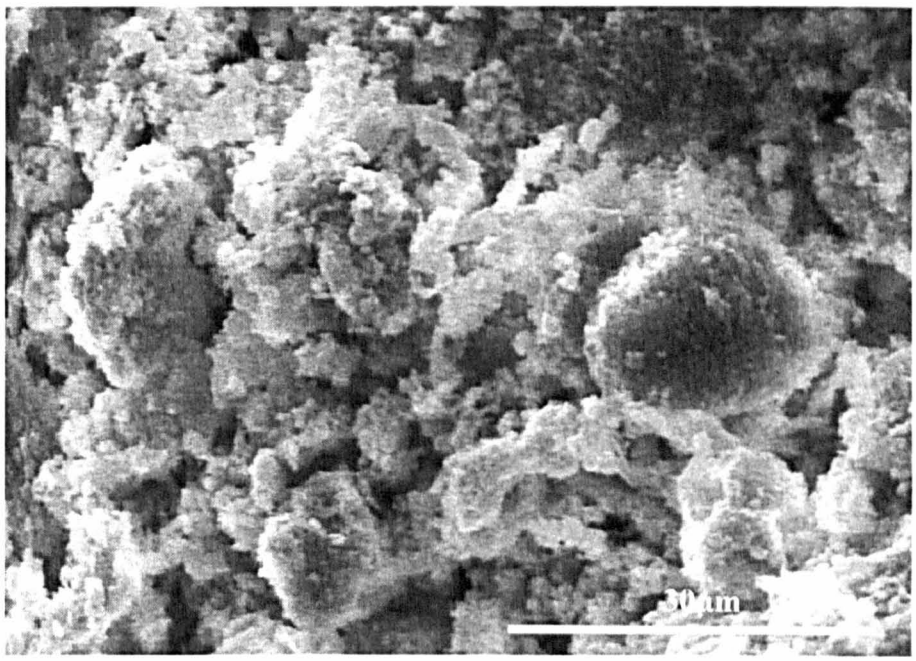

Figure 6.99: SEM photomicrograph of the solid material filtered after the dissolution of Ba-paste in sulphuric acid solution. Microcrystalline barite crystals are formed.

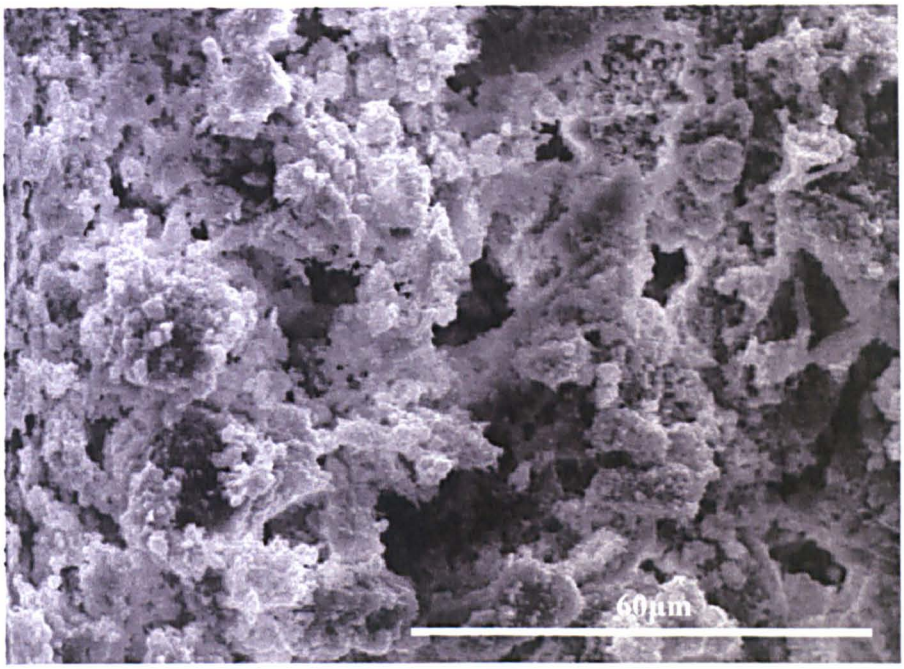

Figure 6.100: SEM photomicrograph of the solid material filtered after the dissolution of Ca2Ba2-paste in sodium sulphate solution. Microcrystalline barite and calcium sulphate hydrate crystals are the main weathering products formed.

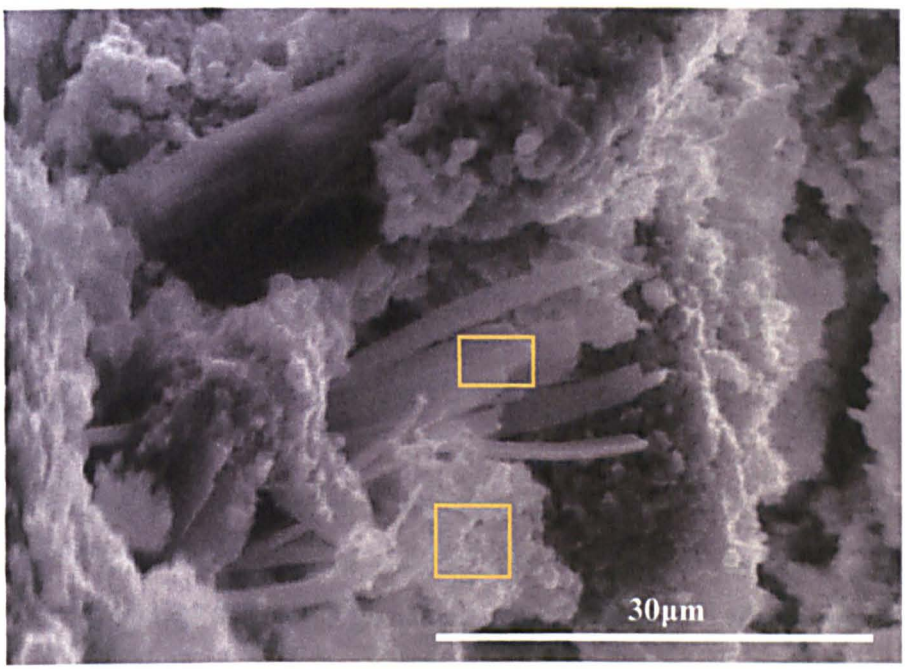

Figure 6.101: SEM photomicrograph of the solid material filtered after the dissolution of Ca2Ba2-paste in sulphuric acid solution. The marked areas indicate the formation of mixed salts of Ba, Ca and S, verified by EDX analysis.

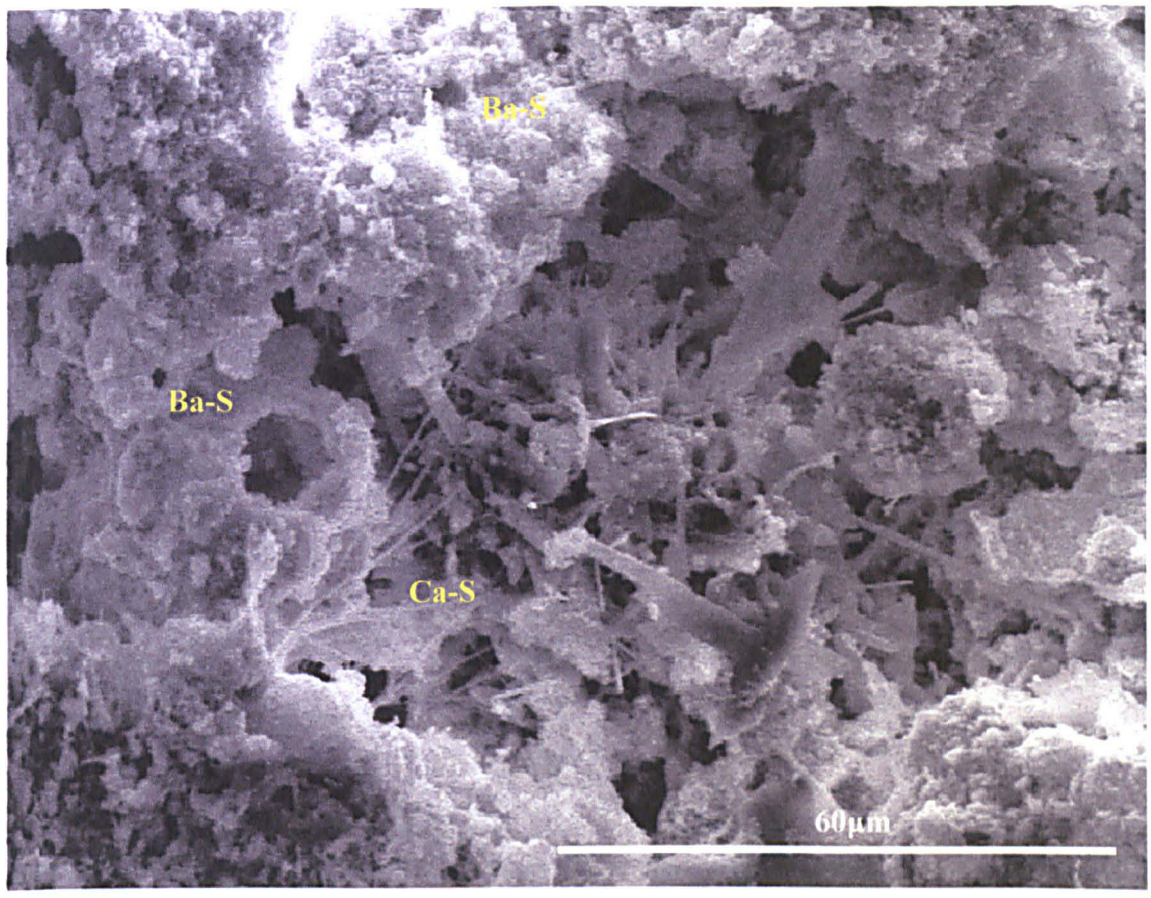

SE Image

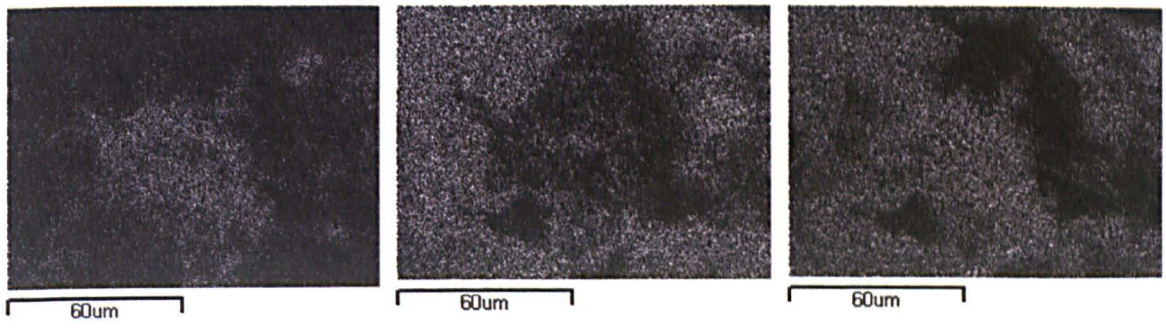

X-ray map: Ca

X-ray map: Ba

X-ray map: S

Figure 6.102: SEM photomicrograph of the solid material filtered after the dissolution of Ca2Ba2-paste in sulphuric acid solution. The marked areas indicate the formation of barite (Ba-S) and calcium sulphate hydrate (Ca-S), based on the X-ray maps of the elements.

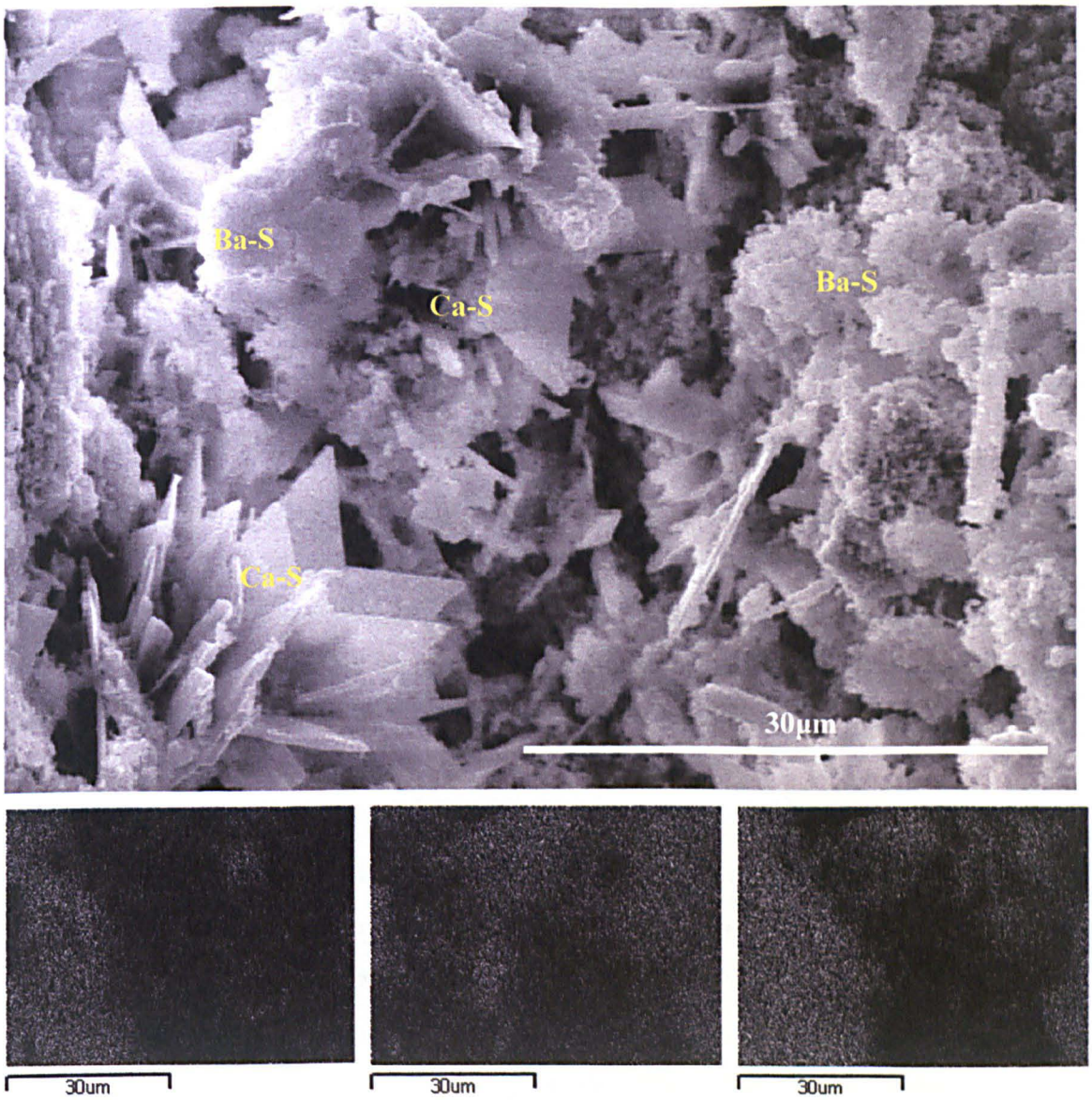

Figure 6.103: SEM photomicrograph of the solid material filtered after the dissolution of Ca2Ba2-paste in sulphuric acid solution. The marked areas indicate the formation of barite (Ba-S) and calcium sulphate hydrate (Ca-S), based on the X-ray maps of the elements.

7 DISCUSSION

7.1 STUDY OF BINARY MIXTURES

The study of binary mixtures helped to determine the effect of barium hydroxide on the microstructure of the lime binder and to estimate the optimum amount of barium hydroxide that could be added to the binder fraction. Moreover, the binary pastes served as 'pure' systems, clear from the effect of aggregates, in order to study the new products formed during setting, as well as the alteration products formed during accelerated weathering tests.

The results of their physical properties showed that the quantity of barium hydroxide has a strong effect on the microstructure of the binder. The presence of barium hydroxide crystals in the binary pastes produced a coarser matrix, which consequently affected the mechanical properties of the mortars. This is more a physical, rather than chemical, effect as it is caused by the grain-size distribution of the barium hydroxide crystals. Crystals with grain-size larger than 80μm diameter act as aggregates and therefore have an influence on the pore-space characteristics of the binder (Maurenbrecher et al., 2001). This was found to affect both binary pastes and LM-mixtures (Figure 7.1).

The correlation between the quantity of barium hydroxide and the porosity characteristics of the lime-binder is given in Figures 7.2 and 7.4. The values determined for the porosity of the binary pastes (around 50%) are in accordance with published data (Arandigoyen et al., 2005) although they are much higher than those found in historic and modern lime-based mortars, due to the absence of aggregates.

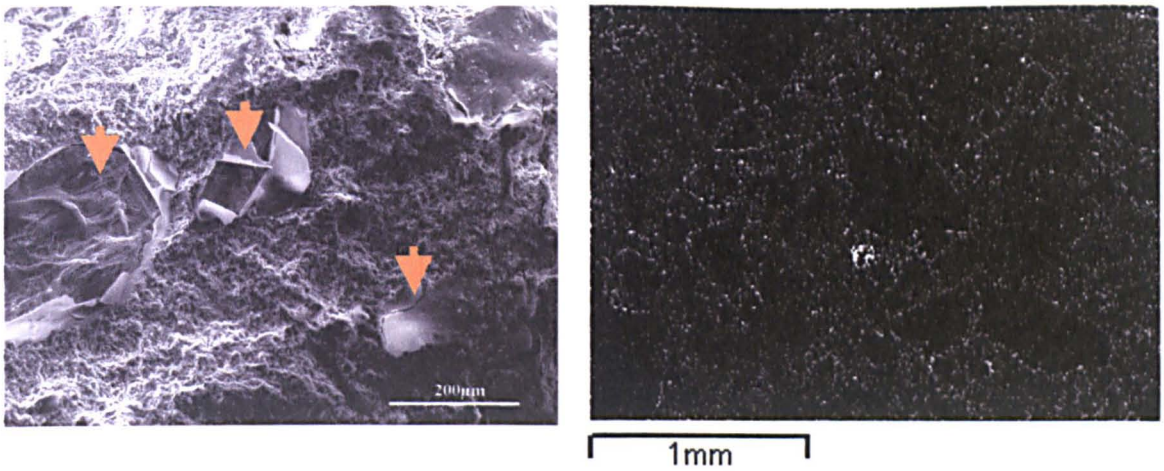

Figure 7.1: SEM photomicrograph from a fractured surface of Ca2Ba2 paste (left) and X-ray Ba^{2+} mapping in a thin section of LM-05 mixture (right). Barium hydroxide crystals larger than 80µm diameter had not completely dissolved in the binder mass.

Figure 7.2 shows that there is no significant relationship between the porosity values and the barium hydroxide concentration. However, the total surface area shows a distinctive trend, with a significant decrease in surface area with increasing concentration of barium hydroxide. This can be explained by the interpretation of the pore-size distribution diagrams (Figures 6.10 to 6.13), where a shift in the main peak, from 100nm to about 1000nm, was observed (i.e. a redistribution of the main pore volume from small to larger pore radius).

Figure 7.3 shows the pore-distribution in the pure lime paste (Ca-paste), which has no barium hydroxide present. The majority of the pores are distributed between a radius of 40 and 200nm, whereas the pore volume due to pores with radius larger than 200nm is close to 88%.

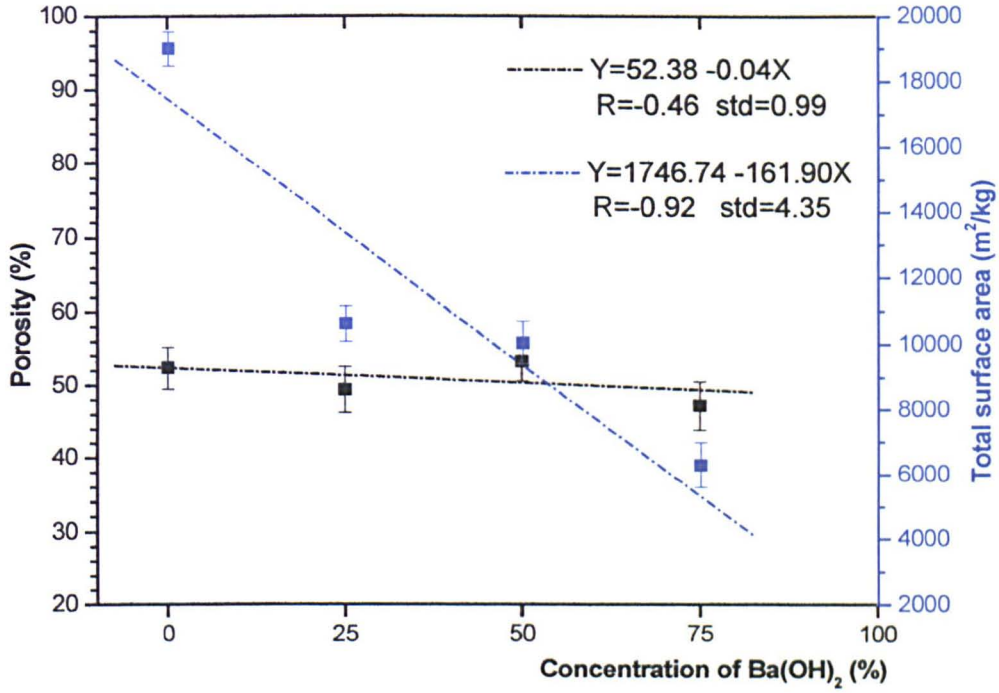

Figure 7.2: Porosity and total surface area values for the binary pastes as a function of barium hydroxide concentration.

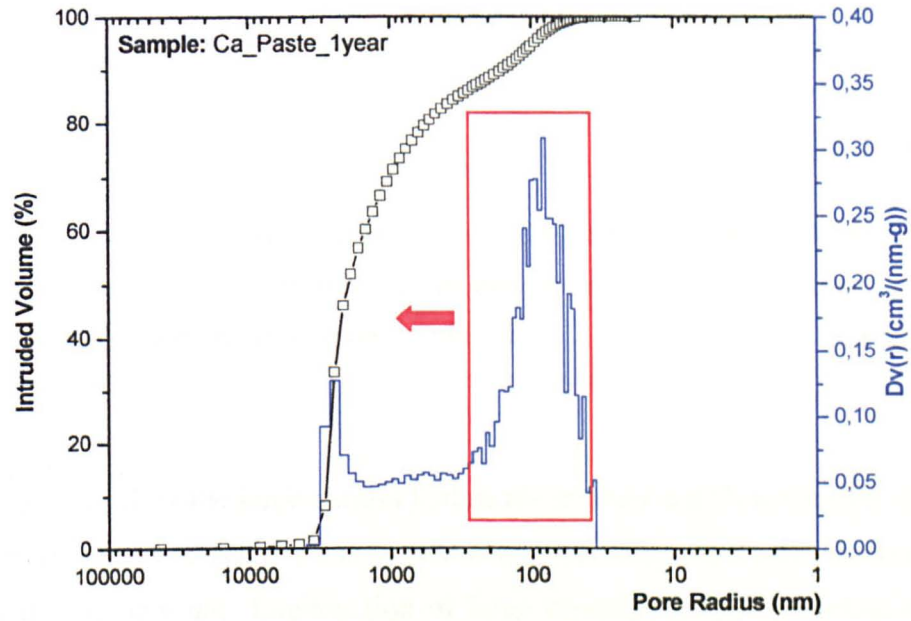

Figure 7.3: Porosity (intruded volume %) and pore-size distribution (Dv(r)) diagrams of Ca-paste. The highlighted peak disappears on addition of barium hydroxide, and a new peak is formed at around 1000nm.

Figure 7.4 shows the variation in pore volume due to pores with radius bigger than 200nm for the different binary mixtures. The successive replacement of lime by barium hydroxide in proportions 25, 50 and 75% resulted in an increase in pore volume (radius > 200nm) by 5, 9 and 10%, respectively. This was confirmed by SEM examination (Figure 6.9).

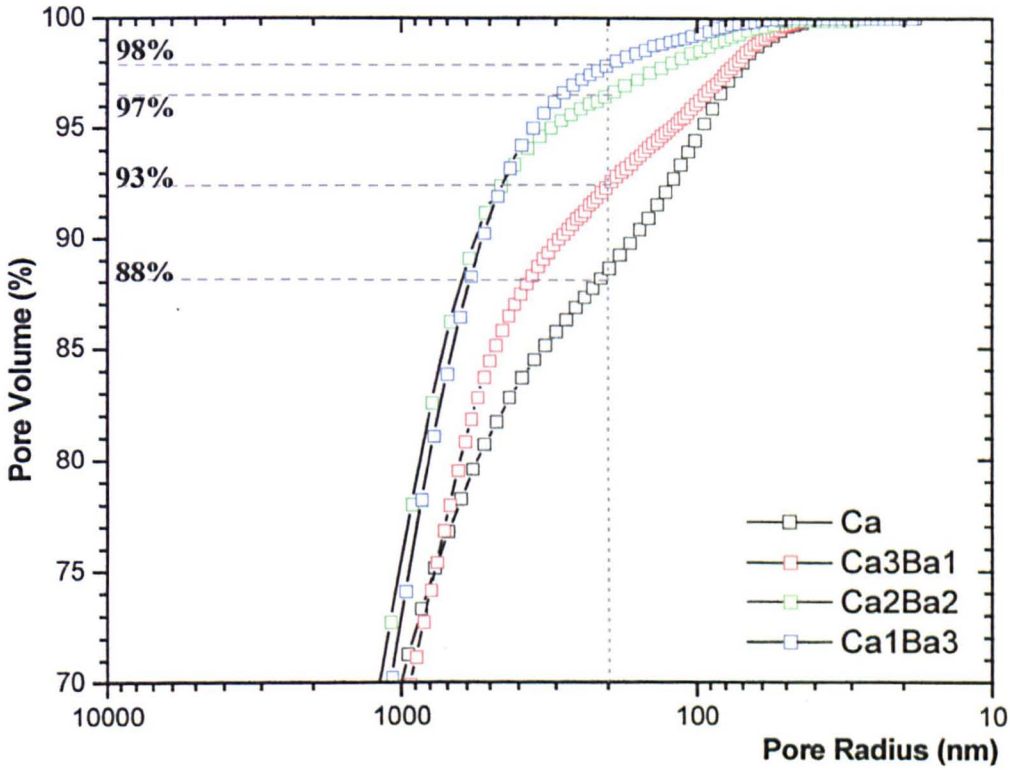

Figure 7.4: Changes in pore volume from pores larger than 200nm for the different binary pastes. Variations in pore volume are due to the presence of large barium hydroxide crystals in the lime-binder.

The defects caused by the large barium hydroxide crystals and their inability to produce homogenous adhesive pastes, is due to their high reactivity with carbon dioxide, present either in the air or water. Examination of large crystals from pure barium hydroxide pastes by SEM, after a one-year setting period, revealed the formation of a thin surface layer of barium carbonate, which acts as a barrier against further dissolution and reactivity (Figure 7.1 and 7.5). The higher reactivity of barium hydroxide, in

comparison to calcium hydroxide, is also evident from the mineralogical (XRD) and thermal analysis (DTA/TG) results (Tables 6.3 and 6.4). For this reason, barium hydroxide has been proposed to be used as an active filter for carbon dioxide gases.

Pastes which consisted of only barium hydroxide did not produce a compact and coherent mass: the samples were very easily crumbled by applying a soft load.

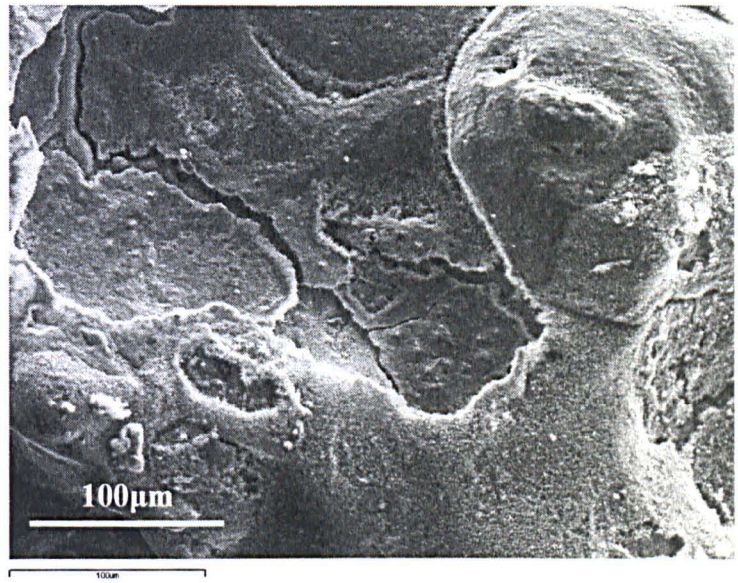

Figure 7.5: Formation of a surface layer of barium carbonate around large barium hydroxide crystals that blocks any further reaction.

The study of binary pastes of barium hydroxide with ceramic and calcium carbonate powder (Table 5.2) proved that barium cannot act as a binding medium on its own. Ceramic pastes with low concentration (10%) in barium hydroxide exhibited a moderate cohesion, mainly caused by the drying of the clay paste. Binary mixtures with higher concentration did not achieve good strength characteristics, since barium hydroxide crystals, of larger than 80µm, played the role of inert inclusions.

Binary pastes with calcium carbonate presented better cohesion than the ceramic pastes. The best characteristics were observed in mixtures containing 25% of calcium carbonate (BaCc25). The better cohesion of these mixtures is attributed to the ability of the

calcium carbonate particles to play the role of nuclii, exchanging Ca^{2+} ions with the barium hydroxide solution, leading to the formation of a barium-calcium carbonate 'solid solution' around the surface of the calcite crystals (Lewin and Baer, 1974).

7.2 SETTING OF MORTAR MIXTURES

The setting and hardening of mortar mixtures is described by the carbonation of both calcium hydroxide and barium hydroxide, and the pozzolanic reactions between the lime binder and the ceramic fragments. The carbonation process of lime includes the dissolution of carbon dioxide (CO_2) in water (Dheilly et al., 2002), and the reaction of the carbonic acid with dissolved calcium hydroxide (Equation 7.1):

$$Ca(OH)_{2(l)} + H_2CO_{3(l)} \rightarrow CaCO_{3(s)}\downarrow + H_2O_{(l)} \qquad (7.1)$$

The above reaction results in the precipitation of calcium carbonate in the binder mass. Calcite is the phase in which, all calcium carbonate phases identified in the XRD patterns are finally transformed, since it is more thermodynamically stable than either aragonite or vaterite (Martinez-Ramirez et al., 2003).

Examination of freshly fractured surfaces under SEM, and thermal analysis of the binder fraction, verified the development of hydraulic phases, which resulted from the reaction of lime with the ceramic material (Figure 7.6).

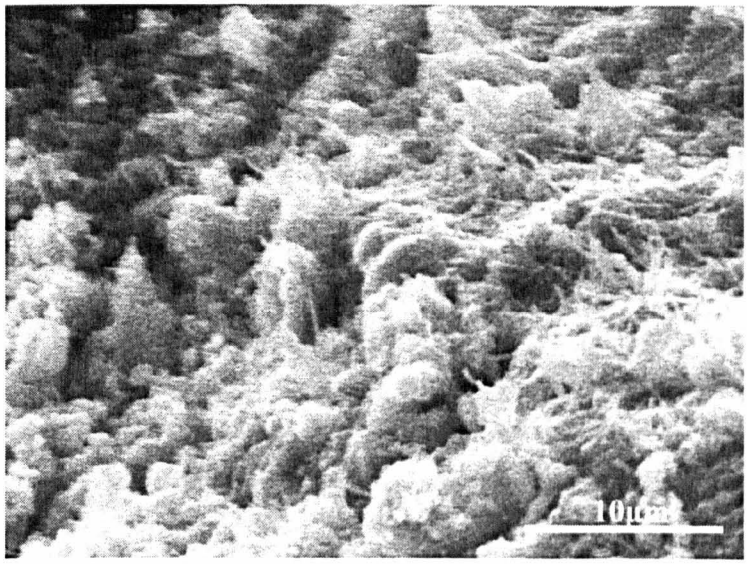

Figure 7.6: Development of hydraulic phases (CSH) through the reaction of lime with the pozzolanic material (ceramic).

The formation of the hydrated phases is described by the following simplified reaction:

$$Ca(OH)_2 + A.S + H_2O \rightarrow CAH + CSH \quad (7.2)$$

(alumino-silicates)

In mixtures that contain barium hydroxide, barium carbonate precipitates in a similar way to calcium carbonate: by the reaction of carbonic acid (Equation 7.3) (Hansen et al., 2003). The precipitation is favoured in an alkaline environment, and does not occur in neutral solutions (Clifton, 1982; Matteini, 1999).

$$Ba(OH)_{2(l)} + H_2CO_{3(l)} \rightarrow BaCO_{3(s)}\downarrow + H_2O_{(l)} \quad (7.3)$$

The evaluation of XRD patterns (Figures 6.24 to 6.27), and thermogravimetric diagrams (Figures 6.36to 6.39) suggests that the carbonation of barium hydroxide is much faster than that of lime. The main diffraction peak of barium hydroxide hydrate [$Ba(OH)_2 \cdot 8H_2O$] at 15° (Figure 6.18) is not present after a three-month setting period in all mixtures. In addition, DTA/TG diagrams do not show any peaks attributed to barium hydroxide. The fast transformation of barium compounds to the carbonate form

influences their chemical stability and contributes to the lower amount of barium ions leached during the electrochemically accelerated leaching test.

Examination of the thin-sections of barium hydroxide mortars by SEM indicated that barium ions (Ba^{2+}) were deposited around calcitic grains and, they were maintained in contact with the surface of the grain (Figure 7.7). The formation of this barium ions liquid film was more prevalent around calcite particles of diameter below 100μm. The thickness of the above film is about 10-15μm (Figure 7.8).

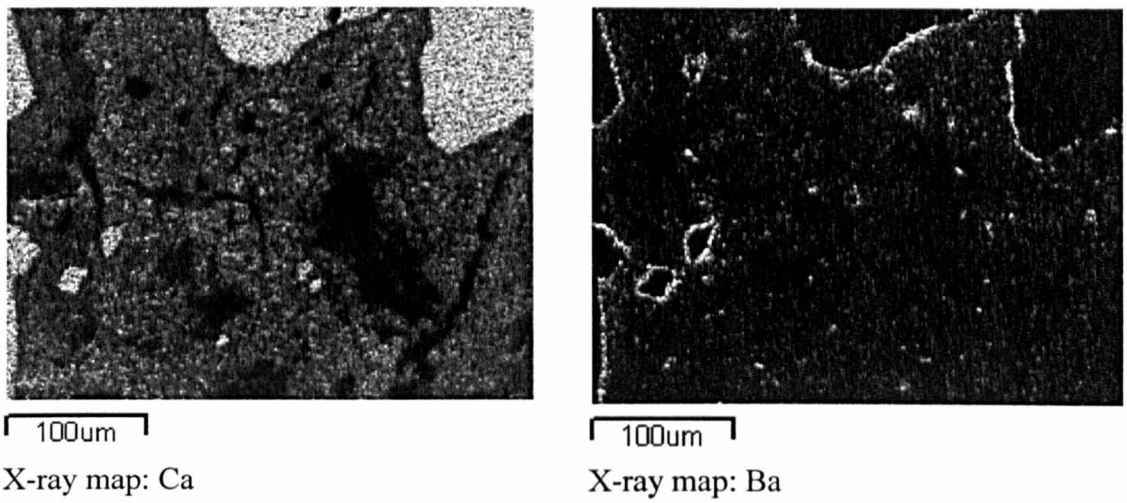

X-ray map: Ca

X-ray map: Ba

Figure 7.7: X-ray maps of calcium (Ca^{2+}) and barium (Ba^{2+}) ions in a thin-section of mixture LM-05. An increased concentration of barium ions is observed around thin calcitic grains.

When barium and calcium ions are present together in solution, the precipitation process leads to the formation of barium - calcium carbonate solid solution (Terada, 1952; Terada, 1953). Those solutions vary in crystal form, depending upon the barium content. The calcite type predominates for a barium carbonate content of up to 70 mole %, whereas the aragonite type predominates when the barium content is higher (Lewin and Baer, 1974). The formation of these solid solutions occurs either by diffusion or precipitation. At room temperature, the diffusion process is very slow (Atkins,

1994:935). The precipitation mechanism assumes that calcium ions move into the calcium-barium solution, which is already formed in the binder at areas of high surface energy, and then co-precipitate with the barium ions when the ion concentrations near the surface of the calcitic grains exceed the solubility product of the solid solution (Lewin and Baer, 1974).

SEM examination of thin sections in conjunction with X-ray elements mapping and linear scanning at the interface areas around small calcitic grains (Figure 7.8, 7.9 and 7.10) revealed that two phenomena are taking place during the setting of barium mortars. The ions exchange of barium ions for calcium ions of the surface layers of calcitic grains and, the formation of a barium carbonate calcium carbonate solid solution around calcitic grains (Figure 7.8).

In Figure 7.8, area '1' corresponds to the ions exchange on the surface of calcitic grain, while area '2' to the solid solution (overlapping of barium and calcium ions) in to the lime binder. The relative concentration of barium and calcium ions around the calcite particles is given in Figure 7.10. The solution observed in the LM-mixtures was rich in barium carbonate at the interface of calcitic grains and it was decreasing concentration (up to 0%) in the interior of the grains. In contrast, the concentration of barium towards the lime-binder mass was decreasing until a constant level.

The formation of these solid solutions offers a new surface in which, new barium carbonate crystals may be directly bonded. Therefore, it acts as a bridge between calcitic aggregates, barium phases and lime binder, contributing to the formation of a compact microstructure in the above described areas.

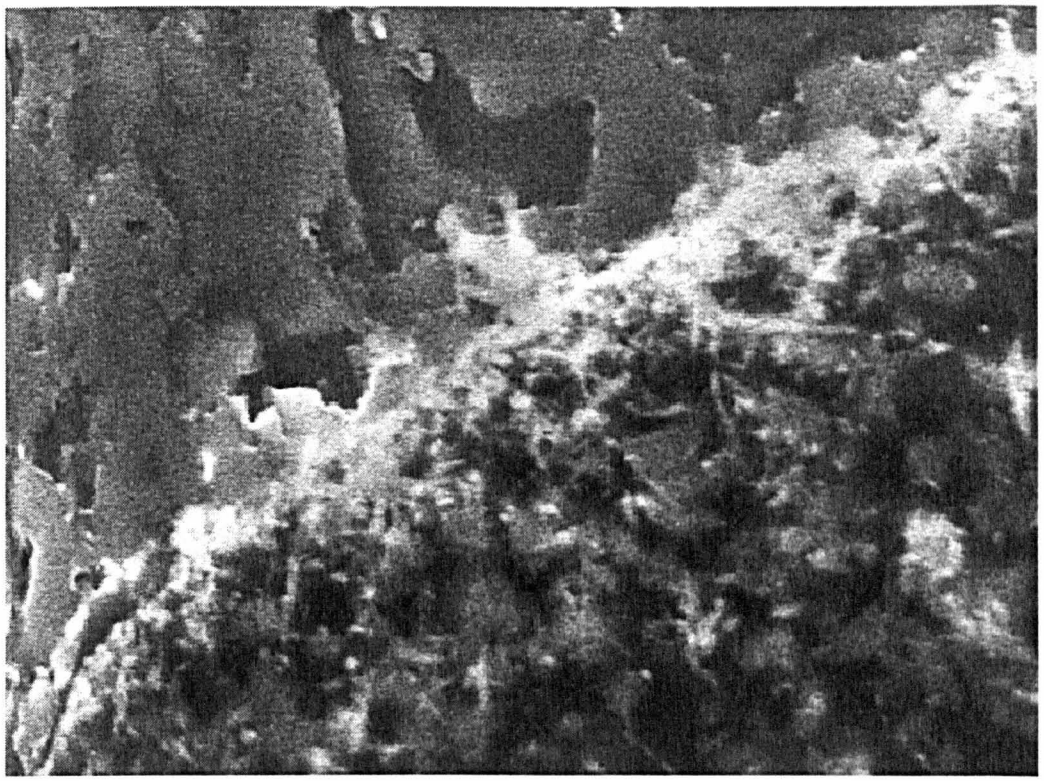

SE image

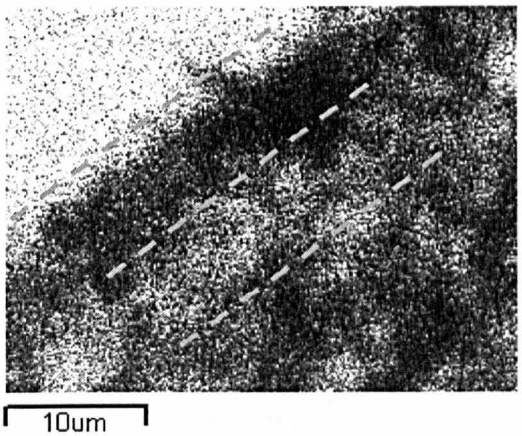

X-ray map: Ca

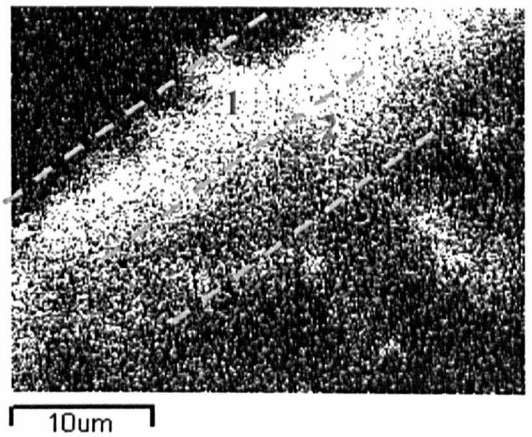

X-ray map: Ba

Figure 7.8: SEM photomicrograph of a thin-section of LM-05. X-ray maps indicate overlap of barium and calcium ions, leading to the formation of a solid solution.

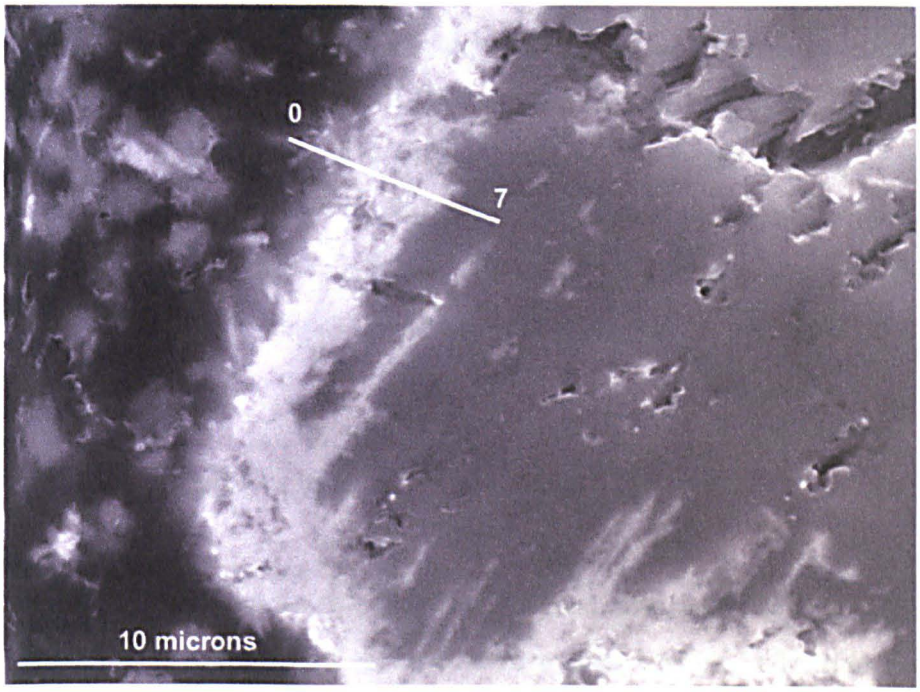

Figure 7.9 Thin section of LM-05 mixture under scanning electron microscope (SE image). The whitish area indicates the formation of the barium film around the surface of the calcitic grain.

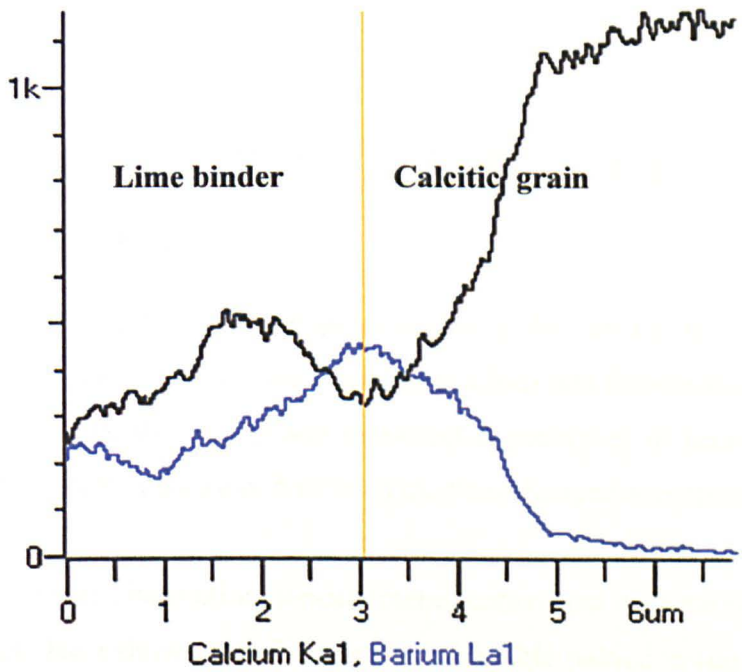

Figure 7.10 Line-scan at the interface zone between calcitic grains and binding material. The binder consists of 75% v/v of calcium hydroxide and 25% v/v of barium hydroxide. The line in the spectrum indicates the border of the calcitic grain.

In mixture LM-06, where barium hydroxide was added as a saturated solution at 80°C, the setting process involved an additional stage. Barium hydroxide precipitated from solution (Equation 7.4) in the initial stage of mixing, due to the cooling of the solution. The ion capacity of the solution is reduced until it reaches room temperature, according to the diagram given in Figure 3.9. When the solution reaches room temperature the precipitation of barium calcium carbonate takes place, according to the procedure previously described.

$$Ba^{2+} + 9OH^{-} + 9H^{+} \rightarrow Ba(OH)_2 \cdot 8H_2O_{(s)}\downarrow \qquad (7.4)$$

The precipitated barium hydroxide has small crystal size and is well distributed in the lime mass. Because of their high specific surface area, barium hydroxide crystals react with the carbonic acid and form barium carbonate. Depending upon the size of the initial particles, unreacted barium hydroxide may remain in the core. Any potential mechanical forces that are created upon anisotropic crystal growth and/or differential volume changes (Hansen et al., 2003) are absorbed by the mortar mass, because of the slow rate of hardening and the high plasticity of lime mortars.

7.3 PHYSICAL PROPERTIES OF MORTAR MIXTURES

The new phases formed through precipitation during the setting of fresh mixtures and the evaporation of water caused several transformations and dimensional changes in the binding material. Since the setting and carbonation processes of lime mortars last for several years, the microstructure of hardened mortars changes over time.

Porosity and pore-size distribution measurements carried out on lime mortars at 28, 90, 180 and 360 days have shown that there is a considerable reduction (up to 20%) in open porosity values (Papayianni and Stefanidou, 2001). These changes modify the porous system and reduce the pore volume of micro- and meso-pores, as well as the specific

surface area of the mortars (Houst and Wittmann, 1994; Houst and Wittmann, 2002; Sahu et al., 2004).

The pore-size distributions of the LM-mixtures, given in Figures 6.49–6.56 show that mixtures LM-03, LM-04 and LM-05 have the same type of pore-volume distribution, with 50% of their total pore volume in pores of radius 1000–3000nm, and almost 20% of their pores concentrated between 50nm and 300nm. The pore-size distribution of LM-06 shows that 70% of the total pore volume is concentrated in the first peak at 700–2000nm, and 10% in the second peak at 50–300nm.

The variation in the porosity and total surface area within the mortar samples with barium concentration in the solid state is given in Figure 7.11.

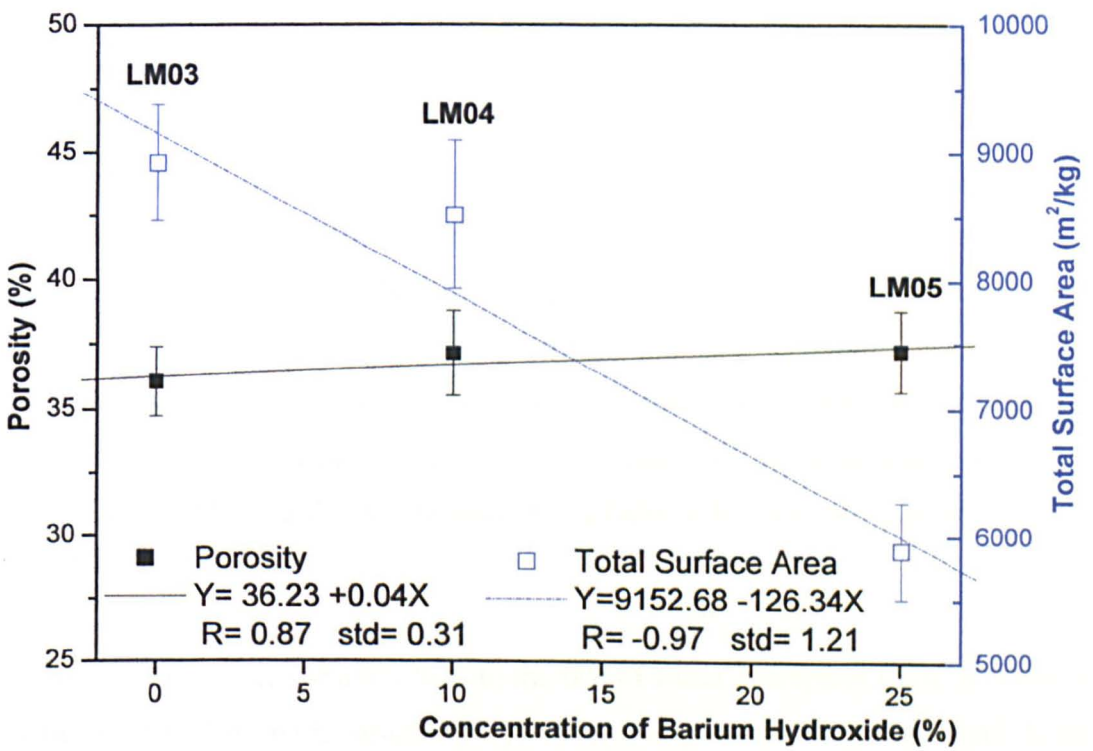

Figure 7.11: Variation of water-accessible porosity and total surface area as a function of barium hydroxide content, in the solid state.

There was no significant difference observed between the water accessible porosity values in the mortar samples, but a significant trend was apparent between the total surface area and barium hydroxide concentration. This is due to the formation of larger pores (>4310.89 nm) within the mortar as the barium hydroxide concentration is increased. Those pores are not accessible by mercury porosimeter and therefore, pore volume distribution of samples does not present any significant differences.

The formation of larger pores affects the performance of the mixtures under continuous loading. The comparison of their microstructure in thin-sections under petrographic and scanning electron microscope, showed that mixtures LM-03, LM-04 and LM-05 had very similar microstructures and only mixture LM-06 was different. There was an extensive network of micro-cracks present in LM-06 (Figure 6.47 and 6.48), attributed to the limited availability of water during setting, due to the fixation of the water molecules in the saturated solution by the precipitated barium hydroxide.

The pore-space characteristics of the mortars control the absorption and diffusion of moisture and aqueous solution within their mass, and therefore affect their durability, deterioration and service life (Martys and Ferraris, 1997; Goual et al., 2000; Arandigoyen et al., 2005). The water absorption diagrams of all mixtures (Figure 6.57) follow the typical behaviour of capillary sorption theories (Martys and Ferraris, 1997), showing a linear increase in the water taken up in the early stages, with the square root of time ($t^{1/2}$). The addition of barium hydroxide forms a homogenous pore structure, which increases the amount of capillary pores, and therefore the amount of the absorbed water. Thus, mixtures LM-04 and LM-05 had increased water absorption coefficients (kg/m^2) of 14.8% and 20.1%, respectively (Table 6.8). Mixture LM-06 showed the lowest increase (1.8%).

Figure 7.12 shows the variation of both the rate of water absorption ($g/m^2\ s^{0.5}$) and water vapour permeability with barium hydroxide concentration, in the solid state. It can be seen that the addition of barium hydroxide results in an increase in the rate of water absorption. It can also be seen that the addition of barium hydroxide in the solid state (mixtures LM-04 and LM-05) causes a linear increase in the water vapour permeability

(lower values correspond to enhanced permeability). The addition of barium hydroxide saturated solution (mixture LM-06) results the formation of a different microstructure, which consist of an extensive network of cracks formed during the setting (Figure 6.47 and 6.48). This network enables the faster evaporation of water vapours and reduces the rate of water absorption.

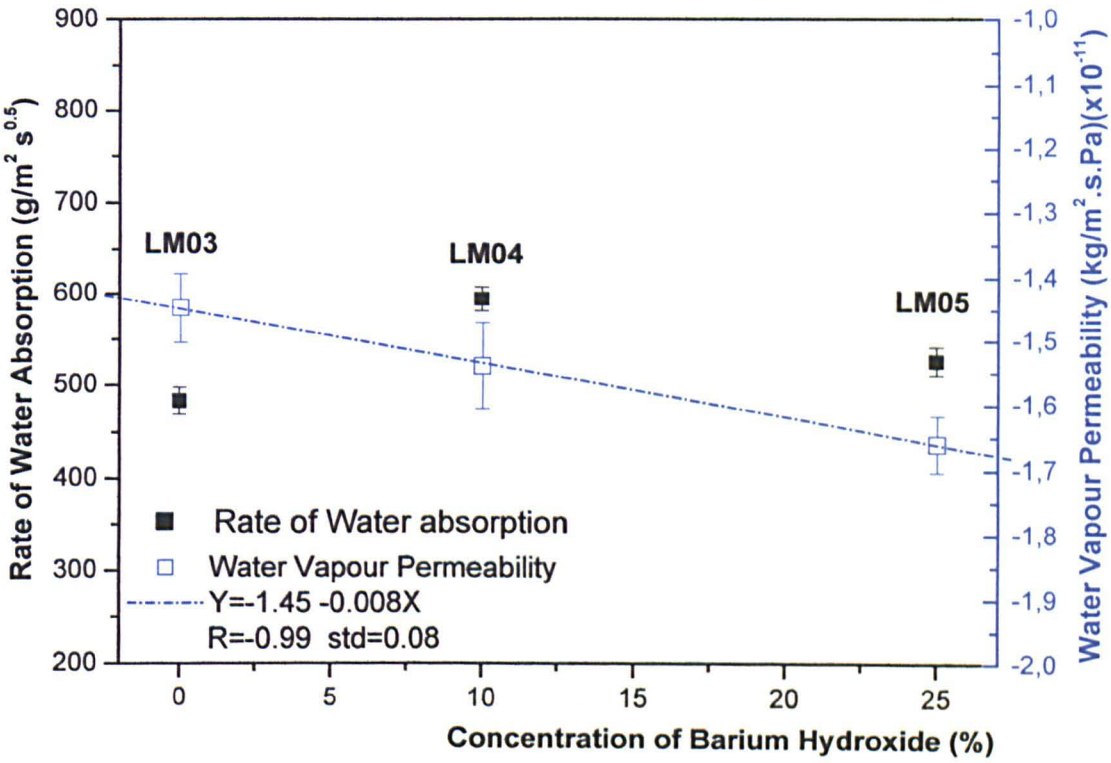

Figure 7.12: Variation in the rate of water absorption and water vapour permeability as a function of barium hydroxide content. The addition of barium hydroxide in the solid state causes a linear increase in water vapour permeability.

An increased water vapour permeability, and the formation of a pore network with larger pores, allows the mixtures with more barium hydroxide to remove the absorbed water from their mass more readily, and hence dry faster, and to absorb and reduce the pore pressure caused during the crystallization of soluble salts. The presence of larger pores provides sites where crystal growth can take place without exerting harmful stresses (Scherer, 1999; Scherer, 2000, Flatt, 2002).

7.4 MECHANICAL PERFORMANCE OF MORTAR MIXTURES

The study of the mechanical properties of the LM-mixtures through unconfined compression and three points loading showed that the addition of barium hydroxide had a significant effect on their performance.

The mechanical strength values are in agreement with the results of other research (Rodrigues and Henriques, 2003), showing an increase in compressive strength of upto 15–21% between three and twelve months.

In general, the compressive strength was shown to decrease with increasing barium hydroxide concentration. In comparison to the reference mixture LM-03, the compressive strength of mixture LM-05, after 12 months, showed the highest reduction (34%), followed by LM-04 (27%) and LM-06 (25%) (Table 7.1). These changes are closely related to the formation of a greater amount of large pores during setting and hardening (Krivtsov and Wiercigroch, 2001; Lanas et al., 2004).

Table 7.1: Variation in the strength of the LM mixtures in comparison to the reference (LM-03).

Sample	**Compressive Strength F_c (MPa)**		**Flexural Strength F_f (MPa)**	
Setting Time (months)	3	12	3	12
LM-03	0.87 ± 0.07	1.06 ± 0.04	1.24 ± 0.07	0.78 ± 0.08
LM-04	0.68 ± 0.06 (-21.84%)	0.77 ± 0.05 (-27.36%)	0.78 ± 0.08 (-37.10%)	0.37 ± 0.08 (-52.56%)
LM-05	0.57 ± 0.06 (-34.48%)	0.70 ± 0.04 (-33,96%)	0.78 ± 0.05 (-37.10%)	0.75 ± 0.07 (-3.85%)
LM-06	0.67 ± 0.05 (-22.99%)	0.79 ± 0.06 (-25.47%)	1.23 ± 0.08 (-0.81%)	0.38 ± 0.09 (-51.28%)

The flexural strength tests showed a considerable decrease in strength between three and twelve months. This phenomenon is attributed to the microstructural changes that take place during setting and, more specifically, to the formation of shrinkage cracks (typical of lime-ceramic fragment mortars) in the external layers of the mortar specimens (Cazalla et al., 2000). Calculation of the carbonation profile showed that at three months the carbonation depth was 0.7–1.0cm, which increased to 1.5–2.0cm after 12 months. The evolution of the carbonation process increased the crack density in the external layers and created fractures, enabling the propagation and diffusion of shrinkage cracks towards the load direction. This finally led to the total failure of the specimen with lower pressure (Schultz, 1996; Li et al., 1998).

Mixture LM-05 showed very similar flexural strength, after twelve months, to that of LM-03 (4% reduction), while the flexural strength of LM-04 and LM-06 was reduced by up to 52% over the same time period (Table 7.1). Da Silva et al. (2002) stated that flexural strength values obtained at different carbonation stages of concrete specimens exhibited a gradual decrease of up to 25% of their initial values. The extensive decrease of flexural strength in the LM mixtures is due to both an increase in crack density in the external layers, and an increase in the large pore population. The values obtained are, however, in accordance with typical flexural strength values measured in historic mortars. Moropoulou et al. (2003) showed that the tensile strength values for historic crushed brick-lime mortars ranges between 0.65–0.50MPa.

From the interpretation of the stress-strain curves (Figure 6.59 to 6.62) and modulus of elasticity values (Table 6.9), the slope of the stress-strain curves for all mixtures, up to 0.5MPa stress, is almost independent of the compressive strength, and therefore the modulus of elasticity values are quite similar (Table 6.9). Mixtures LM-04 and LM-06 show a decrease in the modulus of elasticity of 5.90% and 0.34%, respectively, while mixture LM-05 shows the highest reduction, with a value of 11.12% lower than the reference (LM-03).

The slope of the stress-strain curve, between 0.5MPa and maximum stress, is much steeper for LM-03, which has the highest compressive strength. The mixtures

containing barium hydroxide have flatter slopes, which is an indication of their higher deformability.

The elastic behaviour and deformability of mortars are important properties, which affect the durability of mortars against salt crystallisation. The yield strength and the ratio of modulus of elasticity to flexural strength (E/F_f), and the ratio of compressive to flexural strength (F_c/F_f) have been suggested as parameters that could provide more data on the deformability and elastic behaviour of lime-based mortars (Bromblet, 2000; Bell, 2000:230; Moropoulou et al., 2005b). The yield point or yield strength describes the limit on the stress-strain curves for changing the deformation of the material from elastic to plastic (Bell, 2000:230). When the stress applied to the mixture exceeds its elastic limit (yield point), any internal or external stresses are absorbed (Schafer and Hilsdorf, 1993) through permanent straining, until failure (compressive strength value).

In contrast, the concentration of local stresses in brittle materials results in the formation of internal fractures or micro-cracks. The ratio of the modulus of elasticity to flexural strength (E/F_f) can be considered as an index of flexibility or crack sensitivity (Bromblet, 2000). A high ratio would indicate high sensitivity to cracking.

The ratio of compressive to flexural strength (F_c/F_f) has been found to be proportional to the modulus of elasticity (E) in new mortars (Moropoulou et al., 2005b). Figure 7.13 is a plot of the compressive to flexural strength (F_c/F_f) against the modulus of elasticity (E) for the four mortar mixtures. There is clearly a correlation between samples LM-04, LM-05 and LM-06, but sample LM-03 does not follow this model.

The mechanical behaviour of samples LM-04, LM-05 and LM-06 is affected by the presence of larger pores, which have been created during the setting due to the addition of barium hydroxide.

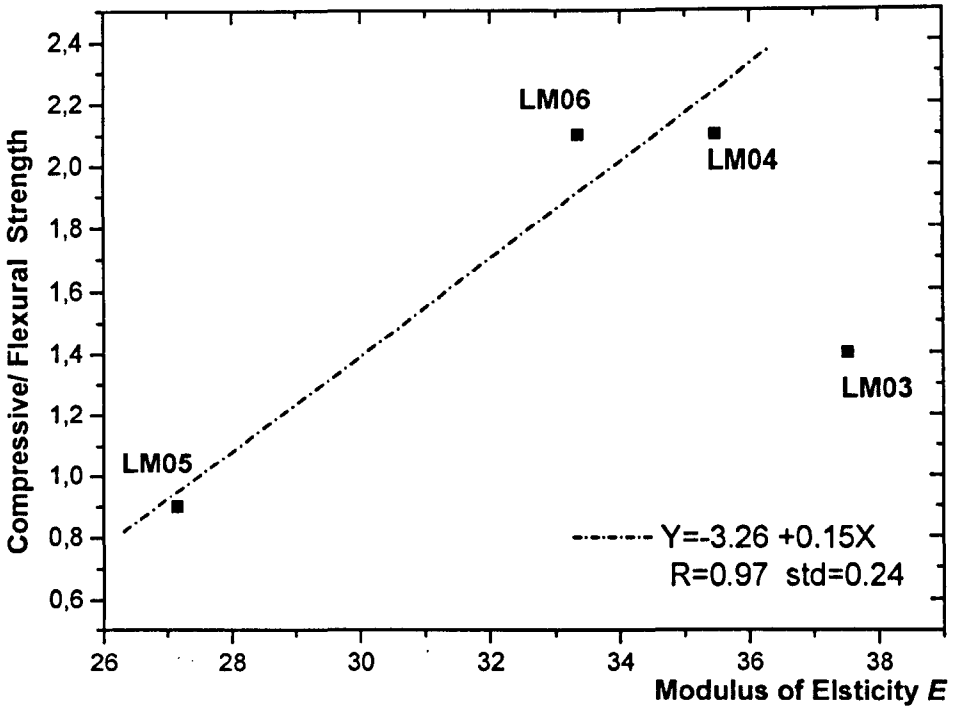

Figure 7.13: A plot of the ratio of the compressive over flexural strength (F_c/F_f) against the modulus of elasticity (E) for the LM mixtures, at twelve months.

Figure 7.14 shows the variation of the modulus of elasticity at the yield point (E') and the compressive/yield strength (F_c/F_y) for the four LM mixtures. These measures of mechanical performance reflect the durability against crystallisation of sulphate salts and help to classify mortars as brittle or ductile according to the amount of plastic deformation which they exhibit (Bell, 2000:230). In general, a correlation is observed between these properties and the order of failure of the LM mixtures (LM06>LM05>LM04>LM03) during the salt crystallisation tests (Figures 6.64 and 6.65).

Figure 7.15 shows the variation of the ratio of the modulus of elasticity to flexural strength (E/F_f) with barium hydroxide concentration. For those samples with barium hydroxide present (LM-04, LM-05 and LM-06), an increase in the barium hydroxide concentration reduces the sensitivity of the mortar to cracking. Only sample LM-05, with 25% barium hydroxide, has less sensitivity to cracking than the reference sample (LM-03), but its standard deviations are, however, quite high.

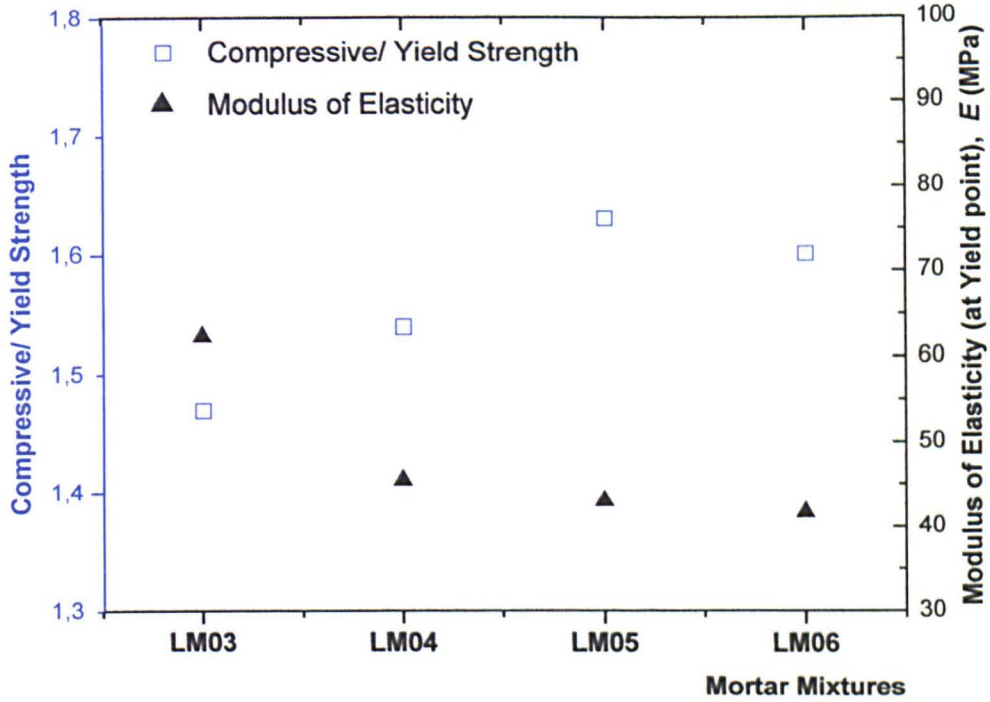

Figure 7.14: The ratio of compressive to yield strength, and the modulus of elasticity at yield point (E') of the LM mixtures at twelve months.

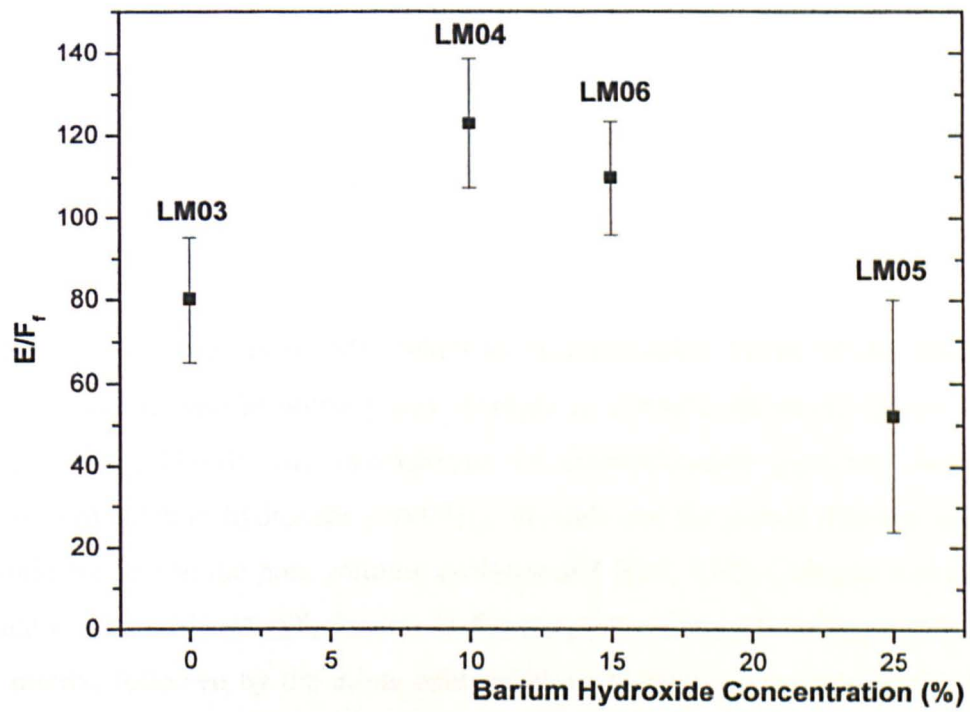

Figure 7.15: Variation in the ratio of the modulus of elasticity to the flexural strength of LM mixtures at twelve months, as a function of the barium hydroxide concentration.

The durability of LM mixtures against accelerated aging tests with sodium sulphate is affected by both the pore-space characteristics and the mechanical performance (as this is expressed by the values of modulus of elasticity at the yield point and the ratio of compressive to yield strength), as well as on the barium content.

XRD patterns show that the barium compounds present in the mortar react with the sulphate ions and form barium sulphate (Figure 6.94 and 6.95). This effectively prevents the formation of the hydrous sodium sulphate, and offers protection against sulphate attack.

7.5 DURABILITY OF MORTAR MIXTURES AGAINST CHEMICAL DEGRADATION

Chemical degradation of mortars is associated with deterioration mechanisms that involve the presence of water or aqueous solutions. Acid attack, dissolution and leaching of the binding medium (hydrated lime) are the main phenomena usually present in lime-based mortars exposed to outdoor environments and lead to their gradual degradation (Cohen and Mather 1991; Sabbioni et al., 2001; Tixier and Mobasher, 2003).

Degradation of mortars is usually linked to decalcification of the binder matrix, and therefore to an increase in porosity and decrease in strength values (Carde et al., 1996; Catinaud et al., 2000). The mechanisms of decalcification generally involve the dissolution of calcium hydroxide [$Ca(OH)_2$] crystals and the partial dissolution of CSH (hydraulic phases) in the pore solution (Adenot and Buil, 1992; Delagrave et al., 1997; Catinaud et al., 2000). Distilled water is the simplest solution inducing decalcification of the matrix, followed by the dilute acid solutions formed in the atmosphere. In order to increase the rate of degradation, twelve-month old mortar specimens were submitted to an electrochemically accelerated leaching test, and the stability of the setting products monitored, as well as any microstructural changes occurring during the test period.

During the test, there is a dynamic chemical equilibrium between the main hydrates, $Ca(OH)_2$ and CSH, and their component ions in the pore water (Equations 7.5 and 7.6) (Brown and Clifton, 1988):

$$Ca(OH)_{2(s)} \leftrightarrow Ca^{2+}_{(aq)} + 2OH^{-}_{(aq)} \quad (7.5)$$

$$C\text{–}S\text{–}H_{(s)} \leftrightarrow Ca^{2+}_{(aq)} + 2OH^{-}_{(aq)} + SiO_{2(s)} \quad (7.6)$$

The applied potential across the specimen forces Ca^{2+} ions to move towards the cathode solution. Thus, the concentration of Ca^{2+} ions in the pore water decreases and more $Ca(OH)_2$ dissolves to maintain the equilibrium. After complete dissolution of the $Ca(OH)_2$, Ca^{2+} ions are supplemented by the CSH phases, which finally degrades to SiO_2 gel (Saito and Deguchi, 2000).

According to their solubility products (Table 3.1), calcium hydroxide [$Ca(OH)_2$] and barium hydroxide [$Ba(OH)_2 \cdot 8H_2O$] are the main products that are expected to be dissolved in the pore water the of LM mixtures. Decalcification of the CSH and the carbonate phases ($CaCO_3$, $BaCO_3$) are secondary reactions also taking place. The dissolution of carbonates in aqueous solution is described by the following reactions (Wilkins et al., 2001):

$$H^{+}_{(aq)} + CaCO_{3(s)} \rightarrow Ca^{2+}_{(aq)} + HCO^{-}_{3(aq)} \quad (7.7)$$

$$HCO^{-}_{3(aq)} + H^{+}_{(aq)} \leftrightarrow H_2CO_{3(aq)} \rightarrow CO_{2(aq)} + H_2O_{(l)} \quad (7.8)$$

Thermal (DTA/TG) and mineralogical (XRD) analysis of the binding material prior to the test showed that only calcite ($CaCO_3$), witherite ($BaCO_3$), portlandite [$Ca(OH)_2$] and low amounts of hydraulic compounds (CSH phases) were present. Barium hydroxide was found to be totally converted to witherite ($BaCO_3$) and barium-calcium carbonate [$BaCa(CO_3)_2$]. Therefore, the main phase that provided ions to the solution was the non-carbonated calcium hydroxide of the lime binder (portlandite).

The above results explain the similar total conductivity values (Figure 6.80) obtained for all of the LM mixtures during the test. The barium ion (Ba^{2+}) concentration is five times lower than the calcium (Ca^{2+}), and therefore the assumption that barium hydroxide reacts very fast with carbon dioxide and is converted to its carbonate form, is strengthened. Finally, the concentration of alkali (K^+, Na^+) that could be leached from the ceramic matrix was below the detection limit of 10μg/ml (ICP analysis).

The amount of ions leached into the pore solutions (Figures 6.81 and 6.82) primarily depends upon the chemical stability of the compounds/phases formed during the setting of the mortars. However, the total amount of ions that pass to both the anode and cathode solution is also dependent upon the pore-space characteristics of the specimens (Bagel' et al., 1997; Catinaud et al., 2000). In Figure 7.16, the rate of water absorption values ($g/m^2\ s^{0.5}$) and maximum concentration of calcium ions leached are plotted for each of the mortar mixtures. There is a clear correlation between the concentration of calcium ions leached (and hence the water accessible pores) and their diffusion speed. The concentration of calcium ions leached cannot, therefore, provide definitive information on the chemical stability of the setting phases formed in the different mixtures.

The decalcification of the binder matrix caused changes on the surfaces of the specimens in contact with the anode and cathode solutions: a considerable amount of degradation was observed due to the loss of the binding medium (Figure 7.17).

In contrast, Ca^{2+} ions leached towards the cathode solution formed a rich layer of calcium hydroxide on the surface of the specimen, which was gradually converted to calcite, after the drying out the solution (Figure 7.18).

Determination of the total porosity of the samples after electrochemically accelerated degradation showed that an increase in water-accessible porosity had been caused (Figure 7.19).

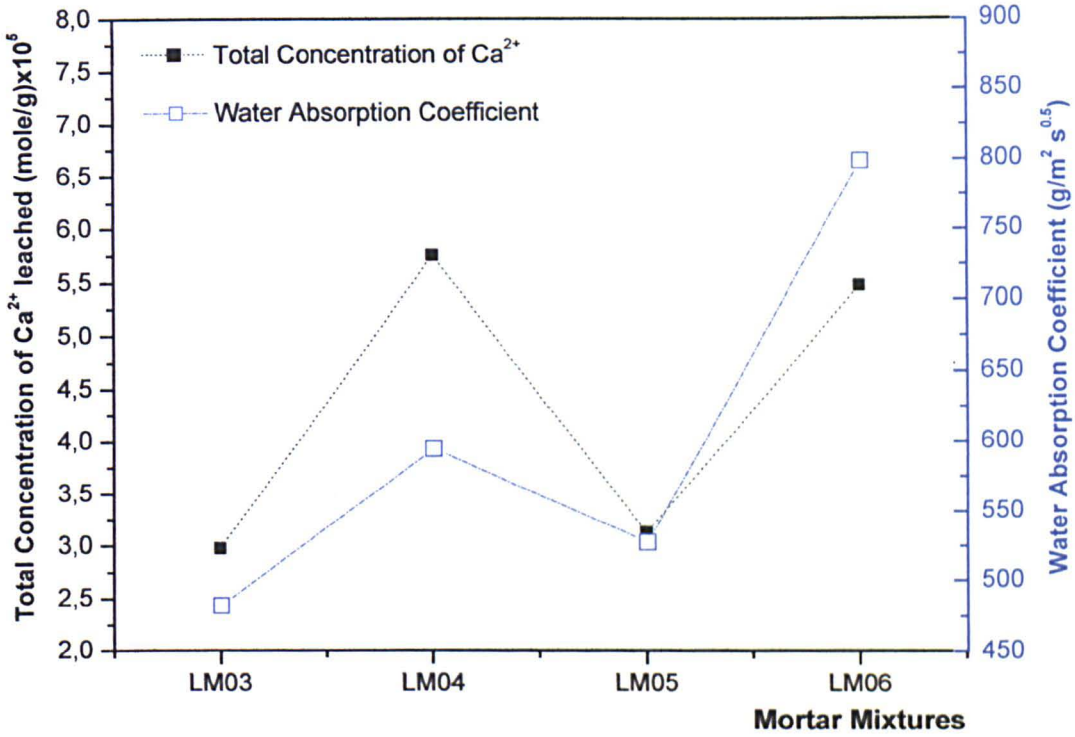

Figure 7.16: Variation in rate of water absorption values (g/m^2 $s^{0.5}$) and maximum concentration (moles/g $x10^5$) of calcium ions leached during the electrochemically accelerated degradation test, for the different mortar mixtures.

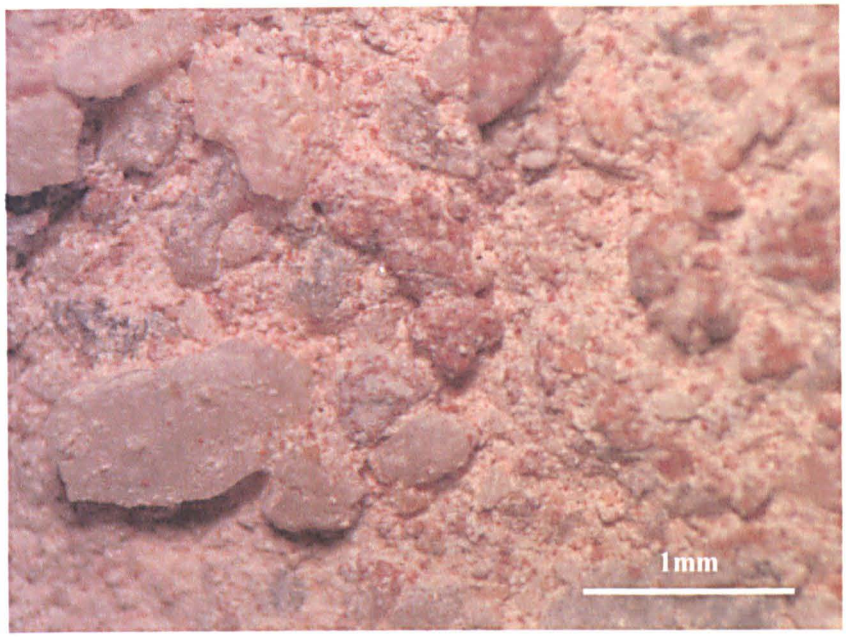

Figure 7.17 Degradation of the specimen in the anode solution due to the leaching of the binding medium.

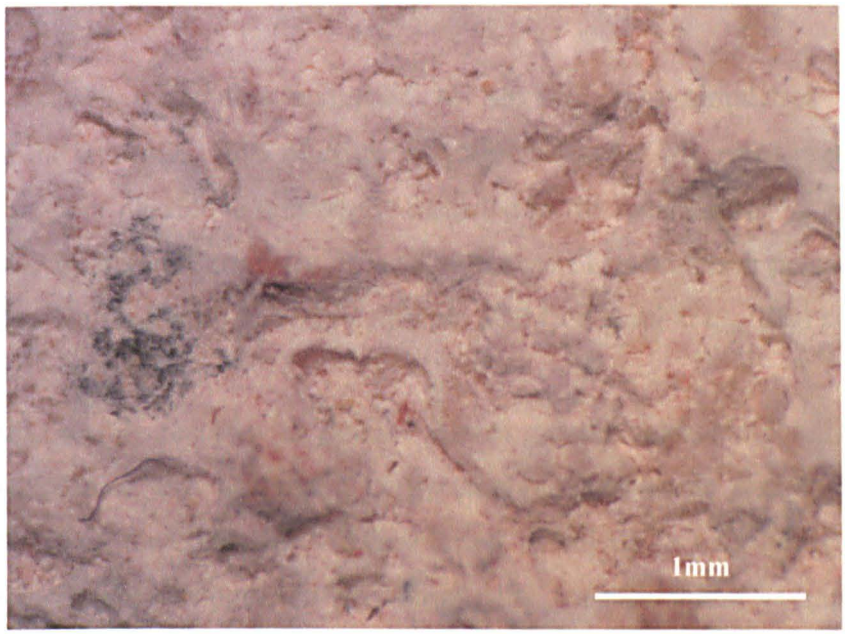

Figure 7.18: Precipitation of a rich layer of calcium hydroxide on the free surface of the specimen in contact with the cathode solution.

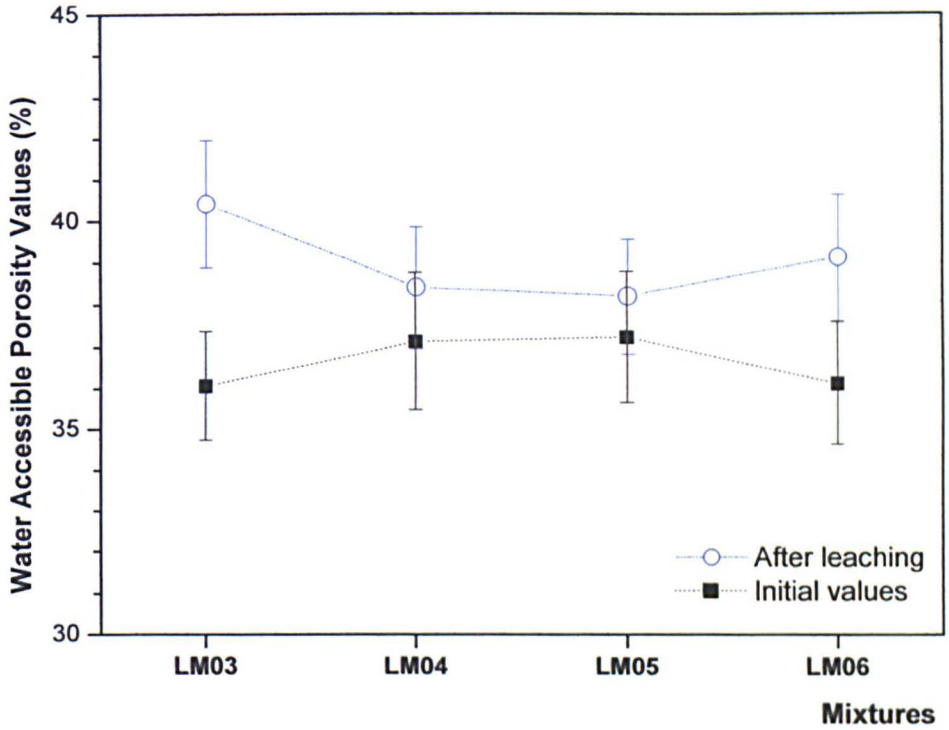

Figure 7.19: Porosity values (%) of the LM mixtures after electrochemically accelerated degradation test.

The LM mixtures were also subjected to an acid rain simulation test, which incorporated the controlled flow of dilute sulphuric acid (0.05M) over the surface of the specimens. Sulphur dioxide is universally regarded as the most damaging species in the atmospheric corrosion of carbonate materials because of its common presence in urban areas, together with its ability to form sulphuric acid (Sabbioni et al., 2001).

Sulphuric acid readily reacts with calcite to form gypsum. In static conditions (humid air), the precipitation and nucleation of gypsum on the calcitic surface is supported (Equation 7.9) and therefore, further dissolution of calcite is inhibited (Booth et al., 1997). Weathering experiments have shown that transformation is rapid and that gypsum formation can occur within a few days under normal atmospheric conditions (Wilkins et al., 2001).

$$CaCO_{3(s)} + H_2SO_{4(aq)} + 2H_2O_{(l)} \rightarrow CaSO_4 2H_2O_{(s)} + H_2CO_{3(aq)} \quad (7.9)$$

When the sulphuric solution flows over the surface of mortars, the dissolved ions (Equation 7.10) are removed by the run-off solution, and therefore the cementing material is weakened.

$$CaCO_{3(s)} + 2HSO^{-}_{4(aq)} \rightarrow Ca^{2+}_{(aq)} + 2SO^{2-}_{(4)(aq)} + H_2CO_{3(aq)} \qquad (7.10)$$

In the acid rain simulation test, a linear increase in the Ca^{2+} ions leached over time was observed. There was clear correlation between the amount of barium hydroxide present in the mortar, and the amount of both Ca^{2+}, and total ions, leached (Figure 7.20). The total amount of Ca^{2+} ions leached was gradually reduced by increasing the amount of barium hydroxide present in the mortar (Figures 7.20 and 7.21).

Figure 7.20 shows that the maximum quantity of Ca^{2+} leached from LM-03 is double, compared to sample LM-05. However, because in sample LM-05, 25% of lime has been replaced by barium hydroxide, values of mixture LM-03 should be multiplied by 0.75 in order to refer to the same amount of Ca. This results to a concentration of Ca^{2+} leached from mixture LM-03, 0.0013 moles/g, which is still 30% higher than LM-05 (0.0010 moles/g).

The quantity of Ca^{2+} leached from the mixtures in the initial stages appears higher than LM-03, because the addition of barium hydroxide introduces a coarser pore structure, which makes those samples more vulnerable to dissolution. Later, when mixtures reach equilibrium with the solution, the concentration of Ca^{2+} ions leached reflects only the solubility of the setting products and the rate of reactions. Therefore, in the first four hours of the experiment (Figure 7.21), mixtures with lower concentration of calcium provide the solution with higher amount of Ca^{2+} ions but, continuously, the total amount of Ca^{2+} ions leached was gradually reduced by increasing the amount of barium hydroxide present in the mortar.

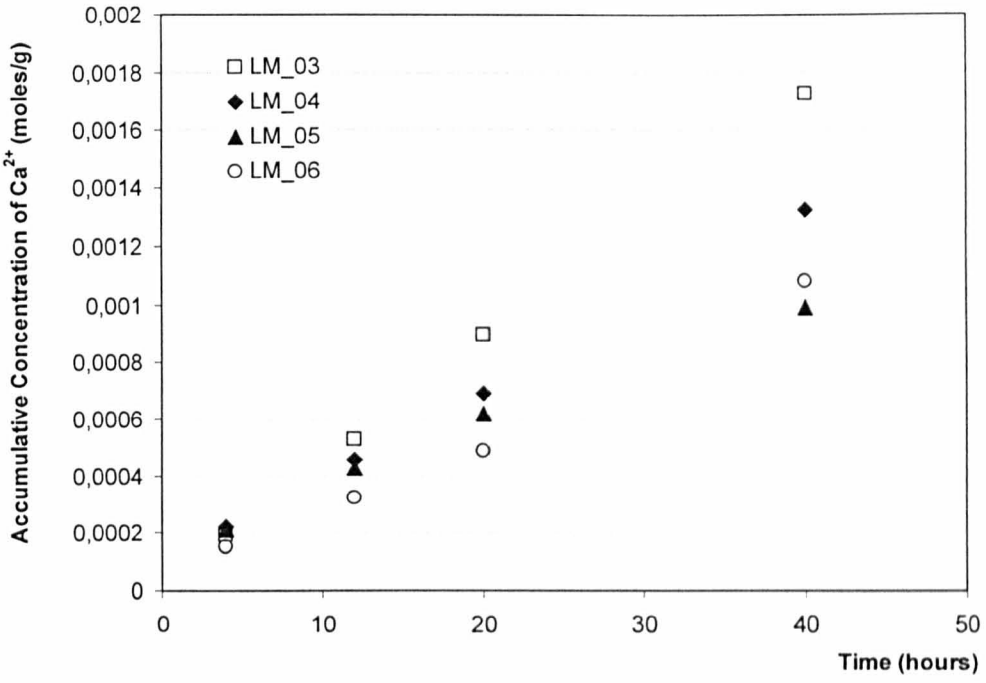

Figure 7.20: Accumulative concentration of calcium ions (moles/g of specimen) leached form the LM mixtures during acid rain simulation test.

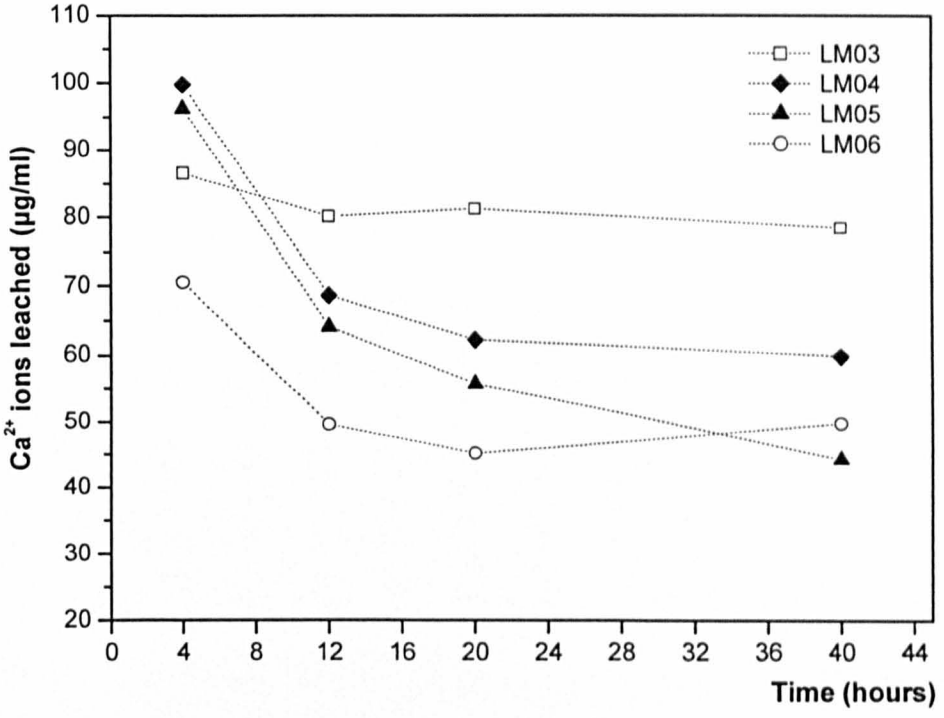

Figure 7.21: Concentration of calcium ions (µg/ml) leached form the LM mixtures during acid rain simulation test.

The reaction of barium carbonate with the sulphuric acid (Equation 7.11) leads to the precipitation of the insoluble barium sulphate.

$$BaCO_{3(s)} + HSO^{-}_{4(aq)} + H_2O_{(l)} \rightarrow BaSO_{4(s)} + HCO^{-}_{3(aq)} \qquad (7.11)$$

The precipitation of barium sulphate at the interface between the non-altered mortar mass and the gypsum layer, forms a barrier (Figure 7.22). This reduces the dissolution rate of the calcitic binder (Figure 7.21). Thus, the depth of the weathering/sulphated layer in the mortars with barium hydroxide gradually reduces, up to 50% (Figure 7.24) of that formed in the reference mixture (LM-03).

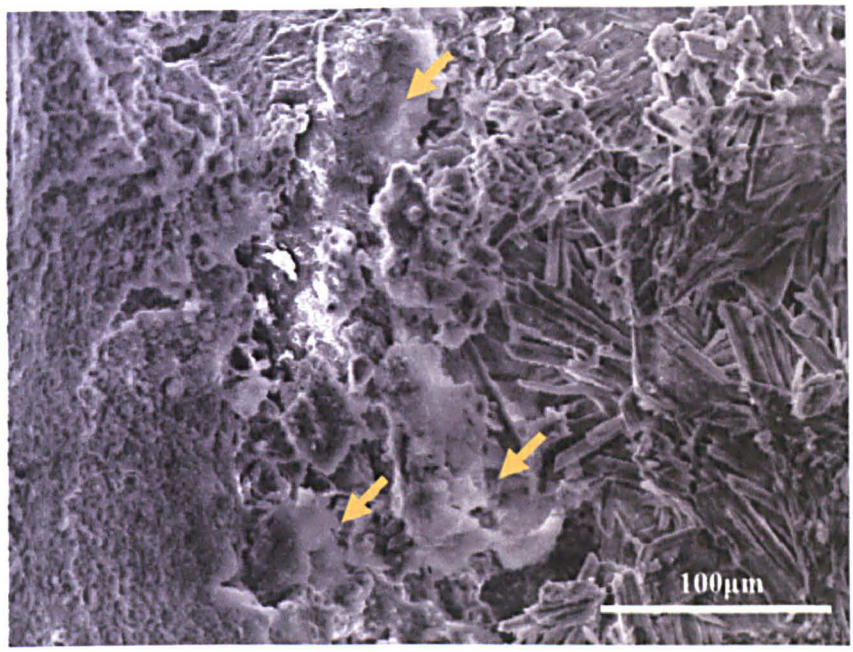

Figure 7.22: SEM photomicrograph of mixture LM-05 after the acid rain simulation test. The layer of barium sulphate ($BaSO_4$) between the altered and the non-affected mass (indicated by arrows) acts as a barrier and prevents further attack of the mortar body.

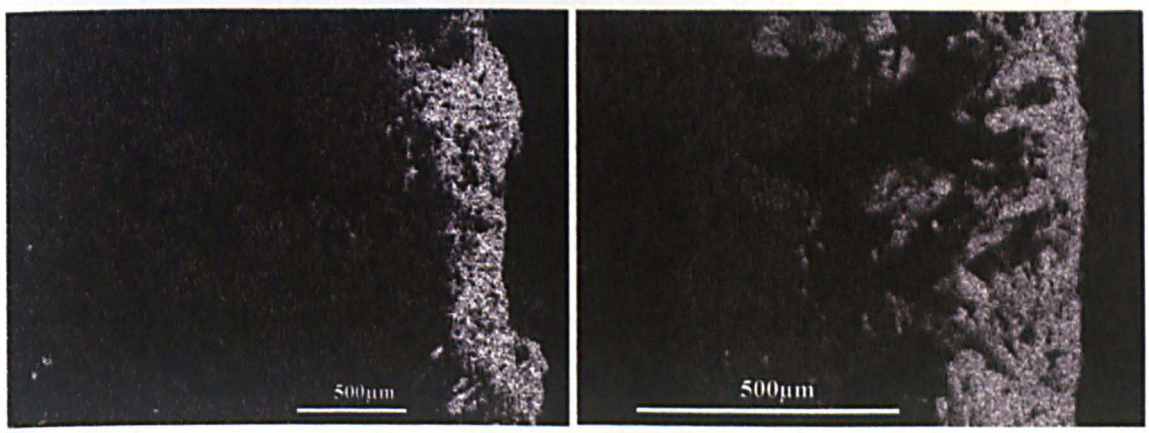

Figure 7.23: X-ray maps of S in mixtures LM-03 (left) and LM-05 (right). The depth of the sulphated layer in mixture LM-05 is half of the one formed in LM-03.

8 CONCLUSIONS AND RECOMMENDATIONS

The experimental procedure followed, and the interpretation of the results obtained, provided the required data for concluding on both the criteria and methodology for the development of new conservation mortars, as well as the effect that barium hydroxide has on their physicochemical properties. The conclusions of this research are presented in three parts, and recommendations for further development of the research are given.

8.1 SETTING PROCESS OF LM-MIXTURES

The setting and hardening of lime-based mortars that contain barium hydroxide (LM-04, LM-05) was described by the carbonation of both calcium hydroxide and barium hydroxide, the precipitation of calcite ($CaCO_3$) and witherite ($BaCO_3$), as well as the formation of a barium calcium carbonate [$BaCa(CO_3)_2$] solid solution. The solid solution existed in areas around calcitic grains of diameter below 100μm. The small grains acted as a nucleus for the formation of the solid solution and supported Ca^{2+} – Ba^{2+} exchange reactions. The areas examined were rich in barium carbonate close to the interface with the calcitic grains, and gradually decreased their concentration, leading to a low, constant, concentration in the lime-binder mass.

In mixture LM-06, where barium hydroxide was added as a saturated solution at 80°C, the setting process included an additional stage, the precipitation of barium hydroxide from the solution as cooling occurred. The crystals of the precipitated barium hydroxide were small and well distributed within the lime mass. After the solution reached constant temperature, the precipitation of barium calcium carbonate took place in the binder mass.

The addition of barium hydroxide saturated solution (mixture LM-06) resulted the formation of a coarse microstructure, which consist of an extensive network of cracks formed during setting. This network resulted in the faster evaporation of water vapours and reduced the rate of water absorption. Finally, the microstructure affected the mechanichal performance of samples under bending fatigue.

Mineralogical (XRD) and thermal analysis results showed that the carbonation of barium hydroxide is much faster than the carbonation of lime. The main peak of barium hydroxide [$Ba(OH)_2 \cdot 8H_2O$] disappeared after a setting period of three months. Consequently, since carbonates are less soluble than hydroxides, the amount of Ba^{2+} ions that could be potentially leached in the initial period of setting is reduced.

8.2 MICROSTRUCTURE AND MECHANICAL PROPERTIES

The addition of barium to the binary pastes was found to affect their microstructure, by forming a more coarse cementing material. Crystals with grain-size larger than 80μm diameter had not completely dissolved in the binder mass and, they acted as aggregates. As a result, they affected the granular distribution of mixtures and, therefore influenced the pore-space characteristics of the binder. However, this was a pure physical, and not chemical, effect, which was dependent upon the grain-size distribution of the barium hydroxide solid fraction used.

The main parameter that was modified was the pore-size distribution of the hardened LM-mixtures, while their total porosity values did not reveal any significant differences. Variations in the pore-size distributions, in comparison with the reference mixture (LM-03), proved to have a positive effect on the durability of the barium-mixtures (LM-04, LM-05 and LM-06).

The shift of the main peak of pore population from the area of 100nm to 1000nm had a side effect on the mechanical properties of the barium mixtures. In comparison to the

reference mixture LM-03, the compressive strength values were reduced: LM-05 exhibited the highest reduction (34%), followed by LM-04 (27%) and LM-06 (25%). However, their values are in between the range of typical lime mortars strength values.

Finally, the total surface area values of the barium-mixtures decreased significantly as the amount of barium hydroxide was increased, while the addition of barium hydroxide in the solid state resulted in a linear increase in vapour permeability.

The above microstructural characteristics found to add a benefit in the performance of barium mixtures against both, chemical and mechanical degradation caused by sulphates.

8.3 CHEMICAL STABILITY

The amount of barium ions that leached during the electrochemically accelerated leaching test was five times lower than that of calcium. This is attributed to the faster transformation of barium compounds to the carbonate form, which is less soluble than the remaining calcium hydroxide. Therefore, it was confirmed that the total amount of ions leached in the pore solutions primarily depends upon the chemical stability of the setting products and the water accessible pores (water absorption coefficient) of the mixtures.

8.4 DURABILITY AGAINST SULPHATES

The interpretation of both mechanical properties and crystallisation test results showed that the durability of the mortar mixture against crystallisation of sulphate salt depends upon the ratio of compressive strength to yield strength (F_c/F_y). The higher the ratio, the more durable the mixture.

The order of failure of the LM mixtures (LM06>LM05>LM04>LM03) during the crystallisation tests showed that the barium-mixtures were more durable. The enhanced

durability of the barium-mixtures against sodium sulphate crystallisation was supported by the partial fixation of sulphates, through the formation of insoluble barium sulphate. Therefore, the deterioration action of hydrous sodium sulphate salts, through their volume expansion, was partially eliminated. In addition, their coarser structure allowed the gradual relaxation of the pore pressure created during salt crystallisation.

In the acid rain simulation test, it was shown that the total amount of Ca^{2+} ions leached was gradually reduced by an increasing amount of barium hydroxide in the mortar. The protective action of the barium compounds was described by the precipitation of barium sulphate at the interface of the non-altered mass, which formed a barrier layer against further dissolution of the calcitic binder. Thus, the depth of the weathering/sulphated layer in the mixture that initially contained 25% of barium hydroxide (LM-05) was reduced to 50% of that formed in the reference mixture (LM-03).

8.5 PRACTICAL APPLICATION

No particular problems were faced during the preparation of the mortar mixtures. The trial application of the barium-mixtures in open air, as support layer for floor mosaics, did not reveal any disadvantages. Finally, all mixtures exhibited very similar colour and surface texture.

From all of the above, it is concluded that barium hydroxide can be used as an additive material in lime-based conservation mixtures, and therefore enhance their durability against sulphate attack. Barium carbonate and barium-calcium carbonate, which are the setting products formed, enhance the durability of the mixtures, either by fixing the sulphate ions, and therefore avoiding the expansion of their hydrous forms, or by forming a barrier layer of barium sulphate, which block the dissolution of the calcitic binder. The optimum quantity of barium hydroxide that can be added to the hydrated lime ranges from 25–30%, depending upon the grain-size distribution of the added material.

Finally, the addition of barium hydroxide during the mixing process of mortars has two main advantages:

1. as an additive material – it results in a homogeneous dispersion in the mortar mass and enhances sulphate resistance; and
2. as a consolidant – it modifies the microstructural properties of the surface layers and eventually supports differential weathering phenomena.

8.6 DEVELOPMENT OF CONSERVATION MORTARS

The main criteria for the development of new conservation mortars should be the raw materials, the texture, and the durability of the original composition. Moreover, the environmental setting of the building/monument, the deterioration parameters of the original mixtures, and how these have been modified today, should always be considered. Finally, the aim of the researchers must be focused on the performance requirements of the new mixture, according to its use and on how this could be achieved by using the same, or similar, raw materials, but modifying the properties, such as mix proportions, microstructure and strength. Compatibility, in terms of appearance, texture, raw materials, strength and microstructure should also be considered. However, the development and final selection of the conservation mortars must be based on the performance requirements initially stated.

Therefore, the study of original mortars is necessary to reveal information about the type of binder and aggregates used, the microstructure and strength level, and the degradation process of the original mixtures. The calculation of the exact mix proportions is not always possible, since chemical transformations occur during setting and weathering causes changes in microstructure. Therefore, more than one mixture should be prepared and tested, in order to choose the one that best fits the performance requirements.

In the above context, the most challenging issue concerning the development of conservation mortars is not to agree how many tests should be used for that purpose, but rather to define a minimum number of tests sufficient to characterise the mortars for the specific purpose.

The following procedure indicates a sequence of tasks that aim to contribute to the establishment of a standard procedure for the design, development and evaluation of conservation mortars. The proposed practice is divided into nine tasks:

1. sampling and characterisation of original mortars and other construction materials;
2. definition of the performance parameters, according to the function, environmental setting and deterioration agents;
3. selection of the raw materials and mix proportions for a set of mixtures;
4. study of fresh mixture properties;
5. study of hardened mixture properties;
6. evaluation of the durability of both mortar mixtures and original construction materials through laboratory tests;
7. interpretation of analytical/experimental data and optimisation of the mixtures;
8. in-field practical application and assessment of performance characteristics; and
9. application and long-term monitoring of the mixtures' performance.

8.7 RECOMMENDATIONS

The interpretation of the experimental results suggested that the durability of mortars against sulphates depends upon the type of sulphates, the chemical composition of the hardened mixtures, as well their pore-space characteristics. Therefore, further studies in this field should be focused on the effect of quantity and maximum grain-size of barium hydroxide on the pore-space characteristics of mortar mixtures, and on how this affects their leaching behavior.

Considering the deterioration mechanisms of barium mortars in sulphate environments, future research projects must study the behavior of barium-mortars in dry deposition processes and the weathering phenomena that take place on the surface of mortars. Moreover, the monitoring of the leaching process and acid-rain simulation tests for longer time period, both in laboratory and on-site, could provide a more accurate prediction of the service life and durability of these mortars.

Mercury and nitrogen porosimetry, total conductivity and pH measurements, along with element concentration analysis (AAS, ICP) may provide further data on the study of deterioration mechanisms.

In the field of deterioration mechanisms, additional work should be done on the study of pore-space characteristics and mechanical properties of mortars after acid attack and electrochemically accelerated tests. Image analysis may be used for evaluating the profile of pore-size distributions from the external surface to the core of the mortar specimens, while point-loading tests could provide information on strength characteristics. Experimental data from these fields could provide information on the performance and service life of both traditional and barium-mixtures, after the initiation of degradation phenomena.

Regarding the chemical stability of setting products, the influence of calcium carbonate powder on the formation of the barium-calcium solid solution, as well as the development of carbonate phases, are two areas of research interest.

Finally, the comparison of mixtures containing barium carbonate instead of barium hydroxide as additive material could serve as an alternative for studying the durability of new mixtures against sulphates.

REFERENCES

Adams, J., Dollimore, D., Griffiths, D.L. (1998). 'Thermal analytical investigation of unaltered $Ca(OH)_2$ in dated mortars and plasters', *Thermochimica Acta*, 324, pp. 67-76.

Adenot, F., Buil, M. (1992). 'Modelling the corrosion of the cement paste by deionized water', *Cement and Concrete Research*, 22, pp. 489-496.

Alessandrini, G., Bugini, R., Folli, L., Realini, M. and Toniolo, L. (1992). 'The compositional ratios of mortars. Comparison between chemical and petrographical methods', in: J.D., Henriques, F., Telmo Jeremias, F. (Eds), *7th International Congress on Deterioration and Conservation of Stone*, 15–18 June, Lisbon, Portugal, pp. 667–675.

Allen G., Allen, J., Elton, N., Farey, M., Holmes, S., Livesey, P., Radonjic, M. (2003). *Hydraulic Lime Mortar for Stone, Brick and Block Masonry*, Donhead, Dorset, UK.

Alvarez, J.I., Martin, A., Garcia Casado, P.J., Navarro, I., Zornoza, A. (1999). 'Methodology and validation of a hot hydrochloric acid attack for the characterization of ancient mortas', *Cement and Concrete Research*, 29, pp. 1061-1065.

Alvarez, J.I., Navarro, I., Garcia Casado, P.J. (2000a). 'Thermal, mineralogical and chemical studies of the mortars used in the cathedral of Pamplona (Spain)', *Thermochimica Acta*, 365, pp. 177-187.

Alvarez, J.I., Navarro, I., Martin, A., Garcia Casado, P.J. (2000b). 'A study of the ancient mortars in the north tower of Pampona's San Cernin church', *Cement and Concrete Research*, 30, pp. 1413-1419.

Ambrosi, M., Baglioni, P., David, P.R., Dei, L., Giorgi, R., Lalli, C., Lanterna, G., Mairani, A., Matteini, M., Rizzi, M., Schonhaut, G. (2000). 'Inorganic consolidants and protectives for architectonic surfaces: experimental tests on Santa Prisca church apse in Rome', in: Guarino, A. (Ed.), *Science and Technology for the Safeguard of Cultural*

Heritage in the Mediterranean Basin, proceedings of the 2nd International Congress, Paris, 5-9 July 1999, Elsevier, Amsterdam, pp. 855-858.

Amoroso, G., Fassina, V. (1983a). 'The abudance, sources and sinks of the most important air pollutants responsible for the deterioration processes in stone', in *Stone Decay and Conservation*, 1st ed., Elsevier, Amsterdam, pp. 54-110.

Amoroso, G., Fassina, V. (1983b). 'The oxidation of sulphur dioxide', in *Stone Decay and Conservation*, 1st ed., Elsevier, Amsterdam, pp. 177-221.

Anzani, A., Baronio, G., Binda, L. (1998). 'Multiple leaf stone masonry as a composite: the role of materials on its behaviour and repair', in: Moropoulou, A., Biscontin, G., Rodrigues, J.D., Erdik, M. (Eds), *Compatible Materials for the Protection of European Cultural Heritage, PACT*, 55, 1, Technical Chamber of Greece, pp. 177-212.

Arandigoyen, M., Perez Bernal, J.L., Bello Lopez, M.A., Alvarez, J.I. (2005). 'Lime-pastes with different kneading water: Pore structure and capillary porosity', *Applied Surface Science* (in press).

Ashurst, J. (1983). *Mortars, Plasters and Renders in Conservation: A Basic Guide*, Ecclesiastical Architect's and Surveyor's Association, London.

Ashurst, J. (1990). 'Mortars for stone buildings', in *Conservation of Building and Decorative Arts*, Vol. 2, Ashurst, J., Dimes, F.G. (Eds), Butterwoths, London, pp. 78-96.

Ashurst, J., Ashurst, N. (1988). *Practical Building Conservation, Volume 3: Mortars Plasters and Renders* , English Heritage Technical Handbook, Gower Technical Press, Hants.

Assimakopoulou-Atzaka, P. (1987). *Syntagma ton Palaiochristanikon Psifidoton Dapedon tis Ellados II, Pelloponisos – Sterea Ellada (Mosaic Pavements from the*

Early-Christian Period in the Hellenic Era II, Peloponnesus – Central Greece). Byzantine Research Centre, Thessaloniki.

Atkins, P.W. (1994). *Physical Chemistry*, Oxford University Press, Oxford.

Baer, N.S. (1982). *Conservation Historic Stone Buildings and Monuments*, National Academy Press, Washington.

Baer, N.S., Sabbioni, C., Sors, A. (Eds) (1991). *Science, Technology and European Cultural Heritage,* proceedings of the European symposium, 13–16 June 1989, Bologna, Italy, Butterworth-Heinemann, Oxford.

Bagel, L., Zivica, V. (1997). 'Relationship between pore structure and permeability of hardened cement mortars: On the choice of effective pore structure parameter', *Cement and Concrete Research*, 27, 8, pp. 1225-1235.

Baglioni P., Rodorico G., Chen Ch.-ch. (2004). 'Nanoparticle technology saves cultural relics: potential for a multimedia digital library', URL: http://memorynet.org/pdf/ baglioni_crete.pdf, (accessed on February 2004).

Bakolas, A., Biscontin, G. Moropoulou, A., Zendri, E. (1998). 'Characterization of structural byzantine mortars by thermogravimetric analysis', *Thermochimica Acta*, 321, pp. 151-160.

Baronio, G., Binda, L., Lombardini, N. (1997). 'The role of brick pebbles and dust in conglomerates based on hydrated lime and crushed bricks', *Construction and Building Materials*, Vol. 11, No. 1, pp. 33-40.

Barsottelli, M., Fratini, F., Giovannini, P., Manganelli, Del Fa C. (1998). 'Transport of fluids in the plaster-masonry system', in: Moropoulou, A., Biscontin, G., Rodrigues, J.D., Erdik, M. (Eds), *Compatible materials for the protection of monuments*, Raphael-COMARECH conference, 15-16 December, Athens, PACT 55, pp. 127–137.

Bell, F.G. (2000). *Engineering Properties of Soils and Rocks*, Blackwell Science, Oxford.

Binda, L., Baronio, G. (1988) 'Survey of brick/binder adhesion in powdered brick, mortars and plasters', *Masonry International Journal*, 2, 3, pp. 87-92.

Binda, L., Baronio, G., Tedeschi, C. (2000). 'Experimental study on the mechanical role of thick mortar joints in reproduced Byzantine masonry', in: Bartos, P., Groot, C., Hughes, J.J. (Eds), *Historic Mortars: Characteristics and Tests*, proceedings of the international RILEM workshop, 12-14 May 1989, Paisley, Scotland, RILEM Publications S.A.R.L., pp. 95-104.

Biscontin, G., Pianna, M., Riva, G. (1981). 'Research on limes and intonacoes of the historical Venetian architecture', in: *Mortars, Cements and Grouts Used in the Conservation of Historic Buildings*, proceedings of the ICCROM Symposium, 3-6 November, Rome, pp. 359-374.

Blanco, M.T., Puertas, F., Palomo, A., Gomez, F. (1989). 'Alteretion of mortars, grouts and plasters in Toledo's cathedral due to humidity', in: *Science, Technology and European Cultural Heritage*, proceedings of the European symposium, 13-16 June, Bologna, Italy, pp. 951-955.

Bland, W., Rolls, D. (1998). *Weathering, an Introduction to the Scientific Principles*, Arnold, London.

Blauer Bohn, C. (2000). 'Analysis of mortars containing pozzolanas', in: Bartos, P., Groot, C., Hughes, J.J. (Eds), *Historic Mortars: Characteristics and Tests*, proceedings of the international RILEM workshop, 12-14 May 1989, Paisley, Scotland, RILEM Publications S.A.R.L., pp. 105-112.

Bokan-Bosiljokov, V. (2001). 'The use of lime mortars for sustainable restoration of ancient buildings', in: Bischoff P.H., Dawe J.L., Schriver A.B., Valsangkar A.J. (Eds),

9th Canadian Masonry Symposium-'Spanning the Centuries with Masonry', proceedings, 4-6 June, Fredericton, New Brunswick, URL: http://www.nrc.ca/irc/fulltext/mortar/, (accessed on September 2003).

Booth, J., Hong, Q., Compton, R.G., Prout, K., Payne, R. M. (1997). 'Gypsum Overgrowths Passivate Calcite to Acid Attack', *Journal of Colloid and Interface Science*, 192, pp. 207-214.

Bouineau, A., Alva, A., Beck, B., Holmstron, I., von Jessen, C., Malliet, J., Massari, I., Mora, P., Peterson, S., Rocard, J., Rossi Doria, P., Sandin, K., van der Scuit, P., Toraca, G., Twilley, J. (1981). 'Working group for the study of mortars and grouts for the conservation of ancient masonry', in: *Mortars, Cements and Grouts Used in the Conservation of Historic Buildings*, proceedings of the ICCROM Symposium, 3-6 November, Rome, pp. 412-414.

Boynton, R.S. (1966). *Chemistry and Technology of Lime and Limestone*, Wiley, New York.

Branda F., Costantini A., Luciani G., Piccioli C. (2000). 'A note on incrustations on a mosaic floor fragment from Punta Epitaffio in Baia', *Studies in Conservation*, 45, pp. 211–13.

Brimblecombe, P., Sabbioni, Cr. (2002). 'Air Pollution Effects on Cultural Heritage Materials in the Context of New Trends emerging from various EC Directives, Instruments, Policies and Standards', Technical Notes of the European Commission Advanced Study Course: "*Science and Technology of the Environment for Sustainable Protection of Cultural Heritage*", Sessions 1-3, 8-19 April, UCL Centre for Sustainable Heritage, London, pp.1-10.

Bromblet, Ph. (2000). 'Properties and durability of air lime-based mortars for limestone repairs on monuments', in: Bartos, P., Groot, C., Hughes, J.J. (Eds), *Historic Mortars:*

Characteristics and Tests, proceedings of the international RILEM workshop, 12-14 May 1989, Paisley, Scotland, RILEM Publications S.A.R.L., pp. 327-338.

Brown, P.W., Clifton, J.R. (1988). 'Mechanism of deterioration in cement-based materials and in lime mortar', *Durability of Building Materials*, 5, pp. 409-420.

BS 1199-1200 (1976). *Specifications for Building sands from natural sources*, British Standard Institution.

BS 1881-121 (1983). *Testing concrete – Part 121: Method for determination of static modulus of elasticity in compression*, British Standard Institution.

BS 4551 (1998a). *Methods of testing mortars, screeds and plasters - Part 1: Physical testing*, British Standard Institution.

BS 4551 (1998b). '*Methods of testing mortars, screeds and plasters - Part 2: Chemical analysis and aggregate grading*, British Standard Institution.

BS 890 (1995). *Specification for building limes*, British Standard Institution.

BS EN 1015-11 (1999). *Methods of test for mortar for masonry — Part 11: Determination of flexural and compressive strength of hardened mortar*, British Standard Institution.

BS EN 1015-18 (2002). *Methods of test for mortar for masonry – Part 18: Determination of water absorption coefficient due to capillary action of hardened mortar*, British Standard Institution.

BS EN 1015-19 (1999). *Methods of test for mortar for masonry – Part 19: Determination of water vapour permeability of hardened rendering and plastering mortars*, British Standard Institution..

BS EN 1015-3 (1999). *Methods of test for mortar for masonry – Part 3: Determination of consistence of fresh mortar (by flow test)*, British Standard Institution.

BS EN 12370 (1999). *Natural stone test methods – Determination of resistance to salt crystallization*, British Standard Institution.

BS EN 1925 (1999). *Natural stone test methods – Determination of water absorption coefficient by capillarity*, British Standard Institution.

BS EN 1936 (1999). *Natural stone test methods – Determination of real density and apparent density, and of total and open porosity*, British Standard Institution.

BS EN 196-1 (1995). *Methods of testing cement - Part 1: Determination of strength*, British Standard Institution.

BS EN 4551-1 (1998). *Methods of testing mortars, screeds and plasters – Part 1: Physical testing*, British Standard Institution.

BS EN 459-1 (2001). *Building lime - Part 1: Definitions, specifications and conformity criteria*, British Standard Institution.

BS EN 459-2 (2001). *Building lime - Part 2: Test methods*, British Standard Institution.

BS EN 459-3 (2001). *Building lime - Part 3: Conformity evaluation*, British Standard Institution.

Building Effects Review Group Report (BERG) (1989). *The Effects of Acid Rain Deposition on Building Materials in the United Kingdom*, HMSO, London.

Camuffo, D. (1992). 'Acid-rain and deterioration of monuments - How old is the phenomenon', *Atmospheric Environment Part B-Urban Atmosphere*, 26, 2, pp. 241-247

Carde Chr., Francois R. (1997). 'Effect of ITZ leaching on durability of cement-based materials'. *Cement and Concrete Research,* 27, 7, pp. 971-978.

Carde, C., Francois, R., Torrenti, J.M. (1996). 'Leaching of both calcium hydroxide and C-S-H from cement paste: modelling the mechanical behavior', *Cement and Concrete Research*, 26, 8, pp. 1257-1268.

Cassar, M., Brimblecombe, P., Nixon, T., Price, C., Sabbioni, C., Sain-Jimezez, C., Van Balen, K. (2004). 'Sustainable solutions in the conservation and protection of historic monuments and archaeological remains: a critical assessment of European research needs', in Sain-Jimenez, C. (Ed), *Air Pollution and Cultural Heritage*, proceedings of the international workshop, 1-3 December, Seville, pp. 249-262.

Catinaud, S., Beaudoin, J.J., Marchand, J. (2000). 'Influence of limestone addition on calcium leaching mechanisms in cement-based materials', *Cement and Concrete Research*, 30, pp.1961-1968.

Cazalla, O., Rodriguez-Navarro, C., Sebastian, E., Cultrone, G., De la Torre, M.J. (2000). 'Aging of lime putty: effects on traditional lime mortar carbonation', *Journal of American Ceramics Society,* 83, 5, pp. 1070-1076.

Charola, A.E., Henriques, F.M.A. (1999), 'Hydraulicity of in lime mortars revisited', in: Bartos, P., Groot, C., Hughes, J.J. (Eds), *Historic Mortars: Characteristics and Tests*, proceedings of the international RILEM workshop, 12-14 May 1989, Paisley, Scotland, RILEM Publications S.A.R.L., pp. 95-104.

Charola, E., Henriques, F. (1998). 'Lime mortars: some considerations on testing standarization', in: McClung, R.C. (Ed), *Use of and Need for Preservation Standards in Architectural Conservation,* ASTM STP 1355, American Society for Testing Materials, West Conshohocken, pp. 142-151.

Charola, E.; Rodrigues, P.; McGhie, A.; Henriques, F. (2004). 'Pozzolanic components in lime mortars: correlating behaviour, composition and microstructure', in: *6th International Symposium on the Conservation of Monuments in the Mediterranean Basin*, conference proceedings, 7-10 April, Lisbon, pp. 403-407.

Charola, E.A., Dupas, M., Sheryll, R.P. and Freund, G.G. (1986). 'Characterisation of ancient mortars: chemical and instrumental methods', in: *Scientific Methodologies Applied to the Works of Art*, proceedings of the symposium, 2–5 May 1984, Florence, Italy, pp. 28–33.

Chiari, G., Santarelli, M.L., Toracca, G. (1992). 'Charatterizzazione delle malte antiche mediante; l' analisi di campioni non frazionati', *Materials and Structures*, 3, pp. 111–37.

Chiari, G., Torraca, G., Santarelli, M.J. (1996). 'Recomendations for systematic instrumental analysis of ancient mortars: The Italian experience', in: Kelley, Stephen, J. (Ed), *Standards for Preservation and Rehabilitation*, ASTM STP 1258, West Conshohocken, pp. 275-284.

Christaras, B. (1998). 'Non-destructive methods used for the estimation of the damage (weathering and cracks) of the building and ornamental stones', in: Moropoulou, A., Biscontin, G., Rodrigues, J.D., Erdik, M. (Eds), *Compatible Materials for the Protection of European Cultural Heritage, PACT*, 55, 1, Technical Chamber of Greece, pp. 213-220.

Church A.H. (1862). 'Stone, Preserving and Colouring; Cements', *British Patent 220*, 28 January.

Church A.H. (1904). 'Treatment of Decayed Stone-work in the Chapter House, Westminster Abbey', *Journal of the Society of Chemical Industry*, 23, pp. 824.

Clifton R.J., Frohnsdorff G.J.C. (1982). 'Stone consolidating materials: a status report', in *Conservation of Historic Stone Buildings and Monuments: Report on the Committee*

on Conservation of Historic Stone Buildings and Monuments, National Materials Advisory Board, Commission on Engineering and Testing Systems, National Research Council, National Academy Press, Washington DC, pp. 287-311.

Cliver, E.B. (1974). 'Tests for Analysis of Mortar Samples', *Association of Preservation Technology (APT) Bulletin*, VI, 1, pp. 68–73.

Cohen, M.D., Mather, B. (1991). 'Sulfate attack on concrete Research needs', *ACI Materials Journal,* 88, 1, pp. 62–69.

Cole, W. Kroone, B. (1960). 'Carbon dioxide in hydrated Portland cement', *American Concrete Institute Journal*, 31, 12, pp. 1275-1295.

Collepardi, M. (1990). 'Degradation and restoration of masonry walls of historical buildings', *Materials and Structures*, 23, pp. 81-102.

COMPASS (2001). *Compatibility of Plasters and Renders with Salt loaded Substrates in Historic Buildings*. Project funded by the European Commission, Fifth Research Technology and Development (RTD) Framework Programme 'Energy Environment and Sustainable Development (EESD)', Reference: EVK4-CT-2001-00047, URL: http://www.cordis.lu/eesd/home.html, (accessed on: April 2005).

Conophagos, C. (1982). 'Concrete and plaster waterproofing in ancient Laurion', in: *Early Pyrotechnology. The Evolution of the First Fire-Using Industries*, Wertime, T.A., Wertime, S.F. (Eds), Smithsonian Institution Press, pp. 117-123.

CORDIS. (2000). *Energy Environment and Sustainable Development (EESD) projects funded by the European Commission.* URL: http://www.cordis.lu/eesd/home.html (accessed on: September 2004).

Corfield, M. (1996). 'Preventive conservation for archaeological sites', in: Roy, A., Smith, P. (Eds), *Archaeological Conservation and its Consequences*, proceedings of the IIC conference, Copenhagen, 26-30 August, pp. 32-37.

Cowper, A.D. (1927). *Lime and Lime Mortars*, Building Research Special Report 9, Her Majesty's Building Research Stationary Office, London, U.K..

Crystallographica Search-Match Software, Version 2.1.1.1, Oxford Cryosystems 1996-2003, available at: www.crystallographica.co.uk

Cultrone, G., Sebastian, T.E., Ortega Huertas, M. (2005). 'Forced and natural carbonation of lime-based mortars with and without additives: Mineralogical and textural changes', *Cement and Concrete Research*, (in press).

da Silva, C.A.R., Reis, R.J.P., Lameiras, F.S., Vasconcelos, W.L. (2002). 'Carbonation-related microstructural changes in long-term durability concrete', *Materials Research*, 5, 3, pp. 287-293.

Deer W.A., Howie R.A., Zussman J. (1996). *An introduction to the rock-forming minerals*, 2nd ed., Pearson Education, Essex.

Degryse, P., Elsen, J., Waelkens, M. (2002). 'Study of ancient mortars from Salassos (Turkey) in view of their conservation', *Cement and Concrete Research*, 32, pp. 1457-1563.

Dei L., Ahle A., Baglioni P., Dini D., Ferroni E. (1997). 'Green degradation products of azurite in wall paintings: identification and conservation treatment', *Studies in Conservation*, 43, pp. 80-88.

Delagrave, A., Gerard, B., Marchand, J. (1997). 'Modeling calcium leaching mechanisms in hydrated cement pastes', in: *Mechanisms of Chemical Degradation of Cement-Based Systems*, E & FN Spon, London, UK, pp. 38-47.

Delalieux, F., Cardell, C., Todorov, V., Dekov, V., Van Grieken, R. (2001). 'Environmental conditions controlling the chemical weathering of the Madara Horseman monument, NE Bulgaria', *Journal of Cultural Heritage*, 2, pp. 43-54.

Dennstedt M. (1884). 'Stone, Preserving and Colouring; Cements', *British Patent 13, 761*, 17 October.

Dheilly, R.M., Tudo, J., Sebaibi, Y., Queneudec, M. (2002). 'Influence of storage conditions on the carbonation of powdered $Ca(OH)_2$', *Construction and Building Materials*, 16, pp. 155-161.

DiBello, M.P., Manganaro, L.J., Aguinaro, E. (1992). "Barium compounds", *Encyclopedia of Chemical Technology*, Wiley and Sons Pub., 3rd Ed., Vol. 3, pp 909 – 931.

Dix, B. (1982). 'The manufacture of lime and its uses in the western Roman provinces', *Oxford Journal of Archaeology*, 1, 3, pp. 331-345.

Doganis, I., Galanos, A., Theoulakis, P., Karatasios, I., Kilikoglou, V. (2003). 'Study of renders and pigments from the Classical temple of Zeus in Nemea, Greece", in: *4th Symposium on Archaeometry of the Hellenic Society of Archaeometry*, Athens 28-31 May (in press).

Dubovoy, V.S., Ribar, J.W. (1990). *Masonry Cement Mortars-A Laboratory Investigation*, Portland Cement Association (PCA), Research and Development Bulletin RD095T, Skokie, USA.

Dunbabin, K.M.D. (1999). *Mosaics of the Greek and Roman World*, Cambridge University Press, Cambridge, pp. 269-290.

Elert, K., Rodriguez-Navarro, C., Pardo, E.S., Hansen, E., Cazalla, O. (2002). 'Lime mortars for the conservation of historic buildings', *Studies in Conservation*, 47, pp. 62-75.

Elert, K., Rodriguez-Navarro, C., Pardo, E.S., Hansen, E., Cazalla, O. (2000). 'Lime mortars for the conservation of historic buildings', *Studies in Conservation*, 47, pp. 62-75.

Elsen, J., Degryse, P., Waelkens, M. (2001). 'Mineralogical and petrographical study of ancient mortars from Sagalassos in view of their conservation', in: Stamatakis, M., Georgali, B., Fragoulis, D. Toumbakari, E.E. (Eds), *8th Euroseminar on Microscopy Applied to Building Materials*, proceedings, 4-7 September, Athens, Greece, pp. 331-337.

English Heritage (2003). *Heritage Counts 2003. The State of England's Historic Environment*, URL: http://www.english-heritage.org.uk/heritagecounts/default.htm, (accessed on: September 2004).

EUROPA (2004). URL: http://europa.eu.int/comm/environment/air/ambient.htm#2 (accessed on: September 2004).

European Materials Research Society (EMRS) Spring Meeting Symposium (1994), 24 - 27 May, Strasbourg, France.

European Parliament (2001). *Technological Requirements for Solutions in the Conservation and Protection of Historic Monuments and Archaeological Remains*, Cassar M. (Ed.), Directorate-General for Research, Directorate A, STOA Programme.

Fassina, V., Favaro, M., Naccari, A., Pigo, M. (2002). 'Evaluation of compatibility and durability of a hydraulic lime-based plaster applied on brick wall masonry of historical buildings affected by rising damp phenomena', *Journal of Cultural Heritage*, 3, pp. 45-51.

Fassina, V., Favaro, M., Naccari, A., Pigo, M. (2002). 'Evaluation of compatibility of hydraulic lime-based plaster applied on brick wall masonry of historical buildings affected by rising damp phenomena', *Journal of Cultural Heritage*, 3, pp. 45-51.

Faucon, P., Gerard, B., Jacquinot, J.F., March, J. (1998). 'Water attack of cement paste: Towards an improved accelerated test?'. *Advanced Cement Research*, 10, pp. 67-73.

Ferroni E., Dini D. (1981). 'Chemical-structural conservation of sulphatized marbles', in: *The Conservation of Stone II*, preprints of the Bologna international symposium, Bologna, 27 – 30 October, pp. 559-566.

Fischer, K. (2000). 'Traditional craftsmanship in modern mortars – Does it work in practice?', in: Bartos, P., Groot, C., Hughes, J.J. (Eds), *Historic Mortars: Characteristics and Tests*, proceedings of the international RILEM workshop, 12-14 May 1989, Paisley, Scotland, RILEM Publications S.A.R.L., pp. 281-286

Fitzner, B. (1993). 'Porosity properties and weathering behaviour of natural stones – Methodology and examples', in: Adda, M. (Ed), *Stone Material in Monuments: Diagnosis and Conservation*, Second Course, Heraklion-Crete, 24-30 May, pp. 43-54.

Flatt, R.J. (2002). 'Salt damage in porous materials: how high supersaturations are generated', *Journal of Crystal Growth*, 242, pp. 435-454.

Franzini, M., Leoni, L., Lezzerini, M. (2000). 'A procedure for determining the chemical composition of binder and aggregate in ancient mortars: its application to moratrs from some medieval buildings in Pisa', *Journal of Cultural Heritage*, 1, pp. 365-373.

Frohnsdorff, G., Masters, L.W. (1980). 'The meaning of durability and durability prediction', *Durability of Building Materials and Components*, Sereda, P.J., Litvan, G.G. (Eds), American Society for Testing and Materials, ASTM STP 691, pp. 17-30.

Ftikos, Chr., Kalos, M. (1985). *Odigies gia ti syntaxi prodiagrafon gia koniamata (Directives for Standards Concerning Mortars)*, Technical Chamber of Greece, Scientific Committee for Building Materials, Athens.

Furlan, V., (1991). 'Causes, Mechanisms and Measurement of Damage to Mortars, Bricks and Renderings', in: Baer, N.S., Sabbioni, C., Sors, A.I. (Eds.), *Science, Technology and European Cultural Heritage*, proceedings of the European symposium, 13–16 June 1989, Bologna, Italy, Butterworth-Heinemann, Oxford, pp. 149-159.

Getty Conservation Institute (2003). *Preservation of lime mortars and plasters, Project Bibliographies Series*, Hansen E.F., Van Balen K., Elert K., Rodriguez-Navarro C., Simon S. (Eds), Los Angeles, URL: http://www.getty.edu/conservation/resources/ bibs, (assessed on: June 2003).

Goins, E. (2000). 'A new protocol for the analysis of historic cementitious materials: Interim Report', in: Bartos, P., Groot, C., Hughes, J.J. (Eds), *Historic Mortars: Characteristics and Tests*, proceedings of the international RILEM workshop, 12-14 May 1989, Paisley, Scotland, RILEM Publications S.A.R.L., pp. 71-79.

Goncalves, T.D. (1998). 'Compatible renders for the conservation of ancient buildings', in: Moropoulou, A., Biscontin, G., Rodrigues, J.D., Erdik, M. (Eds), *Compatible materials for the protection of monuments*, Raphael-COMARECH conference, 15-16 December, Athens, PACT 55, pp. 29-38.

Goodwin, J.F., West, W.H. (1982). 'A Review of the literature on brick-mortar bond', in: *Proceedings of the British Ceramic Society*, 30, 23, pp. 23-37.

Goual, M.S., de Barquin, F., Benmaled, M.L., Bali, A., Queneudec, M. (2000). 'Estimation of the capillary transport coefficient of Clayey Aerated Concrete using a gravimetric technique', *Cement and Concrete Research*, 30, pp. 1559-1563.

Gourdin, W.H., Kingery, W.D. (1975). 'The beginnings of pyrotechnology: Neolithic and Egyptian Lime Plaster', *Journal of Field Archaeology*, 2, pp. 133-150.

Gregerova, M., Pospisil, P. (2001). 'Microscopic methods applied to study of historical mortars and plasters', in: Stamatakis, M., Georgali, B., Fragoulis, D. Toumbakari, E.E. (Eds), *8th Euroseminar on Microscopy Applied to Building Materials*, proceedings, 4-7 September, Athens, Greece, pp. 353-357.

Gregerova, M., Pospisil, P. (2001). 'Microscopic methods applied to study of historical mortars and plasters'in: Stamatakis, M., Georgali, B., Fragoulis, D. Toumbakari, E.E. (Eds), *8th Euroseminar on Microscopy Applied to Building Materials*, proceedings, 4-7 September, Athens, Greece, pp. 353-357.

Groot, C.J.W.P. (1997). 'The Characteristics of Brick and Mortar Considering Mortar/Brick Bond', in: Wu, M., Qian, Y. (Eds), *11th International Brick/Block Masonry Conference*, proceedings, Engineering Construction Standardization (ECS), Shanghai, China, pp. 51-58.

Groot, C.J.W.P., Bartos, P.J.M., Hughes, J.J. (2000). 'Historic Mortars: Characteristics and Tests-Concluding summary and state-of-the-art', in: Bartos, P., Groot, C., Hughes, J.J. (Eds), *Historic Mortars: Characteristics and Tests*, proceedings of the international RILEM workshop, 12-14 May 1989, Paisley, Scotland, RILEM Publications S.A.R.L., pp. 443-454.

Hansen E., Doehne E., Fidler J., Larson J., Martin B., Matteini M., Rodriguez-Navarro C., Pardo E.S., Price C., de Tagle A., Teutonico J.M. and Weiss N. (2003). 'A review of selected inorganic consolidants and protective treatments for porous calcareous materials', *Reviews in Conservation*, 4, pp. 13-25.

Harries, K.A. (1995). 'Concrete construction in early Rome', *Concrete International*, 17, 1, pp. 58-62.

Hayen, R. van Balen, K. van Gemert, D. (2001). 'The influence of production processes and mortar compositions on the properties of historical mortars', in: Bischoff P.H., Dawe J.L., Schriver A.B., Valsangkar A.J. (Eds), *9th Canadian Masonry Symposium- 'Spanning the Centuries with Masonry'*, proceedings, 4-6 June, Fredericton, New Brunswick, URL: http://www.nrc.ca/irc/fulltext/mortar/, (accessed on September 2003).

He, Ch., Osbaeck, B., Makovicky, E. (1995). 'Pozzolanic reactions of six principal clay minerals: Activation, reactivity, assessments and technological effects', *Cement and Concrete Research*, 25, 8, pp. 1691-1702.

Heaton N. (1921). The Preservation of Stone, *Journal of the Royal Society of Arts*, 70, pp. 129-139.

Heikal, M., El-Didamony, M.H., Morsy, M.S. (2000). 'Limestone-filled pozzolanic cement', *Cement and Concrete Research*, 30, pp. 1827-1834.

Hendry, A.W. (2001). 'Masonry walls: materials and construction', *Construction and Building Materials*, 15, pp. 323-330.

Henriques, F., Rato, V., Charola, E. (2004). 'The Influence Of Grain Size distribution on the performance of mortars', in: Kwiatkowski, D., Lofvendahl, R. (Eds), *10th International Congress on Deterioration and Conservation of Stone*, conference proceedings, Stockholm, 27 June-2 July, pp. 1001-1008

Historic Scotland. (2000). '*Conservation Plans: A Guide to the Preparation of Conservation Plans*', Edinburgh.

Hoffmann, D. (1979). 'On the differences in the behaviour of artificially weathered lime plasters and their equivalents found in external structures: a comparative study', in proceedings: *3rd International Congress on the Deterioration and Preservation of Stones*, 24-27 October, Venice, pp. 549-556.

Hoffmann, D., Niesel, K. (1992). 'Pore structure of rendering as a feature of its weathering', in: Delgado Rodrigues, J., Henriques, F., Telmo Jeremias, F. (Eds), *7th International Congress on Deterioration and Conservation of Stone*, proceedings, 15-18 June, Portugal, Lisbon, pp. 611-620.

Hoffmann, D., Niesel, K. (1993). 'Evaluation of lime mortar by physico-technical characteristics', in: *2nd International EUROLIME Meeting*, proceedings, Copenhagen, pp. 37-40.

Hoffmann, D., Niesel, K. (1995). 'Quantifying the effect of air pollutants on renderings and also moisture-transport phenomena in masonry including its constituents', URL: http://www.bam.de/service/publikationen/, (accessed on: September 2004).

Holmstrom, I. (1981). 'Mortars, Cements and Grouts for Conservation and Repair. Some Urgent Needs for Research', in: *Mortars, Cements and Grouts Used in the Conservation of Historic Buildings*, proceedings of the ICCROM Symposium, 3-6 November, Rome, pp. 19–24.

Honeyborne D., Ashurst J., Price C., Ross Keith. (1998). 'Surface treatments', in: *Conservation of Building and Decorative Stone*, Ashurst, J., Dimes, F.G. (Eds), Butterworth Heinemann, Oxford, vol. 2.

Hourmouziadis, G. (1982). 'Ancient Magnesia: from the Paleolithic caves to the palace of Demetrias', in: Capon, M., Capon, R. (Eds), *Magnesia, The Story of a Civilization*, Athens.

Houst, Y.F., Wittmann, F.H. (2002). 'Depth profiles of carbonates formed during natural carbonation', *Cement and Concrete Research*, 32, pp. 1923-1930.

Houst, Y.F., Wittmann, F.H. (1994). 'Influence of water content and porosity on the diffusivity of O_2 and CO_2 through HCP', *Cement Concrete Research*, 24, pp. 1165-1176.

Hughes J.J. (2001). 'The petrography of lime inclusions in historic lime based mortars', in: Stamatakis, M., Georgali, B., Fragoulis, D. Toumbakari, E.E. (Eds), *8th Euroseminar on Microscopy Applied to Building Materials*, proceedings, 4-7 September, Athens, Greece, pp. 359-364.

Hughes, J., Valek, J. (2003). *Mortars in Historic Buildings. A Review of the Conservation, Technical and Scientific Literature*, Historic Scotland, Edinburgh.

Hughes, J.J., Callebaut, K. (2000). 'Practical sampling of historic mortars'. in: Bartos, P., Groot, C., Hughes, J.J. (Eds), *Historic Mortars: Characteristics and Tests*, proceedings of the international RILEM workshop, 12-14 May 1989, Paisley, Scotland, RILEM Publications S.A.R.L., pp. 17-26.

Hughes, J.J., Leslie, A.B., Callebaut, K. (2001). 'The petrography of lime inclusions in historic lime based mortars', in: Stamatakis, M., Georgali, B., Fragoulis, D. Toumbakari, E.E. (Eds), *8th Euroseminar on Microscopy Applied to Building Materials*, proceedings, 4-7 September, Athens, Greece, pp. 359-364.

ICCROM (1981). *Symposium on Mortars, Cements and Grouts used in the Conservation of Historic Buildings*, 3-6 November, ICCROM, Rome.

ICOMOS Charter (*2003*). *Principles for the Analysis, Conservation and Structural Restoration of Architectural Heritage*, ICOMOS, URL: http://www.international. icomos.org/ charters/structures_e.htm, (accessed on: February 2005).

Istoria tou Ellinikou Ethnous (History of the Hellenic Nation) (1985). *Palaioxristianikoi Xronoi (Early Christian Ages)*, Vol Z, Ekdotiki Athinon (Publ.), Athens, Greece, pp. 371–410.

Jedrzejewska, H. (1960). 'Old mortars in Poland: a new method of investigation', *Studies in Conservation*, 5, 4, pp. 132-38.

Kampf, L. (1963). 'Factors affecting bond of mortar to brick', in: *Symposium on Masonry Testing*, American Society for Testing and Materials, ASTM STP 320, pp. 127-141.

Karatasios, I., Watt, D., Colston, B. (2002). 'Characterisation and development of mortars for the conservation of Byzantine floor mosaics', in: Townsend, J.H., Eremin, K., Adriaens, A., (Eds), *Conservation Science 2002*, conference proceedings, 22-24 May, Edinburgh, Scotland, pp. 121-126.

Karaveziroglou, M., Papayianni, I., Penelis, I. (1990). 'Criteria for selecting materials for repair brick masonry', in: *Structural Conservation of Stone Masonry*, proceedings of the International Technical Conference, 31 October – 3 November, ICCROM, Rome, pp. 335-341.

Katyal, N.K., Ahluwalia, S.C., Parkash, R. (1999). 'Effect of barium on the formation of tricalcium silicate', *Cement and Concrete Research*, 29, pp. 1857-1862.

Kilikoglou, V. (1994). 'Scanning electron microscopy' in: Day, P., Wilson, D. 'Ceramic regionalism in prepalatial Central Crete: The Messara imports at EMI to EMIIA Knossos', *Annual of the British School at Athens,* 89, pp. 1-87.

Kingery, W.D., Vandiver, P.B., Prickett, M, (1988). 'The beginnings of pyrotechnology, part II: Production and use of lime and gypsum plaster in pre-pottery Neolithic Near-East', *Journal of Field Archaeology*, 15, pp. 219-244.

Kirkpatrick T. (1978). 'Barium compounds', in: *Encyclopedia of Chemical Technology*, Wiley and Sons Pub., 3rd ed., Vol. 3, pp 463 – 479.

Klemm, D.D., Klemm, R. (1990). 'Mortar evolution in the old kingdom of Egypt', in: Pernicka, E., Wagner, G.A. (Eds), *Archaeometry '90*, proceedings of the International Archaeometry symposium, Birkhauser Verlag, Basel, Switzerland, pp. 445-454.

Krivtsov, A.M., Wiercigroch, M. (2001). 'Molecular dynamics simulation of mechanical properties for polycrystal materials', *Materials Physics and Mechanics*, 3, pp. 45-51.

Krus, M., Kieβl, K. (1998). 'Determination of the moisture storage characteristics of porous capillary active materials', *Materials and Structures*, 31, pp. 522-529.

Kucera, V., Fitz, S. (1995). 'Direct and indirect air pollution effects on materials including cultural monuments', *Water Air and Soil Pollution*, 85, 1, pp. 153-165.

Lambropoulos, V., Giossi, S., Karatasios, I. (2000). 'A comparative study of mortars containing barium hydroxide: application on monuments conservation', in: *9th International Congress on Deterioration and Conservation of Stone*, proceedings, Venice, Italy, 19–24 June, pp. 351-359.

Lanas, J., Alvarez, J.I. (2003). 'Masonry repair lime based mortars: Factors affecting the mechanical behavior', *Cement and Concrete Research*, 33, pp. 1867-1876.

Lanas, J., Perez Bernal, J.L., Bello, M.A., Alvarez Galindo, J.I. (2004). 'Mechanical properties of natural hydraulic lime-based mortars', *Cement and Concrete Research*, 34, pp. 2191-2201.

Lange, D.A, Deford, H.D., Werner, A.M. (1999). 'Microstructural investigation of mortar-unit interaction', *The Masonry Society Journal*, 17, 1, pp. 31-42.

Lea, F.M. (1971). *The Chemistry of Cement and Concrete*, Chemical Publishing Co, New York.

Lewin S. Z. (1966). "The preservation of natural stone, 1839-1965, an annotated bibliography", *Art and Archaeology Technical Abstracts*, 6, 1, pp. 185-277.

Lewin S. Z., Baer N. S. (1974). 'Rationale of the barium hydroxide – urea treatment of decayed stone', *Studies in Conservation*, 19, 1, pp 24-35.

Lewin, S. Z. (1989). 'The susceptibility of calcareous stone to salt decay', in: Zezza, F. (Ed.), *1st International Symposium for the Conservation of Monuments in the Mediterranean Basin*, Bari, pp. 59-63.

Lewin, S.Z. (1981). 'X-ray diffraction and scanning electron microscope analysis of conventional mortars', in: *Mortars, Cements and Grouts Used in the Conservation of Historic Buildings*, proceedings of the ICCROM Symposium, 3-6 November, Rome, pp. 101-131.

Li, Ch., Prikryl, R., Nordlund, E. (1998). 'The stress-strain behaviour of rock material related to fracture under compression', *Engineering Geology*, 49, pp. 293-302.

Lindqvist J. E., Schouenborg B., Sandstrom M., Sandstrom H., Sandin K., Sidmar E. (1994). 'Comprehensive studies of old mortars from three medieval churches in southern Sweeden', in: *Sixteenth Annual International Conference on Cement Microscopy*, proceedings, Richmond, Virginia, USA, pp 306-322.

Ling, R. (1998). *Ancient Mosaics*, British Museum Press, London, pp. 6-18.

Livingston, (1992). 'Geochemical considerations in the cleaning of carbonate stone', in: Webster, R.G.M. (Ed.), *Stone Cleaning and the Nature, Soiling and Decay Mechanisms of Stone*, proceedings of the international conference, 14-16 April, Edinburgh, Donhead, London, pp. 166-179.

Luxan, M.P., Dorrego, F. (1996). 'Ancient XVI century mortar from the Dominican Republic: its characteristics, microstructure and additives', *Cement and Concrete Research*, 26, 6, pp. 841-849.

Maingury, M., Tongazzi, C., Torrenti, J.-M., Adenot, F. (2000). 'Modeling of leaching in pure cement paste and mortar'. *Cement and Concrete Research*, 30, pp. 83-90.

Malinowski, R. (1981). 'Ancient mortars and concretes-Durability aspects', in: *Mortars, Cements and Grouts Used in the Conservation of Historic Buildings*, proceedings of the ICCROM Symposium, 3-6 November, Rome, pp. 341-349.

Maniatis, Y., Tite, M.S. (1981). 'Technological examination of Neolithic-Bronze Age pottery from central and southeast Europe and from the Near East', *Journal of Archaeological Science*, 8, pp. 59-76.

Manzano, E., Bueno, G.A., Gonzalez-Casado, A., del Olmo, M. (1999). 'Mortars, pigments and binding media of wall paintings in the 'Carrera del Daro' in Granada, Spain', *Journal of Cultural Heritage*, 1, pp. 19-28.

Marsh, I.E. (1926). *Stone Decay and its Prevention*, Basil Blackwell, Oxford.

Martinez-Ramirez, S., Puertas, F., Blanco-Varela, M.T., Thompson, G.E., Haneef, S.J., Wood, G.C. (1996). 'Behaviour of lime mortar in atmospheric simulation champers', in: Riederer, J. (Ed), *8th International Congress on the Deterioration and Conservation of Stone*, proceedings, 30 September – 4 October, Berlin, pp. 1557-1563.

Martinez-Ramirez, S., Puertas, F., Blanco-Varela, M.T., Thompson, G.E. (1997). 'Studies of degradation of lime mortars in atmospheric simulation champers', *Cement and Concrete Research*, 27, 5, pp. 777-784.

Martinez-Ramirez, S., Puertas, F., Blanco-Varela, M.T., Thompson, G.E., Almendros, P. (1998). 'Behaviour of repair lime mortars by wet deposition process', *Cement and Concrete Research*, 28, 2, pp. 221-229.

Martinez-Ramirez, S., Sanchez-Cortes, S., Garcia-Ramos, J.V., Domingo, C., Fortes, C., Blanco-Varela, M.T. (2003). 'Micro-Raman spectroscopy applied to depth profiles of carbonates formed in lime mortar', *Cement and Concrete Research*, 33, pp. 2063-2068.

Martinez-Ramirez, S., Thompson, G. E. (1999). 'Wet deposition studies of hydraulic mortars'. *Materials and Structures*, Vol. 32, pp. 606-610.

Martin-Gil, J., Ramos-Sanchez, M.C., Martin-Gil, F.J. (1999). 'Ancient pastes for stone protection against environmental agents', *Studies in Conservation*, 44, 1, pp. 58-62.

Martys, N.S., Ferraris, C.F. (1997). 'Capillary transport in mortars and concrete', *Cement and Concrete Research*, 27, 5, pp. 747-760.

Matteini M. (1999). 'The mineral approach to the conservation of mural paintings: Barium hydroxide and artificial oxalates', in: *Conserving the Painted Past. Developing approaches to wall paintings conservation*, conference post-prints, English Heritage, London, 2-4 December, pp. 110-115.

Matteini M., Moles A., Giovannoni S. (1994). 'Calcium oxalate as a protective mineral system for wall paintings: methodology and analyses', in: Fassina, V., Ott, H., Zezza, F. (Eds), *3rd International Symposium 'The Conservation of Monuments in the Mediterranean Basin: Stone and Monuments: Methodologies for the Analyses of Weathering and Conservation*, proceedings, 22-25 June, Venice, pp. 155-162.

Matteini M., Moles A., Lanterna G., Nepoti M.R. (1996). 'Preliminary monitoring on painted plasters and marble surfaces of a mineral protective treatment based on artificially formed calcium oxalate' in: Realini, M., Toniolo, L. (Eds), *International Symposium II: The Oxalate Films in the Conservation of Works of Art*, proceedings, Milan, 25-27 March, pp. 425-440.

Matteini, M. (1991). 'In review: an assessment of Florentine methods of wall paintings conservation based on the use of mineral treatments', in: Cather S. (Ed.), *The Conservation of Wall Paintings,* proceedings of the symposium organised by the Courtauld Institute of Art and the Getty Conservation Institute, 13-16 July 1987, The Getty Conservation Institute, Los Angeles, pp. 137-148.

Matteini, M. (1999). 'The mineral approach to the conservation of mural paintings: Barium hydroxide and artificial oxalates', in: *Conserving the Painted Past. Developing approaches to wall paintings conservation*, post-prints of the conference, 2-4 December, London, pp. 110 – 115.

Maurenbrecher A.H.P., Trischuk K., Rousseau M.Z. (2001). 'Review of factors affecting the durability of repointing mortars for older masonry', in: Bischoff P.H., Dawe J.L., Schriver A.B., Valsangkar A.J. (Eds), *9th Canadian Masonry Symposium- 'Spanning the Centuries with Masonry'*, proceedings, 4-6 June, Fredericton, New Brunswick, URL: http://www.nrc.ca/irc/fulltext/mortar/, (accessed on September 2003).

Maurenbrecher, A.H.P., Suter, G.T., Trischuk, K., Fontaine, L. (2000). 'Contribution to pointing mortar durability'. in: Bartos, P., Groot, C., Hughes, J.J. (Eds), *Historic Mortars: Characteristics and Tests*, proceedings of the international RILEM workshop, 12-14 May 1989, Paisley, Scotland, RILEM Publications S.A.R.L., pp. 361-369.

McGinley, W.M. (1990). 'IRA and the flexural bond strength of clay brick masonry', *Masonry: Components to assemblages*, Matthys, J.H. (Ed.), American Society for Testing and Materials, ASTM STP 1063, pp. 217-234.

Meng, B. (1993). 'Characterization of pore structure for the interpretation of moisture transport', in: Thiel, M.J. (Ed), *Conservation of Stone and Other Materials*, proceedings of the international congress, RILEM/UNESCO, 29 June-1 July, Paris, E & FN Spon, London, pp. 155-162.

Middendorf, B., Baronio, G., Callebaut, K., Hughes, J.J. (2000). 'Chemical-mineralogical and physical-mechanical investigations of old mortars', in: Bartos, P., Groot, C., Hughes, J.J. (Eds), *Historic Mortars: Characteristics and Tests*, proceedings of the international RILEM workshop, 12-14 May 1989, Paisley, Scotland, RILEM Publications S.A.R.L., pp. 53-60.

Mishara, J. (1982). 'Early Hydraulic Cements', in: Wertime, T.A., Wertime, S.F. (Eds), *The Evolution of the First Fire-Using Industries*, Smithsonian Institution Press, Washington D.C., pp. 125-134.

Moorehead, D.R. (1986). 'Cementation by the carbonation of hydrated lime', *Cement and Concrete Research*, 16, pp. 700-708.

Moriconi, G., Castellano, M.G., Coppelardi, M. (1994). 'Mortar deterioration of the masonry walls in historic buildings. A case history: Vanvitelli's mole in Angona', *Materials and Structures*, 27, pp. 408-414.

Moropoulou, A., Bakolas, A., Aggelakopoulou, E. (2004a). 'Evaluation of pozzolanic activity of natural and artificial pozzolans by thermal analysis', *Thermochimica Acta*, 420, pp. 135-140.

Moropoulou, A., Bakolas, A., Anagnostopoulou, S. (2005a). 'Composite materials in ancient structures', *Cement and Concrete Composites*, 27, pp. 295-300.

Moropoulou, A., Bakolas, A., Bisbikou, K. (1995). 'Characterization of ancient, byzantine and later historic mortars by thermal and X-ray diffraction techniques', *Thermochimica Acta*, 269/270, pp. 770-795.

Moropoulou, A., Bakolas, A., Bisbikou, K. (2000). 'Investigation of the technology of historic mortars', *Journal of Cultural Heritage*, 1, 1, pp. 45-58.

Moropoulou, A., Bakolas, A., Moundoulas, P., Aggelakopoulou, E., Anagnostopoulou, S. (2005b). 'Strength development and lime reaction in mortars for repairing historic masonries', *Cement and Concrete Composites*, 27, pp. 289-294.

Moropoulou, A., Cakmak, A., Labropoulos, K.C., Van Grieken, R., Torfs, K. (2004b). 'Accelerated microstructural evolution of a calcium-silicate-hydrate (C-S-H) phase in

pozzolanic pastes using fine siliceous sources: Comparison with historic pozzolanic mortars', *Cement and Concrete Research*, 34, pp. 1-6.

Moropoulou, A., Cakmak, A.S., Biscontin, G. (1998). 'Criteria and Methodology to Evaluate the Hagia Sophia Crushed Brick/Lime Mortars', in: Moropoulou, A., Biscontin, G., Rodrigues, J.D., Erdik, M. (Eds), *Compatible materials for the protection of monuments*, Raphael-COMARECH conference, 15-16 December, Athens, PACT 55, pp. 39-54.

Moropoulou, A., Cakmak, A.S., Biscontin, G., Bakolas, A., Zendri, E. (2002). 'Advanced Byzantine cement based composites resisting earthquake stresses: the crushed brick/lime mortars of Justinian's Hagia Sophia', *Construction and Building Materials*, 16, pp. 543-552.

Moropoulou, A., Polikreti, K., Bakolas, A., Michailidis, P. (2003). 'Correlation of physicochemical and mechanical properties of historical mortars and classification by multivariate statistics', *Cement and Concrete Research*, 33, pp. 891-898.

Moropoulou, A., Theoulakis, P., Bisbikou, K., Theodoraki, A., Chondros, N. (1993). 'Study of mortars in the Medieval city of Rhodes', in: Thiel, M.J. (Ed), *Conservation of Stone and Other Materials*, proceedings of the international congress, RILEM/UNESCO, 29 June-1 July, Paris, E & FN Spon, London, pp. 394-401.

Mosaics in Situ Project, (2003). *Illustrated Glossarry*, Getty Conservation Institute and Israel Antiquities Authority, URL: http:// www.getty.edu/conservation/, (accessed on April 2004).

Mosquera, M.J., Benitez, D. Perry, S.H. (2002). 'Pore structure in mortars applied on restoration. Effect on properties relevant to decay of granite buildings', *Cement and Concrete Research*, 32, pp. 1883–1888.

Neal, D. (1976). 'Floor mosaics', in: Strong, D., Brown, D. (eds), *Roman Crafts*, London, pp. 241-252.

Newton, R.G., Sharp, J.H. (1987). 'An investigation of the chemical constituents of some renaissance plasters', *Studies in Conservation*, 32, pp. 163-175.

Ntina, A. (1990b). 'Recherches modernes a la paliochristanique ville de Fthiotides Thebes', in: proceedings of the symposium *'Quinze années de Recherches Archéologiques, 1975 - 1990. Bilans et Perspectives'*, 17-22 April, Lyon, pp. 357-370.

Ntina, A. (1990b). 'Palaioxristianika mnimeia sti Thessalia' (Post-Byzantine Monuments of Thessaly-Greece), *Arxaiologia (Archaeologia)*, 34, pp. 87-94.

Okochi, H. (1995). 'Deterioration of concrete structure by acid deposition', *Corrosion Engineering*, 44, pp. 813-827.

Paama, L., Pitkanen, I., Ronkkomaki, H. and Peramaki, P. (1998). 'Thermal and Infrared Spectroscopic Characterization of Historical Mortars', *Thermochimica Acta*, 320, pp. 127–33.

Papayianni, I. (1998), 'Criteria and methodology for manufacturing compatible repair mortars and bricks', in: Moropoulou, A., Biscontin, G., Rodrigues, J.D., Erdik, M. (Eds), *Compatible Materials for the Protection of European Cultural Heritage*, Raphael-INCOMARECH conference, PACT 56, 2, pp. 179-190.

Papayianni, I., Karaveziroglou, M. (1993). 'Aggregate gradation of ancient mortars. Relationship to strength and porosity', in: Thiel, M.J. (Ed), *Conservation of Stone and Other Materials*, proceedings of the international congress, RILEM/UNESCO, 29 June-1 July, Paris, E & FN Spon, London, pp. 493-499.

Papayianni, I., Stefanidou, M. (2001). 'The evolution of porosity in lime-based mortars', in: Stamatakis, M., Georgali, B., Fragoulis, D. Toumbakari, E.E. (Eds), *8th*

Euroseminar on Microscopy Applied to Building Materials, proceedings, 4-7 September, Athens, Greece, pp. 451-457.

Peroni, S., Tersigni, C., Torraca, G., Cerea, S., Forti, M., Guibobaldi, F., Rossi-Doria, P., De Rege, A., Picchi, D., Pietrafitta, F.J. and Benedetti, G. (1981). 'Lime-based mortars for the repair of ancient masonry and possible substitutes', in: *Mortars, Cements and Grouts Used in the Conservation of Historic Buildings*, proceedings of the ICCROM Symposium, 3-6 November, Rome, pp. 63-101.

Perry, H.R., Green, D. (1984). 'Physical and Chemical Data: Vapour Pressures of Pure Substances'. *Perry's Chemical Engineers' Handbook*, Perry R.H. (Ed), McGraw – Hill, 50th edition, New York.

Philips, M. (1994). 'A source of confusion about mortar formulas', *Association for the Preservation of Technology (APT) Bulleting*, 25, 3-4, pp.50-53.

Price, C. (2000). 'Salt Damage in Porous Materials', In: Price , P. (Ed), *An Expert Chemical Model for Determining the Environmental Conditions Needed to Prevent Salt Damage in Porous Materials*, Archetype, London.

Price, C.A. (1996). 'Putting it right: preventive and remedial treatments', *Stone conservation : An overview of current research*, Keys A. (Ed), The J. Paul Getty Trust, Los Angeles.

Puertas, F., Blanco-Valera, M. T., Martinez, S., Accion, F., Alvarez, G. (1992). 'Methodology of Analysis of Stones and Mortars in Monuments', in: D.J., Henriques, F., Telmo Jeremias, F., proceedings of the *7th International Congress on Deterioration and Conservation of Stone*, (Eds),15–18 June, Lisbon, Portugal,, pp. 763–70.

Puertas, F., Blanco-Varela, M.T., Palomo, A., Ortega-Calvo, J.J., Arino, X., Sain-Jimenez, C. (1994). 'Decay of Roman and repair mortars in mosaics from Italica, Spain', *The Science of the Total Environment*, 153, pp. 123-131.

Quenard, D.A., Xu, K., Kunzel, H.M., Bentz, D.P., Martys, N.S. (1998). 'Microstructure and transport properties of porous building materials', *Materials and Structures*, 31, pp. 317-324.

Ransome F. (1866). 'Stone, Preserving; Cements', *British Patent 3729*, 26 October.

Raphael-COMARECH (2000). *Initiative for Compatible Materials Recommendations for the Preservation of the European Cultural Heritage*, Project funded by the European Commission, EC DG X, Reference: R99/II.2.a.11/GR-99/SI2.81089.

Raphael-INCOMARECH (1998). *Compatible Materials for the Preservation of the Protection of European Cultural Heritage*, Moropoulou, A., Biscontin, G., Rodrigues, J.D., Erdik, M. (Eds), 15-16 December, Athens, PACT 55.

Reda Taha, M.M., Shrive, N.G. (2001). 'The use of pozzolans to improve bond and bond strength', in: Bischoff P.H., Dawe J.L., Schriver A.B., Valsangkar A.J. (Eds), *9th Canadian Masonry Symposium-'Spanning the Centuries with Masonry'*, proceedings, 4-6 June, Fredericton, New Brunswick, URL: http://www.nrc.ca/irc/fulltext/mortar/, (accessed on September 2003).

Rendell, F., Jauberthie, R. (1999). 'The deterioration of mortar in sulphate environments', *Construction and Building Materials*, 13, pp. 321-327.

RIBA CPD Course. (2003). 'Introduction to the: design and technology of masonry mortars', Continuing Professional Development for Mortars, CA4.1.10.6.2., URL: http://www.rmc.co.uk/architect/downloads/designandtechnologyofmasonrymortars.pdf, (accessed on: September 2004).

Riccardi, M.P., Duminuco, P., Tomasi, C., Ferloni, P. (1998). 'Thermal, microscopic and X-ray diffraction studies on some ancient mortars', *Thermochimica Acta*, 321, pp. 207-214.

Rice, P.M. (1987). *Pottery Analysis. A sourcebook*, The University of Chicago Press, Chicago.

RILEM Commission 25–PEM. (1980). 'Tentative Recommendations – Recommended tests to measure the deterioration of stone and to assess the effectiveness of treatment methods'. *Materials and Constructions*, 13, 75, pp. 175-253.

RILEM Technical Committee (TC 130-CSL) (1996). *Durability design of concrete structures*, Sarja, A., Vesikari, E. (Eds), E & FN Spon, London, pp. 5-11.

RILEM Technical Committee (TC 167-COM) (2000). *International workshop on Historic Mortars: Characteristics and Tests*, Batros P., Groot C., Hughes J.J. (Eds), Paisley, 12-14 May 1989, RILEM Publications S.A.R.L..

ROCEM (2002). *Roman Cement to Restore Built Heritage Effectively*. Project funded by the European Commission, Fifth Research Technology and Development (RTD) Framework Programme 'Energy Environment and Sustainable Development (EESD)', Reference: EVK4-CT-2002-00084, URL: http://www.cordis.lu/eesd/home.html, (accessed on: April 2005).

Rodrigues, J.D. (1998). 'In the search for tentative recommendations regarding compatible restoration mortars', in: Moropoulou, A., Biscontin, G., Rodrigues, J.D., Erdik, M. (Eds), *Compatible Materials for the Protection of European Cultural Heritage*, Raphael-INCOMARECH conference, PACT 56, 2, pp. 141-147.

Rodrigues, P., Henriques, F. (2003). 'Current Mortars In Conservation: An overview', in: *6th International Conference on Materials Science and Restoration*, conference proceedings, Karlsruhe, 16-18 September, URL: http://www.dec.fct.unl.pt/seccoes/smtc/wd11.htm, (accessed on: April 2005).

Rodriguez-Navarro, C., Cazalla, O., Elert, E., Sebastian, E. (2002). 'Liesegang pattern development in carbonating traditional lime mortars', *Mathematical, Physical and Engineering Sciences*, proceedings, 458, 2025, pp. 2261-2273.

Rodriguez-Navarro, C., Hansen, E., Ginell, W.S. (1998). 'Calcium hydroxide crystal evolution upon aging of lime putty', *Journal of American Ceramics Society*, 81, 11, pp. 3032– 3034.

Rossi-Doria, P.R. (1986). 'Mortars for restoration: basic requirements and quality control', *Materials and Structures*, 19, 114, pp. 445-448.

Rossi-Manaresi, R., Torraca, G. (Eds) (1972). *The Treatment of Stone*, Centro per la Conservazione delle Sculture all' Aperto, Bollogna, pp. 139-144.

Russell J.D. (1987). 'Infrared Methods', in: *A Handbook of Determinative Methods in Clay Mineralogy*, Wilson M.J. (Ed), Blackie and Son, Glasgow.

Rust J. (1861), cited by Tate W., Murchison R., Bonham-Carter A. *Report on the Committee on the Decay of the Stone of the New Palace at Westminster*, London, pp. 126.

Ryu J.-S., Otsuli N., Minagawa H. (2002). 'Long-term forecast of Ca leaching from mortar and associated degeneration'. *Cement and Concrete Research*, 32, pp. 1539-1544.

Sabbioni, C., Zappia, G., Ghedini, N., Gobbi, G., Favoni, O. (1997). 'Black crusts on ancient mortars', *Atmospheric Environment*, 32, 2, pp. 215-223.

Sabbioni, C., Zappia, G., Riontino, C., Blanco-Varela, M.T., Aguilera, J., Puertas, F., Van Balen, K., Toumbakari, E.E. (2001). 'Atmospheric deterioration of ancient and modern hydraulic mortars', *Atmospheric Environment*, 35, pp. 539-548.

Sabbioni,C., Bonazza, A., Zappia, G. (2002). 'Damage on hydraulic mortars: the Venice Arsenal', *Journal of Cultural Heritage*, 3, pp.83-88.

Sahu, S., Badger, S., Thaulow, N., Lee, R.J. (2004). 'Determination of water–cement ratio of hardened concrete by scanning electron microscopy', *Cement and Concrete Composites*, 26, pp. 987–992.

Saito, H., Deguchi, A. (2000). 'Leaching tests on different mortars using accelerated electrochemical method'. *Cement and Concrete Research*, 30, pp. 1815-1825.

Sanchez, J.A., Barrios, J., Barrios, A., De Arellano Agudo, A.R. (1997). 'The shrinkage in lime mortars', *Materiales De Construccion*, 47, 245, pp. 17-28.

Sayre E.V. (1971). 'Direct Deposition of Barium Sulfate from Homogeneous Solution Within Porous Stone', in: Thomson, G. (Ed.), *Conservation of Stone and Wooden objects*, preprints of the New York Conference, 7-13 June 1970, IIC, London, pp. 115–118.

Schafer, J., Hildsdorf, H.K. (1993). 'Ancient and new lime mortars – The correlation between their composition, structure and properties', in: Thiel, M.J. (Ed), *Conservation of Stone and Other Materials*, proceedings of the international congress, RILEM/UNESCO, 29 June-1 July, Paris, E & FN Spon, London, pp. 605–612.

Scherer, G.W. (1999). 'Crystallization in pores', *Cement and Concrete Research*, 29, pp. 1347-1358.

Scherer, G.W. (2000). ,Stress from crystallization of salts in pores', in: *9th International Congress on Deterioration and Conservation of Stone*, proceedings, Venice, Italy, 19–24 June, pp. 187-194.

Schultz, R.A. (1996). 'Relative scale and the strength and deformability of rock masses', *Journal of Structural Geology*, 18, 9, pp. 1139-1149.

Schuster, P.F., Reddy, M.M., Sherwood, S.I. (1994). 'Effects of acid-rain and sulfur-dioxide on marble dissolution', *Materials Performance*, 33, 1, pp. 76-80

Sear, F. (1976). 'Wall and vault mosaics', in: Strong, D., Brown, D. (eds), *Roman Crafts*, London, pp. 231-239.

Shannang, M.J., Yeginobali, A. (1995). 'Properties of pastes, mortars and concretes containing natural pozzolan', *Cement and Concrete Research*, 25, 3, pp. 647-657.

Shelley, J., Wilkins, R., Compton, G., Vilesy, H.A. (2001). 'The effect of surface pretreatment with polymaleic acid, phosphoric acid, or oxalic acid on the dissolution kinetics of calcium carbonate in aqueous acid', *Journal of Colloid and Interface Science*, 242, pp. 378-385.

Siddall, R. (2000). *Plaster, Mortar, Cement & Concrete*, notes for the MSc Course of the Institute of Archaeology 'G123 Conservation: Materials Science', UCL, London, URL: http://www.ucl.ac.uk/~ucfbrxs/limes/G123notes.htm, (accessed on: May 2005).

Skoulikides, Th., Papakonstantinou, P. (1981). 'The mechanism of sulfation by atmospheric SO_2 of limestones and marbles of the ancient monuments and statues I. Observation in situ and measurements in the laboratory; activation energy', *British Corrosion Journal*, 16, 2, pp. 63-69.

Skoulikidis, Th. (1996). 'I chrisi tou idroxidiou tou variou gia ti stereosi tis epifanias petas kai gia prosmixi sto tsimento' (The Use of Barium Hydroxide for the Consolidation of Decayed Stone and as Additive to Cement), *Monument and Environment*, 3, pp. 203–204.

Stewart, J., Moore, J. (1981). 'Chemical Techniques of Historic Mortar Analysis', in: *Mortars, Cements and Grouts Used in the Conservation of Historic Buildings*, proceedings of the ICCROM Symposium, 3-6 November, Rome, pp. 297–310.

Striegel, M.F., Guin, E.B.B., Hallett, K., Sandoval, D., Swingle, R., Knox, K., Best, F., Fornea, S. (2003). 'Air pollution, coatings, and cultural resources', *Progress in Organic Coatings*, 48, 2-4, pp. 281-288.

Swallow, P., Carrington, D. (1995). 'Limes and lime mortars-Part one', *Journal of Architectural Conservation*, 1, 3, pp. 7-25.

Taylor, G.D. (2000). *Materials in Construction. An Introduction*, Pearson Education Limited, Essex.

Technical Advice Notes (TAN) 1 (2003). *Preparation and Use of Lime Mortars*, Technical Conservation Research and Education Division, Historic Scotland, Edinburgh.

Terada, J. (1952). 'Rhombohedral crystals of Ba-Ca and Sr-Ca double carbonates', *Journal of the Physical Society of Japan*, 7, pp. 432-434.

Terada, J. (1953). 'Crystal structure of the Ba, Sr, and Ca triple carbonates', *Journal of the Physical Society of Japan*, 8, 2, pp. 432-434.

Teutonico, J.M., Ashall, G., Garrod, E., Yates, T. (1999). 'Acomparative study of hydraulic lime-based mortars', in: Bartos, P., Groot, C., Hughes, J.J. (Eds), *Historic Mortars: Characteristics and Tests*, proceedings of the international RILEM workshop, 12-14 May 1989, Paisley, Scotland, RILEM Publications S.A.R.L., pp. 339-349.

Teutonico, J.M., McCaig, I., Burns, I., Ashurst, J. (1994). 'The Smeaton project: factors affecting the properties of lime-based mortars', *APT Bulletin*, 25, 3-4, pp. 32-49

The Northwest Masonry Guide (2000). *Requirements for Rain Resistant Masonry Construction: The Efflorescence Phenomenon*, URL: http://masonryinstitute.com/guide/part4/construction_a2_pg4.html, (accessed on: April 2003).

Theoulakis, P., Giannoulaki, M., Poulimenea, S., Karatasios, I., Kilikoglou, V., Themelis, P. (2004). 'Deterioration layers and crust formations on two Hellenistic excavated marble sculptures. Analytical and theoretical approach', in: Kwiatkowski, D., Lofvendahl, R. (Eds.), *10th International Congress on Deterioration and Conservation of Stone "STONE 2004"*, proceedings, 27 June - 2 July, Stockholm, Vol. I, pp. 43-50.

Theoulakis, P., Karatasios, I., Sotiropoulos, Ag., Kilikoglou, V. (2004). 'The selection of stone for historic buildings repair. The use of Cypriot stone in the Medieval city of Rhodes', in: *6th International Symposium on the Conservation of Monuments in the Mediterranean Basin*, 7 - 10 April, Lisbon, pp. 352-360.

Theoulakis, P., Moropoulou, A., (1999). 'Salt Crystal Growth as Weathering Mechanism of Porous Stone on Historic Masonry', *Journal of Porous Materials*, 6, pp. 345-358.

Tixier, R., Mobasher, B. (2003). 'Modeling of damage in cement-based materials subjected to external sulfate attack. II: comparison with experiments', *Journal of Materials in Civil Engineering*, 15, 4, pp. 314-322.

Torfs, K., Van Grieken, R. (1997). 'Chemical relations between atmospheric aerosols, deposition and stone decay layers on historic buildings at the Mediterranean coast', *Atmospheric Environment*, 31, 15, pp. 2179-2192.

Torraca, G. (1988). *Porous Building Material: Material Science for Architectural Conservation*, 3rd ed., ICCROM, Rome.

Torrii, K., Taniguchi, K., Kawamura, M. (1995). 'Sulphate resistance of high fly ash content concrete', *Cement and Concrete Research*, 25, 4, pp. 759-768.

Tsuyuki, N., Watanabe, R., Koizumi, K., Unemura, Y., Machinaga, O. (2000). 'Effects of barium salt on the fixation of chloride ions in hardened mortars'. *Cement and Concrete Research*, 30, pp. 1435-1442.

Tsuyuki, N., Watanabe, R., Koizumi, K., Unemura, Y., Machinaga, O. (2000). 'Effects of barium salt on the fixation of chloride ions in hardened mortars'. *Cement and Concrete Research*, 30, pp. 1435-1442.

Twilley J. (1984). 'The relationship of microstructure to treatment variable in the consolidation of limestone with barium compounds', in: *12th Annual Meeting of the American Institute for Conservation (AIC)*, preprints, Los Angeles, California, Washington DC, pp.79-85.

Umemura, Y., Tsuyuki, N., Harada, H. (1998). 'Effect of WE water – reducing agents on the chloride ion fixation and permeability to hardened mortars', *Concrete Research Technology*, 9, 2, pp. 115-125.

UNESCO (1985). *Conventions and Recommendations of UNESCO Conserning the Protection of the Cultural Heritage*, UNESCO, Paris.

University of Illinois Urbana/Champaign (2000). Department of Materials Science and Engineering, URL: http://matse1.mse.uiuc.edu/concrete/hist.html, (assessed on: May 2002).

Van Balen, K, Van Gemert, D. (1994). 'Modeling lime mortar carbonation', *Materials and Structures*, 27, pp. 393-398.

Van Balen, K., Toumbakari, E.E, Blanco-Varela, M.T., Aguilera, J., Puertas, F., Palomo, A., Sabbioni, C., Riontino, C., Zappia, G. (1999a). 'Environmental deterioration of ancient and modern hydraulic mortar (EDAMM)', *Research Report N° XX on European Commission - Directorate-General XII*, Protection and Conservation of European Cultural Heritage, Project No Env4-CT95-0096.

Van Balen, K., Toumbakari, E.E, Blanco-Varela, M.T., Aguilera, J., Puertas, F., Palomo, A., Sabbioni, C., Zappia, G., Riontino, C., Gobbi, G. (1999b). 'Procedure for mortar identification: a proposal', in: Bartos, P., Groot, C., Hughes, J.J. (Eds), *Historic*

Mortars: Characteristics and Tests, proceedings of the international RILEM workshop, 12-14 May 1989, Paisley, Scotland, RILEM Publications S.A.R.L., pp. 61-70.

Van Balen, K., Toumbakari, E.E., Blanco-Valera, M.T., Aquilera, J., Puertas, F., Palomo, A., Sabbioni, C., Riontino, C., Zappia, G. (1999). *Environmental Damage to Ancient and Modern Mortars (EDAM)*, Project No ENV4-CT95-0096, Research Report No XX, Diractorate-General XII for Science, Research and Development.

Van Balen, K., Van Gemert, D. (1994). 'Modelling lime mortar carbonation', *Materials and Structures*, 27, pp. 393-398.

Vecchio, S., La Ginestra, A., Frezza, A., Ferragina, C. (1993). 'The use of thermoanalytical techniques in the characterization of ancient mortars', *Thermochimica Acta*, 227, pp. 215-223.

Veiga, R.M., Aguiar, J., Silva, A.S., Carvalho, F., (2001). 'Methodologies for characterisation and repair of mortars for ancient buildings', *Historical Constructions*, Lourenço, P.B., Roca P. (Eds.), Guimarães, pp. 353-363.

Vekinis, G., Kilikoglou, V. (1998). 'Mechanical performance of quartz-tempered ceramics: Part II, hertzian strength, wear resistance and applications to ancient ceramics', *Archaeometry*, 40, 2, pp. 281-292.

Venice Charter - International Charter for the Conservation and Restoration of Monuments and Sites (1964). ICOMOS, URL: http://www.international.icomos.org/venicecharter2004/index.html, (accessed on: May 2004).

Verita, M. (2000). 'Technology and deterioration of vitreous mosaic tesserae', *Reviews in Conservation*, 1, pp. 65-76.

Vitruvius. *The Ten Books on Architecture*, translated by Morgan, M.H. (1960), Dover Publications, New York.

Vos, H.B. (1975). 'Waterabsorption and drying of materials', in: *The Conservation of Stone*, proceedings of the international symposium, 19-21 June, Bologna, Italy, pp. 679-694.

Wallace, W. (1865). 'On ancient mortars', *Chemical News*, pp. 185-186.

Warnes A.R. (1926). *Building Stones; their Properties, Decay, and Preservation*, Ernest Benn Ltd., London.

Watt, D., Colston, B. (2000). 'Investigating the effects of humidity and salt crystallisation on medieval masonry', *Building and Environment*, 35, pp. 737-749.

Whitbread, I.K. (1986). 'The characterization of argillaceous inclusions in ceramic thin sections', *Archaeometry*, 28 , 1, pp 79-88.

Whitbread, I.K. (1989). 'A proposal for the systematic description of thin sections towards the study of ancient ceramic technology', in: Maniatis Y. (Ed), *25th International Symposium of Archaeometry*, proceedings, Elsevier, Amsterdam, pp. 127-138.

Wild, S., Khatib, J.M., O'Farel, M. (1997). 'Sulphate resistance of mortar containing ground brick clay calcinated at different temperatures', *Cement and Concrete Research*, 27, 5, pp. 697-709.

Wilkins,S. J., Compton, R.G., Viles, H.A. (2001). 'The effect of surface pretreatment with polymaleic acid, phosphoric acid, or oxalic acid on the dissolution kinetics of calcium carbonate in aqueous acid', *Journal of Colloid and Interface Science*, 242, pp. 378-385.

Yates, T. (2003). 'Mechanisms of air pollution damage to brick, concrete and mortar', in Air Pollution Reviews: *The Effects of Air Pollution on the Built Environment*, Brimblecombe, P. (Ed), Imperial College Press, London, pp.107-132.

Zacharopoulou, G. (1998). 'The renascence of lime based mortar technology. An appraisal of a bibliographic study', in: Moropoulou, A., Biscontin, G., Rodrigues, J.D., Erdik, M. (Eds), *Compatible Materials for the Protection of European Cultural Heritage, PACT*, 55, 1, Technical Chamber of Greece, pp. 89-114.

Zappia, G., Sabbioni, C., Pauri, M. and Gobbi, G. (1994). 'Mortar damage due to airbone sulfur compounds in a simulation chamber', *Materials and Structures*, 27, pp. 469-473.

Zappia, G., Sabbioni, C., Riontino, C., Gobbi, G., Favori., O. (1998). 'Exposure tests of building materials in urban atmosphere', *The Science of the Total Environment*, 224, pp. 235-244.

Zhang, B. (1998). 'Relationship between pore structure and mechanical properties of ordinary concrete under bending fatigue', *Cement and Concrete Research*, 28, 5, pp. 699-711.

APPENDICES

A TRAINING UNDERTAKEN DURING THE RESEARCH PROGRAMME

List of Publications

Scientific Journals

i. Maravelaki-Kalaitzaki, P., Bakolas, A., Karatasios, I., Kilikoglou, V. (2005). 'Hydraulic-lime mortars for the restoration of historic masonry in Crete', *Cement and Concrete Research*, 35, 8, pp. 1577-1586.

International Conference Proceedings (peer–reviewed)

ii. Karatasios, I., Anamaterou, E., Mantzana, E., Chrisopoulos, D. (2005). 'Past practice and future perspectives in the field of mosaics conservation in Greece', paper accepted for oral presentation in the: *9th ICCM conference 'Lessons Learned: Reflecting on the Theory and Practice of Mosaic Conservation'*, 29 November-3 December, Hammamet, Tunisia.

iii. Theoulakis, P., Karatasios, I., Sotiropoulos, Ag., Kilikoglou, V. (2004). 'The selection of stone for historic buildings repair. The use of Cypriot stone in the Medieval city of Rhodes', in proceedings of the: *6th International Symposium on the Conservation of Monuments in the Mediterranean Basin*, 7-10 April, Lisbon, pp. 352-360.

iv. Theoulakis, P., Giannoulaki, M., Poulimenea, S., Karatasios, I., Kilikoglou, V., Themelis, P. (2004). 'Deterioration layers and crust formations on two Hellenistic excavated marble sculptures. Analytical and theoretical approach', in

proceedings of the: *10th International Congress on Deterioration and Conservation of Stone "STONE 2004"*, Kwiatkowski, D., Lofvendahl, R. (Eds.), Stockholm 27 June – 2 July, Vol. I, pp. 43-50.

v. Theoulakis P., Karatasios I., Stefanis A., Kilikoglou V. (2003). 'Environmental Monitoring and Deterioration Phenomena of Historic Buildings: The Case of Retzep Pasha Mosque in Rhodes, Greece', in proceedings of the: *International Conference on Environmental Monitoring of our Cultural Heritage-Sustainable Conservation Solutions*, 13 – 14 November, Edinburgh, Chapter 9, pp 1-34.

vi. Doganis, I., Galanos, A., Theoulakis, P., Karatasios, I., Kilikoglou, V. (2003). "Study of renders and pigments from the Classical temple of Zeus at Nemea, Greece", in proceedings of the: *4th Symposium on Archaeometry of the Hellenic Society of Archaeometry*, 28-31 May, Athens, (in press).

vii. Karatasios, I., Theoulakis, P., Lampropoulos, V., Kilikoglou, V., Chryssopoulos, D. (2003). "Characterization of construction materials of wall mosaics from Dafni Monastery, Athens", in proceedings of the: *4th Symposium on Archaeometry of the Hellenic Society of Archaeometry*, 28-31 May, Athens, (in press).

viii. Karatasios, I., Theoulakis, P., Kylikoglou, V., Colston, B., Watt, D., Lampropoulos, V. (2002). "Analytical and Microscopic Techniques for the Study of Mortars from the Floor Mosaics of Thebes, Greece", in proceedings of the: *8th International Conference for the Conservation of Mosaics*, 3-5 November, Thessaloniki, (in press).

ix. Karatasios, I., Watt, D., Colston, B. (2002). "Characterisation and development of mortars for the conservation of Byzantine floor mosaics", in proceedings of the International Conference: *Conservation Science 2002*, 22-24 May, National Museum of Scotland, Edinburgh, pp. 121-126.

x. Theoulakis, P., Karatasios, I., Sotiropoulos, A., Vallatos, D., Kilikoglou, V. (2001). 'The use of Cypriot sandstone on the monuments of the medieval city of Rhodes. Physicochemical compatibility with the local sandstone' (in Greek), in proceedings of the International Conference: *15 Years of Restoration Works in the Medieval City of Rhodes,* 14–18 November, Rhodes, (in press).

xi. Karatasios, I., Kilikoglou, V., Moustakis, G., Theoulakis, P. (2001). 'Methodology applied for the physicochemical analysis and the study of deterioration phenomena of the Byzantine wall-paintings, at the Medieval city of Rhodes. Analysis of the construction materials' (in Greek), in proceedings of the International Conference: *15 Years of Restoration Works in the Medieval City of Rhodes,* 14–18 November, Rhodes, (in press).

xii. Moustakis, G., Theoulakis, P., Karatasios, I., Kilikoglou, V., (2001). 'Methodology applied for the physicochemical analysis and the study of deterioration phenomena of the Byzantine wall-paintings, at the Medieval city of Rhodes. Study of the deterioration phenomena' (in Greek), in proceedings of the International Conference: *15 Years of Restoration Works in the Medieval City of Rhodes,* 14–18 November, Rhodes, (in press).

xiii. Lampropoulos V., Ghiosi S., Karatasios I., (2000). "A comparative study of mortars containing barium hydroxide ($Ba(OH)_2$). Application on monument's conservation". *IX International Congress on the Deterioration and Conservation of Stone*, 19 - 24 June, Venice, Italy, Vol. 2, pp. 351-359.

Conservation Proposals - Technical Reports

xiv. Kilikoglou, V., Theoulakis, P., Karatasios, I., Stefanis, A., Paulopoulos, G. '*Conservation Proposal for the Building and Decorative Materials of Retzep Pasha Mosque, in the Medieval City of Rhodes*' (in Greek). The project was funded by the Greek Ministry of Culture and the Municipality of Rhodes, October 2004.

xv. Theoulakis, P., Karatasios, I. *'Mineralogical and Physicochemical Study of Ceramics and Building Stones from Dafni Monastery, in Athens'* (in Greek). The project was funded by the Greek Ministry of Culture, April 2004.

xvi. Kilikoglou, V., Theoulakis, P., Karatasios, I. *'Conservation Proposal for the Decorative Materials of the Doorframe of Souleiman Mosque, in the Medieval City of Rhodes'* (in Greek). The project was funded by the Greek Ministry of Culture, May 2003.

xvii. Karatasios, I., Kilikoglou, V. *'Physicochemical Analysis of the Byzantine Wall Paintings from Aghia Aikaterini, in the Medieval City of Rhodes'* (in Greek). The project was funded by the Greek Ministry of Culture, February 2002.

xviii. Kilikoglou, V., Theoulakis, P., Karatasios, I. *'Physicochemical Study of Mortars and Plasters from the Spanish Inn, in the Medieval City of Rhodes'* (in Greek). The project was funded by the Greek Ministry of Culture, February 2001.

xix. Moraitou, G., Karatasios, I., Kordas, G. *'Preventive Conservation of Keghree Opus Sectile, in the Archaeological Museum of Isthmia'* (in Greek). The project was found by the Greek Ministry of Culture, May 1999.

Additional Training

i. 'Experiencing Archaeology: Analyses, hypotheses and dirty knees', *Fitch-Wiener Labs Seminar Series on "Science-based Archaeology"*, given by Dr Rodger Doonan (Department of Archaeology, University of Sheffield), organised by the Fitch Laboratory, British School at Athens and the Wiener Laboratory, American School of Classical Studies at Athens. Held in Athens, 2 March 2005.

ii. 'Elemental Analysis by X-ray Spectroscopy Techniques'. Research training seminar provided by THERMO Electron Corporation and HELLAMCO S.A., held in Athens, Greece, 15 February 2005.

iii. 'Ancient Greek Painting in the Making: The Role of Analytical Techniques towards an Art Historical Interpretation', *Fitch-Wiener Labs Seminar Series on "Science-based Archaeology"*, Dr Hariclia Brecoulaki (Univeristy of Paris I - Sorbonne), organised by the Fitch Laboratory, British School at Athens and the Wiener Laboratory, American School of Classical Studies at Athens. Held in Athens, 26 January 2005.

iv. 'X-ray Powder Diffraction. The RIETVELD method'. 2nd Workshop of the Hellenic Crystallographic Association, held at the Department of Physics, National University of Athens, 13-14 October 2004.

v. 'Finishing your thesis and preparing for the viva'. Research training course organised by De Montfort University, held in Leicester, 12 February 2003.

vi. Personal training on the Scanning Electron Microscopy, by Dr Vassilis Kilikoglou, at the Institute of Materials Science, NCSR 'Demokritos', in Athens, Greece.

vii. Personal training on the X-ray Diffraction Analysis, by Dr Vassilis Psycharis, at the Institute of Materials Science, NCSR 'Demokritos' and by Demitris Fragoulis, at TITAN Cement Industry, both in Athens, Greece.

viii. Personal training on the Thermal-Thermogravimetric Analysis, by Dr Aris Papageorgiou, at TITAN Cement Industry, in Athens, Greece.

ix. Personal training on the point-loading compressive test by Dr George Vekinis and Dr Vassilis Kilikoglou, at the Institute of Materials Science, NCSR 'Demokritos', in Athens, Greece.

x. Personal training on the Fourier Transformed Infrared Spectroscopy (FTIR) by Dr Vassilis Verganelakis, at the Institute of Materials Science, NCSR 'Demokritos', in Athens, Greece.

Teaching Experience

i. 'Conservation of Stone – Part I, Practice', Teaching Assistant, Department of Conservation of Antiquities and Works of Art, TEI of Athens. Academic years 2002-2005, (80 hours per semester).

ii. 'Conservation of Mosaics – Part II, Practice', Teaching Assistant, Department of Conservation of Antiquities and Works of Art, TEI of Athens. Academic years 2003-2004, (40 hours per semester).

Participation in Research Programmes

i. European Commission funded program 'Investigation of the effect of airborne particles deposition on the surface of stone monuments. Cleaning and surface protection methods'.
(January 2004, due to finish December 2006).
Participants: Technological Educational Institution of Athens; University of Aegean; and NCSR 'Demokritos'.

ii. European Commission funded program 'Laser for stonework restoration'.
(July 2003, due to finish December 2006).
Participants: National Gallery of Athens and Museum Al. Soutsou; Byzantine and Christian Museum; 'Lithou Sintirisis' Ltd.; 'Compucon' Ltd.; 'Spirit' Ltd.; Institute of Technology and Research; and Technological Educational Institution of Athens.

iii 'Study of the mechanical behaviour of Byzantine stone masonry, decorated with wall mosaics. Restoration proposals for the Dafni Monastery'.
(October 2002 – June 2004).
Participants: Directorate for Technical Research on Restoration, Greek Ministry of Culture and Department of Civil Engineering, National Technical University of Athens.

iv Shelby White- Leon Levy Programme for Archaeological Publication: 'Archaeological and archaeometric study of glass debris found in a Hellenistic glass factory on Rhodes, Greece'.
(March 1999, due to finish December 2005).
Participants: Harvard University and ΚΒ΄ Archaeological Ephorate of Dodecanese

Conferences Attended

i. '9th International Conference on Environmental Science and Technology', organised by the Global Network for Environmental Science and Technology and the Department of Environmental Studies, University of Aegean, held in Rhodes, Greece, 1-3 September 2005.

ii. 'Recent Preoccupations Concerning Textiles, Leather and Legislation', ICOM Interim Meeting, held in Athens, Greece, 20-24 April 2004.

iii. '4th Symposium on Archaeometry of the Hellenic Society of Archaeometry', held in Athens, 28-31 May 2003.

iv. 'Conservation and Exhibition of Restored Works of Art. Technical and Aesthetically Problems', one day meeting organised by the Byzantine and Christian Museum, held in Athens, on 29 January 2003.

v. '8th International Conference for the Conservation of Mosaics', organised by the ICCM, ICCROM and Getty Conservation Institute, held in Thessaloniki, 3-5 November 2002.

vi. '5th International Meeting for the Restoration of the Acropolis Monuments', organised by the Greek Ministry of Culture, held in Athens, 4-6 October 2002.

vii. 'Conservation Science 2002', conference organised by the National Museums of Scotland, held in Edinburgh, on 22-24 May 2002.

viii. '15 Years of Restoration Works in the Medieval City of Rhodes', international conference organised by the Greek Ministry of Culture and UNESCO, held in Rhodes, 14–18 November 2001.

ix. '8th Euroseminar on Microscopy Applied to Building Materials', held in Athens, Greece, 4-7 September 2001.

x. '1st International Conference Hyalos, Vitrum, Glass. History and Conservation of Glass and Vitreous materials in the Hellenic world', organised by NCSR 'Demokritos', held in Rhodos, 1-4 April 2001.

xi. 'IX International Congress on Deterioration and Conservation of Stone', organised by the Instituto Veneto per i Beni Culturali, held in Venice, 19-24 June 2000

B BASIC PRINCIPLES OF ANALYTICAL TECHNIQUES

B.1 X-ray Powder Diffraction

X-ray diffraction is a non-destructive analytical technique for identification of the various crystalline forms, known as 'phases', of the compounds present in solid materials and powders. The minimum amount of samples required is from a few milligrams to 1g. Powder samples must be grounded bellow 70μm.

Solid matter can be described as amorphous or crystalline. In crystalline materials the atoms are arranged in a regular pattern, and there is as smallest volume element that by repetition in three dimensions describes the crystal lattice. A crystal lattice is a regular three-dimensional distribution (cubic, rhombic, etc.) of atoms in space. These are arranged so that they form a series of parallel planes separated from one another by a distance *d*, which varies according to the nature of the material. For any crystal, planes exist in a number of different orientations, each with its own specific d-spacing.

X-rays are electromagnetic radiation similar to light, but with a much shorter wavelength. They are produced when electrically charged particles of sufficient energy are decelerated. In an X-ray tube, the high voltage maintained across the electrodes draws electrons toward a metal target (the anode). X-rays are produced at the point of impact, and radiate in all directions. Tubes with copper targets, which produce their strongest characteristic radiation (Kα1) at a wavelength of about 1.5 Angstroms, are commonly used for geological applications.

If an incident X-ray beam with wavelength *lambda* (λ) encounters a crystal lattice, general scattering occurs. Although most scattering interferes with itself and is eliminated (destructive interference), diffraction occurs when scattering in a certain direction is in phase with scattered rays from other atomic planes (Figure 1).

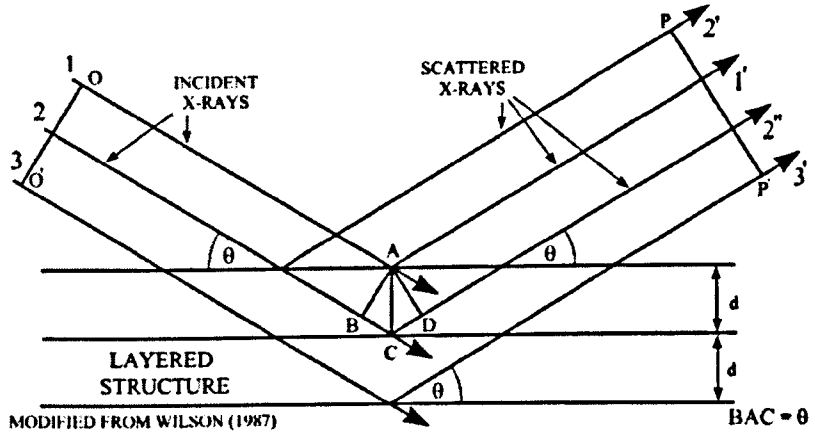

Figure 1: Scattering of X-rays on the parallel planes of the crystal lattice

Under this condition the reflections combine to form new enhanced wave fronts that mutually reinforce each other (constructive interference). The relation by which diffraction occurs is known as the Bragg law or equation:

$$2\,d\sin\theta = \lambda_0 \qquad \text{(Bragg law)}$$

where:

d = lattice interplanar spacing of the crystal

θ = X-ray incidence angle (Bragg angle)

λ = wave length of the characteristics X-rays

Because each crystalline material has a characteristic atomic structure, it will diffract X-rays in a unique characteristic pattern. By varying the angle *theta* (θ), the Bragg's Law conditions are satisfied by different *d*-spacings in polycrystalline materials. Plotting the angular positions and intensities of the resultant diffracted peaks of radiation produces a pattern which is characteristic of the sample. The identification of diffractograms is achieved by comparing the x-ray diffraction patterns, obtained from an unknown sample with an internationally recognised database containing reference patterns for more than 700.000 phases.

B.2 Scanning Electron Microscopy

Scanning electron microscopy is used primary for the study of the surface and of the micro-structure of materials at very high magnifications. SEM magnifications can go to more than 300.000.

During SEM inspection, a beam of electrons is focused on a spot volume of the specimen, resulting in the transfer of energy to the spot. These bombarding electrons, also referred to as primary electrons, dislodge electrons from the specimen itself. The dislodged electrons, also known as secondary electrons, are attracted and collected by a positively biased grid or detector, and then translated into a signal. To produce the SEM image, the electron beam is swept across the area being inspected, producing many such signals. These signals are then amplified, analyzed, and translated into images of the topography being inspected. Finally, the image is shown on a CRT.

Aside from secondary electrons, the primary electron beam results in the emission of backscattered (or reflected) electrons from the specimen. Backscattered electrons possess more energy than secondary electrons, and have a definite direction. As such, they can not be collected by a secondary electron detector, unless the detector is directly in their path of travel. All emissions above 50 eV are considered to be backscattered electrons.

SEM may be equipped with an EDX analysis system to enable it to perform compositional analysis on specimens. EDX Analysis stands for Energy Dispersive X-ray analysis. It is a technique used for identifying the elemental composition of the specimen, or an area of interest thereof. It is sometimes referred to also as EDS or EDAX analysis. The EDX analysis system works as an integrated feature of a scanning electron microscope (SEM), and can not operate on its own without the latter.

During EDX Analysis, the specimen is bombarded with an electron beam inside the scanning electron microscope. The bombarding electrons collide with the specimen atoms' own electrons, knocking some of them off in the process. A position vacated by an ejected inner shell electron is eventually occupied by a higher-energy electron from

an outer shell. To be able to do so, however, the transferring outer electron must give up some of its energy by emitting an X-ray.

The amount of energy released by the transferring electron depends on which shell it is transferring from, as well as which shell it is transferring to. Furthermore, the atom of every element releases X-rays with unique amounts of energy during the transferring process. Thus, by measuring the amounts of energy present in the X-rays being released by a specimen during electron beam bombardment, the identity of the atom from which the X-ray was emitted can be established.

The output of an EDX analysis is an EDX spectrum, which normally displays peaks corresponding to the energy levels for which the most X-rays had been received. Each of these peaks is unique to an atom, and therefore corresponds to a single element. The higher a peak in a spectrum, the more concentrated the element is in the specimen. An EDX spectrum plot not only identifies the element corresponding to each of its peaks, but the type of X-ray to which it corresponds as well.

B.3 Fourier Transform Infrared Spectroscopy

Fourier Transform Infrared Spectroscopy, or FTIR Analysis, is a failure analysis technique that provides information about the chemical bonding or molecular structure of materials, whether organic or inorganic. It is used in failure analysis to identify unknown materials present in a specimen, and is usually conducted to complement EDX analysis.

The technique works on the fact that bonds and groups of bonds vibrate at characteristic frequencies. A molecule that is exposed to infrared rays absorbs infrared energy at frequencies which are characteristic to that molecule.

During FTIR analysis, a spot on the specimen is subjected to a modulated IR beam. The specimen's transmittance and reflectance of the infrared rays at different frequencies is translated into an IR absorption plot consisting of reverse peaks. The resulting FTIR spectral pattern is then analyzed and matched with known signatures of identified materials in the FTIR library.

Unlike SEM inspection or EDX analysis, FTIR spectroscopy does not require a vacuum, since neither oxygen nor nitrogen absorb infrared rays. FTIR analysis can be applied to minute quantities of materials, whether solid, liquid, or gaseous. When the library of FTIR spectral patterns does not provide an acceptable match, individual peaks in the FTIR plot may be used to yield partial information about the specimen.

Single particles are sufficient enough for material identification through FTIR analysis. Organic contaminants in solvents may also be analyzed by first separating the mixture into its components by gas chromatography, and then analyzing each component by FTIR.

B.4 Thermal Analysis

Thermal analysis comprises a group of techniques in which a physical property of a substance is measured as a function of temperature, while the substance is subjected to a controlled temperature programme. In differential thermal analysis, the temperature difference that develops between a sample and an inert reference material is measured, when both are subjected to identical heat-treatments. The related technique of differential scanning calorimetry relies on differences in energy required to maintain the sample and reference at an identical temperature.

DTA involves heating or cooling a test sample and an inert reference under identical conditions, while recording any temperature difference between the sample and reference. This differential temperature is then plotted against time, or against temperature. Changes in the sample which lead to the absorption or evolution of heat can be detected relative to the inert reference.

Differential temperatures can also arise between two inert samples when their response to the applied heat-treatment is not identical. DTA can therefore be used to study thermal properties and phase changes which do not lead to a change in enthalpy. The baseline of the DTA curve should then exhibit discontinuities at the transition temperatures and the slope of the curve at any point will depend on the microstructural constitution at that temperature.

A DTA curve can be used as a finger print for identification purposes, for example, in the study of clays where the structural similarity of different forms renders diffraction experiments difficult to interpret. The area under a DTA peak can be to the enthalpy change and is not affected by the heat capacity of the sample.

DTA may be defined formally as a technique for recording the difference in temperature between a substance and a reference material against either time or temperature as the two specimens are subjected to identical temperature regimes in an environment heated or cooled at a controlled rate.

B.4 Inductively Coupled Plasma Optical Emission Spectrometry

ICP-AES is short for optical emission spectrometry with inductively coupled plasma. ICP-AES is an emission spectrophotometric technique, exploiting the fact that excited electrons emit energy at a given wavelength as they return to ground state. The fundamental characteristic of this process is that each element emits energy at specific wavelengths peculiar to its chemical character. Although each element emits energy at multiple wavelengths, in the ICP-AES technique it is most common to select a single wavelength (or a very few) for a given element. The intensity of the energy emitted at the chosen wavelength is proportional to the amount (concentration) of that element in the analyzed sample. Thus, by determining which wavelengths are emitted by a sample and by determining their intensities, the analyst can quantify the elemental composition of the given sample relative to a reference standard.

ICP-AES analysis requires a sample to be in solution. Thus, interstitial waters can be analyzed simply, requiring only dilution in most cases. Igneous rocks, sedimentary rocks, and sediments, however, must be dissolved. This can be achieved either by a combined acid attack employing HF, HNO_3, and HCl acids, or by a $LiBO_2$ flux-fusion technique similar to that used for XRF preparation.

The plasma is formed by argon (Ar) gas flowing through a radiofrequency field where it is kept in a state of partial ionisation, i.e. the gas consists partly of electrically charged particles. This allows it to reach very high temperatures of up to approx. 10.000°C. At high temperature, most elements emit light of characteristic wavelengths which can be measured and used to determine the concentration.

Using standard spectroscopic techniques (e.g., background corrections), sequential ICP-AES can provide extremely flexible and rapid analysis of a number of up to 40 elements and ICP-AES is consequently a multi-element technique. In terms of sensitivity, ICP-AES is generally comparable to flame atomic absorption, i.e. detection limits are typically at the µg/L level in aqueous solutions.

B.6 Mercury Intrusion Porosimetry

The method of mercury porosimetry is used to give an indication of the approximate pore volume and distribution within a porous material. This is done by infiltrating the material with mercury under a controlled applied pressure. The pressure can be related to the pore size using the assumption of cylindrical pores.

In a pore of circular cross-section or radius r, the surface tension of liquid within the capillary acts to force the liquid back, and is applied along the line of contact with the edge. The surface tension force tends to force the liquid out of the capillary. The magnitude of this force is given by $2\pi r\gamma$, where γ is the surface tension force per unit area, and in the direction of the axis of the capillary by $2\pi r\gamma\cos\theta$, where θ is the contact angle. In equilibrium, this force is balanced by the pressure forcing the liquid into the pore, $\pi r^2 p$. Balancing these forces gives the Washburn (1921) equation:

$$r = -\frac{2\pi\cos\theta}{p}$$

To measure the pore volume intruded at an applied pressure, it is necessary to place the sample to be tested within a sealed pressure vessel into which mercury is forced. The volume of mercury intruded is determined by measuring the change in resistance of a wire suspended in a capillary tube leading into the mercury.

C LEACHING

Leaching is regarded as the dissolution of a solid by an aqueous chemical solution. The degradation phenomenon called 'leaching' in mortar involves the dissolution of various components in the pore water of cement/lime paste. Elements that are bound in poorly soluble phases, like the constitutive phases of the mortars matrix, are only likely to be released if the matrix is becoming dissolved. This process can be complicated by secondary reactions, such as precipitation, adsorption, or the formation of complexes. Solubility is an important parameter in leaching processes, as it determines which transport process/processes are present.

Depending on their grade of solubility, four groups of elements can be distinguished:

- Elements that remain soluble at all pH values, e.g. Na^+, K^+;
- Elements that are soluble in acidic solutions but precipitate in alkaline ones, e.g. Ca^+, Cd^+;
- Elements that are reminiscent of (2) but which redissolve partially or totally in more strongly alkaline solutions (amphoteric behaviour), e.g. Al^{3+}, Zn^{2+}, Pb^{2+}, Cu^{2+};
- Elements that may be present in the solution in the oxo-anionic form, e.g. CrO_4^{2-}, AsO_4^{3-}.

The leaching rate in a cement/lime-based material is not easily described. The phenomena involved are complex and coupled, at the surface as well as in the solid.

The main parameters influence the leaching process incorporate:

- the chemical composition of the additive or admixture;
- . the chemical composition of the water (e.g. pH, complexing compounds);
- . the solubility of the leached component;
- . the rates of reaction;
- . diffusion properties, i.e. concentration gradients;
- . material properties (e.g. buffer capacity, porosity, permeability, L/S-ratio);
- . adsorption and ion exchange

These factors can be sorted under two fundamental issues: equilibrium and kinetics. Depending on the leaching situation, one of these two issues can be more or less dominant.

D ELECTROCHEMICAL CELLS

An electrochemical cell consists of two electrodes, in contact with an electrolyte, an ionic conductor (which may be a solution, a liquid, or a solid). An electrode and its electrolyte comprise an electrode compartment.

A galvanic cell is an electrochemical cell that produces electricity as a result of the spontaneous reaction occurring inside it. An electrolytic cell is an electrochemical cell in which a non-spontaneous reaction is driven by an external source of courent.

In an electrochemical cell, the reduction and oxidation processes responsible for the overall reaction are separated in space: oxidation takes place in one electrode compartment and reduction takes place in the other compartment. As the reaction proceeds, the electrons released in the oxidation at one electrode

$$Red_1 \rightarrow Ox_1 + ve^-$$

travel through the external circuit and re-enter the cell through the other electrode. There they bring about reduction:

$$Ox_2 + ve^- \rightarrow Red_2$$

The electrode at which oxidation occurs is called the anode; the electrode at which reduction occurs is called the cathode.

In an electrolytic cell, electrons are forced through the circuit by an external source. Although the cathode is still the site of reduction, the negative electrode whereas the anode, the site of oxidation, is positive.

REFERENCES

Atkins, P.W. (1998). *Physical Chemistry*, Oxford University Press, Oxford.

Andersson, Å. (2000). 'Leaching of Hazardous Substances from Concrete Constituents', PhD Thesis, Chalmers University of Technology, Department of Building Materials, Göteborg.

EUR 17869 EN (1997). European Commission Report, Development of a leaching method for the determination of the environmental quality of concrete, EC Directorate-General Science, Research and Development, DGX11/C/5-Programme SM&T.

Moszkowicz, P., Barna, R., Sanchez, F., Bae, H., R., Méhu, J., (1997). 'Models for leaching of porous materials', *Waste Materials in Construction: Putting theory into Practice*, Proceedings, Wascon, Elsevier Science, pp. 491-500.